Towards exploration tools for high purity quartz: an example from the South Norwegian Evje-Iveland pegmatite belt

Submitted by Benjamin Richard Snook to the University of Exeter as a thesis for the degree of Doctor of Philosophy in Earth Resources, January 2014.

I certify that all material in this thesis which is not my own work has been identified and that no material has been previously submitted and approved for the award of a degree by this or any other University.

Signature: .....

Benjamin Richard Snook, January 2013

ABSTRACT

High purity quartz (HPQ), generally defined as containing <50 ppm trace elements, is of increasing economic significance due to its use in new types of high tech components (computer chip and semiconductor manufacture) and green technology (silicon wafer production for photovoltaics). Current HPQ deposits (such as hydrothermal veins and leuco-granites/alaskites) are extremely rare and volumetrically small. Unless significant new deposits are found, increasing demand for HPQ will raise its price, elevating the strategic nature of this limited commodity. The large volumes and simple mineralogy of pegmatites and the high chemical purity of their constituents make them an attractive target for HPQ. As yet, however, there are no detailed criteria on which to explore for HPQ in pegmatites. In order to develop such criteria, there needs to be a greater understanding of the nature and genesis of pegmatite-hosted HPQ deposits. The Evje-Iveland pegmatite field of the Bamble-Evje pegmatite cluster, southern Norway was targeted due to its well constrained geological setting and previously identified potential for HPQ. Studies initially focussed on understanding the genesis of the Evje-Iveland pegmatites, before investigation of the formation mechanisms of HPQ.

The Evje-Iveland pegmatite field contains approximately 350 major bodies of internally zoned, weakly peraluminous/metaluminous, REL-class, NYF-type pegmatites, usually consisting of (from margin to centre) a border zone facies of fine grained quartz and plagioclase, a coarser wall zone of quartz, plagioclase and biotite, an intermediate zone of megacrystic K-feldspar with graphic intergrowths of quartz and a massive quartz core. The pegmatites have a relatively simple mineralogy (essentially granitic), with accessory REE-bearing phases. The pegmatites typically have sharp contacts concordant with country rock foliation, but, at Iveland, evidence of country rock anatexis is observed. The Landsverk 1 pegmatite contains brecciated feldspar and replacement quartz, the latter interpreted to be of ‘hydrothermal’ origin.

The nearby Høvringsvatnet granites were investigated as a potential source for the Evje-Iveland pegmatites. However, no spatial control could be identified on pegmatite characteristics with distance from the granites (e.g. degree of

fractionation, geochemistry) and there was found to be a significant age discrepancy (approximately 70 Ma) between the Høvringsvatnet granites (982.9±3.9 to 979.7±3.8 Ma) and the Evje-Iveland pegmatites (variable, but clustered around 910.5±1.6 Ma). From field observations (including the clear in situ formation of pegmatites at Iveland) and geochemical modelling, it is interpreted that the pegmatites formed by 15 – 30% partial melting of country rock gneisses and metagabbros. Due to the proximity and similarity in timing of emplacement of the nearby Rogaland Igneous Province, the pegmatites are likely to have formed from the same trigger which caused partial melting of deep crust responsible for the adjacent Province; crustal thinning, down thrusting of crust and the intrusion of crustal tongues into the mantle during the end of the Sveconorwegian Orogeny.

Studies on the nature and formation of quartz in the pegmatites were based on CL imaging in scanning electron microscope (SEM) and laser ablation inductively coupled plasma mass spectrometry (LA-ICP-MS). It is demonstrated that there is little spatial or internal consistency in the trace element content of magmatic quartz which limits its suitability as a source of HPQ. However, replacement quartz shows trace element contents below 50 ppm, so may constitute HPQ, but compared with magmatic quartz typically shows relatively elevated levels of Al (10 – 400 ppm) and Li (1 – 25 ppm), low Ge (<1 ppm) and a complete absence of Ti. Different quartz types and domains (revealed by SEM-CL) show distinct $\delta^{18}O$ values; magmatic quartz shows $\delta^{18}O$ of 8 to 9‰ , typical of granitic quartz, whereas late stage, low trace element zones in hydrothermal quartz show $\delta^{18}O$ values -8 to 11‰, likely to have crystallised from variably meteoric and magmatic fluids. As such, it is proposed that HPQ in the Evje-Iveland pegmatites was generated by secondary processes involving relatively low temperature, externally derived hydrothermal fluids, rather than as a result of the formation of the pegmatite bodies themselves. Additionally, it has been demonstrated that an associated granite is not necessary for pegmatite generation, so exploration areas for pegmatite-hosted HPQ needn’t be limited to regions around plutons. Exploration activities should be underpinned by field observations of pervasive hydrothermal reworking, and occurrences of HPQ identified from CL-SEM imaging and elemental and O isotope analyses.

ACKNOWLEDGMENTS

I am extremely grateful to my supervisors Ben Williamson, Axel Müller and Frances Wall for their constant advice, guidance and cajoling. The research project could not have been possible without funding from the Camborne School of Mines (CSM) and the Norwegian Geological Survey (NGU), and I gratefully acknowledge the Institute of Materials, Minerals and Mining, the Society for Economic Geologists and The Geological Society, London for their generosity in providing additional funding which enabled vital field work, research and presentations at a variety of international conferences. Thank you all.

I would also like to thank all of the laboratory staff at the NORDSIM facility, Swedish Natural History Museum, for their guidance and patience in my work on U-Pb dating and O isotopes, both during and after my trip to Stockholm. Similarly, I am thankful for the advice and laboratory access provided by the friendly academics and technical staff at both at the CSM and NGU facilities. There are too many to list, but Bernard Bingen deserves particular mention for his unquestioning devotion of time in zircon preparation.

I offer my gratitude to the friends I shared an office with, and encouragement to those left to finish. Both professional and personal life has been unparalleled for the duration of my studies.

Finally, I will remain eternally grateful for the support of my non-university friends, to Ali and to my parents. I couldn't have done it without you.

Contents

FIGURES

TABLES

1. INTRODUCTION

1.1 Project rationale

Naturally occurring high purity quartz (HPQ), which is defined as containing less than 50 ppm trace elements (Harben, 2002), is of increasing economic significance due to emerging applications in the production of high-tech components such as computer chips and semiconductors and in green technologies, particularly for silicon wafer production for photo-voltaic cells (Glover et al., 2012). The production of solar panels has increased rapidly over the last 5 years (Fig. 1.1.1). However, HPQ is extremely rare as suitable deposits, mainly in hydrothermal veins and granitic rocks, are typically volumetrically small. Unless significant new deposits are found, increasing demand for HPQ will raise its price, elevating the strategic nature of this limited commodity. The Silicon Solar Resources Group (www.ssrg.com.sg 2013) suggests that present consumption of HPQ is growing at 20% p.a.; currently at approximately 3.5 Mt p.a., this is forecast to double by 2015.

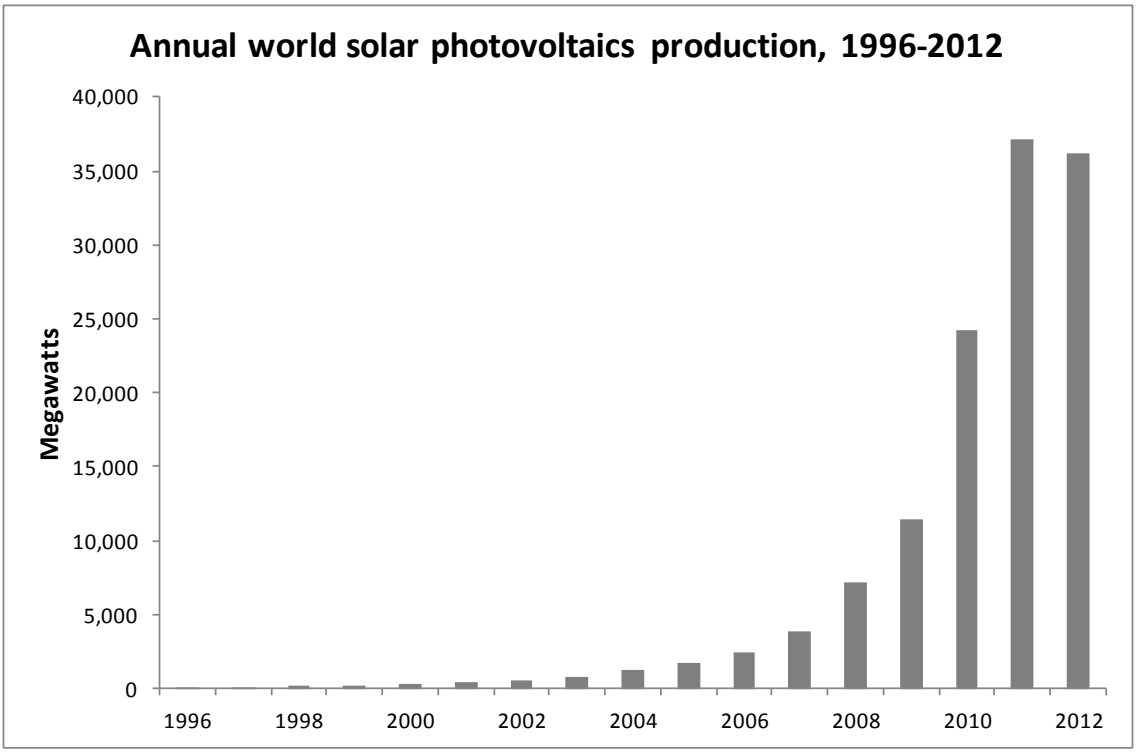

Fig. 1.1.1 Production increase of photovoltaics (after data from the Earth Policy Institute, 2013)

Ensuring security of supply for HPQ requires the identification of deposits in a broader range of countries, particularly in Europe, and possibly of a different kind to those currently in production e.g. low volume granitic pods and

hydrothermal veins. A prerequisite for developing exploration tools for such deposits is to gain a better understanding of their nature and mechanisms of formation. The large volumes and simple mineralogy of pegmatites and the often high chemical purity of their constituents (Glover et al., 2012) make them an attractive target for HPQ.

This study aims to address these issues through a detailed investigation of HPQ occurrences in the Evje-Iveland pegmatite field, located between the villages of Evje and Iveland in south Norway (see Fig. 1.1.2). The location was chosen as the Evje-Iveland pegmatites were determined to contain quartz of a “relatively high purity” by Larsen et al. (2000), which was corroborated during exploration activities by the Norwegian Geological Survey (NGU). The field contains a range of well exposed pegmatites due to historical small scale mining activity and has an extensive mineral collecting history. Additionally, a number of studies have been undertaken to determine the regional geology, tectonic history, structural evolution, mineralogy and age of rocks in the area (e.g. Bjørlykke, 1935; Bingen et al., 2005, 2008a, 2008b; Hendersen and Ihlen, 2004; Pedersen, 1981; and Pedersen and Konnerup-Madsen, 1994, 2000). Previous studies have been undertaken on the genesis of the pegmatites, which can act as a useful counterpoint to this investigation (e.g. Bjørlykke, 1937; Pedersen and Konnerup-Madsen, 1994; several unpublished MSc theses - Andersen, 2001; Fought, 1993; Stockmarr, 1994).

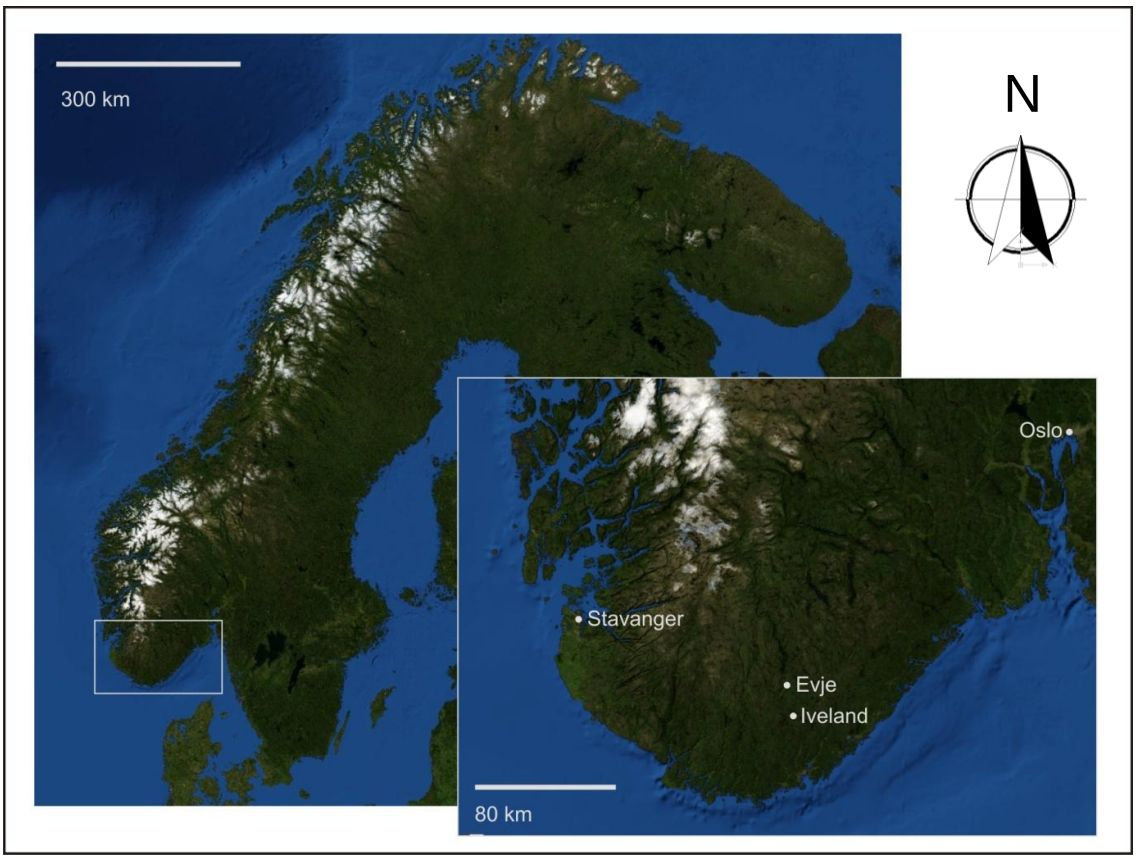

Fig. 1.1.2 Location map of the study area (after ArcGIS My Map, 2012)

Pegmatites have long been utilised as important sources of gems, feldspar and mica but are of increasing importance for 'critical' metals and high purity quartz (e.g. London and Kontak, 2012 and references therein). However, in many instances their origin is inferred rather than fully studied, and despite numerous studies, the exact mechanisms of pegmatite formation remain controversial. The majority view is that pegmatites form as a result of equilibrium crystallisation of coexisting granitic melt and flux bearing fluids at or below the hydrous granitic liquidus, as initially proposed by Jahns and Burnham (1969), discussed further in *Chapter 2.3.2*. However, other workers (Boos, 1954; Stewart, 1978; Simmons et al., 1995, 1996; Martin and De Vito, 2005) suggest alternative modes for pegmatite genesis, based upon models of partial melting and anatexis of host country rock.

Previous studies of pegmatites of the Evje-Iveland belt of south Norway have suggested that they represent late stage fractionates of melt vestiges from the adjacent Høvringsvatnet granite complex (Bjørlykke, 1937). Larsen et al. (2000), referring to previous work (principally by Bjørlykke, 1937), suggested

that the Evje-Iveland pegmatites and Høvringsvatnet granites are closely related and probably formed from a common limited parental source. Larsen (2002) refers to a LREE-enriched, HREE-deficient 'parent melt' with a 'late magmatic volatile phase', and suggests that the pegmatites were derived from 'primitive parental magmas'. Conflictingly, some authors (e.g. Pedersen and Konnerup-Madsen, 1994) discuss how the Høvringsvatnet granites may represent the parent magma of the granite pegmatites but subsequently report a significant temporal difference (~100 Ma) between the granites and the pegmatites based on unpublished data and student theses (Pedersen and Konnerup-Madsen, 2000).

1.2 Aim of the study and hypotheses to test

The aims of this study were to 1) determine the origin and evolution of the Evje-Iveland pegmatites; whether they represent late stage melts from the Høvringsvatnet granites or the products of low degree partial melting of local country rocks and 2) determine the nature and origin of quartz in the pegmatites; whether HPQ was formed by magmatic (pegmatite-forming) processes or a later hydrothermal overprint. Resolving these aims may have significant implications for the generation of comparable pegmatite fields, and aid in the exploration for new sources, high-purity quartz and other commodities associated with pegmatites.

In order to address the aims of this study, five specific hypotheses were tested:

- There is no spatial control on pegmatite characteristics with distance from the granite (e.g. degree of fractionation, geochemistry);
- There is a significant age discrepancy between the Høvringsvatnet granites and the Evje-Iveland pegmatites;
- The Evje-Iveland pegmatites formed by partial melting of country rock gneisses and metagabbros;
- Quartz chemistry is homogenous throughout individual pegmatites in Evje-Iveland;

- HPQ was generated by secondary processes (possibly at the magmatic-hydrothermal transition) such as hydrothermal alteration or secondary overprinting i.e. recrystallisation. The generation of HPQ is therefore (at least) a two stage process, whereby primary quartz (of variable purity) forms within a pegmatite, and is subsequently replaced by newly formed high purity quartz.

1.3 Objectives

The first three hypotheses were tested by studying the geochemical relationship between the Evje-Iveland pegmatites and the Høvringsvatnet granites to compare the nature of their source. Whether the pegmatites represent residual melts following the crystallisation of the Høvringsvatnet granites, were generated by melting of country rocks, or are from an alternative source is extremely difficult to determine from major and trace element compositions, due mainly to complications in acquiring single and suites of whole-rock samples from individual pegmatites for geochemical modelling (given the very coarse grain size of pegmatites). However, as a shared source is not implicit simply from a coeval age (and vice versa), additional evidence will be required. For example, source characteristics can be broadly assessed using the I- and S-type classification proposed by Chappell and White (1974) and updated by White and Chappell (1983), to indicate whether the granites and pegmatites had a meta-igneous or meta-sedimentary source.

In addition to investigating the geochemical link between the pegmatites and granites, their temporal relationship was determined through U-Pb isotope dating. Previous age determinations generally show large uncertainties; 845±12 Ma and “about 800 Ma” (after Pedersen and Konnerup-Madsen, 2000) for the pegmatites and 945±53 Ma (Pedersen, 1981) and 971+63/-34 Ma (Andersen et al., 2002) for the Høvringsvatnet granite. Although relatively precise ages for the Evje-Iveland pegmatites are provided by Scherer et al. (2001) (910.5±1.6 Ma) and Andersen (2001) (909±5 Ma), the ages are based on five U-Pb isotope ratios from a piece of gadolinite from an unknown pegmatite. As such, clarification of the currently uncertain temporal relationship between the

pegmatites and Høvringsvatnet granite is crucial in understanding whether the granites and pegmatites are genetically related i.e. whether the pegmatites represent more evolved equivalents of the granites, or that the pegmatites and granites are unrelated.

Müller et al. (2008) demonstrated that quartz from the south Norwegian Froland pegmatite field maintains a consistent trace element signature both between and within pegmatites; this is an economic necessity for HPQ deposits due to the requirement to produce a consistent quartz product. The homogeneity of pegmatite quartz (hypothesis 4) will be tested through targeted sampling and studying mineral chemistry (LA-ICP-MS on quartz).

The role of secondary processes in the generation of HPQ (hypothesis 5) will be assessed by studying field relations, variation in the chemistry of a variety of pegmatite minerals, macro- and microscopic textures of minerals and mineral chemistry. This will be supplemented by determining the oxygen isotope ratios and mineral chemistry of pegmatitic quartz in order to better understand the mode of formation of the pegmatites (i.e. source, magmatic evolution, metasomatism, hydrothermal overprinting) and to explain the nature and existence of HPQ.

Müller et al. (2008) showed that quartz from the Froland pegmatites underwent multiple reworking events at micro-scale. Structures resulting from quartz overprinting (healed fractures, diffusion fronts, re-crystallised quartz domains) are revealed by scanning electron microscope cathodoluminescence (SEM-CL). A better understanding of the formation of these microstructures may lead to a better understanding of the large scale processes responsible for HPQ formation. The oxygen isotope analyses of these different generations of quartz will aid in developing appreciation of the origin of the melts/fluids from which the quartz crystallised and which caused the overprinting and re-crystallisation. The crystal domains of the different quartz and feldspar generations are commonly rather small (<200 µm), and to resolve their individual oxygen isotope ratios therefore required the high spatial resolution of ion probe analysis. This type of approach has been successfully applied to igneous quartz by Valley and

Graham (1996), who showed that $\delta^{18}O$ in a single quartz grain can vary by up to 13‰, over 400 μm.

1.4 Thesis structure

The thesis is comprised of 6 chapters in total (**Introduction** included), with associated appendices:

Chapter 2 (**Literature review**) provides a review of the geological setting of the Evje-Iveland pegmatite belt, an introduction to pegmatites and an appraisal of HPQ.

Chapter 3 (**Methodologies**) discusses the various methodologies employed in this investigation to attempt to achieve the aims outlined above, including field and sampling campaign, sample preparation, analytical techniques and ultimately quality assurance and control.

Chapter 4 (**Results**) presents the results from this investigation, including field observations, geological maps, whole rock and mineral qualitative and quantitative data.

Chapter 5 (**Discussion**) discusses the results of the study, providing an interpretation of pegmatite genesis and the formation of HPQ. Investigation of the genesis of the pegmatites combines data from the field, geochemistry and geochronology, whilst imaging, in-situ beam techniques and stable isotope geochemistry were utilised to elucidate HPQ formation. Additionally, the validity of the techniques employed during the investigation are assessed

Chapter 6 (**Conclusions**) summarises the main findings to resolve the outlined aims, with additional discussion of aspects worthy of further study.

Appendix 1 consists of a summary of samples collected during the course of this investigation. **Appendix 2** consists of data tables for geochemical results.

2. LITERATURE REVIEW

2.1 The Sveconorwegian Orogeny

2.1.1 Components of the Sveconorwegian Orogeny

The Sveconorwegian Orogeny (SNO) resulted from the collision of Fennoscandia/Laurentia with Amazonia during the formation of Rodinia at the end of the Mesoproterozoic (Pedersen et al., 2009). Collision, which began at around 1140 Ma, with final convergence at 970 Ma, caused polyphase imbrication of terranes at the edge of Fennoscandia, with the resultant belt comprising, east to west, of a Palaeoproterozoic Eastern Segment and four transported terranes (Idefjorden, Kongsberg, Bamble, and Telemarkia (possibly exotic)) (Bingen et al., 2008b). This is illustrated in Fig. 2.1.1**.**

The **Fennoscandia foreland** is composed of Palaeoproterozoic crust of the Svecofennian belt and the Transcandinavian Igneous Belt (TIB; granitoids and porphyries (1850-1660 Ma) showing limited deformation and a general alkali-calcic signature) (Högdahl et al., 2004). This continental basement was intruded by several generations of Mesoproterozoic and younger magmatic rocks (granites and dolerites; Söderlund et al., 2005).

The **Eastern Segment** predominantly consists of 1800-1640 Ma variably metamorphosed gneissic granitoids (compositionally similar to the TIB) intruded by volumetrically minor magmatic suites (variably mafic or granitic, 1560-1200 Ma) (Högdahl et al., 2004). Pre-SNO amphibolites facies metamorphism (the Hallandian event) is dated at 1460-1410 Ma by U-Pb in zircon (Söderlund et al., 2002). The intensity of SNO-related reworking and metamorphism increases from north to south and from east to west (Bingen et al., 2008b).

The **Idefjorden Terrane** is 1660 – 1520 Ma, consisting mainly of calc-alkaline and tholeiitic plutonic and volcanic rocks associated with greywacke-bearing metasedimentary sequences, with general younging towards the west (e.g. Bingen et al., 2001). The Terrane displays a general N-S to NW-SE orogenic foliation, and is perceived to represent a palaeo-arc setting (Bingen et al., 2005).

The **Bamble and Kongsberg Terranes** mainly consist of 1570 – 1460 Ma calc-alkaline plutonic suites associated with quartzite and greywacke-dominated metasedimentary complexes (Andersen et al., 2004a). The quartzite-rich complexes also contain mica gneiss, sillimanite-rich gneiss and minor orthoamphibole-cordierite rocks (Bingen et al, 2008b). The Bamble Terrane hosts the 1200 – 1180 Ma (U-Pb in zircon) gabbro-tonalite Tromøy complex, 1170 – 1150 Ma granite-charnockite metaplutons, 1060 Ma pegmatites and 990 – 920 Ma post-collisional granite plutons (Andersen et al., 2004a).

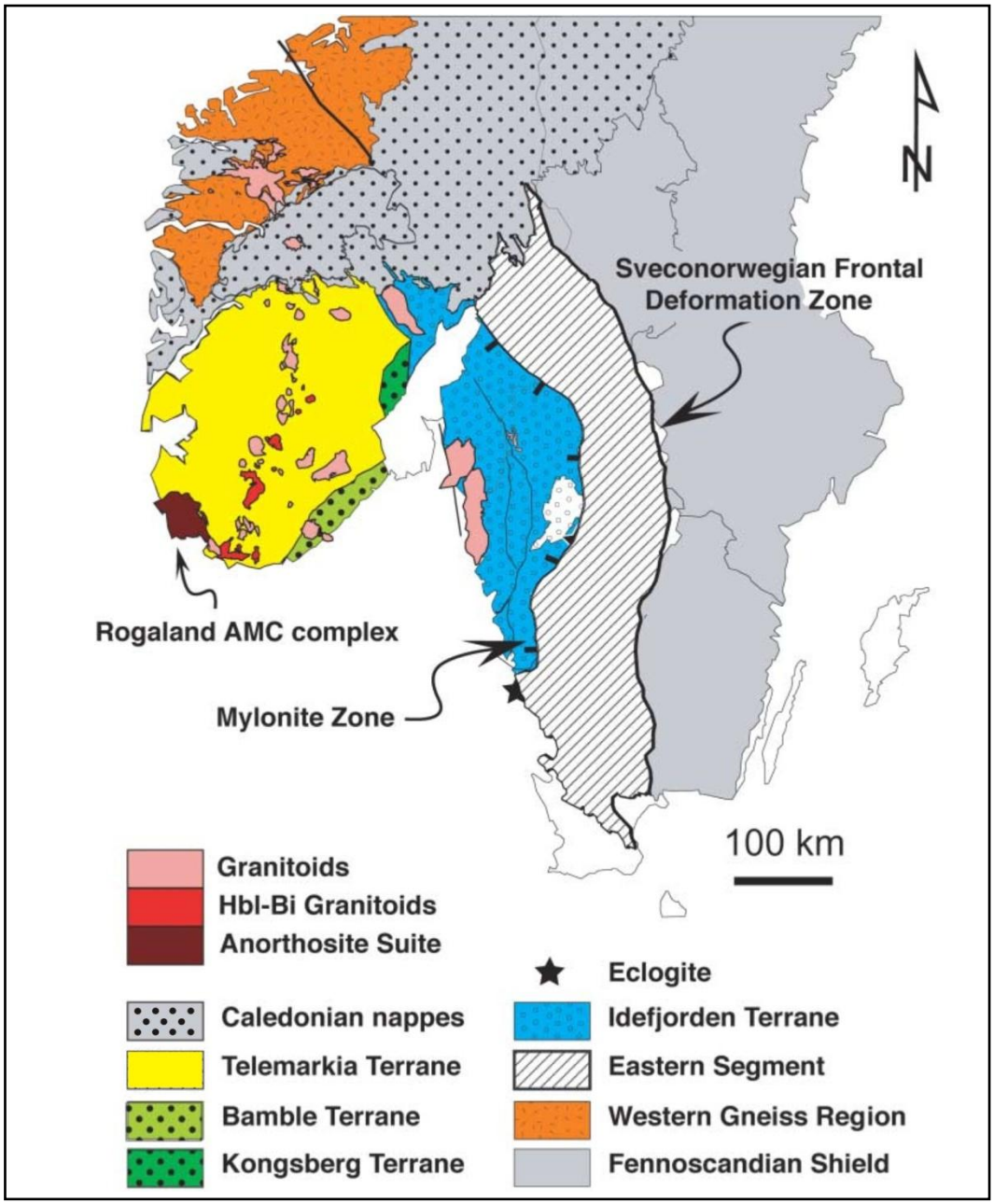

Fig. 2.1.1 Simplified map of geological terranes present in southern Scandinavia (after Brueckner, 2009)

From geophysical data, the Bamble and Kongsberg Terranes form two tectonic wedges overlying the Telemarkia Terrane (Ebbing et al., 2005). The Kongsberg Terrane displays a steep N-S trending SNO foliation, with a peak amphibolite facies assemblage (Andersen and Munz, 1995). The Bamble Terrane has a pronounced NE-SW trending structural grain/strong planar fabric, isoclinal folds and lithological banding (Kullerud and Dahlgren, 1993). Peak P-T conditions are granulite facies estimated at 0.7±0.11 GPa and 793±58°C (Harlov, 2000).

Two phases of metamorphism are recorded; the first is limited to the Bamble Terrane at 1140 – 1125 Ma, as recorded in amphibolite facies and granulite facies rocks which have been dated by U-Pb in zircon (1125±46 and 1124±8 Ma; Knudsen and Andersen, 1999), in monazite (1145±3 to 1127±6 Ma; Bingen et al., 2008a) and titanite in marble (1137±2 Ma; Cosca et al., 1998). Peak metamorphism was at sillimanite granulite facies at 1137±1 Ma (from U-Pb in monazite; Bingen et al., 2008a). The second phase affected both the Bamble and Kongsberg Terranes. Monazite with a U-Pb age of 1107±9 Ma exists within the Bamble Terrane, with titanite ages between 1106±2 and 1091±9 Ma (Bingen et al., 2008a). These ages overlap with the main cluster of amphibole $^{40}Ar/^{39}Ar$ cooling ages of 1099±3 to 1079±5 Ma, recorded in amphibolite and granulite rocks (Cosca et al., 1998). 1107±9 Ma (Bingen et al., 2008a) represents a point of regional cooling and unroofing in the Bamble Terrane. Critically, both events (at 1140 – 1125 and 1110 – 1080 Ma) are recorded in one sample from the amphibolite-facies domain in Bamble, indicating the two events cannot be attributed to two separate tectonic units (Bingen et al., 2008b).

The Porsgrunn-Kristiansand Fault Zone (PKF), which forms the boundary between the Bamble and Telemarkia Terranes, is a southeast dipping SNO thrust zone reworked as an extensional detachment. The thrust zone is associated with northwest verging folds developed under amphibolite-facies conditions and the intrusion of pegmatite bodies (Henderson and Ihlen, 2004). The age of the thrusting is not defined, but must be younger than the 1132±3 Ma Morkheia monzonite suite deformed along the shear (Heaman and Smalley, 1994). Thrusting most likely post-dates the peak of the most widespread event of amphibolite-facies metamorphism recorded in the Bamble and Kongsberg

Terranes (approximately 1110 Ma) and may overlap with regional cooling recorded at 1090 – 1080 Ma. Secondary titanite may relate to reactivation of the shear zone or reheating in relation to metamorphism in the Telemarkia footwall of the shear zone at 994±30 Ma, with titanite and amphibole ages suggesting further late-SN cooling between 910 and 860 Ma (Heamon and Smalley, 1994; Bingen et al., 2008b).

The **Telemarkia Terrane** was affected by a voluminous magmatic event at 1520-1480 Ma, with no older magmatic rocks positively identified (Bingen et al., 2005). These volcanic and plutonic suites are interlayered with quartzite metasedimentary sequences (older than c. 1350 Ma), and are intruded and unconformably overlain by several magmatic suites and sediments (between 1280 and 1130 Ma) (Bingen et al., 2001). SNO plutonism is manifest in Telemarkia, consisting of 1050 – 1035 Ma granodiorite to granite suites, 1030 – 1000 Ma syn-collisional granitoids, 970 – 930 Ma post-collisional monzodiorite to granite plutons and the 930 – 920 Ma Rogaland anorthosite-mangerite-charnockite complex (e.g. Schärer et al., 1996; Bingen and van Breemen, 1998). The Telemarkia Terrane is composed of four distinct sectors (the Telemark, Hardangervidda, Suldal and Rogaland-Vest Agder; Bingen et al., 2005); the eastern Telemark sector is the largest and most pertinent to this study. It must be noted that the Rogaland sector is adjacent to the Evje-Iveland pegmatite belt (80 km to the west), and is essentially only 10 Ma older (e.g. Duchesne et al., 1999; Schärer et al., 1996). Crustal heating associated with the Rogaland complex, possibly including that from crustal thinning and underplating, is a potential source of the heat for partial melting to produce the pegmatites of Evje-Iveland (discussed in *Chapter 5.1.2*).

The central part of the Telemark sector is composed of low-grade supracrustal rocks, consisting of four main stratiform sequences (Andersen et al., 2004b). The lowest is a suite of 1510 – 1500 Ma bimodal volcanic rocks of the Rjukan group. This is overlain by the quartzite-dominated Vindeggen group, which is in turn overlain unconformably by 1170 – 1140 Ma bimodal volcanic rocks which interlayered with metasediments (Bingen et al., 2008b). The uppermost post-1120 Ma sequence is made up of immature clastic sediments. Metamorphic

grade increases towards the northeast to amphibolite-facies, dated in an amphibolite boudin by U-Pb in zircon at 1014±1 Ma (Bingen et al., 2008a). Towards the south, supracrustal rocks abut a NE-SW trending amphibolite-facies gneiss complex which has been dated by titanite at 913 – 901±7 Ma, probably reset by late-SNO high grade metamorphism (Heaman and Smalley, 1994). The Telemark sector is bounded to the west by the N-S trending Mandal-Ustaoset Fault, forming in the north a ductile shear zone and a brittle normal fault system by which the Telemark sector is downthrown. Southwards, the Mandal-Ustaoset Fault merges into the N-S structures characteristic of the gneisses.

The Telemarkia and Idefjorden are separated by the southwesterly dipping Vardefjell Shear Zone, which is characterised by amphibolite-facies banded gneiss containing extensive amphibolite layers and boudins dated by U-Pb in zircon at 1012±7 to 1008±14 Ma (Bingen et al., 2008a). Deformation of the amphibolites along the shear is syn- or post-peak metamorphism at c. 1010 Ma, and may have continued until 985±5 Ma (Bingen et al., 2008a).

2.1.2 A four stage model for the SNO

A four stage model has been proposed by Bingen et al. (2008b), consisting of the Arendal phase (1140 – 1080 Ma), Agder phase (1050 – 980 Ma), Falkenberg phase (980 – 970 Ma) and Dalane phase (970 – 900 Ma).

The start of the Arendal phase corresponds with the oldest recorded Sveconorwegian high-grade metamorphism (c. 1140 Ma) within the Bamble Terrane at Arendal (Bingen et al. 2008b). Its formation is best interpreted as being due to early-Sveconorwegian 1140 – 1080 Ma collision between the Telemarkia and Idefjorden Terranes, resulting in the development of the Bamble and Kongsberg tectonic wedges (containing lithologies characteristic of the enclosing terranes) (Ebbing et al., 2005).

Bingen et al. (2008b) suggested a geotectonic model where, at 1220 Ma, NW subduction under Telemarkia of an oceanic basin produced the 1200 – 1180 Ma Tromøy volcanic arc and potentially a granite batholith (now the 1200 Ma

Drivheia gneiss) in southern Telemarkia. At 1140 Ma, collision between the Telemarkia and Idefjorden Terranes caused the formation of an orogenic wedge (Bamble and Kongsberg Terranes), resulting in crustal thickening (with southwest directed shortening) and peak metamorphism under intermediate pressure granulite facies conditions (1140 – 1125 Ma Arendal granulites). At 1110 Ma, continued convergence produced high-grade metamorphism within the newly formed wedges and locally into the Idefjorden Terrane, with eventual thrusting of the Bamble Terrane onto the Telemarkia ramp (the PKFZ) and, at 1080 Ma, post-thrust regional cooling. Unconformable and post-1120 Ma clastic sediments may indicate foreland or intramontane basin formation related to mountain building and tectonic stripping of the Bamble and Kongsberg Terranes. Tectonic inactivity within the SNO belt followed the unroofing of these terranes, from 1080 – 1050 Ma (Bingen et al., 2008b).

The Agder phase (1050 – 980 Ma) was the main SN event. This probably resulted from an oblique continent-continent collision between Fennoscandia and another large continent (potentially Amazonia). This phase is characterised by tectonic imbrications and crustal thickening in the central part of the orogeny (including deformation, metamorphism and magmatism in the Idefjorden and Telemarkia Terranes) (Bingen et al., 2008b).

The phase was initiated in 1050 Ma when the Idefjorden Terrane was underthrust and buried to a depth of 35 – 50 km; amphibolite- to granulite-facies metamorphism records pressures of 1.0 – 1.5 GPa (Bingen et al., 2008a). This metamorphism is coeval with the intrusion of high-K calc-alkaline granodiorite plutons (1050 – 1030 Ma Feda and Fennefoss augen gneiss suites) in the Telemarkia Terrane (Bingen and van Breeman, 1998). These suites may represent the final stage of an active continental margin setting in the belt, or melting of a protolith with an active margin signature as a result of crustal thickening (Bingen et al., 2008b). Crustal thickening in the Telemarkia Terrane (as suggested by synchronous metamorphic records) began at 1035 Ma, with the oldest evidence recorded in low-grade metamorphic lithologies, which subsequently cooled shortly after 1030 Ma (Stein and Bingen, 2002). From zircon, monazite and molybdenite geochronology (in western Telemarkia at

least) high-grade metamorphic conditions prevailed until 900 Ma (Bingen et al., 2008b). Synchronous to Telemarkian thickening, monazite and titanite age data suggest unroofing in the Idefjorden terrane at 1025 Ma; the implication is that this exhumation of high pressure rocks took place in a convergent setting (Bingen et al., 2008b). The Vardefjell Shear zone accommodated deformation between the two terranes at 1010 – 985 Ma defined by dating of amphibolite-facies metamorphism and fabric-parallel titanite respectively (Bingen et al., 2008a). This deformation is approximately coeval with high-grade metamorphism in the Telemarkia hanging wall of the shear zone (1014 Ma). The high pressure metamorphism of the Idefjorden Terrane differs from the medium-pressure metamorphism displayed in Telemarkia. This, along with a westerly-increasing volume of syn-collisional magmatism, further contrasts the warmer thermal nature of the Telemarkian lithosphere relative to the Idefjorden Terrane (Bingen et al., 2008b).

During the Falkenberg phase, high-grade metamorphism (980-970 Ma) related to crustal thickening propagated eastwards into the Eastern segment. The inclusion of eclogite relics (914±14 Ma) indicates burial of Fennoscandia crust to at least 50 km (with subsequent exhumation to a middle crustal level), this being the last undisputable evidence for convergence in the SNO belt (Bingen et al., 2008b).

The Dalane phase represents a period of relaxation/gravitational collapse from 970 to 900 Ma (Bingen et al., 2006). The lack of late-orogenic sedimentary units within Fennoscandia suggests continental thinning was primarily due to crustal extension, as opposed to erosion. Two high grade domains (the southern Eastern Segment and western Telemarkia) were exhumed to upper crustal levels post-970 Ma, producing large scale gneiss dome/core complex-like structures (Bingen et al, 2008b). The interpretation of the southern Eastern Segment is as a large asymmetric metamorphic core complex. E-W to WNW-ESE trending fold structures and high strain zones are perceived as evidence for combined N-S shortening and E-W extension and formed during crustal flow associated with uplift of high-pressure rocks to a mid-crustal level (Möller et al., 2007). Initially rapid exhumation (970 Ma) was followed by relatively slower

uplift and regional cooling (960 – 920 Ma). Exhumation of the Eastern Segment is synchronous with the formation of N-S trending steep, normal shear zones at the front of the orogeny (Andréasson and Rodhe, 1994) and intrusion of the orogenically concordant Blekinge-Dalarna dolerites in the foreland of the SN belt (Söderlund et al., 2005). In western Telemarkia, amphibolite- to granulite-facies can be interpreted as forming a large scale gneiss dome (progressively exhumed after 970 Ma; Bingen et al., 2006) which may include the high grade South Telemark gneisses. Doming was instigated between 970 – 940 Ma and again at 930 – 910 Ma, and was associated with voluminous post-collisional monzodiorite-granite plutonism, local-scale decompression melting and a regional drop in pressure (Vander Auwera et al., 2003). In the Telemarkia and Idefjorden Terranes there was comparatively limited exhumation post-970 Ma. Shallow plutons and discordant veins indicate predominantly brittle upper crustal conditions and an extensional setting at 970 – 900 Ma (Hellström et al., 2004).

2.2 Regional tectonics and geological setting for the Evje-Iveland pegmatites

The Evje-Iveland pegmatites (comprehensively described by Bjørlykke, 1935) occur in the Setesdalen region of southern Norway, within the Telemark block of the Fennoscandian shield (Fig. 2.1.1 and Fig. 2.2.2). They were likely generated in the closing stages of the Sveconorwegian orogeny, where the Bamble Complex was thrust over the Telemark Block along the Porsgrunn-Kristiansand Fault Zone (Pedersen and Konnerup-Madsen, 2000). The Telemark block is now separated from the Kongsberg-Marstrand block to the east and the Bamble-Lillesand block to the southeast by the Kristiansand-Bagn shear zone (Pedersen and Konnerup-Madsen, 2000), and from the Hardangevidda-Rogaland block to the west by the NS trending Mandel Ustaoset lineament, which terminates southwest of southern Setesdal (Bingen et al., 2005). The country rocks are variously a pre- and syn-SNO metamorphic suite, with a series of syn- and post-orogenic igneous complexes. During the SNO, where metamorphism occurred at upper greenschist to mid-amphibolite facies in the period 1060 to 970 Ma, igneous activity dominated, with the majority of granites

emplaced along N-S to NNE-SSW lineaments i.e. orthogonal to the direction of Sveconorwegian collision (Pedersen and Konnerup-Madsen, 2000).

The metamorphic rocks of southern Norway can be broadly divided into two suites; granitic gneisses and banded gneisses. The granitic gneisses are composed of granitic orthogneisses and augen gneisses which have plutonic protoliths. The banded gneisses are variably mafic and felsic, with additional metamorphosed clastic sediments and basaltic tuffs. The gneisses have been dated at approximately 1130 – 1030 Ma by Rb-Sr whole rock and U-Pb zircon dating (Knudsen et al., 1997; Bingen and van Bremen, 1998) which is believed to indicate the onset of SNO metamorphism.

2.2.1 Geology of the Setesdalen metamorphic basement

The geology of the Setesdalen area (which hosts the Bamble-Evje pegmatites) has been summarised by several authors, but perhaps most effectively by Pedersen and Konnerup-Madsen (2000). Their geological map of the Setesdalen region is shown in Fig. 2.2.1, which covers the majority of the field area. Initially, a pre-SNO basement complex was formed, which was overlain by supracrustal (immature clastic) and infracrustal (bi-modal anorogenic igneous) rocks. The Sveconorwegian orogeny caused amphibolite facies metamorphism of these country rocks, with granitoids being emplaced in the closing stages of the orogeny. In Pedersen and Konnerup-Madsen's report (2000), the pegmatites are suggested to have been emplaced during the final stages of the SNO.

As previously mentioned, the metamorphic rocks of southern Norway are typically gneisses, those around the pegmatites of Evje-Iveland pegmatite field being pre-SNO basement. Banded gneisses are common, consisting of alternating bands of amphibolites, granodioritic biotite-hornblende gneisses, K-feldspar-garnet gneisses and cummingtonite-rich gneisses. They have been metamorphosed to upper amphibolite to lower granulite facies, dated using the whole rock Rb-Sr isochron method at 1350±80 Ma (Pedersen, 1981).

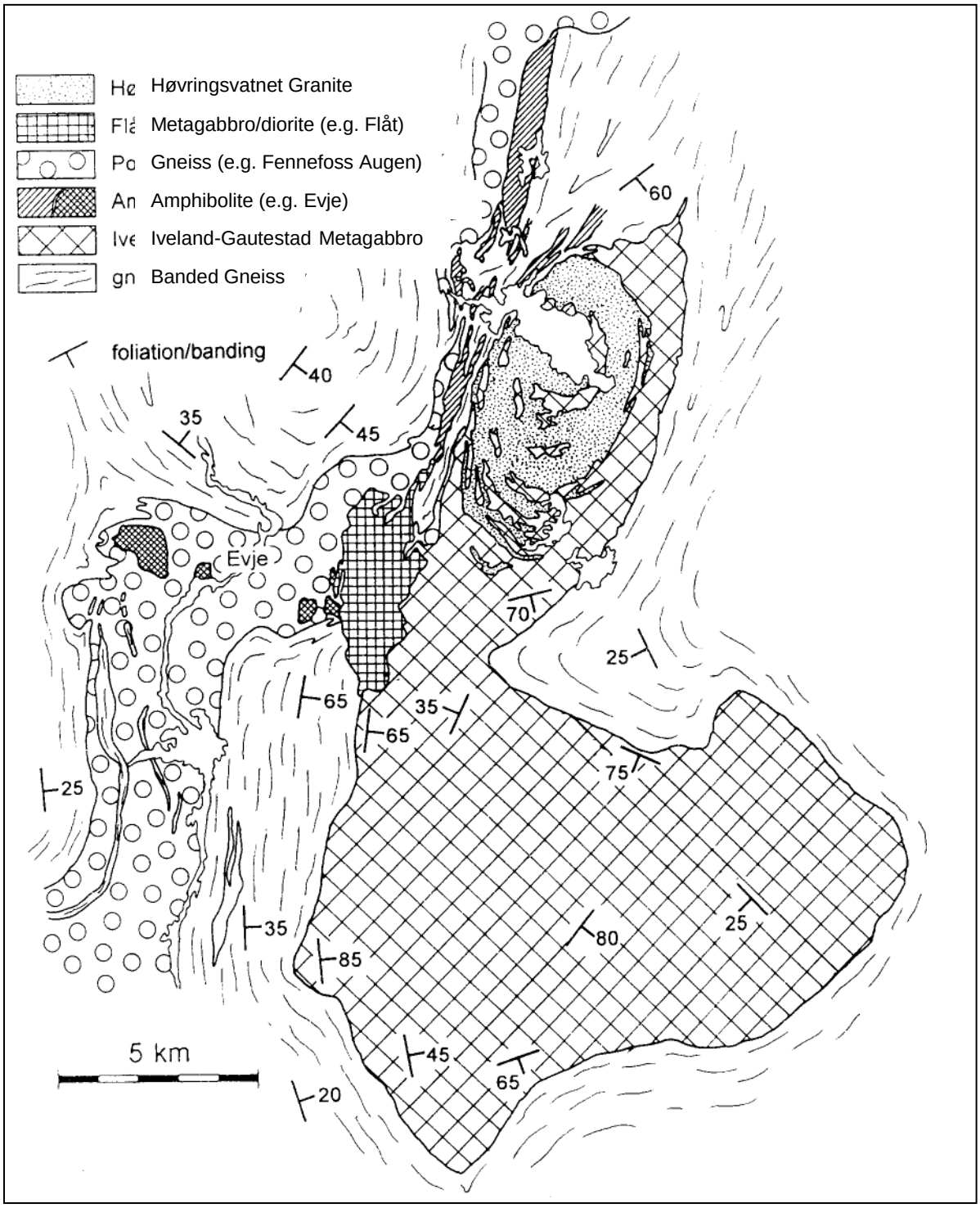

Fig. 2.2.1 Geological map summarising the study area (Pedersen and Konnerup-Madsen, 2000)

The main expression of basic rocks in the Setesdalen metamorphic basement complex covers an area of approximately 160 km^2 and was originally described as a norite (Barth, 1947). However, the unit is more complicated, actually consisting predominantly of the layered Iveland-Gautestad intrusion with subordinate Evje amphibolite and Mykleås ferrodiorites (which is now considered part of the Flåt complex); the latter two units are younger than the

former representing early Sveconorwegian magmatism (Pedersen, 1993; Pedersen and Konnerup-Madsen, 2000).

The Iveland-Gautestad intrusion (after Pedersen and Konnerup-Madsen (2000)) is composed of metamorphosed ultramafic to felsic rocks. The protolith types are gabbronorites (occasionally olivine bearing) grading to diorites and quartz diorites. The intrusion was discordantly emplaced into isoclinally folded mafic mid to upper amphibolite grade banded gneisses. Igneous layering is common, as are relict igneous orthopyroxenes; olivine is more rare. The resulting complex was subsequently metamorphosed to form the Iveland-Gautestad metagabbroic complex (IGMC). Field evidence in Pedersen et al. (2009) suggests that the emplacement of different pulses of magmas were separated by periods of deformation, which implies that the intrusion can be considered as syn-kinematic. In the north of the IGMC are ultramafic units; hornblendite and pyroxene-hornblendite lenses, gabbronorites and layered diorites, all cut by tonalitic/gabbroic dykes, with hornblende pyroxenites and lherzolitic peridotites occurring to the south (Rønholt, 1990). These ultramafics are thought to represent types of peridotitic and pyroxenitic cumulates (Pedersen and Konnerup-Madsen, 2000). Locally, Fe-Ni-Cu sulphide mineralisation occurs as disseminations to blebs and bands (e.g. the ‘ore’ diorite of the Flåt diorite), with textures, minerals and chemical characteristics similar to orthomagmatic segregative mafic/ultramafic deposits which can be found elsewhere in the Bamble area (Brickwood, 1986).

The tectono-magmatic environment has been suggested as that of a destructive plate margin (Pedersen and Konnerup-Madsen, 2000). Coarse grained amphibolites occur as xenoliths in the finer IGMC which occurs east/southeast of Høvringsvatnet granite (Fig. 2.2.1), and are more deformed than their host, containing calc-silicate lenses (i.e. these amphibolites were likely deformed at depth). Compositional trends of the IGMC are typical for low to medium K_2O, tholeiitic to calc-alkaline basaltic rock suites, and provide a continental margin signature. The ultramafic rocks are high in Mg, Ni and Cr, and are low in K, P and Ti, which indicates early stage fractionation of Mg phases (such as olivine and pyroxene). U-Pb dating performed on euhedral unzoned zircons from

coarse grained diorite from the southern part of the IGMC provided an age of 1279±3 Ma, which represents emplacement and cooling of the complex (Pedersen and Konnerup-Madsen, 2000). Multicollector ICP-MS (MC-ICP-MS) data from Pedersen et al. (2009) provided zircon ages of 1285±8 and 1271±11 Ma. Sm/Nd dating failed to constrain an age due to scatter in the data which reflects assimilation of older crustal material by the basic melt. An Rb/Sr whole-rock (coarse grained diorite) isochron for these rocks appear to give an age of 1040 Ma, which could be a subsequent syn-SNO metamorphic event (Pedersen and Konnerup-Madsen, 2000) related to the progressive assembly of Rodinia.

2.2.2 Sveconorwegian magmatism in the Setesdalen region

The Setesdalen experienced two events of potassic/ultrapotassic magmatism (Pedersen and Konnerup-Madsen, 2000) as a result of the onset of the SNO, at approximately 1030 Ma and 970 – 900 Ma. This activity ultimately produced the Setesdalen Igneous Province.

1) Early Magmatism (~1030 Ma) – Pedersen and Konnerup-Madsen (2000) suggest emplacement of diorites (subsequently the Evje amphibolite), large elongate complexes of granodiorites and granites (which were subsequently deformed to form the feldspathic and porphyritic Fenefoss augen gneiss) and highly evolved ferrodiorites (the Flåt diorite (which itself is composed of the Mykleås diorite and the ‘ore’ diorite)). Chemical analyses of these early magmatic rocks indicate that they are calc-alkaline and highly potassic.

The Fennefoss augen gneiss, which represents deformed granodiorites, is a 45 km long body orientated NNW-SSW. Suggested ages are 1031±2 Ma (Pedersen and Konnerup-Madsen, 2000), 1035 Ma (Bingen, 1998) and 1026±26 Ma (Pedersen, 1981). Associated deformed granites have been mapped as the Grimsvatn augen gneiss, but are combined with the augen gneiss for ease. Crenulate to cuspate contacts between the granodiorite protolith and the diorites imply that the emplacement time between the granodiorite and the diorites was short, and the intermingling of magmas at the contact zone indicates that the granodiorites had not yet consolidated upon intrusion of the diorites. The augen gneiss is also seen to cut deformed

conglomerates of the Byglandsfjorden group which, locally, were both deformed at 1000 Ma i.e. syn-SNO (Pedersen et al., 2009).

The Flåt diorite is composed of the Mykleås diorite and the 'ore' diorite. The Mykleås diorite is porphyritic with plagioclase phenocrysts (suggested age 1034±2 Ma (Pedersen and Konnerup-Madsen, 2000)), whereas the 'ore' diorite is of the same composition but more equigranular. This diorite hosts the ore body of the Flåt nickel mine, which ceased operations in 1944 but is still open to the public. The ore is generally heterogeneous, ranging from disseminated to massive sulphide ore, containing pyrite, pyrrhotite, pentlandite and chalcopyrite. NB: What has been described historically as a diorite has, in this study, been identified and referred to as a metagabbro i.e. a crystalline rock composed of plagioclase and mafic minerals (pyroxenes/hornblendes) which has variable development of a metamorphic (amphibolitic/gneissic) fabric.

The Evje amphibolite occurs as xenoliths within the Fennefoss Augen gneiss, typically as black, fine grained dioritic rock, with localised mm veins of hornblende. It is composed of plagioclase, hornblende, various sulphide and oxide phases with lesser garnets and biotites (which probably reflect the assimilation of older gneisses). The IGMC contains less Y, Zr and Nb and more Rb, Sr and Cr than the Evje amphibolite, implying that the amphibolite represents enriched MORB/ocean island amphibolites, and therefore, the subduction of MORB within the continental destructive margin of the IGMC (Pedersen and Konnerup-Madsen, 2000).

2) Late Magmatism (~970 - 900 Ma) – Magmatism at this stage consisted of small plutons, variably with associated dykes, which were bi-modal in nature; granitic with related monzodiorite, monzonite or syenite (i.e. a progression to lower relative silica contents). Four of these plutonic complexes were generated (Pedersen and Konnerup-Madsen, 2000). These are the Høvringsvatnet granitic intrusion, which lies within the field study area, and the Neset, Grendi and Åraksbø intrusions (14, 8 and 34 km from the Høvringsvatnet granite respectively), which cover roughly ellipsoid-shaped areas of up to 35 km^2. Whilst the orientation of these ellipsoid intrusions vary, the complexes overall

are aligned NNW-SSE. Each intrusion displays different characteristics dependant on its evolution, but all contain a monzonite-monzodioritic phase and a granitic (occasionally porphyritic) phase. Field evidence (cuspate and crenulated internal contacts in the smaller bodies) alludes to a co-existence of melts (Pedersen and Konnerup-Madsen, 2000).

The Høvringsvatnet granite forms an approximately elliptical NNE-SSW trending body. It is emplaced in the northern-most part of the IGMC. Well defined cone sheet and bell jar systems indicate that the granite was emplaced at a high crustal level (Anderson, 1936), and, as evidenced from the presence of roof pendants and xenoliths, erosion has been limited to roof level. After Pedersen and Konnerup-Madsen (2000), the principle granites are medium to coarse grained with K-feldspar phenocrysts, which increase in size towards the centre of the intrusion and become absent distally. Within the granite is a lesser component of monzonite which is typically dark to light grey and medium grained, with no preferred mineral orientation. It locally forms hybrids at the granite contact. Fine, aphyric granites occur in the southeast of the intrusion, and locally within the phaneritic material. The granite displays a weak fabric; parallel biotites or flat aggregates of biotite and hornblende, which becomes more developed distally. The cone sheets of the inner system are made up of monzonites, whereas the intermediate and outer systems are individual (locally up to 20) sheets of granite and intermediaries of spotted monzonite (containing biotite $\pm$ amphibole). Marginal sheets of aplite are also present. $^{87}Sr/^{86}Sr$ values from Pedersen, 1981, are always above 0.709 for granitic material and principally above 0.707 for monzonitic material (all samples were above 0.7059), typical of an S-type signature.

The work of Pedersen and Konnerup-Madsen (1994) contains whole rock Rb-Sr isochrons for each of the intrusive complexes. The emplacement of monzonites at Neset occurred at 969±18 Ma. Granitic material and monzonite dykes at Høvringsvatnet have a reported age of 900±53 Ma (which were previously reported by Pedersen (1981) as 945±53 Ma (Rb-Sr whole-rock isochron) and have subsequently been dated at 971+63/-34 Ma (Andersen et al., 2002)). At Grendi, the predominant coarse granites have an age of 973±74 Ma, with a

finer granitic component recorded at 1004±200 Ma; it is suggested that this finer component may represent melts generated during the Sveconorwegian orogeny. Finally, porphyritic granites and monzonites comprising the Åraksbø complex have been dated at 971±16 Ma.

As a final stage to SNO-related activity in the Setesdalen area, the Evje-Iveland pegmatites were emplaced into the IGMC with minor E-W tholeiitic dykes between 900 – 800 Ma and ~620 Ma respectively, during a tensional stage, possibly reflecting one or more attempts at continental break up. Bjørlykke (1937) suggested that residual Høvringsvatnet magma remained liquid due to a high country rock temperature and was emplaced by orogenic pressures throughout the country rock, forming the discrete pegmatite bodies. Alternatively, basic melts may have generated higher hear flows, causing partial melting within the crust to produce REE rich pegmatite melts (Pedersen and Konnerup-Madsen, 2000).

2.2.3 The Evje-Iveland pegmatites

The pegmatite field (Fig. 2.2.2) contains around 350 major pegmatite bodies (since 1884 approximately 260 have been mined for high purity ceramic K-feldspar) which were emplaced within basement banded gneisses (Pedersen and Konnerup-Madsen (2000) provide a detailed description of the IGMC). Eight pegmatites were chosen for this study on the basis of geographical distribution (Fig. 2.2.2), mineralogical diversity, completeness of exposure and ease of sampling. These were (with decreasing northing) Landsverk 1, Kåbuland, Li Gruva, Slobrekka, Hovåsen, Solås, Iveland and Steli. The pegmatites are granitic in composition, and are classified as rare-element pegmatites (Pedersen and Konenrup-Madsen, 2000) of the NYF (Niobium-Yttrium-Fluorine) family (Černý and Ercit, 2005) with variable contents of a range of rare metal and REE minerals.

Their mixed REE type (Černý and Ercit, 2005; see *Chapter 2.3.2*) may suggest an origin by partial melting of lower crustal lithologies; one of the targets of this investigation is to investigate their source. It has been suggested that the pegmatites are related to the Høvringsvatnet granites (Bjørlykke, 1937; Larsen

et al., 2000) and that they mark the terminal stages of late/post Sveconorwegian activity in the region. However, the work of Pedersen and Konnerup-Madsen (2000) synthesise a variety of ages for the pegmatites between 845±12 Ma and ~800 Ma, suggesting the pegmatites are too young for this to be true. In addition, another age for the Evje-Iveland pegmatites is 910.5±1.6 Ma, which is based on U-Pb isotope ratios of five pieces of gadolinite (Scherer et al., 2001); the exact origin of the dated gadolinite crystals is not known.

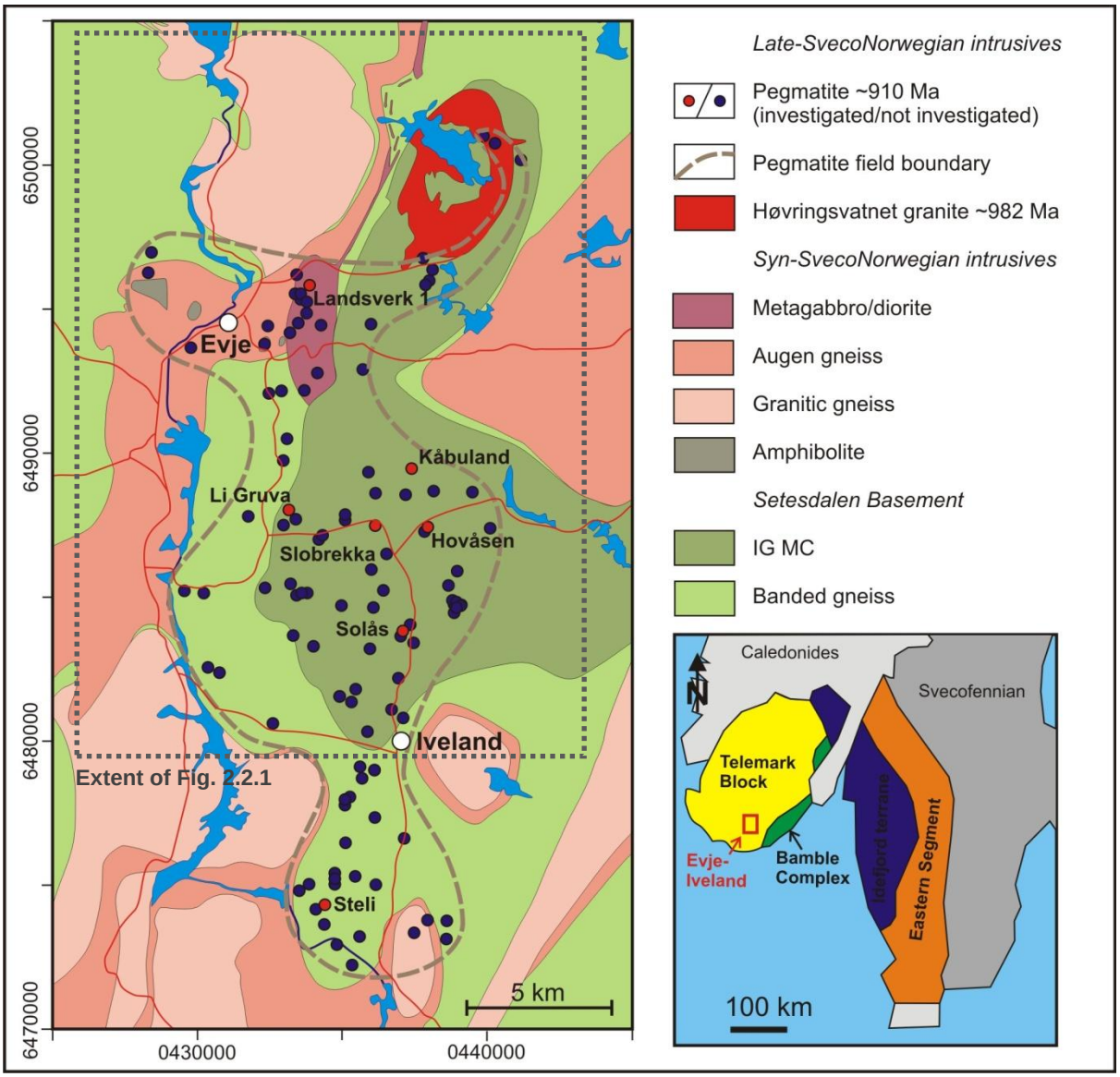

Fig. 2.2.2 Geological map of the study area, with investigated pegmatites shown as red dots (after Pedersen, 1981; Pedersen and Konnerup-Madsen, 2000; Pedersen et al., 2009. Inset map of southern Norway and Sweden from Bingen et al., 2008b)

Classically, pegmatites are thought to represent highly evolved end members of an originally granitic melt (as summarised by London, 2008). Previous

interpretations of the Evje-Iveland pegmatites have echoed this, the pegmatites having been described as late stage fractionation products of melt vestiges from the Høvringsvatnet granite complex (e.g. Bjørlykke, 1937), which has been supported by later authors (e.g. Pedersen and Konnerup-Madsen, 1994). This interpretation was clearly underpinned by the close spatial link between the pegmatites and the Høvringsvatnet granites (Fig. 2.2.2).

Other geological summaries of the area appear to accept the genetic link between the granites and the pegmatites, mainly as they do not offer alternative explanations (e.g. Larsen et al., 2000). Some literature implies that the pegmatites are not linked to the Høvringsvatnet granites however, but still fail to provide an alternative. For example, Larsen (2002) demonstrates an evolutionary trend in Sr/Rb, Ba/Rb and K/Rb values in K-feldspar moving progressively SSE from the granites (with the Gjerstad suite augen gneiss/Agder basement complex contact acting as a possible conduit), whilst stating that it is unlikely that the Evje-Iveland pegmatites and the Bamble pegmatites are genetically related. This north to south control was suggested by Larsen et al. (2000), who demonstrated that the degree of fractionation and quantity of trace elements in quartz increased towards the south. Conflictingly, preliminary work by Müller and Ihlen (2011) indicates that quartz chemistry is extremely varied, and shows little consistency either within pegmatites or throughout the field.

2.2.4 Geological summary for the Setesdalen region

The geological evolution of the Setesdalen area during the SNO can be summarised chronologically as follows (after Pedersen and Konnerup-Madsen, 2000 unless otherwise referenced):

Formation of a pre-Sveconorwegian basement – heterogeneous gneisses were intruded by calc-alkaline granitoids (1350 – 1300 Ma) and by what was to become the IGMC (1279 Ma). Geochemistry (their calc-alkaline nature and trends in Hf isotope data) suggests the event involved the growth of juvenile crust in a continental margin setting (Pedersen et al., 2009), with possible subduction followed by magmatism and regional pre-Sveconorwegian upper

amphibolite facies metamorphism. Granitic magmas from Setesdal with mafic coeval counterparts (approximately 1265 Ma) do not share a Hf ratio, which implies that the mafic magmatic event probably didn't contribute to crustal development in the region (Pedersen et al., 2009). A change in the Hf isotopic composition occurred at 1220 – 1210 Ma due to input of additional juvenile material from a depleted mantle source, likely a result of the intrusion of significant volumes of mantle derived mafic melts into the lower crust. Granitic and granodioritic gneisses which crystallised at a similar time in central Telemark show a similar Hf isotope signature which suggest this underplating event had a regional impact (Pedersen et al., 2009).

Uplift, erosion and peneplanisation under anorogenic conditions – rifting induced bi-modal volcanism, which was followed by clastic sediment deposition (the Byglandsfjorden group). Infracrustal granites provide an age of 1150 – 1100 Ma for this. Minor diorites (the protolith for the Evje Amphibolite) and gabbros may also have been emplaced at this stage.

Granitoid emplacement, regional deformation and metamorphism – the Fennefoss augen gneiss (1031 Ma), metamorphic resetting of the IGMC (Rb-Sr age of 1040 Ma) and ages from sites further west in Norway indicate an age of 1060 – 1040 Ma for the onset of the Sveconorwegian orogeny. Associated metamorphism was in the amphibolite facies, possibly with associated syn-orogenic calc-alkaline granites and ferrodiorites.

Ending of the Sveconorwegian orogeny – this was marked by the emplacement of K-rich bimodal granites and monzonite complexes (which display a within plate signature) in Setesdalen, with an age of intrusion of 980 – 975 Ma. Their largely undeformed nature and high crustal position define an intermittent stage of post-Sveconorwegian uplift and peneplanisation.

Late/post-Sveconorwegian activity – the emplacement of the Evje-Iveland pegmatites and minor E-W tholeiitic dykes occurred between ~900 – 800 Ma and ~620 Ma respectively, and represent a tensional stage, possibly reflecting one or more attempts at continental break up. Basic melts may have generated

higher hear flows, which could have induced crustally derived REE rich pegmatite melts.

2.3 An introduction to pegmatites

2.3.1 Pegmatite definition

From a very comprehensive review of pegmatites, London (2008) states that texture plays as important a part in defining a body of rock a pegmatite as crystal size and composition, and recommends the following definition:

"*An essentially igneous rock, commonly of granitic composition, that is distinguished from other igneous rocks by its extremely coarse but variable grain-size* [Fig. 2.3.1]*, or by an abundance of crystals with skeletal, graphic* [Fig. 2.3.2]*, or other strongly directional growth-habits* [Fig. 2.3.3]. *Pegmatites occur as sharply bounded homogenous to zoned bodies within igneous or metamorphic host-rocks* [Fig. 2.3.4]."

Fig. 2.3.1 Coarse grain size; K-feldspar megacrysts in massive quartz. Slobrekka pegmatite

Fig. 2.3.2 Graphic quartz; skeletal quartz intergrowths in K-feldspar. Solås pegmatite

Fig. 2.3.3 Zoning; Massive K-feldspar outer core (top), with intermediate zone of quartz/plagioclase with garnet crystallisation horizons (line rock). Crystallisation propagation appears to be downwards. Li Gruva pegmatite

Fig. 2.3.4 Pegmatite (white, excavated core zone) sharply contacting the host Iveland-Gautestad metagabbroic complex (grey). Kåbuland pegmatite

This definition will be generally accepted throughout this investigation. Additionally, London (2014) states that the internal and generally concentric mineralogical and grain size zonation typically demonstrated by pegmatites is conspicuous and distinctive; this has been recognised since 1949 by Cameron et al., who developed the nomenclature (moving from the margin to the centre of the body) utilised today; the border zone, the wall zone, the intermediate zones and the core.

The border zone is a fine grained (approximately 2 – 5 mm) granitic facies, up to a few cm thick which wholly surrounds the pegmatite body.

The wall zone is a thicker (up to 1 m) and coarser grained variant of the border zone, displaying 1 – 2 cm crystals of feldspar, quartz and biotite. Anisotropic orientation of crystal growth typically develops in the wall zone.

Intermediate zones are characterised by an increase in crystal size (up to several metres) and a dominance of a single crystal phase, typically K-feldspar

(variably intergrown with skeletal quartz), microcline, plagioclase and spodumene (London, 2008). Intermediate zones are typically concentric in the thickest parts of the body, but may pinch out laterally as the pegmatite thins in lenticular bodies. Where present, preferential crystal orientation is continued in this component, and may define a succession of intermediate zones.

The core represents a typically homogenous, continuous and monomineralic mass at the approximate centre of the pegmatite. Cores of quartz are common, but pegmatites may also display various proportions of perthite and albite (London, 2008).

An extensive synthesis of zonation in pegmatites by London (2014) defines the controlling fundamentals of internal evolution as the bulk composition of pegmatite melt, the magnitude of liquidus undercooling prior to pegmatite crystallisation, isothermal fractionation, constitutional zone refining (the formation of a migratory boundary layer liquid relatively rich in fluxes) and far field chemical diffusion. The phenomenon of pegmatite zonation is closely linked with their formation mechanism, and as such will be discussed further in *Chapter 2.3.2*.

2.3.2 Pegmatite genesis

Despite focussed investigations into pegmatite formation since 1949 (Cameron et al.), the numerous summary reviews published to this day (London, 2005b; Simmons, 2007; London, 2009; Thomas et al., 2012; London and Morgan, 2012; London, 2014) suggest that the processes responsible for pegmatite genesis are still not fully understood. Pegmatites are acknowledged to generally form by a process of fractional crystallisation of a granitic melt (e.g. London, 2008; Thomas et al. 2012), but it has been suggested that low-degree partial melts produced around plutons in orogenic environments could form pegmatite melts by anatexis (e.g. Boos, 1954; Stewart, 1978; Simmons, 2007; Simmons et al., 1995, 1996; Martin and De Vito, 2005).

Generally considered to have provided the foundation for pegmatite genetic studies, Jahns and Burnham (1969) produced the model for pegmatite genesis

most widely accepted in the 70s and 80s. The model suggested that pegmatites form by equilibrium crystallisation of undercooled granitic melts and hydrous fluids at or below the hydrous granite liquidus, and that pegmatites owe their distinctive zonal and textural characteristics to the buoyant separation of aqueous vapour from silicate melts, producing K-rich upper portions and Na-rich lower zones of individual pegmatites. Previous work by Jahns and Tuttle (1963) had apparently supported this.

However, later work by London (2005a) suggested water saturation is not required in early pegmatite crystallisation; B, F, P and Li are critical in lowering crystallisation temperature, decreasing nucleation rates, decreasing melt polymerisation, decreasing viscosity, increasing diffusion rates and increasing solubility. Essentially, fluxes serve to minimise nuclei formation whilst maximising diffusion, producing fewer, larger crystals. Additionally, experimental work (Webber et al., 1999; Morgan and London, 1999) indicates that proposed cooling rates for pegmatite forming melts are much more rapid than conventional petrology would suggest and that they should cool quicker than crystallisation can follow, varying from days/months to decades/centuries, evidenced by ubiquitous textural evidence of rapid crystal growth rates, skeletal/graphic quartz, growth towards the core and comb structure tourmaline.

The distinctive zonal and textural pegmatite features previously identified have been replicated in experiments that employ Constitutional Zone Refinement (CZR) of melts that are undercooled pre-crystallisation (London, 2008 and 2009); this has become a widely accepted possible formation mechanism (e.g. Thomas et al., 2012; London, 2014). The method requires disequilibrium crystallisation from a flux bearing (but not necessarily rich) granitic melt that is undercooled by 100 – 300°C. A lag time between cooling and initiation of crystallisation initiation produces a supersaturated melt, so that when nucleation and crystallisation commence, fluxes accumulate in a boundary layer ahead of the crystallisation front. The solidus of the boundary layer is lowered by the fluxes, and the front becomes progressively enriched in incompatible phases as crystallisation continues (London, 2009 and 2014); back-diffusion of fluxes is excluded due to high viscosity and the rate of crystal growth. Melt boundary

layers formed by this process would represent the last silicate liquids to crystallise in pegmatites, which apparently explains the tendency in pegmatites for abrupt transitions from simple to evolved mineral and rock compositions. This doesn't correlate closely with the core zone described previously nor the Evje-Iveland pegmatites (see **CHAPTER 4** for further description), which routinely contain REE minerals in intermediate zones, with the presumably final core zone comprised of massive quartz rather than a flux rich hydrothermal assemblage; the core is not representative of an incompatible element enriched melt and is typically massive. In the final stages of crystallisation an aqueous vapour phase may evolve, producing miarolitic cavities and evolved suites of pegmatite minerals (London, 2005b).

Pegmatites typically display line rocks or unidirectional solidification textures (USTs) which occur mainly in the footwall and are aplitic portions which display pronounced mineralogical layering characterised by fine grained garnet/tourmaline and albite/quartz masses in alternating bands (Simmons, 2007). The classically accepted model for formation was that of Jahns and Tuttle (1963), where periodic loss of water vapour acted as a mechanism for quenching by relief of pressure. Layering through significant undercooling has also been proposed (London, 2005a) and diffusion-controlled oscillatory nucleation and crystallisation from a strongly and rapidly undercooled melt was interpreted to form line rocks in pegmatite-aplite dikes by Webber et al. (1997) as a result of triggers e.g. thermal, chemical or pressure quenching. This texture is discussed further in *Chapter 4.1.5*.

Perhaps the most all-encompassing review of potential pegmatite formation mechanisms is that compiled by Thomas et al. (2012). Their suggestions for competing models for the internal evolution of granitic pegmatites include:

1) Precipitation from an aqueous fluid phase
2) Crystallisation of silicate liquid through an aqueous fluid interface
3) Crystallisation from a hydrous silicate gel
4) Crystallisation from a flux rich silicate liquid
5) Crystallisation of a granitic melt from margins to centre with CZR

1) Precipitation from an aqueous fluid phase (occurring in a manner similar to hydrothermal veins) has been criticised (e.g. London, 2011) as aqueous fluids lack the solute transport capacity necessary to crystallise large bodies of pegmatite and because of the lack of hydrothermal alteration assemblages in the majority of pegmatites.

2) Crystallisation of silicate liquid through an aqueous fluid interface (after Landes (1933) requires a concentration of water and other constituent elements into residual magma within a granitic intrusion, with post-pegmatite crystallisation followed by later mineralisation by hydrothermal fluids. The mechanism again lacks the solute transport capacity, and produces crystallisation rates of thousands of years, which have been deemed too slow (Webber et al., 1999; Thomas et al., 2012).

3) Crystallisation of quartz pegmatites from a silicate gel has been proposed (e.g. Thomas and Davidson, 2012a) as a potential mechanism; the gel medium allowing diffusion of only the aqueous species (through suppression of convection/advection), reducing the opportunity for nucleation (which favours the growth of larger crystals) and accounting for massive quartz cores (which implies the transport of huge quantities of silica) (Thomas et al., 2012). As silica gel inclusions become increasingly common towards the quartz cores of the pegmatites, they are considered to demonstrate increasing water and alkali carbonate concentrations in the melt (Thomas and Davison, 2012a), and as such the gel hypothesis (at least as a late stage process) is not considered unreasonable (Thomas et al., 2012).

4) Crystallisation of pegmatites from flux-rich silicate melts (which contain a high, but undefined, H_2O concentration) has been the most widely adopted mechanism for pegmatite formation since Jahns and Burnham (1969) published their classic model. Concentrations of melt inclusions (construed to be trapped melts; Thomas and Davidson, 2012b) suggest H_2O contents as high as 10% and 20% (g/g), which, in combination with fluxes (OH^-, CO_2, HCO_3^-, CO_3^{2-}, SO_4^{2-}, PO_4^{3-}, H_3BO_3, F, Cl, Li, Na, K, Rb, Cs, Be, and B (Thomas and Davison, 2012b; Thomas et al., 2012)), would require little undercooling of the melt. As

with CZR, fluxes serve to reduce melt viscosity, and aid in producing large crystals by increasing element diffusion and crystal growth rates whilst limiting nucleation opportunities. Thomas et al. (2012) suggest that the anisotropy in pegmatitic textures may arise from this rapid crystallisation; viscosities are so low that suspended crystals cannot form within the melt, so must crystallise from the margins. Conflictingly, London (2014) demonstrates pegmatite crystallisation temperatures of 450°C (with up to 250°C of undercooling) which causes pegmatite viscosities, as a whole, to be extremely high. The viscosity of hydrous granite at 700°C is likened to asphalt (105 Pa·s), and at 450°C to pitch (108 Pa·s), implying that neither crystal settling nor convection can be legitimate mass transfer mechanisms (London, 2014). Instead, it is proposed that the development of a flux rich boundary layer ahead of the crystallisation front generates the conditions necessary for pegmatite crystallisation.

5) Crystallisation of a granitic melt from the margins to centre was first described by Cameron et al. (1949), and has been accepted in most models (Thomas et al., 2012). Within this framework London (2008, 2009) combined undercooling with flux concentration via CZR to compensate for high viscosities and to account for macro-crystallisation and the occurrence of zonation. The model depends on the pegmatite melt matching that of a H_2O undersaturated haplogranite (Ab-Or-Qtz) minimum; in contrast Thomas and Davidson (2012b) demonstrate water saturation. Conflicting opinions arise with viscosity as mentioned previously, with Thomas et al. (2012) believing that freely-diffusing mineral constituents (in a non-supportive low-viscosity melt) are necessary not only for progressive inward crystallisation, but for the transport of pegmatite melts away from their source. Additionally they state that, despite the boundary layer, residual melt would act instead as a “compositional buffer”, limiting compositional evolution.

In their summary, Thomas et al. (2012) suggest that in fact pegmatites are unlikely to form by a single method, and recommend that a “complex interplay” of model components are ultimately responsible for the formation of pegmatites and their textures.

2.4 Pegmatite classification

Modern pegmatite classification schemes are strongly influenced by the depth-zone classification of granitic rocks published by Buddington (1959), and the Ginsburg et al. (1979) classification which categorized pegmatites according to their depth of emplacement and relationship to metamorphism and granitic plutons. Černý's (1991b) revision of that classification scheme is essentially the most widely used classification of pegmatites today. His classification is a combination of depth of emplacement, metamorphic grade and minor element content. His 1991 classification has 4 main categories or classes. These are Abyssal (high grade, high to low pressure), Muscovite (high pressure, lower temperature), Rare-Element (low temperature and pressure), and Miarolitic (shallow level). The Rare-Element Classes are subdivided based on composition into LCT and NYF types. The NYF group displays a progressive accumulation and enrichment of Nb, Y and F (with additional Be, REEs, Sc, Ti, Zr, Th and U), fractionated from subaluminous to metaluminous A- and I-type granites generated from a variety of processes involving depleted crust or mantle contributions. The peraluminous LCT group is characterised by Li, Cs and Ta (with Rb, Be, Sn, B, P and F) predominantly derived from S-type granites (with a limited I-type contribution). Mixed NYF and LCT groups may exist, such as those generated by contamination of NYF plutons by digestion of undepleted supracrustal rocks.

In 2005, Černý and Ercit provided a refinement of the 1991-classification, where they propose five classes of granitic pegmatite: *abyssal* (AB), *muscovite* (MS), *muscovite – rare-element* (MSREL), *rare-element* (REL) and *miarolitic* (MI) (summarised in Table 2.3.1). The classes (with the exception of the MS type) are further divided into subclasses according to their mineralogical and geochemical characteristics. Further subdivision of the REL and MI subclasses into types and subtypes is defined by differences in geochemical signatures or P-T conditions of solidification (as suggested by variable suites of accessory minerals) in which the rare-element class is further subdivided into types and subtypes. The system does not include peralkaline lithologies, and also excludes contaminated or hybridized (such as by reaction with country rocks) pegmatites. This scheme has been used in most modern pegmatite studies.

Table. 2.4.1 The class system of geological, paragenetic and geochemical classification of granitic pegmatites, with comparative petrogenetic families (Černý and Ercit, 2005; Černý et al., 2012)

CLASS	**Subclass**	Type	*Subtype*	Family
ABYSSAL (AB)	AB-HREE			NYF
	AB-LREE			
	AB-U			NYF
	AB-BBe			LCT
MUSCOVITE (MS)				
MUSCOVITE – RARE ELEMENT (MSREL)	MSREL-REE			NYF
	MSREL-Li			LCT
RARE-ELEMENT (REL)	REL-REE	allanite-monazite		
		euxenite		NYF
		gadolinite		
	REL-Li	beryl	beryl-columbite	
			beryl-columbite-phosphate	
		complex	spodumene	
			petalite	
			lepidolite	LCT
			elbaite	
			amblygonite	
		albite-spodumene		
		albite		
MIAROLITIC (MI)	MI-REE	topaz-beryl		NYF
		gadolinite-fergusonite		
	MI-Li	beryl-topaz		
		MI-spodumene		LCT
		MI-petalite		
		MI-lepidolite		

Increasing P-T

In addition to the CLASS-**subclass**-*type*-subtype hierarchy (which, in spite of the requirement for extensive knowledge of formation environment, is referred to as descriptive), Černý and Ercit (2005) propose an apparently more genetic scheme: petrogenetic families. They propose two end members of a continuum: Niobium-Yttrium-Fluorine (NYF) and Lithium-Cesium-Tantalum (LCT). These acronyms stand for the rare elements most conspicuously concentrated in the pegmatite mineralogy; in NYF, for example, these may include columbite (Nb), fergusonite (Nb, Y), gadolinite (Y, Nd), polycrase Y, Nb), thortveitite (Y), xenotime (Y), allanite (Y), fluourite (F) and topaz (F). It is becoming apparent

that the classification of pegmatites as either NYF or LCT types is favourable over the original class system (e.g. Černý et al., 2012).

2.4.1 Geological classes

The classes of pegmatite (AB, MS, MSREL, REL and MI; Černý and Ercit (2005)) are initially defined on the basis of pressure (and temperature) conditions that characterise their host rock suites; these do not however necessarily represent the consolidations of the syn- to post-kinematic pegmatites (and granites) themselves. The P-T conditions recorded represent a regional maximum as they characterise peak metamorphism which usually predates pegmatite intrusion. The temporal difference between peak metamorphism and intrusion is greatest in AB pegmatites and minimal (if not absent) in MS. Individual classes may be subdivided on the basis of geochemical signature, and these subclasses may be further divided (by differences in mineral assemblages, geochemical signature or conditions of consolidation) into pegmatite types and subtypes (Černý and Ercit, 2005). Essentially, pegmatite classes are defined by geological criteria, with additional division allowing the incorporation of geochemical features, mineral assemblages and textures (which reflect P-T conditions of pegmatite intrusion), which “serves to place a given pegmatite into a gross geological context, and into a descriptive geochemical-paragenetic category”.

Abyssal (AB) class

These pegmatites are hosted within the majority of the P-T range of the granulite (and upper-amphibolite) facies, excluding extremely high pressures. The class also included pegmatites of intermediate depth but dehydrated high-temperature host terranes. Abyssal pegmatites typically represent products of partial melting and/or metamorphic re-equilibration and typically conform to the metamorphic fabric of the host when emplacement was synkinematic. Migmatitic leucosomes are common, whereas voluminous masses (e.g. anatectically derived granites with interior and distal pegmatite zones) are rarer. Even less abundant are abyssal pegmatites with a granitic source (after Bushev and Koplus, 1980); magmatic differentiation and fractionation are virtually absent in abyssal pegmatite populations. Mineralisation is rarely economic, and

is limited to High Field Strength Elements (HFSEs; U, Th, Y, REEs, Nb, Zr). Host rocks may be subject to multiple episodes of metamorphism, and pegmatite generation may not be coincide with peak P-T conditions; indeed, pegmatites are commonly related to relatively late processes connected with thermally-consistent melting during uplift.

Four subclasses are defined for the abyssal pegmatites, predominantly on the basis of geochemical abundances and the resulting mineralogical relationships of U and Th to Y, LREEs, HREEs and Nb:

- AB-HREE: Pegmatites with relatively abundant Nb, causing most U and Th to be concentrated as substitute elements in Y-REE-Nb oxide minerals (euxenite, samarskite, fergusonite and pyrochlore).
- AB-LREE: Pegmatites with relatively diminished Nb and HREEs, and abundant LREEs; most U and Th is present as substitute elements between silicate and phosphate phases (allanite and monazite).
- AB-U: Pegmatites with insignificant Nb, Y and REEs, causing the majority of U and Th to exist as uraninite and thorite respectively (i.e. structurally key elements in species of their own).
- AB-BBe: Pegmatites enriched in B and Be, predominantly peraluminous in nature, characterised by high pressure species and developed mainly in complex environments during multi-stage events (after Grew et al., 2000). The extent of departure from truly granitic compositions is not currently defined.

Muscovite (MS) class

These pegmatites are typically conformable with host rocks of high pressure amphibolite facies, displaying a kyanite-sillimanite metamorphic progression, and are a product of either partial melting or a “very restricted extent of differentiation of anchi-autochtonous palingenetic granites” (Černý and Ercit, 2005). Field evidence (enclaves of unaltered metamorphic assemblages) and a lack of fractionation are proposed as evidence that the conditions of magma generation, intrusion and pegmatite formation were extremely similar to those of their kyanite-sillimanite host rocks. The pegmatites are usually devoid of exotic

mineral assemblages, but instead contain ceramic-grade feldspar, quartz and industrial mica (the source of the original name, which is retained for lack of better terminology). Further subdivision is unnecessary due to the simple silicate mineralogy and lack of mineralisation in most examples (Černý and Ercit, 2005).

Muscovite – Rare-element (MSREL) class

This category contains pegmatites historically placed between the MS or REL classes; it is perceived that a distinct class is now justified, with two broad but mutually distinctive subclasses (Černý and Ercit, 2005). Pegmatites of the MSREL class are hosted in a metamorphic environment intermediate to that of the MS and REL classes. Typically, unlike MS pegmatites, they are discordant to the metamorphic foliation of their host rock (and in some examples display regional zonation with respect to source granites). MSREL pegmatites contain both high quality economically viable muscovite and concentrations of rare element minerals (beryl, cassiterite, columbite-group, REE-Nb-U oxides, and Li silicates) that may be close to economic (Černý and Ercit, 2005).

Rare-element (REL) class

Historically, this class has been subject to most investigation. It includes pegmatites differentiated from granitic plutons, primarily emplaced at intermediate/shallow depths that display an economic concentration of rare element oxides and silicates in more fractionated zones. Two subclasses have been suggested by Černý and Ercit (2005); REL-REE and REL-Li.

REL-REE pegmatites are sourced from post- to anorogenic metaluminous to peraluminous granites at variable crustal depths in primarily extensional settings. REL-Li pegmatites represent those emplaced on low pressure upper greenschist to amphibolite-facies host rocks, fractionated mostly from syn- to late-orogenic peraluminous granites in predominantly compressional regimes. The REL-REE subclass is typified by characteristic HFSEs, and is divided into three types; *allanite-monazite* (with a significant proportion of LREEs), *euxenite* (significant Y, a variable HREE/LREE ratio and negligible Be) and *gadolinite*

(significant HREEs, Y and Be). All types are P, B and S depleted, with a limited presence of Li, Rb and Ce (Černý, 1991a).

REL-Li pegmatites are considered the most diverse subclass in the proposed system; rare alkalis, Be, Sn, Ta, B, P and F are accumulated by progressive fraction, reflecting a range of solidification conditions. The proposed types are *beryl*, *complex*, *albite-spodumene* and *albite*; these are further divided into subtypes.

The *beryl* type is typically manifested as the *beryl-columbite* subtype. Be and Nb-Ta vary in their exact abundances, but are typically present in high concentrations. *Beryl-columbite-phosphate* pegmatites are less common than the *beryl-columbite* subtype, but are still frequent. Proportions of beryl, columbite group and phosphate minerals are variable, with the anionic and transition metal composition of the source melt potentially producing microlite and wyllieites (Černý and Ercit, 2005).

Complex type pegmatites are characterised by significant proportions of Li aluminosilicates, and a highly developed internal structure. The subtypes of this class are defined by their Li aluminosilicate mineral assemblages, which are dictated by parental bulk composition and P-T conditions. The most common of the *complex* pegmatites is the *spodumene* subtype, which is thought to form at 3 to 4 kbar. The *petalite* subtype form at lower pressures (1.5 to 3 kbar) but higher temperatures. The general paragenetic and geochemical characteristics of these two subtypes are very similar. Less common are *lepidolite* pegmatites, which display increased Mn over Fe, significant amounts of microlite minerals and relatively abundant tourmaline. *Elbaite* pegmatites, apparently transitional from the *lepidolite* subtype, are less common again, containing (in addition to elbaite) boron minerals and miarolitic cavities. The *amblygonite* subtype contains pegmatites with amblygonite-montebrasite minerals and may be more widely spread than currently thought, due to non-indentification of amblygonite in the field (Černý and Ercit, 2005).

Albite-spodumene pegmatites are a product of high pressure conditions and display an unusual bulk composition consisting of predominantly albite and quartz, minor K-feldspar and the highest concentrations of Li in any pegmatite. Zoning in *albite-spodumene* pegmatites is essentially absent, but phenocrysts of spodumene and K-feldspar may display inward growth textures. *Albite* pegmatites are the least common of the REL-Li subclass. These have with albite dominant over quartz which is dominant over K-feldspar, spodumene or lepidolite, and variable zoning (Černý and Ercit, 2005).

Miarolitic (MI) class

The pegmatites of this class are characterised by an abundance of cavities, formed from a gas phase exsolved from the pegmatite melts. The miaroles indicate the pegmatites form at shallower depths, due to a lower constraining pressure. Two subclasses are proposed, based on differing mechanisms of gas exsolution. In MI-REE pegmatites, volatiles are released due to a reduction in pressure, whereas in MI-Li pegmatites gas is exsolved by a combined chemical and pressure quench (Černý and Ercit, 2005). With suitable pathways however, expelled volatiles may escape from the pegmatite melts, reducing the volume or indeed number of cavities produced. Suggestions conflicting with the perceived shallow emplacement depths of these pegmatites (based on equilibrium relationships in Li rich systems) have been disproved due to confirmation regarding the “disequilibrium course of crystallisation of Li-rich pegmatites” and “consolidation from a supercooled melt some 200°C below the liquidus surface” (London, 2005a) which shift crystallisation conditions into the stability field of spodumene. In light of this, Černý and Ercit (2005) suggest MI-REE and Mi-Li of pegmatite crystallise in near-identical conditions, but completely fail to account for the differing Li phases (e.g. lepidolite, petalite) present in MI-Li pegmatites. MI-REE pegmatites are associated with anorogenic granites intruded at shallow depths. The subclass is split into two types on paragenetic and geochemical criteria, but many examples of intermediate types exist. *Topaz-beryl* pegmatites can exist purely displaying the nomenclature minerals, but most occurrences contain an accessory suite of Li micas (zinnwaldite), fluorite, Nb, Ta and Ti minerals and REE phosphates. The *gadolinite-fergusonite* type represents an extreme equivalent of the *topaz-beryl* type, defined by a concentration of REE

and Nb>Ta minerals with lesser accessory phases (Ti oxides, Sc silicates, zircon, aeschynite and ferrocolumbite).

The MI-Li subclass is related to similar granites that produce REL-Li pegmatites, and may develop as a result of local gradation. Additionally, vapour exsolution is promoted by the greatly reduced solubility of H_2O in the source melt as a result of stabilisation of B and Li silicates. Tourmalines are present (occasionally exclusively) as B is the main component responsible for the chemical quench. The basis of subdivision of this subclass is predominantly the principal Li-aluminosilicate within the pegmatite bodies. However, it is admitted that a majority phase is difficult to identify, and sometimes not present. Additionally, fluid pressure and degree of undercooling play an important role in defining mineral assemblages. Assemblages between individual pockets may not be in equilibrium, producing a series of related pegmatites which cannot be concisely reconciled to a specific type.

Beryl-topaz pegmatites are renowned gem-producers, and typically occur as dykes within more diverse pegmatites. *MI-spodumene* types may, confusingly, be either spodumene deficient or enriched. *MI-petalite* pegmatites are so called as petalite is their principal Li aluminosilicate, despite being present in low quantities. *MI-lepidolite* types however are enriched in the nomenclature mineral, with the *Mi-spodumene* and *MI-petalite* pegmatites grading into it.

2.4.2 Petrogenetic families

The classification of pegmatites into families is based upon the provenance of granitic pegmatites which have been derived by ‘igneous differentiation from diverse plutonic sources’. The ‘families’ classification scheme encompasses a wide variety of pegmatite groups, from individual granites/pegmatites to fields of related suites. As mentioned, the families are defined as either NYF or LCT, based on the REEs most concentrated during fractionation, as well as general enrichment trends. Černý and Ercit (2005) emphasise that enrichment in the three typical elements will not be equal in magnitude or occurrence within pegmatite populations, and as such it is recommended that this scheme is currently kept as general as possible, with further subdivision into specific

categories with well-defined sequences of crustal environment-protolith-process-granite-pegmatite generation as documentation and understanding develops.

Additionally, the elements characteristic of each group are not mutually exclusive. Early, less fractionated LCT pegmatites may contain minerals indicative of NYF pegmatites (e.g. REE phosphates, allanite, euxentite) and extensively evolved NYF pegmatites may contain Li minerals distinctive of the LCT family. However, this atypical mineralisation is usually minimal. Pegmatite populations with a combined signature are assigned to a mixed NYF+LCT family (Černý and Ercit, 2005), and the majority of cases can be rationalised as the contamination of NYF granites by LCT melts. As this combination of families is based upon the presence of “significant quantities of both suites of typical minerals” with no effort made to define ‘significant’, it appears that the majority of pegmatites can qualify as mixed type.

NYF pegmatites

These pegmatites are characterised by an elemental suite of Nb>Ta, Ti, Y, Sc, REE, Zr, U, Th and F (as fluorite or topaz) (Černý and Ercit, 2005). Associated granites show considerable textural and geochemical variation (homogenous to differentiated), but are typically subaluminous to metaluminous A- to I- types (with limited peraluminous/peralkaline examples), with moderate fractionation histories (Ercit, 2005). LREEs are typically enriched to 100 – 800 times chondritic (but may show depletion), whereas HREEs are commonly apparent. Radiogenic and stable isotope signatures are consistent, with $\delta^{18}O$ data centred on a single maximum of about 8.0‰ (Černý, 1991a). NYF pegmatites correspond with REL-REE and MI-REE subclasses; the MSRELL-REE subclass may be classified as such if proof of plutonic derivation is demonstrable.

Černý and Ercit (2005) summarise multiple formation mechanisms for NYF melts based on geological, isotopic and geochemical evidence and petrological-geochemical considerations:

1. Direct differentiation from mantle derived basaltic magmas;

2. Melting of mid/lower crustal protoliths which have been previously modified by an episode of melting which caused LCT elements to be mobilised but the NYF elements to be conserved;
3. Melting of undepleted juvenile igneous lithologies in an orogenic setting;
4. A combination of processes 2 and 3;
5. Melting of sialic crust (Si and Al rich upper crust) pre-enriched in NYF elements by mantle derived fluids (including bimodal gabbro-granite suites).

LCT pegmatites

These pegmatites are characterised by relatively high concentrations of Li, Rb, Cs, Be, Sn, Ta>Nb, with additional B, P and F (but not as fluorite or topaz) (Černý and Ercit, 2005). Associated granites are typically peraluminous (to varying degrees) and of S- and/or I-type. Fractionation and textural diversity is usually high within the intrusive bodies. LREEs are enriched to 10 – 100 times chondritic, with $\delta^{18}O$ data indicating a bimodal distribution peaking at 8.5 and 11.5‰ (Černý, 1991a), which represent the two principle sources of LCT fertile granites (Černý and Ercit, 2005):

1. Anatexis of undepleted upper to middle crust metasedimentary and metavolcanic protoliths;
2. Limited anatexis of basement variably metamorphosed igneous rocks.

LCT pegmatites correspond with REL-Li and MI-Li subclasses, with possible future inclusion of the MSREL-Li subclass when proof of plutonic derivation is demonstrable.

2.5 High Purity Quartz (HPQ)

2.5.1 Potential defects within quartz

The chemical and physical properties of quartz are defined by its actual rather than stoichiometric structure; this is fundamentally controlled by the thermodynamic conditions during mineralisation and hydrothermal and metamorphic process. As such, specific structures, chemistries and physical properties can be utilised for geological studies and specific technical

applications (Götze, 2009). The occurrence of these processes means that completely pure quartz (that with an 'ideal structure') is essentially impossible. Impurities, or defects, occur as point defects, linear dislocations and mineral/fluid inclusions (Götze, 2009); Fig. 2.5.1.

Point defects are uncommon but arise due to a) incorporation of non silica ions in lattice and interstitial positions (e.g. Götze (2009), Jung (1992) and Müller et al. (2011)), b) a variety of displaced atoms c) Si/O vacancy defects. They may be defined as intrinsic (involving atoms from the host; vacancies, interstitial and excess atoms) or extrinsic (foreign atoms). The defects may be further classified as diamagnetic or paramagnetic depending on electronic structure (Götze, 2009). Si^{4+} is subject to limited simple substitutions due to its small ionic radius and high valence; Al^{3+} (with a resulting e^{-1} hole in the nearest O^{2-}) is the most common, whilst Ti and Fe may be also be incorporated (Götze, 2009). Pegmatitic quartz typically displays small concentrations of point defects, with more trace element point defects, but specific defects may depend on quartz genesis: $[TiO_4/H^+]^0$ centres are metamorphic, $[TiO_4/H^+]^0$ are igneous (Götze et al., 2004).

Dislocations are the most abundant linear defects within quartz, and are typically either edge or screw types. Dislocations either initiate during the condensation of point defects during crystal growth or during mechanical/thermal overprinting (where the type and number of dislocations is systematic of specific growth conditions), or from mechanical effects/rapid cooling post-crystallisation (Götze, 2009). During the development of quartz crystals, mineralising fluids and/or paragenetic minerals may be incorporated physically within the structure as fluid or mineral inclusions. These are indicative of the crystallisation environment, and significantly affect the trace-element composition of the quartz. Fluid inclusions not only dictate the chemistry of quartz, but may also influence the melting behaviour of the mineral (Götze, 2009).

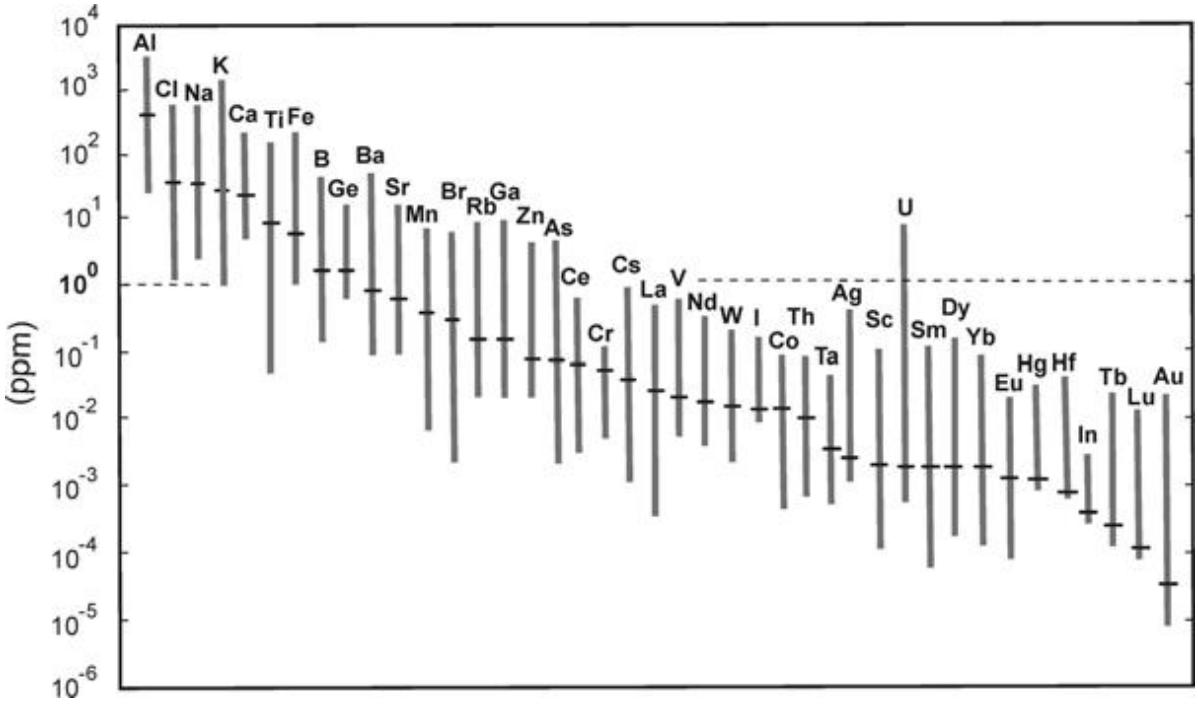

Fig. 2.5.1 Average abundance of trace elements in quartz (from Götze, 2009)

When determining implications for uses of HPQ, there is a strong need to differentiate between structural impurities and solid and liquid inclusions. Inclusions are typically removed during processing by mineral dressing, but structural impurities can only be partially removed; this is time consuming and expensive. Jung (1992) suggests that only Al, B, Ge, Fe, H, K, Li, Na, P and Ti are “true structural impurities, while Ca, Cr, Cu, Mg, Mn, Pb, Rb and U are manifested as contamination by microscopic solid and fluid inclusions”. Substitutional impurities (Ti, Fe and Ge) are those which compete with Si^{4+} for a place in the quartz crystal lattice. Interstitial impurities are essentially charge compensators which balance substitutional impurities such as Li^{+} or Na^{+} to balance the missing charge from Al^{3+} (substitution). H is rare in igneous quartz, and is more common in quartz from dilute aqueous solutions such as veins. This type of quartz displays lamellar growth structures and highly asymmetric distribution of structural impurities which cause sectoral and concentric zonation. Zoning is caused by selective accumulation of certain elements along specific orientations, causing abrupt compositional changes (e.g. Tanner et al., 2013). Indeed, highly uneven distributions of impurities are limited to lamellar hydrothermal quartz in veins; structural impurities in igneous and metamorphic quartz are more evenly distributed throughout crystals.

Müller and Koch-Müller (2009) summarise that natural quartz should have an atomic ratio of Al^{3+}+Fe^{3+}+Be^{3+} to P^{5+}+H^{+}+Li^{+}+Na^{+}+K^{+} in the charge neutrality equation of 1; Müller et al. (2009) suggest a ratio of 1: 1 to 1.5 for Al+Fe:Li+K+P+H manifested in the quartz, the correlation of which is improved by the presence of OH^{-}, which increases the Al+Fe/Li+K+P if added to Li, K and P (as it effectively reduces the charge). If a sample already has a high Al+Fe/Li+K+P, then OH^{-} (with Al and Fe) will balance this. Igneous quartz may preferentially incorporate hydrogen as OH^{-} in lieu of Li, K and P, producing a high H/Li+K+P ratio. A high H/Li+K+P ion ratio in igneous quartz (over hydrothermal or metamorphic) suggests that igneous quartz preferentially incorporates hydrogen as OH^{-} over Li, K and P, with molecular H_2O likely related to water bearing micro pores and fractures, rather than fluid inclusions which were not apparent.

The definition by Harben (2002) of HPQ (naturally occurring material containing less than 50 ppm trace elements), whilst functionary, does not deal with specific impurities. Müller et al. (2007) developed a HPQ classification based not only on total impurities, but on the concentration limits of certain elements, proposing upper concentration limits of 25 ppm for Al and 10 ppm for Ti. In 2011 the authors developed this concept further, stipulating the sum of 9 elements (Na, K, Li, Al, Ca, Fe, Ti, B and P) analysed within quartz crystals (single grain analysis) or processed quartz sand (bulk product analyses) must be less than 50 ppm to warrant classification as ‘high purity’. Furthermore, Müller et al. (2011) provided upper permissible limits for each element; Al <30 ppm, Ti <10 ppm, Na <8 ppm, K <8 ppm, Li <5 ppm, Ca <5 ppm, Fe <3 ppm, P <2 ppm and B <1 ppm.

2.5.2 Quartz in pegmatites

Larsen et al. (2004) summarise that trace element distributions in granitic and pegmatitic quartz are highly sensitive to igneous fractionation processes, potentially recording the origin and the evolution of granitic pegmatites. Simply assessing the trace element assemblage seems to be insufficient in determining the source(s) of the parent melt; the trace elements appear to be of more use in defining fractionation trends, mineral facies and relative differences between

melts. Larsen et al. (2000) summarise that, traditionally, high temperature (β-) quartz accommodates higher concentrations of impurities in its atomic structure than the lower temperature α variety. The study suggests that in the Evje-Iveland pegmatite field, less fractionated pegmatite melts contain elevated Ti, Mg, Ca and Cr and more fractionated (and therefore cooler) melts higher Fe, Li and B. This is (broadly) supported by Larsen et al. (2004); K, Fe, Be and Ti are concentrated in early quartz, P, Ge, Li and Al are concentrated in late quartz.

The interpretation is that Ti, Be and K are compatible in quartz, and Ge, P Li and Al incompatible. Al, Li and to some extent Fe show irregular trends during fractionation, with Be and K (and, with Rb, Ti) and Ge and P clearly decreasing and increasing respectively. This is likely a result of these elements only occurring at one structural site in the quartz atomic lattice. Therefore, as substitutions for Si, they are strongly confined to the atomic lattice structure of quartz and hence are not easily influenced by subsolidus processes (excepting Be) (Larsen et al. 2004).

Ti and Ge show simple substitutions for Si, having the same 4^+ charge. P^{5+} and an equivalent molar fraction of Al^{3+} (to balance the pentavalent ion) act as coupled substitutions (also potentially involving B and Fe, but these are such in insignificant quantities that they can be ignored). Li, Na, K, Be, Fe, B, Sr, Rb, Ba and remaining Al act as stuffed derivatives or interstitial charge compensators (Larsen et al., 2004). Larsen (2000) states the total concentration of structural impurities rises with the degree of differentiation and that therefore Ge/Ti, Ge/Be, P/Ge and P/Be ratios in quartz are sensitive to fractionation, in much the same way as Rb/Sr and Rb/K of K-feldspar. Ge/Ti in quartz is the most robust during subsolidus processes in the igneous system, and is therefore considered most suitable for petrogenetic interpretations (Larsen et al., 2004).

Larsen et al. (2000) suggest that primary fluid inclusions are common in pegmatite quartz from the Evje-Iveland field, but that they vary in proportion and size. The majority are subhedral and of the H_2O-CO_2-NaCl type. Quartz from the intermediate zone contains inclusions of low to medium salinity with 10 – 15 vol% CO_2; core inclusions are low salinity with 5 – 10 vol% CO_2. Dominant

electrolytes are Cl^- and Na^+. Secondary inclusions are compositionally similar to primary, but occasionally show evidence of liquid immiscibility with a carbonic and aqueous phase. Inclusions in pegmatite quartz are also described by Thomas and Davidson (2012a and 2012b) as melt and trapped silicate gels, respectively. The water contents of the melt inclusions (typically in excess of 10% (g/g)) are the result of melt-melt immiscibility processes, and indicate the melt is of an extremely low viscosity and not necessarily undercooled (Thomas and Davidson, 2012b). The silicate gel inclusions become increasingly common towards the quartz cores of the pegmatites, and are considered to demonstrate increasing water and alkali carbonate concentrations in melt (Thomas and Davidson, 2012a).

Grey scale contrasts observed in quartz under SEM-CL are caused by a heterogeneous distribution of lattice defects (e.g. Si and O vacancies and/or broken bonds) and trace elements in the crystal lattice (i.e. atomic substitutions) (e.g. Sprunt, 1981; Perny et al., 1992, Götze et al., 2005). Whilst the physical background of the quartz CL is not fully understood (Müller et al., 2008), the structures revealed supply information about crystallisation, deformation and fluid driven overprinting, in a manner similar to a geological map. CL structures can be related to both external deviatoric stress and internal stress at grain scale due to the strong thermal contraction of quartz. In Froland pegmatite quartz, thin, dark, intra and transgranular healed cracks and irregular quartz domains of low luminescence extending from healed cracks are common (Müller et al., 2008). Diffuse alteration rims, locally wavy zoning sub-parallel to grain boundaries and contacts may result from diffusional processes. All darker, secondary zones present in the Froland quartz are depleted in Al, Ti and K (relative to primary host quartz) i.e. there has been a late-stage fluid driven purification event, which leads to a significant reduction in trace element concentrations if secondary quartz makes up a significant proportion of the material (Müller et al., 2008).

2.5.3 Industrial applications

The applications of quartz (Table 2.5.1) are varied with end use and price dependant on deposit quality and size (Fig. 2.5.2); a bulk product in the glass

industry, quartzites for refractory material, HPQ crystals in the piezo and optical industries, fused silica in semi-conductor packaging and Si metal for Si alloys. Granulometric properties of the raw material are critical when quartz is utilised as casting material in foundry sands. Chemical purity (to prevent discolouration) and grain size consistency (for regular melting behaviour) are vital quartz parameters in the glass industry (Götze, 2009).

Table. 2.5.1 Genesis, provenance, properties and industrial application of differing quartz types (Götze, 2009)

Quartz type	Desirable properties	Preferred application
Magmatic/postmagmatic quartz of alaskite 'Iota quartz'	Chemical Purity	Synthetic high-purity silica material
Pegmatitic and hydrothermal quartz	Chemical purity, perfect crystal order	Optical and piezo quartz, quartz synthesis (lascas), solar silicon
Metamorphic quartzite	SiO_2 up to 98%	Refractory materials
Metamorphogenic mobilizates	Chemical purity	Quartz synthesis (lascas)
Sedimentary quartz sands	Chemical purity, granulometric properties	Glass and foundry industry, cristobalite, quartz powder
Sedimentary quartzite	Chemical purity, cryptocrystalline silica	Refractory materials

Perfectly crystalline quartz of extremely high purity (e.g. sub 1 ppm Al) is required as a growth medium for the synthesis of hydrothermal quartz. This HPQ is utilised as a growth medium and as fabrication material for semiconductor and Si-based solar panel construction (both as wafers for the solar cells and as glass cover slips (Glover et al., 2012). Manufacture is necessary as the majority of natural quartz is unsuitable for optical and piezo quartz); approximately 1000 t/y of synthetic hydrothermal quartz is produced in 350 – 400°C 100 – 120 MPa autoclaves, utilising pegmatitic and hydrothermal quartz (lascas) as high purity raw materials for crystal growth (Götze, 2009). Pegmatite quartz is also used in insulating tiles in NASA space shuttles, and in the mirrors of observatory telescopes (Glover et al., 2012).

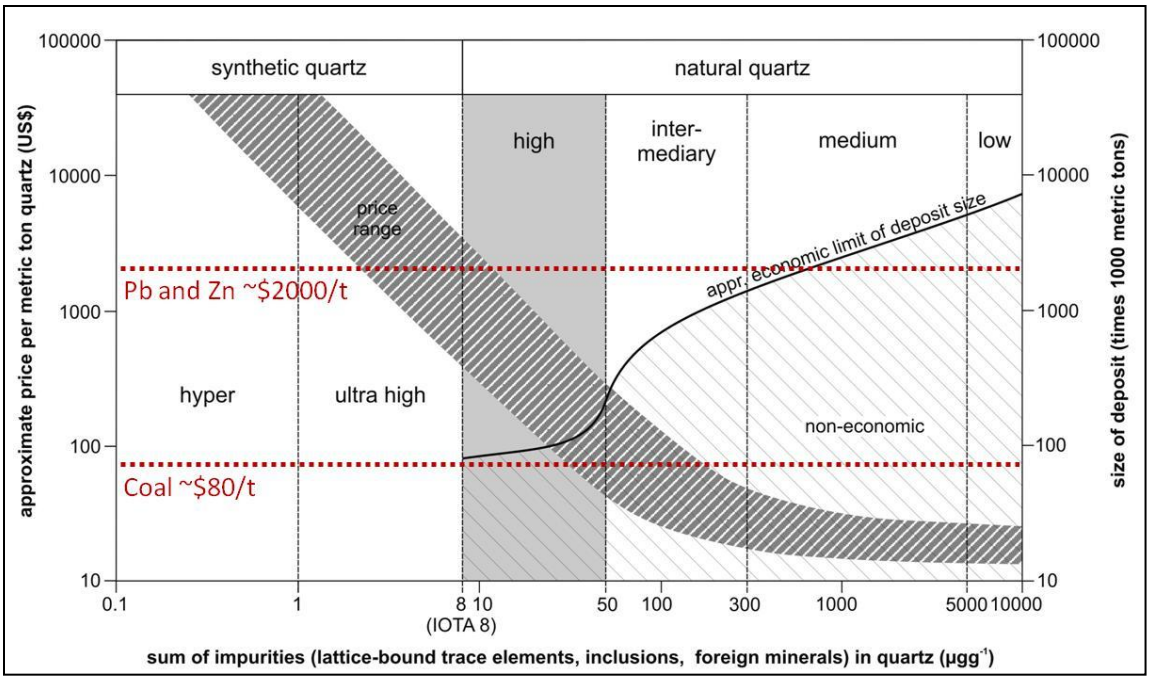

Fig. 2.5.2 Economic schematic indicating the classification of quartz, their value (Müller, 2011) and position relative to other saleable material (Pb, Zn and coal prices from InfoMine, December 2011)

3. METHODOLOGIES

3.1 Field techniques and sampling

3.1.1 Field mapping

Field mapping was carried out in two campaigns during September 2010 and June 2011, focussing on the Evje-Iveland pegmatites in general and the pegmatites of the Landsverk area, respectively. The work included geological mapping of the pegmatites, lithological descriptions, structural and textural studies and extensive sampling for geochemical analyses. Sites were chosen based on:

- ease and safety of access;
- exposure of pegmatite body (i.e. pegmatites which have been mined and are therefore visible) and country rock;
- completeness, showing a high proportion of the internal architecture of the body;
- position within the pegmatite field with the aim of studying a representative range of pegmatite bodies, from simple pegmatites to evolved pegmatites displaying replacement units.

As discussed in Chapter 2.2.3 eight pegmatites were selected for detailed studies: Landsverk 1, Kåbuland, Li Gruva, Slobrekka, Hovåsen, Solås, Iveland and Steli. Geological mapping was performed using 1:10,000 scale base map field slips generated from the Norwegian State Authority's Norgeskart facility (http://www.norgeskart.no/adaptive2/default.aspx?gui=1&lang=2) and then digitally annotated in Corel Draw using State Authority paper maps (Best. nr: 447, Kartblad 1512-3, 2009). In-field location was performed utilising a Garmin 60s GPS with 1:50,000 scale digital base maps and a Silva Ranger Type 15 compass.

3.1.2 Sampling

'Whole rock' and mineral (from crystal centre where possible) samples, 263 in total, were collected from each pegmatite. 'Whole rocks' were sourced from granitic border zones, where the crystal size was typically 2 mm. Approximately 5 kg was collected to ensure that the samples were representative. Further

justification for this sampling method is provided in *Chapter 5.1.3*. Where exposed, granitic border zones were sampled at the base and the roof of the pegmatite for comparison. Sampling of specific minerals was more selective as particular minerals from particular zones were desirable, and as such were targeted when observed. Sampling of 'whole rocks' and minerals was performed with either a steel geology hammer or steel sledge hammer. Weathered surface materials were removed in the field to reduce the amount of material transported back to the laboratory. Samples were stored in either ziplocked LDPE polybags or drawstrung Hubco Sentry spunbonded polyester fabric bags and assigned unique identification numbers (DDMMYY-##) which were recorded in a field note book along with the 13 figure sample location reference (UTM 32V WGS84) format. Some mineralogical samples are popular with mineral collectors, and as such the chances of finding them (aside from immediately after a fresh blast) are incredibly low. Because of this, some samples (110910-14 to 110910-26) were purchased from a local reputable mineral dealer.

3.1.3 Sample summary

A summary of collected samples is provided in APPENDIX 1. Attention should be made to the sample number (as described in *Chapter 3.1.2*), which represents different field campaigns. Samples from 2010 and 2011 (DDMM10-## and DDMM11-## respectively) were collected and analysed as part of this study. Samples from 2008 (DDMM08-##; the majority of the K-feldspar and biotite samples) and 2009 (DDMM09-##; the majority of whole rock samples) were collected by Axel Müller of the NGU (a supervisor of this project) and analysed by NGU laboratories and ACME Analytical Laboratories in Vancouver, Canada respectively as part of a preliminary study. They are included as they are entirely relevant to the field area. All sample preparation and analytical procedures (e.g. the laboratory used, sample handling, standard reference materials, analytical conditions) were the same for all sample material pertinent to this study, so the samples will be discussed synonymously in the following chapters, with distinction/clarification made if necessary. The data for samples collected in 2008, 2009 and for this study are included in the same tables (APPENDIX 2).

3.2 Sample preparation

3.2.1 Mineral sample preparation for SEM, CL and LA-ICP-MS

Scanning Electron Microscopy (SEM), cathodoluminescence (CL) and laser ablation inductively coupled plasma mass spectrometry (LA-ICP-MS) investigations were performed exclusively on polished thick sections, prepared at the NGU. Material was selected based on apparent homogeneity and lack of weathering and mineral inclusions. The material was cut into tablets, approximately 20x40x10 mm in size, with a circular saw. The tablets were then bonded to glass thin section slides (25x50 mm) using Epofix resin. The tablets were subsequently ground flat (to ensure perfectly horizontal analysis surfaces) on a Knuth Rotor, initially using a 220 and then a 1000 silicon carbide disk (approximately 20 seconds each disk). The precursor stage to the polishing process was lapping of the sample faces on a Logitech LP50 for four minutes using F600 silicon carbide slurry; this ensured a thickness of approximately 200 µm, which would allow the section to withstand subsequent laser ablation analysis. All slurries were water based, as no minerals in the rock were water soluble. The samples were then cleaned before final polishing using a Stuers Planapol-V counter-rotating polisher. A perforated pad K hard cloth was initially employed with six minutes of polishing using a 6 µm diamond slurry followed by four minutes using 3 µm diamond slurry. The sample faces were finished on a soft felt pad with 1 µm diamond slurry for about four minutes until a suitable finish was produced. Samples for SEM and CL analysis were carbon coated to a thickness of approximately 25 µm.

3.2.2 Sample preparation for XRF

For each mineral sample, approximately 0.2 kg of macroscopic homogeneous megacrysts were crushed to a <1 mm grain size using a REUTSCH BB200 rock crusher. Grains containing inclusions of foreign minerals were removed by careful hand picking (microscopic mineral inclusions however cannot be removed entirely by this procedure). The purified and washed sample material was milled to ~40 µm in agate pots. Approximately 3 g of the powder was fused at 1030°C for 60 minutes to determine loss on ignition (LOI) gravimetrically, which gave an approximate measure of volatile content (e.g. H_2O and CO_2). For major element determinations, 0.6 g of the sample powder used was fused in a

Pt-crucible with 4.2 g of lithium tetraborate flux ($Li_2B_4O_7$) at 1120°C and then cast into a graphite platen to produce a visually flat and homogeneous glass disc. For trace elements, pressed powder pellets were prepared with 9.6 g of powdered sample and 2.4 g of Licowax wax binding agent (Hoechst C).

3.2.3 Sample preparation for ICP-AES, ICP-MS

Solution inductively coupled plasma atomic emission spectrometry (ICP-AES) and inductively coupled plasma mass spectrometry (ICP-MS) was performed on specific whole rock material at ACME labs. The complete 5 kg sample was crushed and ground down to ~40 µm using the methods discussed in *Chapter 3.2.2*.

3.2.4 Sample preparation for zircon U-Pb isotope determinations

Age determinations by U-Pb Secondary Ion Mass Spectrometry (SIMS) on zircons were carried out on three samples from the Høvringsvatnet granite (a syenomonzonite (220609-03), a biotite granite (220609-04) and a biotite rich granite (220609-01)) and on samples from the Slobrekka, Li Gruva, Steli, Solås and Hovåsen pegmatites. After initial magnetic separation (granites at approximately 1 – 2 A, 5 – 10°, pegmatites at 0.5 A, 5 – 15°), zircons were handpicked under the microscope and assembled along with a set of standard zircons (aged 1065 Ma (sample 91500; Wiedenbeck et al., 1995)) to form a block, according to procedures described on http://www.nrm.se/nordsim.

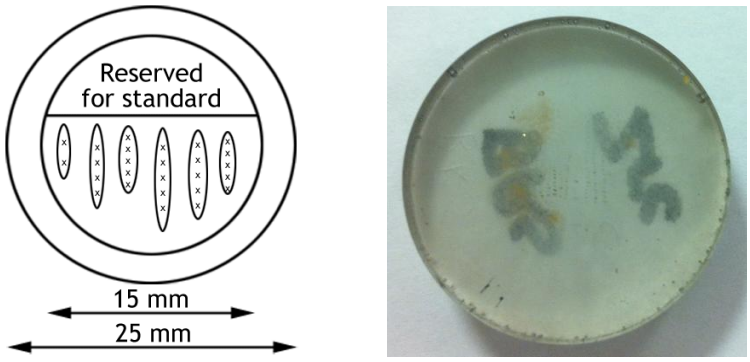

Fig. 3.2.1 The 25 mm block layout for NORDSIM isotope analyses (from http://www.nrm.se/nordsim)

Fig. 3.2.1 (from the NORDSIM, Swedish Museum of Natural History website) demonstrates the required block layout for material to be analysed at the

isotope facility. Whilst the holder accepts a 25 mm block, the sample holder of the ion-microprobe has an edge which partly covers the puck. For that reason the grains are located in the centre of the mount, at a minimum of 5 mm from the edge.

The block was made up from Stuers Epofix resin and hardener, and polished with a Struers RotoPol-31 with a Struers RotoForce-4. Due to the size of the zircons (down to sub 100 μm), polishing consisted of progressive 1 to 2 minute runs on MD-Pan felt pads with 6 μm and 3 μm diamond slurry, with the samples and pad sprayed periodically with an alcohol lubricant and diamond aerosol. Between each stage, cleaning occurred with water and soap, with material dried with a spray of compressed air. As polishing progressed metamict material from within the zircons plucked out as it was friable, diminishing the polish quality of the mount. As such, hand polishing occurred with 1 μm diamond slurry and alcohol lubricant until an acceptable finish (monitored by optical microscope) was produced.

Once mounted and polished, SEM-CL and SEM-BSE (backscattered electron) images were taken of every granite and pegmatite zircon respectively to define zoning, fractures and areas not damaged by radiation (i.e. metamict). This would expedite the subsequent analyses, as suitable SIMS points (i.e. the avoidance of replacement structures/rims/overgrowths which would give varying ages; oscillatory zoning is acceptable e.g. Whitehouse and Kamber (2005)) had already been determined. Examples are illustrated in Fig. 3.2.2.

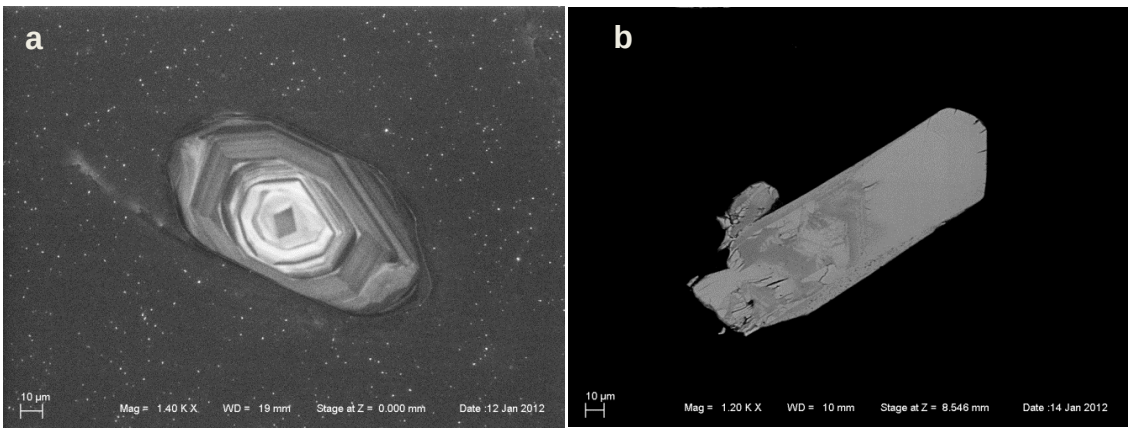

Fig. 3.2.2 Example zircons from the biotite granite (a; CL image) and the Slobrekka pegmatite (b; BSE image)

Fig. 3.2.3 illustrates the zircon block in its entirety, which was ultimately gold coated to 120 angstroms.

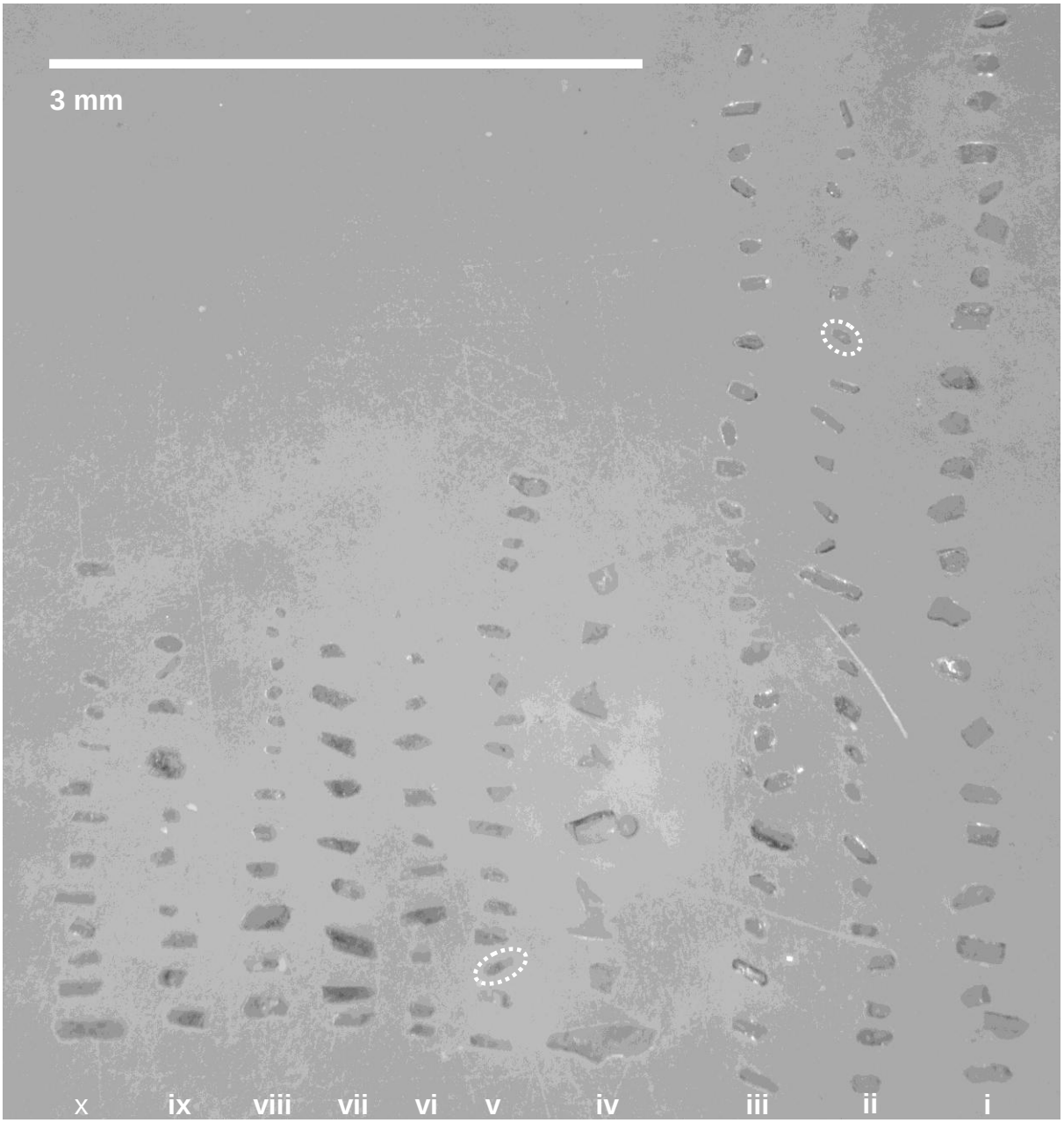

Fig. 3.2.3 Zircon 25 mm block (same size as that visualised in Fig. 3.2.3) composition; a syenomonzonite (i), a biotite granite (ii) and a biotite rich granite (iii) from the Høvringsvatnet granites and the Slobrekka (v), Li Gruva (vi), Steli (vii), Solås (viii) and Hovåsen (xi) pegmatites. Standards are row iv, and row x are zircons from a Froland pegmatite, not relevant to this study. White rings indicate the zircons in Fig. 3.2.2

3.2.5 Sample preparation for O isotope analysis

Material for O isotope analyses by SIMS was taken directly from the quartz samples previously analysed by LA-ICP-MS as discussed in *Chapter 3.2.1*. Essentially, the thick sections were cut into ~5 x 2 mm fragments, glass slide

included, using a small circular saw. These were then mounted ‘quartz up’ into a resin block according to the specifications on the NORDSIM website (http://www.nrm.se/nordsim), as discussed in *Chapter 3.2.4*. This process is summarised for the Landsverk 1 material in Fig. 3.2.4. Polishing occurred as discussed previously, and once mounted and polished, SEM-CL images were taken of each quartz slice to define zoning. Standard reference material (sample NBS 28 (Hut, 1987)) was embedded at the NORDSIM facility, and the block was re-polished appropriately.

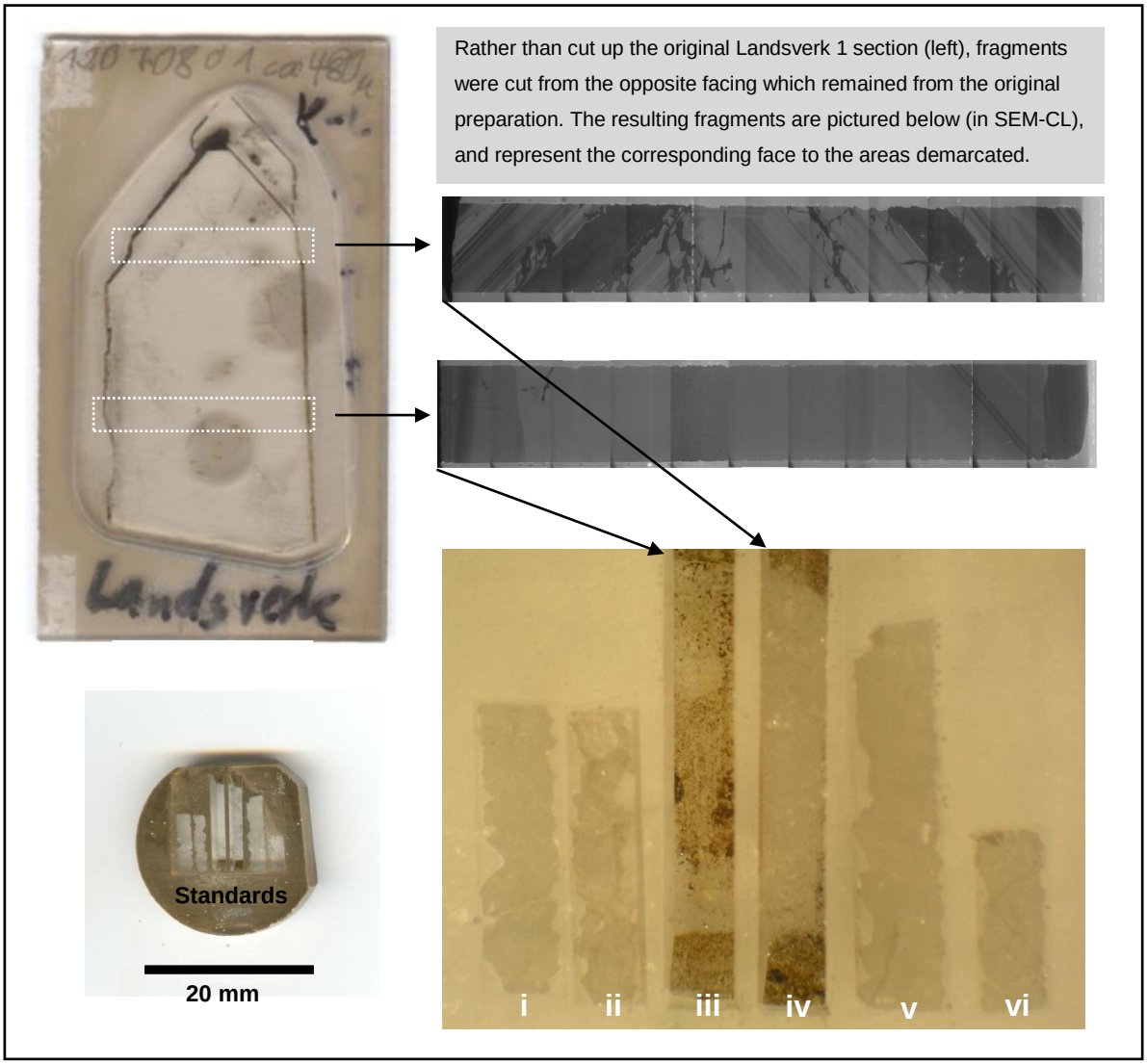

Fig. 3.2.4 Construction of the quartz block for O-isotope SIMS analyses. Once fragments had been cut for Steli core (i), Steli outer zone (ii), Landsverk 1 crystal base (iii), Landsverk 1 crystal tip (iv), Solås core (v) and Solås outer zone (vi), these were mounted in a resin block with standards, polished and ultimately gold coated

3.3 Analytical techniques

3.3.1 SEM and CL analyses

SEM and CL analyses were carried out at the Geological Survey of Norway (NGU), Trondheim on a Leo 1450 VP analytical SEM with a Centaurus bialkali CL detector. Working conditions varied slightly, but typically the stage had a working distance of 15 – 20 mm (to allow the introduction of the CL detector) with the chamber at a working pressure of 20 Pa. The applied accelerating voltage and current at the sample surface were 20 kV and 3 nA, respectively. The BIALKALI CL detector has a response range from 300 (violet) to 650 nm (red), peaking in the violet spectrum range at around 400 nm. The CL images were collected from one scan of 43 s and an image output of 1024 × 768 pixels with and 256 grey levels.

3.3.2 XRF analyses

Major and trace element compositions of feldspars and micas were determined by X-ray fluorescence spectrometry (XRF) using a Phillips PW1480 spectrometer equipped with a Sc/W X-ray tube at the NGU. Major element analysis was carried out on fused glass discs for Na_2O, MgO, Al_2O_3, SiO_2, P_2O_5, K_2O, CaO, TiO_2, MnO and Fe_2O_3. The total Fe concentration was calculated as Fe_2O_3 wt.%. The limits of detection (LOD) are 0.1 wt.% for SiO_2, Al_2O_3, and Na_2O, and 0.01 wt.% for Fe_2O_3, TiO_2, MgO, CaO, K_2O, MnO, and P_2O_5. For trace elements, analyses were carried out on pressed powder pellets. The surfaces of the pellets were analysed for Rb, Sr, Y, Zr, Nb, Ba, Pb, Th, U, Sc, V, Cr, Co, Ni, Cu, Zn, Ga, Mo, As, Sb, Sn, Ce, Nd, La, W, Cs, Ta, Pr, Hf, S, Cl and F. The LOD was 10 $\mu g g^{-1}$ for Zn, Ni, Co, Mo, Nb, Zr, Y, Sr, Rb, and Th, 5 $\mu g g^{-1}$ for As, and 1000 $\mu g g^{-1}$ for S, Cl, and F.

3.3.3 'Whole rock' analysis by ICP-AES and ICP-MS

Whole rock sample solutions were analysed by ICP-AES and ICP-MS for major and trace elements respectively at the ACME Analytical Laboratories in Vancouver, Canada in two batches, using sets of internationally recognized standards, according to procedures described on http://acmelab.com/pdfs/Acme_Price_Brochure.pdf.

The analysis package is titled ‘Total Whole Rock Characterization 4AB1’, and involves two subpackages, with hydrofluoric acid as the digestion agent. 4A02 is referred to as “a classical whole-rock analysis for 11 major oxides and several minor elements by ICP-AES following a lithium borate fusion and dilute acid digestion of a 0.2 g sample pulp. The package includes loss on ignition (LOI) by sintering at 1000°C (package code 2A05) and Leco analysis for total carbon and sulphur (package code 2A12)”. 4B02 “incorporates two separate ICP-MS analyses to optimize determination of a 45-element suite of trace elements. Rare earths and refractory elements report from a lithium borate decomposition (same as that used in Group 4A) to give total abundances. Precious metals, base metals and their associated pathfinder elements (highlighted in adjacent element table) are generated from an aqua regia digestion (same as package code 1DX1)” (http://acmelab.com/pdfs/Acme_Price_Brochure.pdf). As such, a 10 g sample pulp was required.

ICP-AES was used to determine SiO_2, Al_2O_3, Fe_2O_3, CaO, MgO, Na_2O, K_2O, MnO, TiO_2, P_2O_5, Cr_2O_3, Ba, C, S, Cu, Ni, Pb, SO_3, Sr, V_2O_5, Zn, and Zr, and to determine LOI. ICP-MS was used to determine Au, Ag, As, Ba, Be, Bi, Cd, Co, Cs, Cu, Ga, Hf, Hg, Mo, Nb, Ni, Pb, Rb, Sb, Sc, Se, Sn, Sr, Ta, Th, Tl, U, V, W, Y, Zn, Zr, La, Ce, Pr, Nd, Sm, Eu, Gd, Tb, Dy, Ho, Er, Tm, Yb and Lu.

3.3.4 Trace element analysis by LA-ICP-MS

Laser ablation ICP-MS was used to determine the in situ concentrations of 17 elements (including Al, Li, Ti and Ge) in quartz. The analyses were performed on the double-focusing magnetic sector field mass spectrometer model ELEMENT XR from Thermo Scientific which is combined with the NewWave UP193FX excimer laser at the NGU. The 193 nm ArF laser had a repetition rate of 10 Hz, a spot size of 75 µm, and energy fluence of about 5 J/cm^2 on the sample surface. A rastered area of approximately 150×200 µm was ablated on the surface of the standards and the quartz samples. The approximate depth of ablation (determined using an optical microscope) was about 30 µm. The carrier gas for transport of the ablated material to the ICP-MS was He mixed with Ar. Further information on the measurement procedure is discussed by Flem et al. (2002) and Flem and Müller (2012).

3.3.5 U-Pb isotopes

A Cameca IMS1270 multi-collector equipped large-format ion microprobe at the NORDSIM facility was utilised to generate high spatial resolution U-Pb data from igneous zircons. A defocused O^{2-} primary beam projected a 60 µm aperture on to the sample, which generated elliptical, flat bottomed craters of approximately 20 µm in length in the larger granite zircons (Whitehouse and Kamber, 2005); spatial resolution in the smaller, more structurally complex pegmatite zircons was further enhanced by application of the field aperture in the secondary ion optics, which reduced the actual analysed region admitted to the mass spectrometer down to approximately 10 µm. An energy window of 60 eV was utilised, the detection device was a single ion-counting electron multiplier, with mass calibration maintained with an automatic routine in the Cameca CIPS software (Whitehouse and Kamber, 2005). Further details of analytical methods for U-Pb analyses are provided by Whitehouse et al. (1997, 1999), with QA/QC techniques discussed in *Chapter 3.4.4*.

3.3.6 Quartz O isotope analysis

O isotopes were analysed at NORDSIM. Measurements were performed with the same Cameca IMS1270 multi-collector equipped large-format ion microprobe, in a manner described in detail by Nemchin et al. (2006a), for ^{16}O and ^{18}O. A 20 keV Cs^{+} primary beam (+10 kV primary, −10 kV secondary) of approximately 5 nA was used in aperture illumination mode to sputter a 15 µm sample area, with a normal incidence electron gun providing charge compensation. Fully automated runs comprised a 180-s pre-sputter period, followed by 240 s of data acquisition using two Faraday detectors in the multicollector system. Incorporated into the procedure was within-run beam centering in the field aperture using transfer deflectors and within-run mechanical optimisation of the entrance slit position (Whitehouse and Nemchim, 2009). Additional protocols are discussed in Nemchin et al. (2006b).

3.4 QA/QC

3.4.1 ACME ICP-AES and -MS

Using the method of Howarth and Thompson (1976), at a 95% confidence level, it is apparent that over 85% of elements analysed in the initial ACME batch have a precision of better than 10%, with only La, Ce and V demonstrating a precision worse than 20%. 90% of elements analysed in the second ACME batch have a precision of better than 5%, with only Be and Sc demonstrating a precision worse than 10%.

Utilising the same duplicate data as that used for the Howarth-Thompson assessment (Howarth and Thompson, 1976) Fig 3.4.1 demonstrates the strong correlation between four duplicated pulp samples, with R^2 values of essentially 1. The major element plots correspond to analyses for SiO_2, Al_2O_3,Fe_2O_3, MgO, CaO, Na_2O, K_2O, TiO_2, P_2O_5, MnO and Cr_2O_3. The trace element plots correspond to analyses for Ni, Sc, Ba, Be, Co, Cs, Ga, Hf, Nb, Rb, Sr, Ta, Th, U, V, Zr, Y, La, Ce, Pr, Nd, Sm, Eu, Gd, Tb, Dy, Ho, Er, Tm, Yb and Lu.

From comparison with analyses of standard reference material SO-18 (the reference material utilised by ACME labs for all ICP-AES and -MS analyses), the analytical error associated with the 2009 data ranged within 2.56% (4.19 2s.d.) of the absolute concentration of major elements based on 4 measurements of the standard, and typically within 6.9% (0.20 2s.d.) of the absolute concentration of minor/trace elements (Ni was an exception at 14.20% (11.95 2s.d.)). The analytical error associated with the 2010 data typically ranged within 2.05% (2.29 2s.d.) of the absolute concentration of major elements based on 6 measurements of the standard, and typically within 8.30% (3.38 2s.d.) of the absolute concentration of minor/trace elements (excluding the final measurement of standard, which demonstrated analytical error of up to 12% (22 2s.d) for some trace elements e.g. Tm).

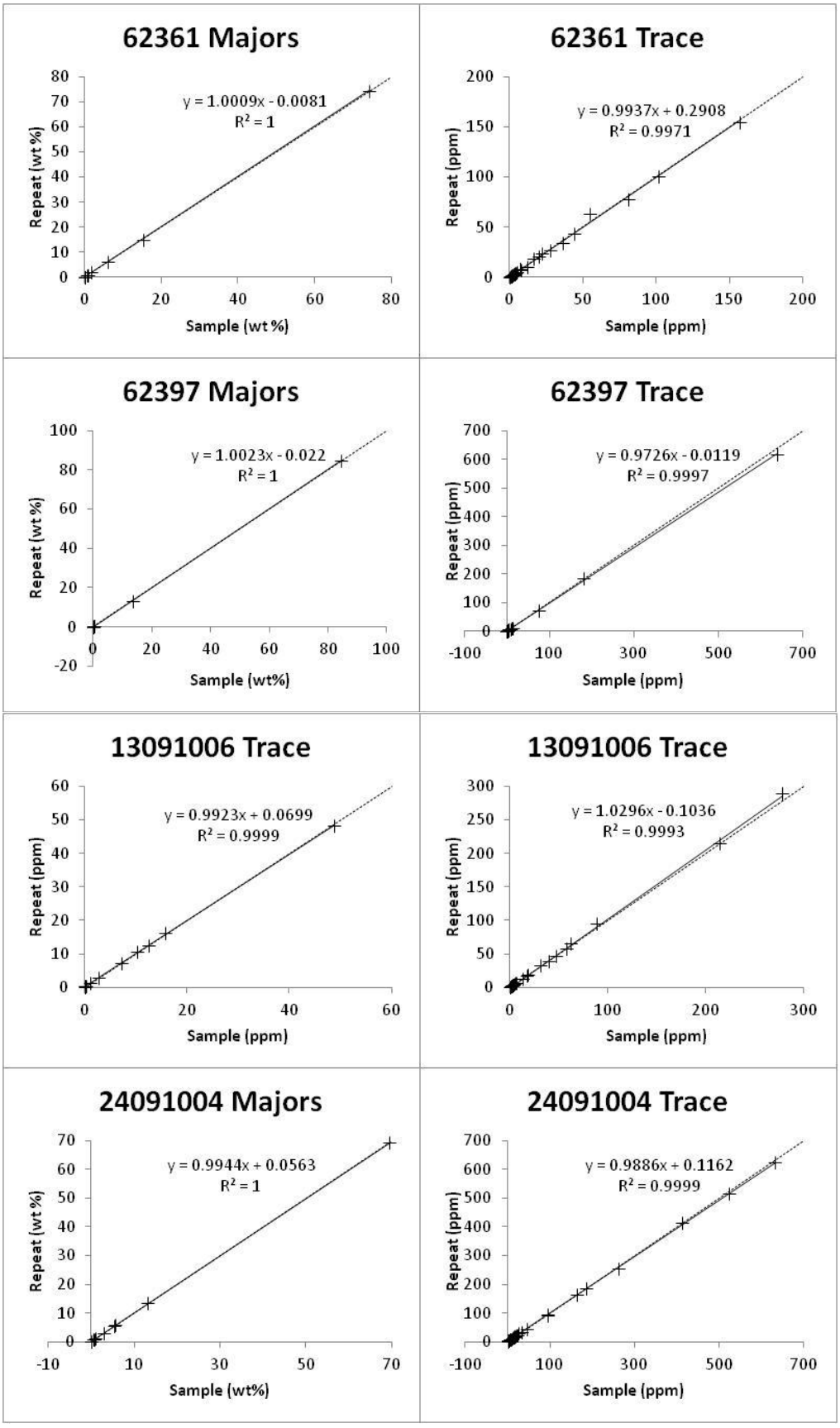

Fig. 3.4.1 Measurements of samples (sample number given) and their repeat to demonstrate repeatability in ACME ICP-AES (for majors) and -MS (for trace), using R^2 as a degree of correlation.

3.4.2 XRF

NGU were able to provide the following data on analytical error (Tables 3.4.1 and 3.4.2), which reflect the total uncertainty of analyses performed at their XRF laboratory. The figures are synthesised from year-long accuracy and precision results from repeats of standards, and also incorporate uncertainty inherent in sample preparation.

Table 3.4.1 Analytical error associated with major element XRF analyses in K-feldspar

Element	**SiO_2**	**Al_2O_3**	**Fe_2O_3**	**TiO_2**	**MgO**	**CaO**	**Na_2O**	**K_2O**	**MnO**	**P_2O_5**
Sample	± %	± %	± %	± %	± %	± %	± %	± %	± %	± %
07070802	0.64	0.127	0.005	0.005	0.005	0.005	0.04	0.254	0.005	0.005
09070819	0.64	0.127	0.005	0.005	0.005	0.005	0.04	0.254	0.005	0.005
09070820	0.64	0.127	0.005	0.005	0.005	0.005	0.04	0.254	0.005	0.005
28060907	0.64	0.127	0.005	0.005	0.005	0.005	0.04	0.254	0.005	0.005
28060908	0.64	0.127	0.005	0.005	0.005	0.005	0.04	0.254	0.005	0.005
10070814	0.64	0.127	0.005	0.005	0.005	0.005	0.04	0.254	0.005	0.005
10070824	0.64	0.127	0.005	0.005	0.005	0.005	0.04	0.254	0.005	0.005
10070831	0.64	0.127	0.005	0.005	0.005	0.005	0.04	0.254	0.005	0.005
12070802	0.64	0.127	0.005	0.005	0.005	0.005	0.04	0.254	0.005	0.005
13091007	0.64	0.127	0.005	0.005	0.005	0.005	0.04	0.254	0.005	0.005

Table 3.4.2 Analytical error associated with trace element XRF analyses of K-feldspar. All samples contain elements in the lower Quantity bracket, except Pb, Rb, Sr and Ba, which fall in the upper Quantity bracket. Samples contain Cs in the lower Quantity bracket, except for 09070819 and 09070820, which contain Cs in the upper Quantity bracket

Element	**Concentration**	**Error (%)**
Co, Cr, Cu, Ga, Mo, Nb, Ni, Pb, Rb, Sr, Th, U, V, Y, Zn	< 50 ppm	< 10
	> 50 ppm	< 5
Ag, As, Ba, Cd, La, Nd, Sc, Sn, W, Zr	< 50 ppm	< 20
	> 50 ppm	< 10
Ce, Ge, Hf, Sb, Sm, Ta, Tl, Yb	< 50 ppm	< 30
Bi, Br, Cs, Hg, I, Se, Te	< 100 ppm	< 50
	> 100 ppm	< 25
F, Cl, S	< 1 %	< 50
	> 1 %	< 25

3.4.3 LA-ICP-MS

External calibrations were performed using three silicate glass reference materials produced by the National Institute of Standards and Technology, USA: NIST SRM 610, 612 and 614. In addition, NIST SRM 1830 soda-lime float

glass (0.1% m/m Al_2O_3) and the certified reference material BAM No.1, amorphous SiO_2 glass from the Federal Institute for Material Research and Testing, Germany, were used. Certified, recommended and proposed values for these reference materials were taken from the certificates of analysis where available, or otherwise from the web site for Geological and Environmental Reference Materials (GeoReM, 2012). The isotope ^{29}Si was chosen as internal standard. Each isotope mass was scanned 15 times sequentially. At least three analyses were performed on each quartz sample. All reference materials were measured at the beginning of the analytical sequence. In addition NIST SRM 612 was analysed repeatedly (every 12^{th} sample) throughout the sequence to document instrumental drift. An Ar blank was run before each reference material and sample measurement. The background signal was subtracted from the instrumental response of the reference material before normalisation against the internal standard, to avoid memory effects between samples and to limit instrument drift. The calculation of absolute element concentrations was performed by applying Excel worksheet macros. A weighted linear regression model, including several measurements of the different reference materials, was used to define the calibration curve for each element. The analysis spots were located in clear quartz crystal domains without visible (applying 1000x magnification) fluid and mineral micro inclusions. Ten sequential measurements on a "SiO_2 blank" crystal were used to estimate the limits of detection (LOD) which were based on 3× standard deviation (3σ). LODs are listed in APPENDIX 2. The analytical error ranged within 9% of the absolute concentration of the element based on 20 measurements of the NIST SRM 612, with critical elements (Al, Li, Ti, Ge) typically displaying an error of 3%.

Figs. 3.4.2 to 3.4.5 represent LA-ICP-MS runs, plotting elemental ppm against progressive time i.e. the order in which the analyses were taken. The figures demonstrate that there is no apparent instrument-induced trend between measurements, which, combined with the subtraction of background signal from blank runs and the calibration of the data with standard measurement, testifies to the validity of the data set.

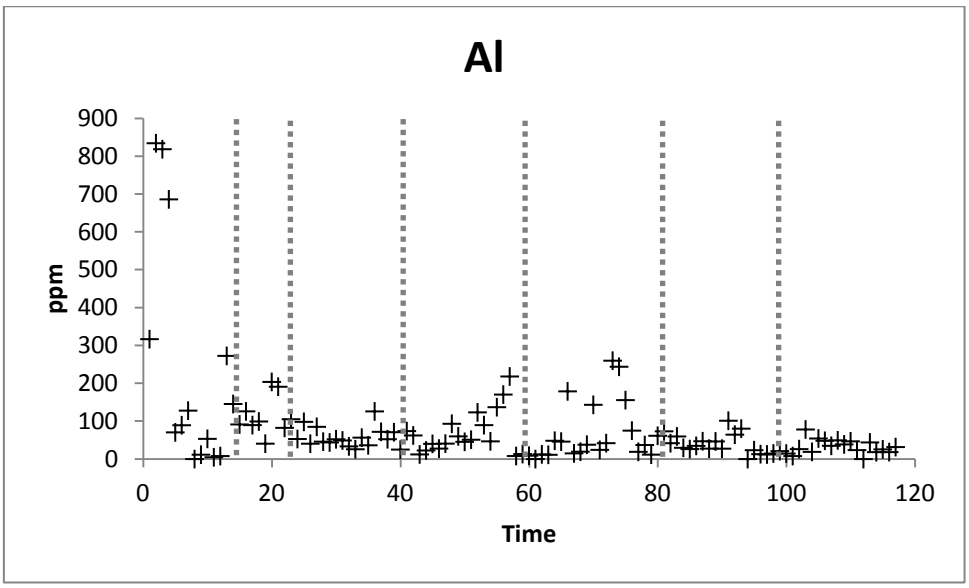

Fig. 3.4.2 Progressive LA-ICP-MS analyses of Al demonstrating a lack of machine-induced drift. Grey bars mark the transition between pegmatite bodies

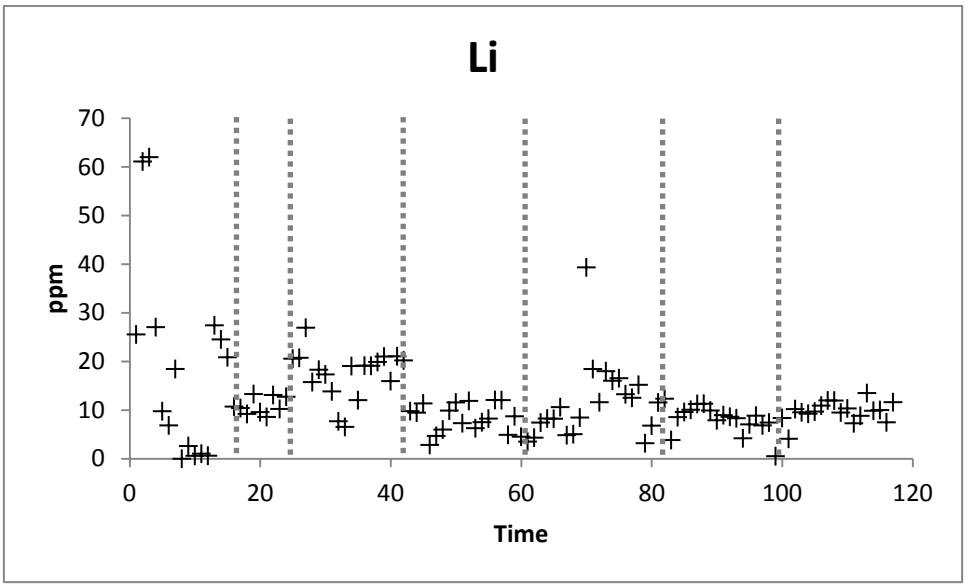

Fig. 3.4.3 Progressive LA-ICP-MS analyses of Li demonstrating a lack of machine-induced drift. Grey bars mark the transition between pegmatite bodies

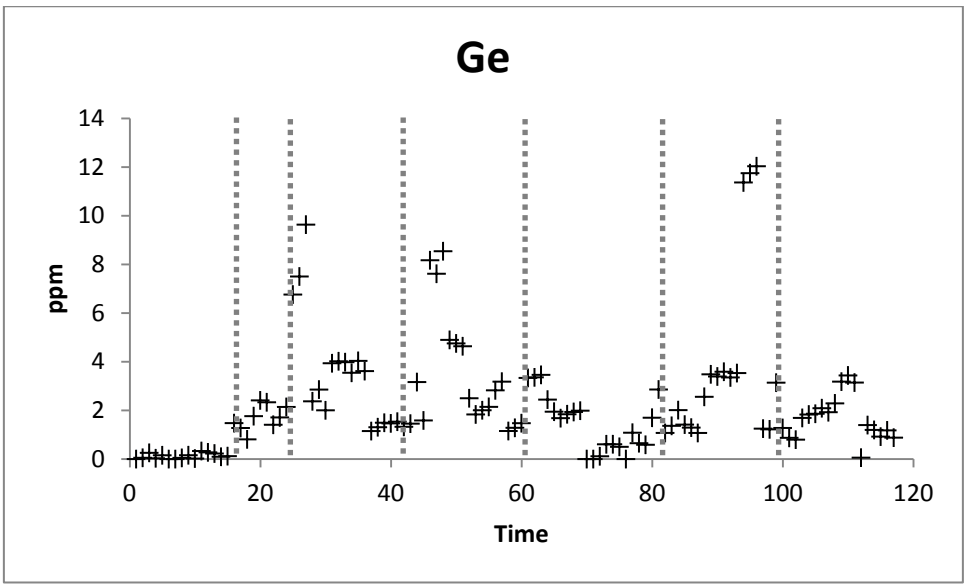

Fig. 3.4.4 Progressive LA-ICP-MS analyses of Ge demonstrating a lack of machine-induced drift. Grey bars mark the transition between pegmatite bodies

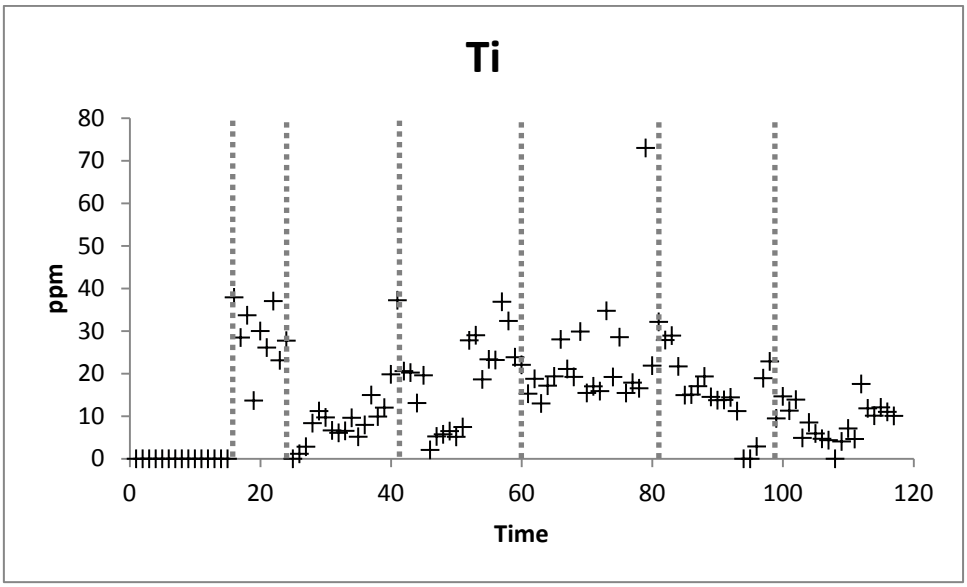

Fig. 3.4.5 Progressive LA-ICP-MS analyses of Ti demonstrating a lack of machine-induced drift. Grey bars mark the transition between pegmatite bodies

Detailed petrographic examination of the polished thick sections prior to analysis coupled with high-resolution optical control during laser ablation allowed the selection of ablation areas free of mineral and fluid micro inclusions. Additionally, the samples were examined by SEM-CL to guarantee the chemical homogeneity of the ablation area. Natural quartz may show small-scale (<500 µm) growth zoning, alteration structures or healed fractures with variable trace element content which are apparent under SEM-CL (e.g. Müller et al., 2008). If these structures lie in the sampling area and are smaller than the ablation

raster, the trace element concentrations of the structures will be averaged. As the same material cannot be ablated twice, duplicates could not be run.

3.4.4 SIMS

For both U-Pb and O isotope investigations, analytical drift was monitored by alternating between the analysis of the sample and standard. For U-Pb dating of zircons, a standard was analysed after every four sample analyses which was reduced to every six analyses for the central bulk of the run, and then returned to every four analyses as the run was due to finish. Error ellipses demonstrating confidence are displayed on the produced isochrones (**Chapter 4.8**). For O isotope determinations in quartz, sample analyses were made in groups of four, with standards run at intervals; seven standard measurements at the initiation, six the second time, and two thereafter.

According to Whitehouse and Nemchin (2009), there are several parameters which can impact the quality of SIMS analyses; in essence these include sample mounting, polishing and sample standard orientation. All sample surfaces are required to be the same height; this was ensured by a stringent polishing regime. Additionally, it is indicated that orientation progressive analyses along the x-axis of the mount is likely to produce better accuracy; Figs. 3.4.6 and 3.4.7 illustrate that this was adhered to. The reason for this is attributed to “differences in centring of the secondary beam in the two directions, as well as possible effects from the electron gun steering coils” (Whitehouse and Nemchin, 2009).

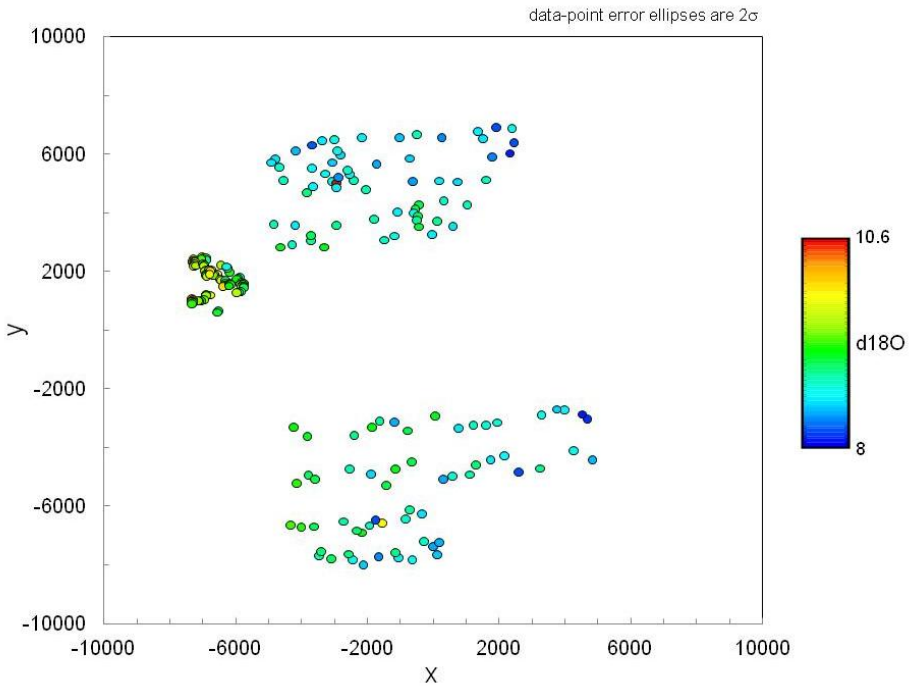

Fig. 3.4.6 Spatial distribution of $\delta^{18}O$ values for the Steli (upper) and Solås pegmatites (standards to left)

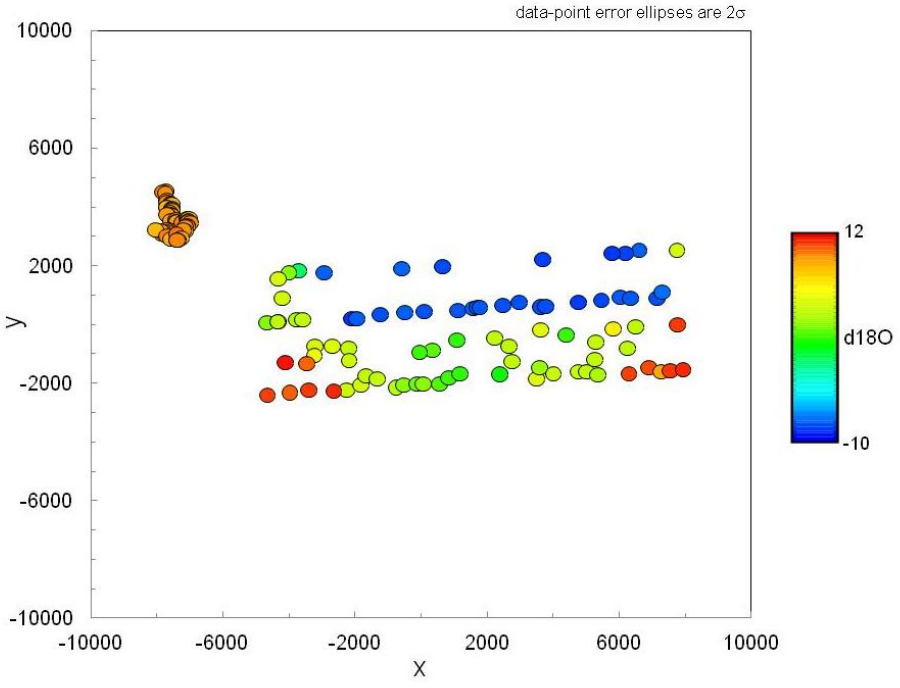

Fig. 3.4.7 Spatial distribution of $\delta^{18}O$ values for the Landsverk 1 quartz crystal base (upper) and tip (lower) (standards to left)

At the time of data acquisition, slight concern was expressed as to the size of the quartz fragments in the mount and the resulting possibility of edge effects. These would result from the block holder, which overlaps the edge of the block

whilst in the ion probe. In particular, it was feared that the upper parts of the Landsverk crystals would be too close to the edge of the block, and therefore the $\delta^{18}O$ values returned would be biased. As such, post-acquisition, the data was assessed for validity. Simply by observing the values produced, it is apparent that $\delta^{18}O$ values are consistent, and indeed often display an expected symmetry (despite several being beyond the suggested 6000 coordinate (Fig. 3.4.6 and 3.4.7). This is supported by comparison to the standard quartz analyses; these standards were taken consistently throughout the analysis series, and show no drift.

This expected symmetry is particularly well displayed in Fig. 3.4.8, which shows the Landsverk 1 material and a graphical representation of $\delta^{18}O$ distribution. It clearly demonstrates how discrete $\delta^{18}O$ populations fall into defined spatial domains which can be correlated exactly with domains defined by CL. Critically, domains at both ends of the section show consistent values, which suggests that edge effects in these analyses are negligible. From comparison with the standard reference material, which has a $\delta^{18}O$ value of 9.50‰ (NBS 28; Hut, 1987), all data is reported with 6% accuracy (0.57 2s.d.).

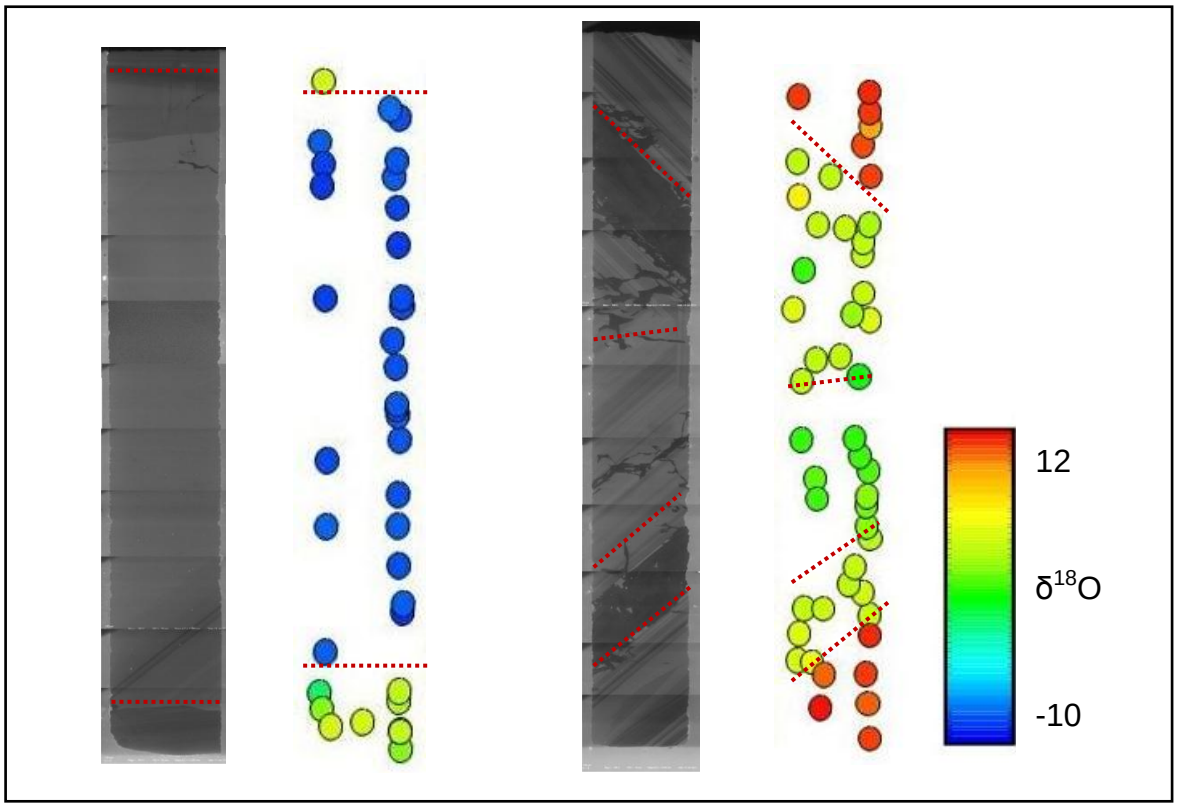

Fig. 3.4.8 Distribution of $\delta^{18}O$ values for the Landsverk 1 quartz crystal base (left) and tip (right)

4. RESULTS

4.1 Field observations; the Evje-Iveland pegmatite field

The Evje-Iveland pegmatites were found to be fundamentally granitic in composition, with principal mineral phases of quartz, plagioclase and K-feldspar. Common minerals include biotite and muscovite in splays and packs respectively, with ubiquitously minor (sub 1%) quantities of magnetite and garnet and a variety of rare metal/REE accessory phases (summarised in Table 4.1.1). The pegmatites are zoned (as classically described by Cameron et al., 1949), with a border zone (up to 0.5 m wide, displaying a fine granitic texture), a megacrystic wall zone (with >3 cm crystals of quartz, plagioclase and biotite), an intermediate zone (typically massive K-feldspar supported by plagioclase) and a core zone (typically pure and massive quartz with crystal sizes of up to several metres). In addition, late-pegmatitic replacement units are observed at Solås and Landsverk 1, characterised by greenish amazonite and bladed cleavelandite splays (a Na-rich variety of albite) overgrowing/replacing existing pegmatite minerals (pinkish microcline and albite respectively) and topaz, spessartine, beryl and tourmaline. These REE-depleted replacement units indicate secondary metasomatic stages.

The pegmatites consist of sheet-like bodies which have a variable but generally shallow dip (excepting Kåbuland and Landsverk 1 which are near vertical), a thickness of 4 to 15 m and a strike length of 10 to 50 m. Host rocks are typically banded basement gneisses, the IGMC or metagabbros (the Flåt diorite; Fig. 2.1.3). Contacts are often sharp and generally concordant with the foliation in the country rocks. The pegmatites show contact reaction aureoles, with the (approximately 3 cm) alteration of amphibole to biotite. However, at Iveland, there is clear evidence that partial melting of the country rocks contributed melts to the pegmatite (see Fig. 4.1.1). Felsic melts locally form pegmatite pockets, with classic zoning of quartz and feldspar intergrowths (border zone), a pure quartz core zone and localised magnetite. The residue from partial melting consists of biotite-rich schlieren.

Table 4.1.1 Summary of magmatic mineral assemblages of the studied pegmatites. C = very common, c = common, r = rare, R = very rare, XR = extremely rare, m = observed microscopically, blank cell = absent, () = uncertain

	Pegmatite						
Mineral	Landsverk 1	Kåbuland	Hovåsen	Slobrekka	Li Gruva	Solås	Steli
			BULK				
K-feldspar	C	C	C	C	C	C	C
Plagioclase	C	C	C	C	C	C	C
Quartz	C	C	C	C	C	C	C
Biotite	C	C	c	C	C	c	C
Muscovite	c	c	C	c	r	c	c
			ACCESSORIES				
Beryl			c	R		c	R
Topaz						R	
Cleavelandite	R					R	
Garnet	R		r	r	r	R	r
Magnetite	c	c	m	r		r	
Ilmenite	c			r		r	
Tourmaline						R	
Sulphide			m	m		m	
			REE MINERALS				
Aeschynite		(R)		XR		XR	
Allanite	m	r		r		r	
Columbite			r			r	R
Euxenite	(XR)	(R)					
Fergusonite	XR	r		XR		R	
Gadolinite				r			
Monazite	R				XR	m	XR
Polycrase	R	r		R	XR	R	
Thorveitite		XR					
Xenotime	m	XR	XR	XR		m	
Zircon	m			m		m	

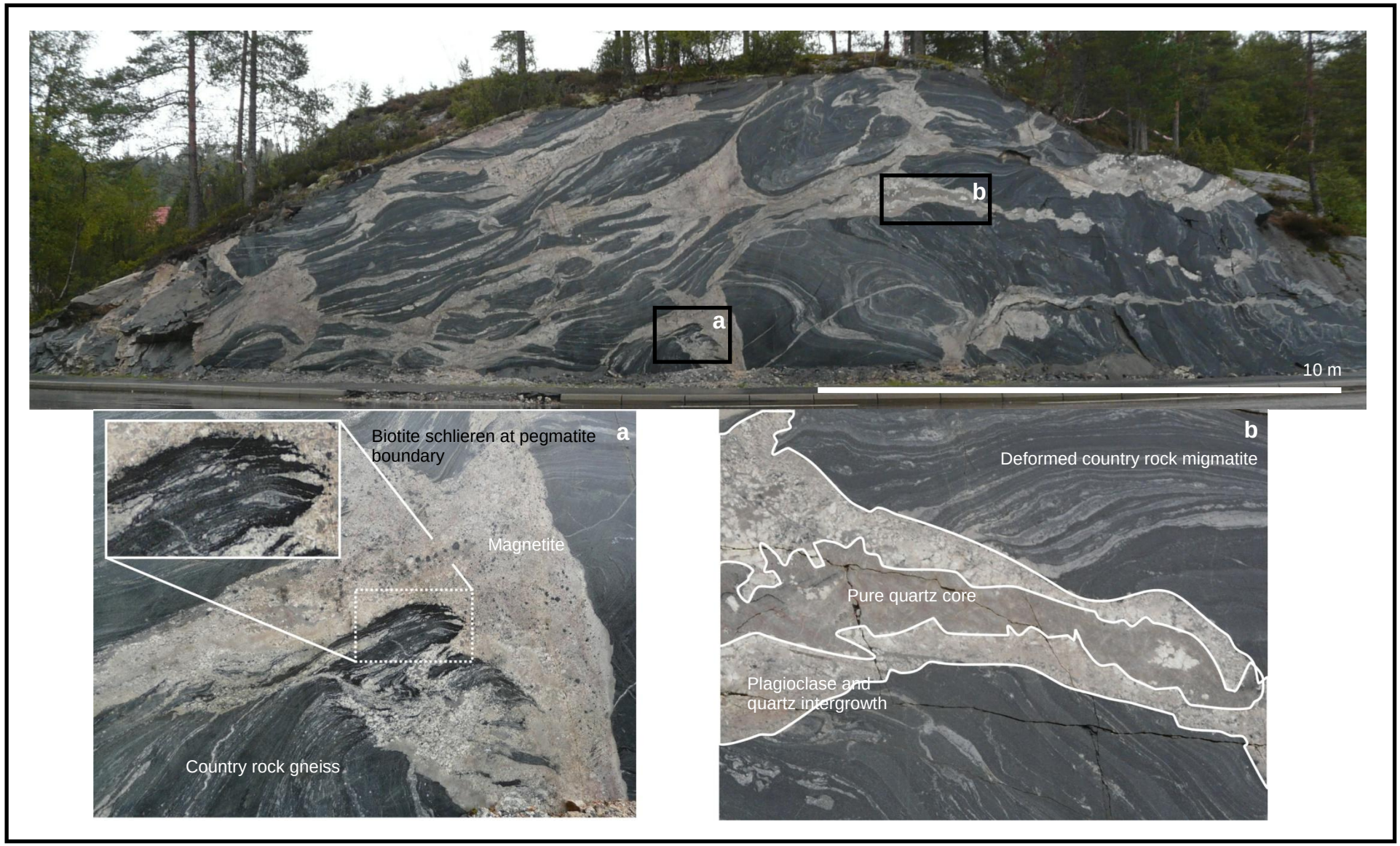

Fig. 4.1.1 Iveland section consisting of country rock gneisses cross cut by pegmatite bodies. Areas **a** and **b** show biotite schlieren and pegmatite morphology respectively

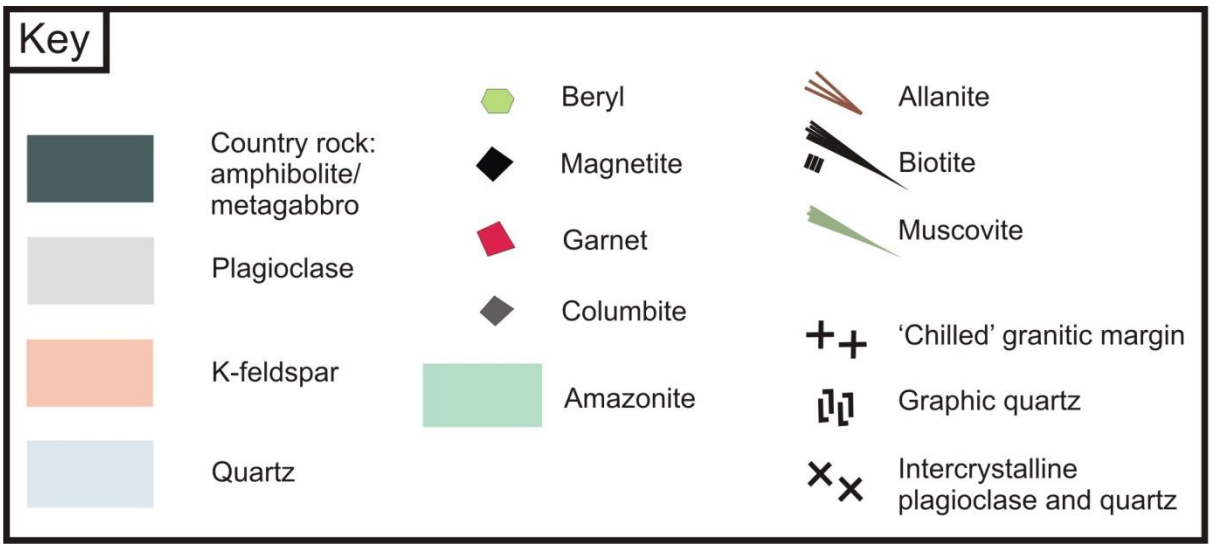

Fig. 4.1.2 Key for the symbols used in subsequent graphics

4.1.1 Landsverk 1

The Landsverk 1 pegmatite crops out over an area of approximately 130 x 40 m in the northern part of the pegmatite field (Figs. 2.1.3 and 4.1.3). Emplaced within the Flåt diorite/meta-gabbro, the internal structure of this 25 m thick pegmatite is difficult to define due to extensive hydrothermal brecciation of large parts of the pegmatite. All primary pegmatite minerals have undergone widespread fracturing and brecciation with subsequent quartz infill. In the brecciated areas, fragments of K-feldspar megacrysts appear to remain chemically unaltered (Fig. 4.1.4). In the south eastern roof of the pegmatite the primary texture of the pegmatite is essentially preserved. Here, K-feldspar forms large megacrysts of up to 3 m, and are associated with 4 m biotite splays (Fig. 4.1.5), which are variably altered to magnetite. Plagioclase masses appear to be spatially coincident to muscovite sheaves. It can be noted that muscovite generally occurs in the centre of the pegmatite, whereas biotite is concentrated in the roof. Mineralogical observations are summarised in Table 4.1.2.

Table 4.1.2 Mineralogical observations of the Landsverk 1 pegmatite

Observed primary mineralogy	Quartz, K-feldspar, plagioclase, biotite, muscovite, fergusonite, monazite, cleavelandite
Macroscopic classification	Hydrothermally overprinted (breccciated) REL-REE allanite-monazite/euxenite with cleavelandite-amazonite replacement units

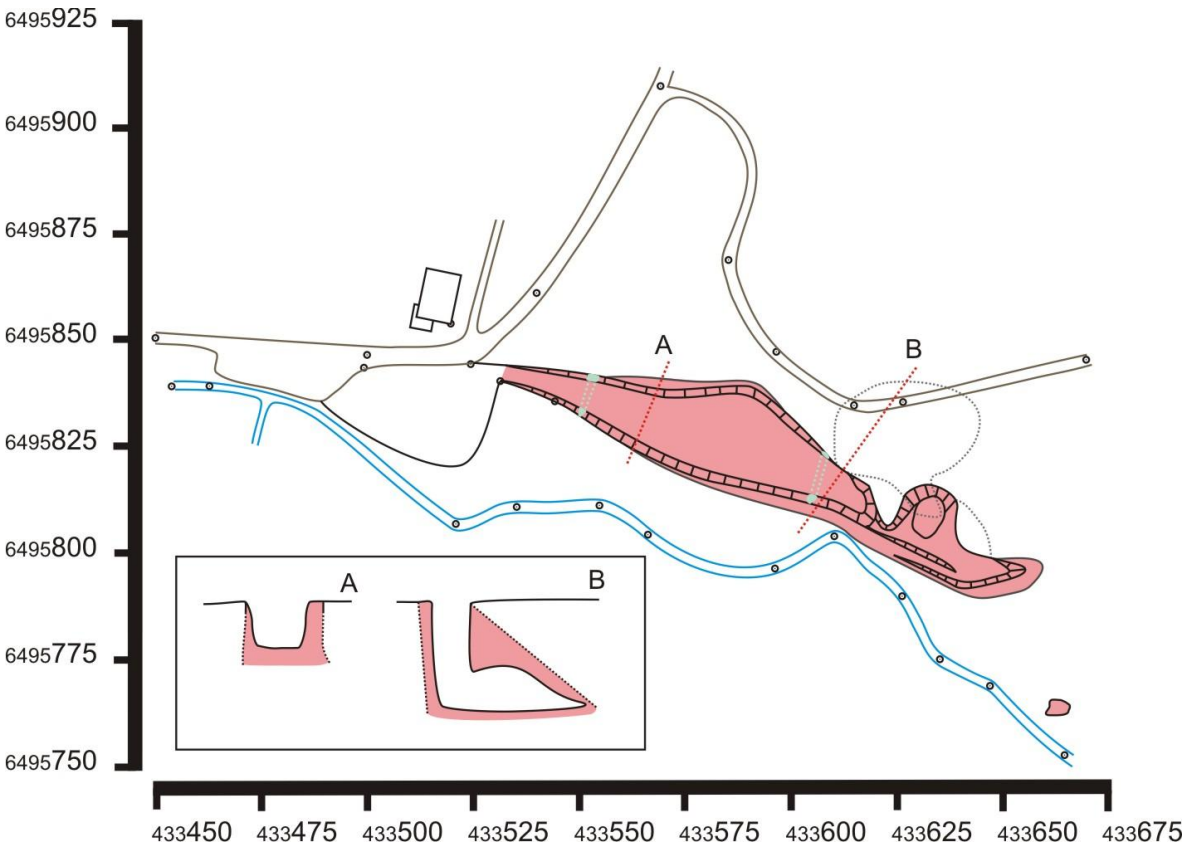

Fig. 4.1.3 Schematic geological map (plan view; easting/northing) of the Landsverk 1 pegmatite (pink areas containing amazonite replacement units in turquoise) and surrounding area (road in brown, stream in blue). Inset are sections along transects A and B. Country rock (Flåt diorite/meta-gabbro) not demarcated

Fig. 4.1.4 Brecciated K-feldspar (pink) healed by late hydrothermal quartz (white)

Fig. 4.1.5 Biotite in the roof of the Landsverk 1 pegmatite; variably replaced by magnetite (pseudomorphs of magnetite after biotite), potentially due to hydrothermal overprinting

The upper part of the pegmatite displays less of an overprint; K-feldspar remains more intact, and hydrothermal quartz is less prevalent. There are two localised zones of amazonite and cleavelandite. Along the contact with the country rock, crystal size is reduced to 10 cm and plagioclase/albite is highly fractured and altered to epidote (for approximately 5 cm). A hydrothermal assemblage (outlined in Fig. 4.1.6 and Table 4.1.3) can be observed, and is typically concentrated in metre-sized cavities. Pyrite and epidote were observed in significant quantities in a 1 m thick quartz vein 200 m to the northwest along pegmatite strike.

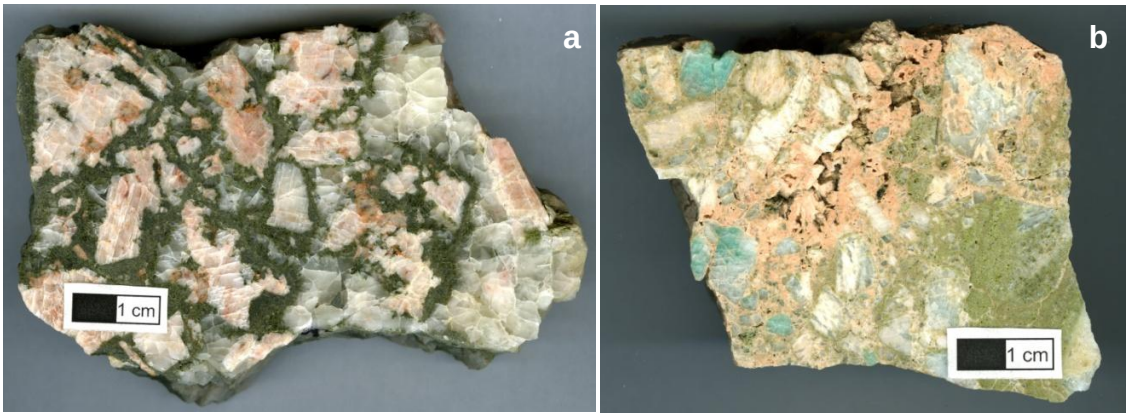

Fig. 4.1.6 Hydrothermal mineral assemblage observed in the Landsverk 1 pegmatite. a) Pink K-feldspar cemented by epidote and milky-grey hydrothermal quartz (dominant on the right). b) Amazonite and white K-feldspar is brecciated and cemented by epidote, quartz and pink albite. The albite appears to represent the final stage of crystallisation

Table 4.1.3 Paragenetic diagram for the hydrothermal assemblage of the Landsverk 1 pegmatite. Relative timing relations were established from mineral textures

Hydrothermal Mineral	Relative timing of crystallisation
Quartz	
Albite	
Pyrite	
Epidote	
Stipnomelan	
Calcite	
Fluorite	
Chlorite	
Quartz (in adularia)	
Black clays	
White clays	
Turquoise gel	
Stibnite	

4.1.2 Kåbuland

Internal dimensions and zoning are not clear within this pegmatite, as it is tabular, steeply dipping to the northeast and the core has been almost entirely excavated. Its approximate area in plan view is 60 x 15 m, with a possible thickness of 15 m (Fig. 4.1.7). The host IGMC is medium grained (0.5 cm crystals), consists of 50% plagioclase and 50% amphibole, lacks foliation and is enriched in biotite at the pegmatite contact due to alteration of amphibole.

The pegmatite itself consists unusually of either pure quartz or plagioclase at the contact, with crystals approximately 5 cm in size before grading into quartz and plagioclase intergrowths with localised graphic quartz. Crystal size increases towards the core which contains 1.5 m masses of quartz and K-feldspar. Biotite appears to be limited to the roof of the pegmatite, and there are localised examples of radial splays in feldspar around black minerals which represent radioactively induced cracks. Mineralogical observations are summarised in Table 4.1.4.

Table 4.1.4 Mineralogical observations of the Kåbuland pegmatite

Observed primary mineralogy	Quartz, K-feldspar, plagioclase, biotite, magnetite, allanite, aeschynite, polycrase, fergusonite, xenotime
Macroscopic classification	REL-REE, allanite-monazite/euxenite

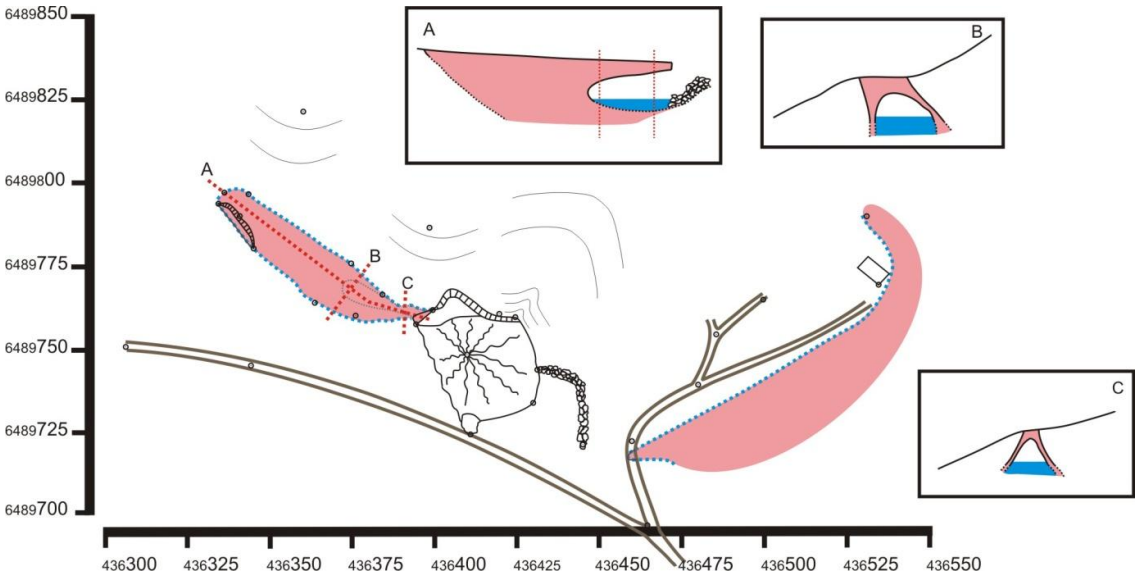

Fig. 4.1.7 Schematic geological map (plan view; easting/northing) of the Kåbuland pegmatite (shown in pink) and surrounding area (road in brown, spoil tip in black, water levels in solid blue). Insets are sections through transects A, B and C. Country rock (Flåt diorite/meta-gabbro) not demarcated

4.1.3 Hovåsen

The Hovåsen pegmatite (see Fig. 2.1.3) is contained within IGMC host rocks which have been locally enriched in biotite and are deformed adjacent to the contact. The pegmatite covers an area in plan view of 100 x 15 m and has a visible thickness of 10 m. It displays a 5 cm border of fine/medium grained

biotite rich granitic facies at the boundary which grades into quartz, plagioclase and biotite intergrowths for 10 cm. This grades into biotite-free quartz and plagioclase for 50 cm before the pegmatite proper begins.

The core is comprised of 3 m quartz masses, typically with smokey rims. Plagioclase phenocrysts up to 1 m in size exist, and often display albite rims; albite also encapsulates 20 cm crystals of beryl. Packs (up to several metres in size) of muscovite (2 cm crystals) are variably associated with colombite crystals of up to 20 cm in length. Locally, fractures and cavities are filled with fine muscovite and drusy quartz respectively. In one part of the lower core, abundant garnets form line rocks with quartz, plagioclase and muscovite. Mineralogical observations are summarised in Table 4.1.5.

Table 4.1.5 Mineralogical observations of the Hovåsen pegmatite

Observed primary mineralogy	Quartz, K-feldspar, plagioclase, biotite, muscovite, garnet, columbite, beryl
Macroscopic classification	MSREL-REE

4.1.4 Slobrekka

The Slobrekka pegmatite (Fig. 4.1.8) which is hosted by amphibolite country rock, covers an area of 200 x 35 m and has a visible thickness of 10 m. The contact is irregular and is variably sharp (where the country rock appears to be more mafic and therefore was possibly more resistant to melting) to gradational (where the country rock is more felsic), with the country rock appearing to be partially melted and assimilated. The pegmatite locally intrudes the country rock with elongate offshoots and stringers variably concordant with the fabric of the country rock (which occasionally displays a deflected cleavage at the contact). Within the pegmatite and adjacent to the contact, a fine (0.5 to 1 cm) granitic borer zone grades into quartz, plagioclase, muscovite and biotite intergrowths, with localised quartz megacrysts, graphic quartz, allanite and magnetite. The progressive zoning is described below. Rare element minerals (allanite, gadolinte and polycrase) tend to form in the upper part of the core. Mineralogical observations are summarised in Table 4.1.6.

Zone 1 – Chaotic intergrowths of 0.3 cm quartz, biotite, plagioclase and K-feldspar. Localised megacrysts (5 cm) of quartz and K-feldspar, with 3 cm biotite, 2 cm euhedral magnetite and minor allanite.

Zone 2 – Irregular but short (1 cm) transition to coarser (1 to 10 cm) quartz and plagioclase. Very localised muscovite.

Zone 3 – Massive 50 cm K-feldspar megacrysts (locally intruded/cracked with quartz infill) with interstitial massive quartz crystals up to 1.5 m in length. Contains limited muscovite and garnet throughout, with one megacrysts of biotite.

Zone 4 – The crystal boundary of the plagioclase is planar, but with an irregular internal zonation of a graphic quartz front. Coarse plagioclase crystals exist within the core, with interstitial quartz, plagioclase and muscovite (and minor garnets). Chaotic quartz and plagioclase intergrowths occur distally.

Table 4.1.6 Mineralogical observations of the Slobrekka pegmatite

Observed primary mineralogy	Quartz, K-feldspar, plagioclase, biotite, muscovite, garnet, magnetite, allanite, gadolinite, polycrase
Macroscopic classification	REL-REE, gadolinite

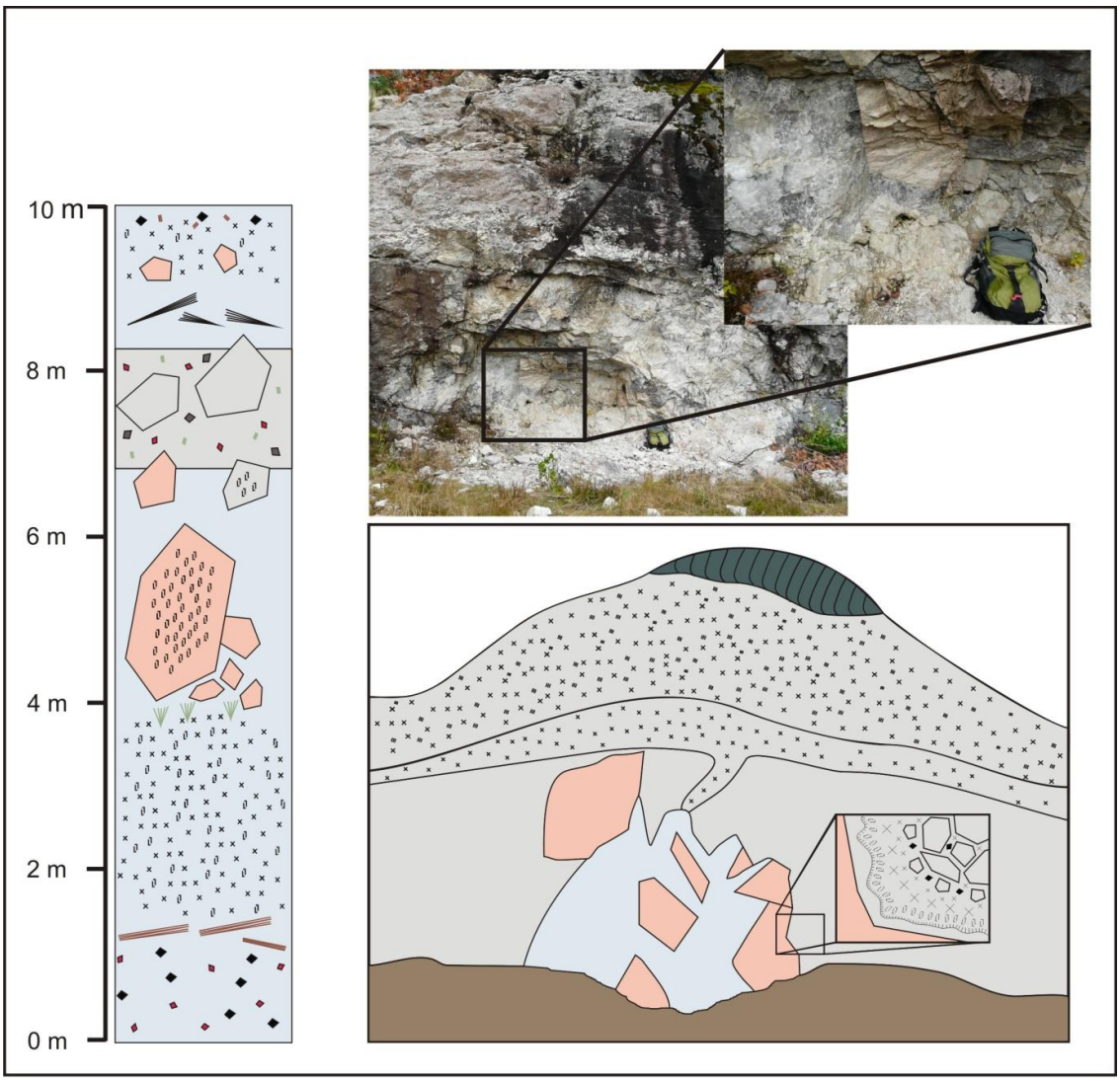

Fig. 4.1.8 Schematic log and section of the Slobrekka pegmatite. The photograph corresponds with the underlying schematic, illustrating a massive quartz core with euhedral pink K-feldspar megacrysts, encased in massive plagioclase/quartz/biotite intergrowths. The profile was taken 50m to the east through the pegmatite 'proper', and shows a quartz dominant mineralogy with a suite of accessory minerals.

4.1.5 Li Gruva

Emplaced in metagabbro, the Li Gruva pegmatite (Fig. 4.1.9) covers an area of 1300 x 200 m, varies in thickness from 15 to 40 m, and appears to dip at a shallow angle towards the west. At the contact in the cupola of the pegmatite (i.e. the centre of the upper dome), there is a metre layer of K-feldspar with graphic quartz. This pinches out distally, and is underlain by a fine quartz and feldspar microgranite facies, which grades into a fine quartz, feldspar and biotite intergrowth zone with localised biotite splays (0.3 m) and 0.2 m K-feldspar megacrysts.

The wall rocks of pegmatites are known to contain unidirectional solidification textures (USTs) which represent magmatic layering; inwardly extended and flared crystals of feldspar and mica (e.g. London, 2008) and stripes or trains of garnet line rocks (e.g. Hönig, 2010). London (2008) suggests that liquidus undercooling (of 150 – 250°C) and nucleation delay, in addition to isothermal subsolidus fractional crystallisation, constitutional zone refinement and far field chemical diffusion, are required for the development of orientated textures and indeed the internal zonation of pegmatites in general (London 2014). Hönig (2010) echoes that undercooling and rapid, multistage non-equilibrium crystallisation from a water saturated melt is necessary for the development of USTs, and qualifies the production of garnet line rocks as a form of magmatic layering which requires the formation of a boundary chemical layer bordering the crystallisation front. Oscillatory crystallisation (the so called 'swinging' of the eutectic) at this boundary causes repeated saturation of essential elements (i.e. Fe and Mn), and hence episodic garnet crystallisation. Li Gruva contains USTs in both the roof (defined by biotite splays; Fig. 4.1.10) and the base (defined by garnet trains; Fig. 4.1.11) of the pegmatite.

Growing into the pegmatite from the upper border zones are 1 – 2 m biotite splays. They cut into a 3 m thick quartz and feldspar zone, which also hosts an apparently massive 1 m thick plagioclase layer. The base of the quartz/feldspar zone appears to have acted as a nucleation front for another series of 3 m biotite splays growing into the core zone, which consists of massive quartz with 5 m masses of upwardly growing K-feldspar. USTs are defined in the base by 0.5 – 8 cm garnet trains, regularly spaced at approximately 20 cm, Mineralogical observations are summarised in Table 4.1.7.

Table 4.1.7 Mineralogical observations of the Li Gruva pegmatite

Observed primary mineralogy	Quartz, K-feldspar, plagioclase, biotite, garnet, monazite, polycrase
Macroscopic classification	REL-REE, euxenite. However, the pegmatite is extremely deficient in REEs, and borders on being part of the abyssal class

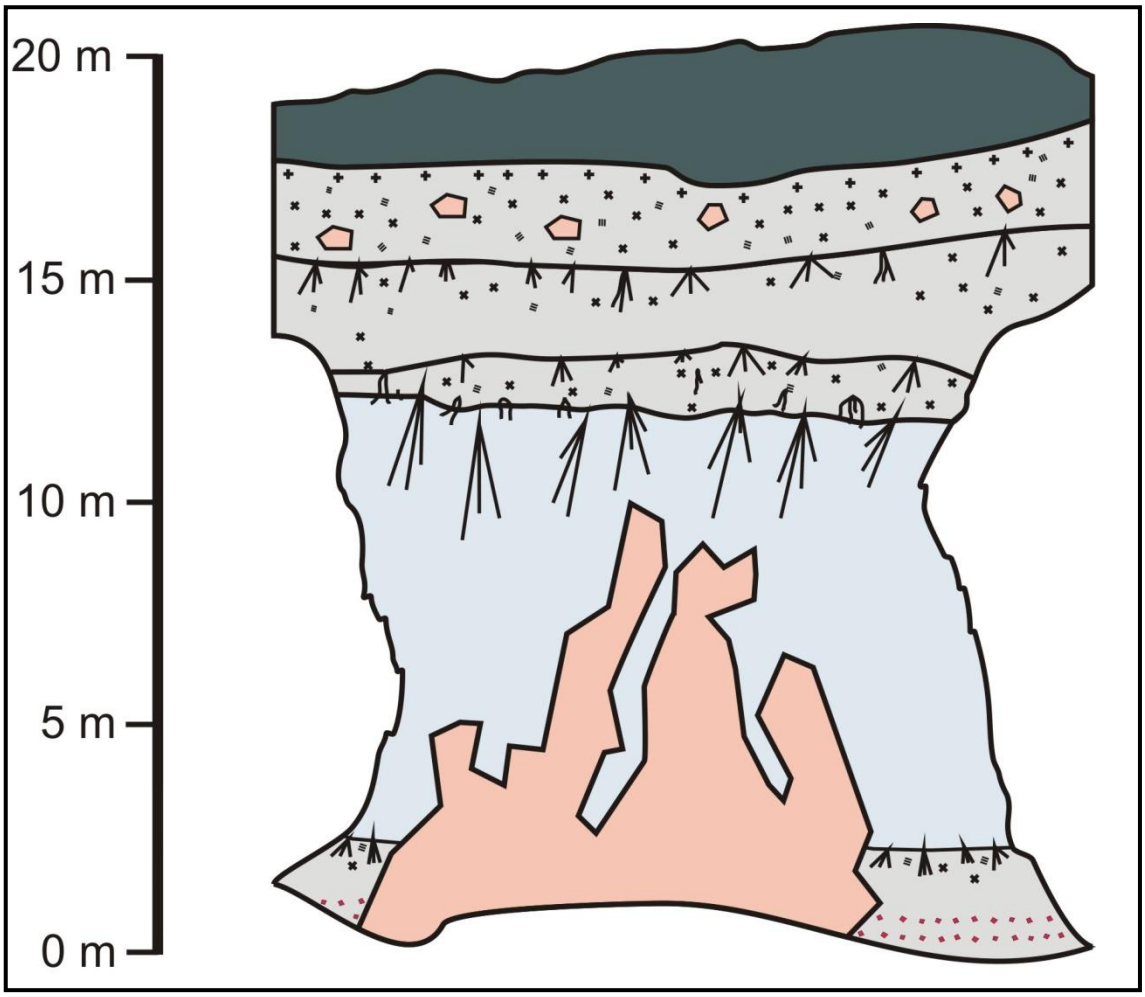

Fig. 4.1.9 Schematic log of the Li Gruva pegmatite, capped by IGMC host rocks (dark green). The roof of the pegmatite contains a granitic facies grading into coarsely intergrown plagioclase, quartz and biotite. Below this are several layers of biotite-rich pegmatite with comb-textures (unidirectional solidification textures) meaning that the crystal growth direction was away i.e. down from the upper contact. The core is composed of massive quartz and idiomorphic K-feldspar. Garnet and biotite line rocks in the base of the pegmatite are represented schematically, and are accurately represented in Fig. 4.4.11

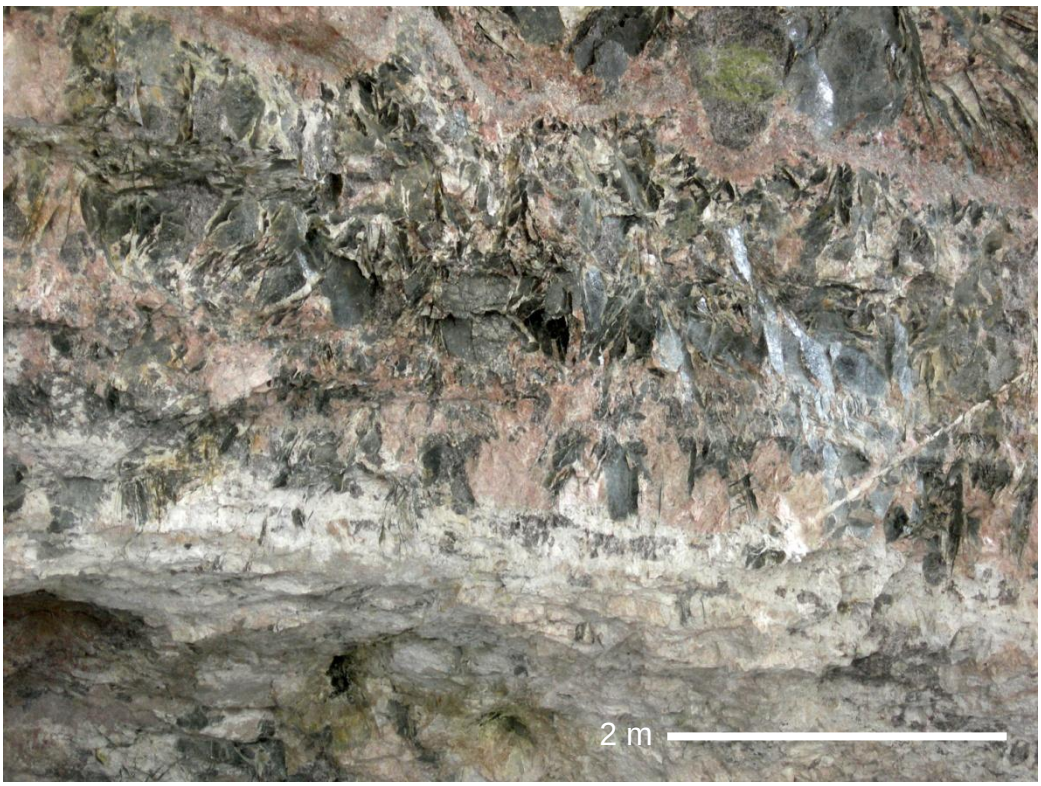

Fig. 4.1.10 Line rock in the roof of Li Gruva

Fig. 4.1.11 Line rock at the base of Li Gruva (from Müller et al., 2012). The UST is defined by layers of garnet which either abut or continue beneath K-feldspar megacrysts

4.1.6 Solås

This pegmatite (see Fig. 4.1.12) comprises a 5 m thick body which covers an area of 200 x 15 m in plan view, with an overlying (approximately 10 m above) concordant secondary pegmatite body which is 1.5 m thick and covers an area of 80 x 10 m. The country rock is foliated IGMC (with approximately equal proportions of amphibole, biotite and plagioclase). The contact between the pegmatite and metagabbro is relatively sharp; 5 cm of fine quartz, feldspar and biotite irregular intergrowths occur into the pegmatite, with 2 cm of biotite-enrichment within the host.

Allanite and garnets occur towards the base of the pegmatite, growing generally upwards (in some cases, allanite grows through garnet crystals), with magnetite, minor polycrase and increasing K-feldspar in the lower intermediate zone. In the base of the core is an amazonite/cleavelandite zone, with associated garnets, beryls and topaz. Overlying this are metre-sized K-feldspar and plagioclase masses with muscovite, which reduce in size in an upper region of quartz, feldspar and biotite intergrowths with biotite splays. The pegmatite is capped by the ubiquitous granite (0.5 to 1.5 cm crystals) facies. Mineralogical observations are summarised in Table 4.1.8.

Table 4.1.8 Mineralogical observations of the Solås pegmatite

Observed primary mineralogy	Quartz, K-feldspar, plagioclase, cleavelandite, amazonite, biotite, muscovite, garnet, beryl, topaz, allanite, colombite, polycrase, fergusonite, aeschynite
Macroscopic classification	REL-REE, allanite-monazite with amazonite and cleavelandite replacement units

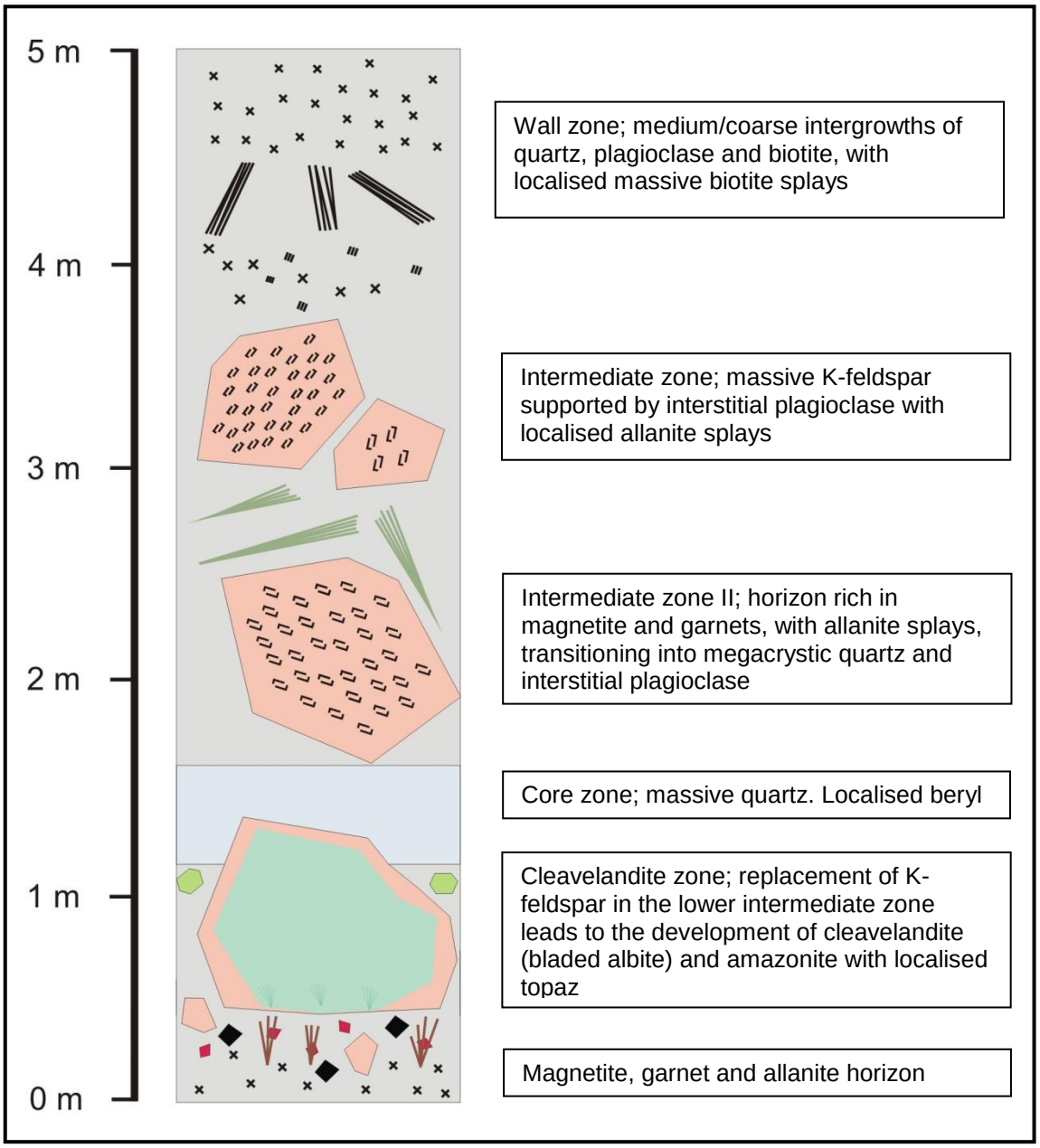

Fig. 4.1.12 Schematic log of the Solås pegmatite

4.1.7 Steli

The Steli pegmatite (Fig. 4.1.13) is approximately 100 x 20 m in plan view, 5 m thick and tabular, intruding banded meta-gabbro/gneiss. The body is more vertically symmetrical than the other pegmatites under investigation, with upper and lower border facies of microgranite (0.5 cm crystals), approximately 0.5 m thick, grading into coarser quartz, feldspar and biotite intergrowths (0.5 m thick zone).

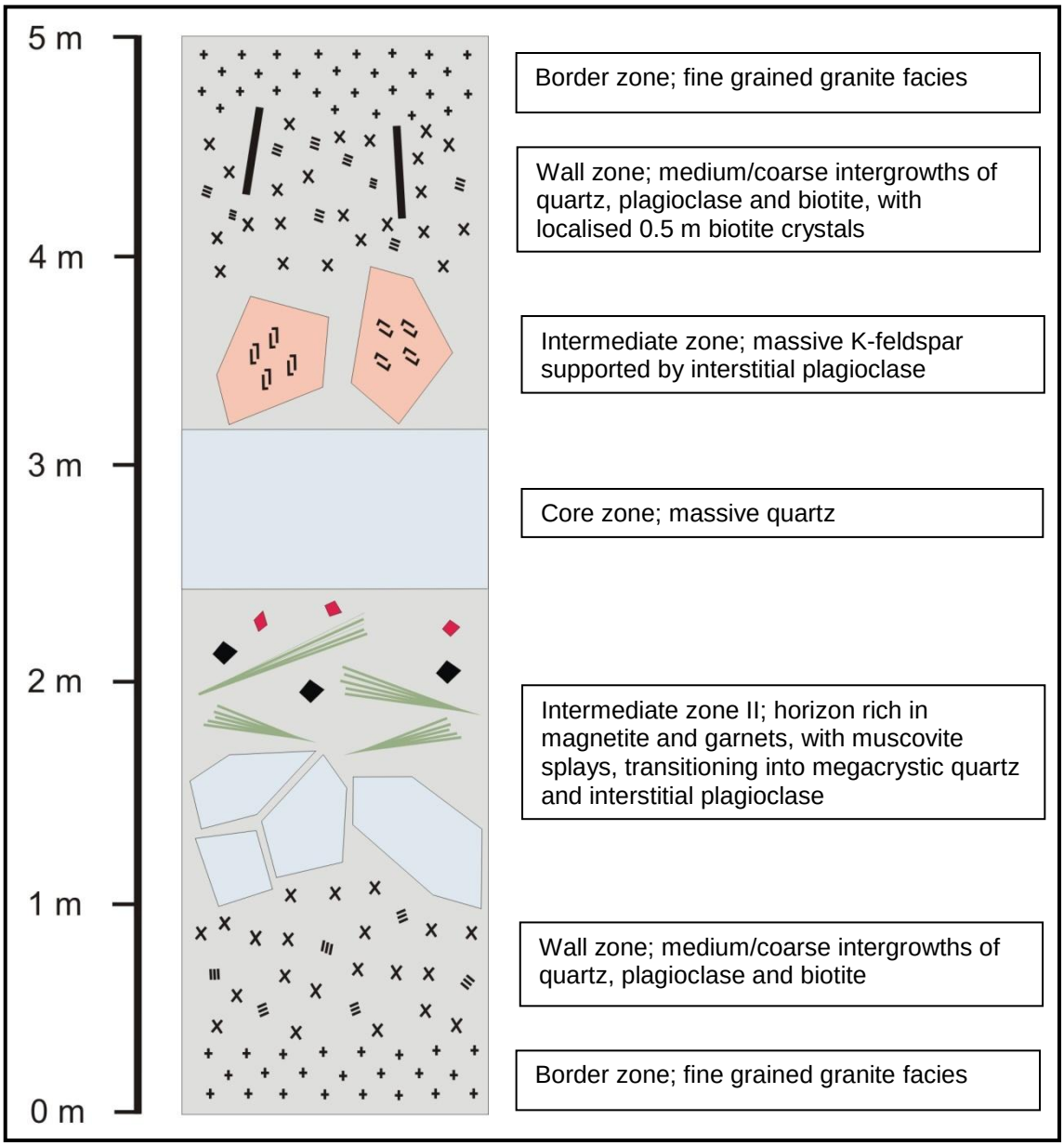

Fig. 4.1.13 Schematic log of the Steli pegmatite

The core is composed of massive quartz with 1 m sized packs of muscovite, bounded above by K-feldspar. Magnetite occurs locally in conjunction with garnets (which appear to form in late stage veins). Beryl, colombite and monazite occur in the east and south of the pegmatite respectively, defining distinct mineral zones (beryl has only been described historically, occurring in the eastern bottom of the pegmatite when the mine was active (no longer exposed) (Axel Müller, pers. comm., 2011)). 0.5 m biotite crystals occur in the upper wall zone. Mineralogical observations are summarised in Table 4.1.9.

Table 4.1.9 Mineralogical observations of the Steli pegmatite

Observed primary mineralogy	Quartz, K-feldspar, plagioclase, muscovite, magnetite, garnet, columbite.
Macroscopic classification	REL-REE, allanite-monazite with transition to MSREL-REE

4.1.8 Iveland

The Iveland pegmatite(s) (Fig. 4.1.1) are exposed in a road cut, and as such estimations of their size are difficult. From field evidence, the pegmatites appear to have been emplaced within a ductile environment, with the country rock gneisses directly contributing melts to the pegmatites. The pegmatites consist of a series of variably connected lenses ranging in size from 10 cm to 3 m, which generally show little mineralogical variation. The larger apophyses demonstrate typical pegmatite morphology, with a massive quartz core and a border zone of intergrown plagioclase and quartz; it is this material which makes up the majority of the pegmatite. Magnetite crystals are present locally, interstitial to the quartz and plagioclase in the intergrowth border zone.

The pegmatite/country rock contact is undulose, with either discordant or concordant contact relationships. Locally, where country rock has partially melted, thermally resistant Fe-bearing minerals, including biotite schlieren have remained. Mineralogical observations are summarised in Table 4.1.9.

Table 4.1.10 Mineralogical observations of the Iveland pegmatite

Observed primary mineralogy	Quartz, plagioclase, magnetite (biotite restite)
Macroscopic classification	Not attempted (and hence not included in table **4.1.1**) due to lack of characteristic minerals

4.2 Field observations; the Landsverk pegmatites

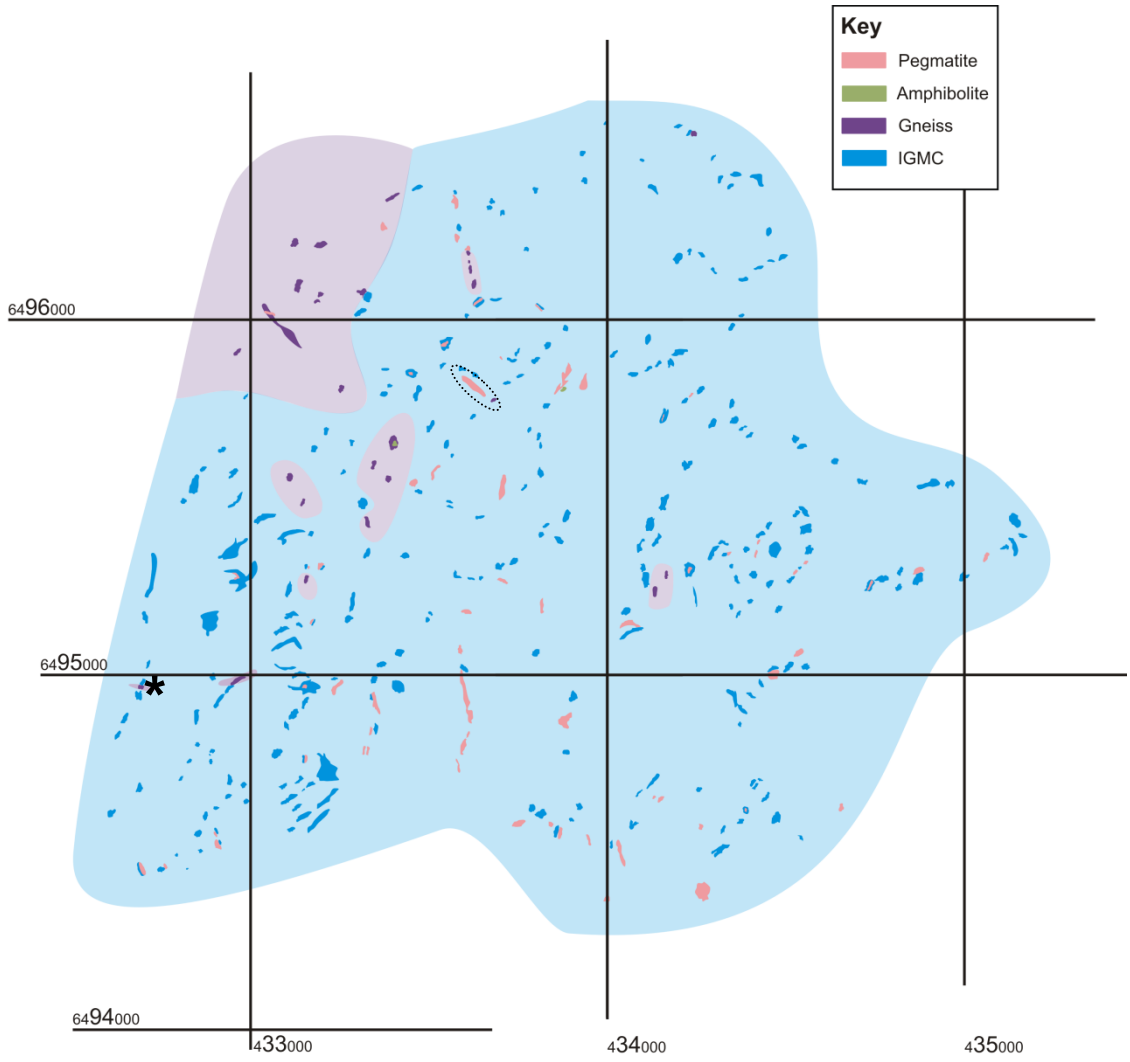

Fig. 4.2.1 Geological map of the Landsverk 1 region (see Fig. 2.1.3).Observed outcrop is in solid colour, inferred geology is shown as a transparent overlay. The Landsverk 1 pegmatite is ringed in dashed black. Asterisk marks location of Fig. 4.2.6. Gridlines are 1 km square

A large number of pegmatite bodies were observed (Fig. 4.2.1), varying in size from 1 x 1 m pods to 70 x 40 m lenses. Orientation varied, with several bodies striking NE-SW, and other bodies (including Landsverk 1) and a large number of quartz veins striking NW-SE to NNW-SSE and dipping to the east. A 1.5 m thick quartz vein orientated 161/54 E 300 m east of Landsverk 1 was seen to contain pyrite and epidote; members of the hydrothermal mineral suite representative of overprinting at Landsverk 1. This adds credence to the concept that a late stage event is responsible for the structures orientated

NNW-SSE. This orientation of NNW-SSE with a variable dip to the east can be observed in the metamorphic foliation of the limited gneiss exposures.

Pegmatite composition is relatively primitive, with quartz and plagioclase as the primary components with localised K-feldspar megacrysts. The quartz and plagioclase was typically present as medium grained interlocking crystalline masses, and occasionally as graphic intergrowths within K-feldspar. The texture and mineralogy of the poorly exposed pegmatites was consistently comparable with that of the wall/intermediate zones of better exposed pegmatites (both within and outside of the Landsverk 1 area), suggesting that massive cores are probably present. Quartz was however observed as wide lenticular veins and pod-like masses within the medium crystalline quartz-feldspar groundmass, and this is the material typically sampled for assessment of quartz purity. Micas were not common, particularly in the smaller pegmatites, and rare magnetite was the only accessory mineral identified.

The pegmatites appeared to be unaffected by secondary recrystallisation events; primary pegmatite structures were identifiable, with visible megacrystic zones appearing intact (unlike those demonstrated in Figs. 4.1.4 and 4.1.6). However, localised examples of quartz masses appeared to be quite saccaroidal upon sampling and, in one instance, the intermediate zone adjacent to the mass appeared to be quartz deficient. Whether this is a function of weathering or incomplete dissolution, remobilisation and recrystallisation is unclear, but the orientation of the pegmatite appears to be NNW-SSE i.e. the same orientation as that of the structures which may be representative of a recrystallisation event (Landsverk 1 and the pyrite epidote vein).

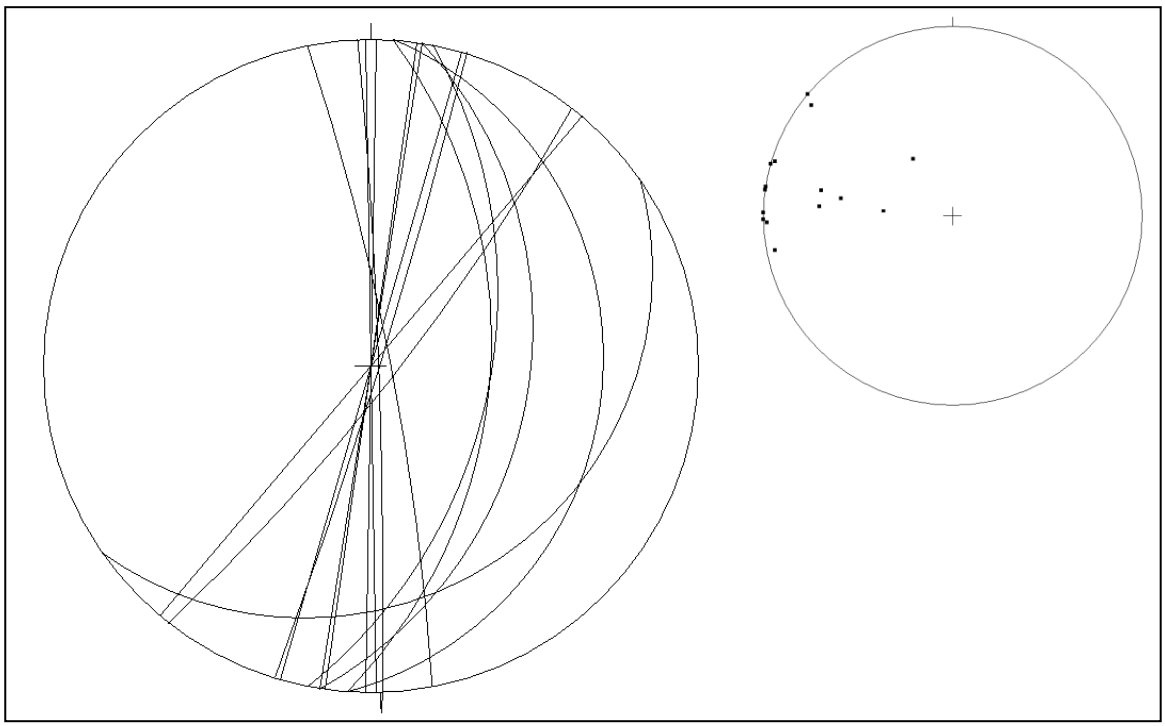

Fig. 4.2.2 Stereographic projection of orientations in gneisses from the Landsverk mapping area (planes, with summary poles)

The vast majority of gneissic banding in the mapping area (Fig. 4.2.2) is orientated NNE-SSW, dipping steeply to the east. This correlates closely with the oldest phase of deformation observed in the field (depicted in Fig. 4.2.6) which was initially interpreted as representing the Adger phase of the Sveconorwegian orogeny (Bingen et al., 2008b). The Adger phase initiated at 1050 Ma, with principal activity from 1035 to 980 Ma. The Fennefoss Augen gneiss has been dated variably to 1031±2 Ma (Pedersen and Konnerup-Madsen, 2000), 1035 Ma (Bingen, 1998) and 1026±26 Ma (Pedersen, 1981); the orientation of the principal banding in the gneisses and the oldest phase of deformation likely result from this deformation event.

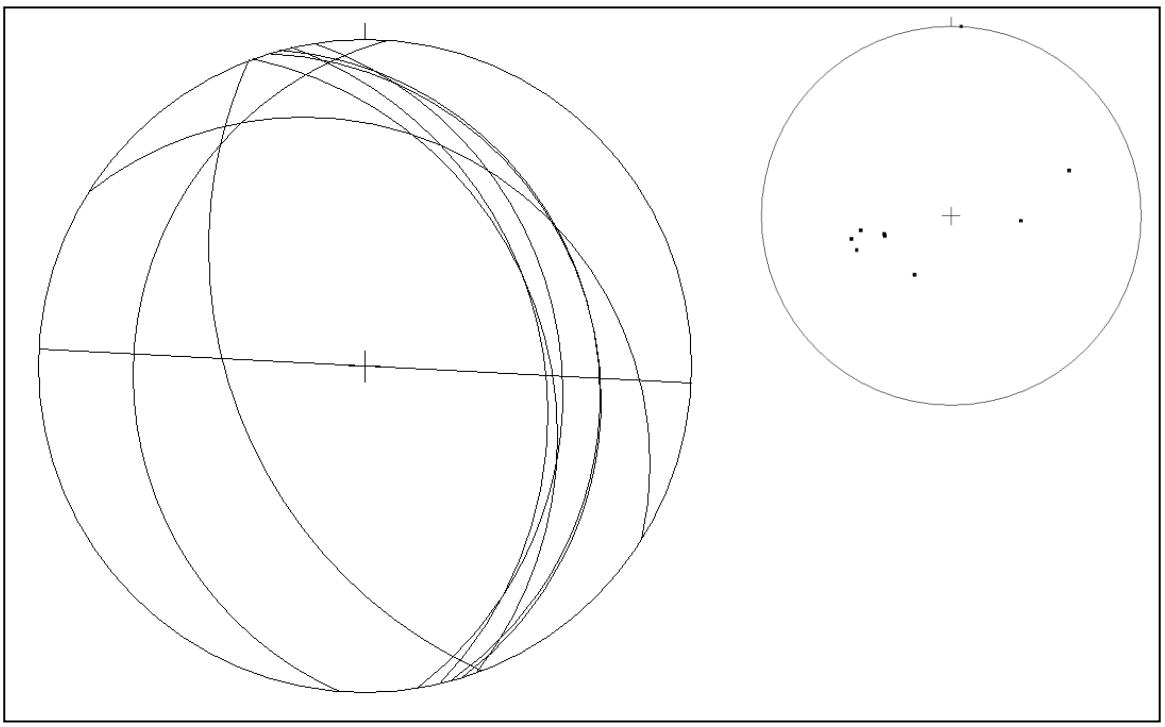

Fig. 4.2.3 Stereographic projection of measurable pegmatite bodies from the Landsverk mapping area (planes, with summary poles)

Almost all the pegmatites within the mapping area (Fig. 4.2.3) strike NNW-SSE, which corresponds with the youngest phase of deformation identified in Fig. 4.2.6; the implication is that the pegmatites represent the final phase of deformation in the region. NW-SW contraction/E-W extension occurred during the latter stages of the Dalane phase (970 – 900 Ma; Bingen et al., 2008b), which pre-dated and was synchronous with suggested ages of pegmatite emplacement; it is likely that the structures resulting from Dalane phase deformation acted as pathways for late stage fluids/pegmatite melts.

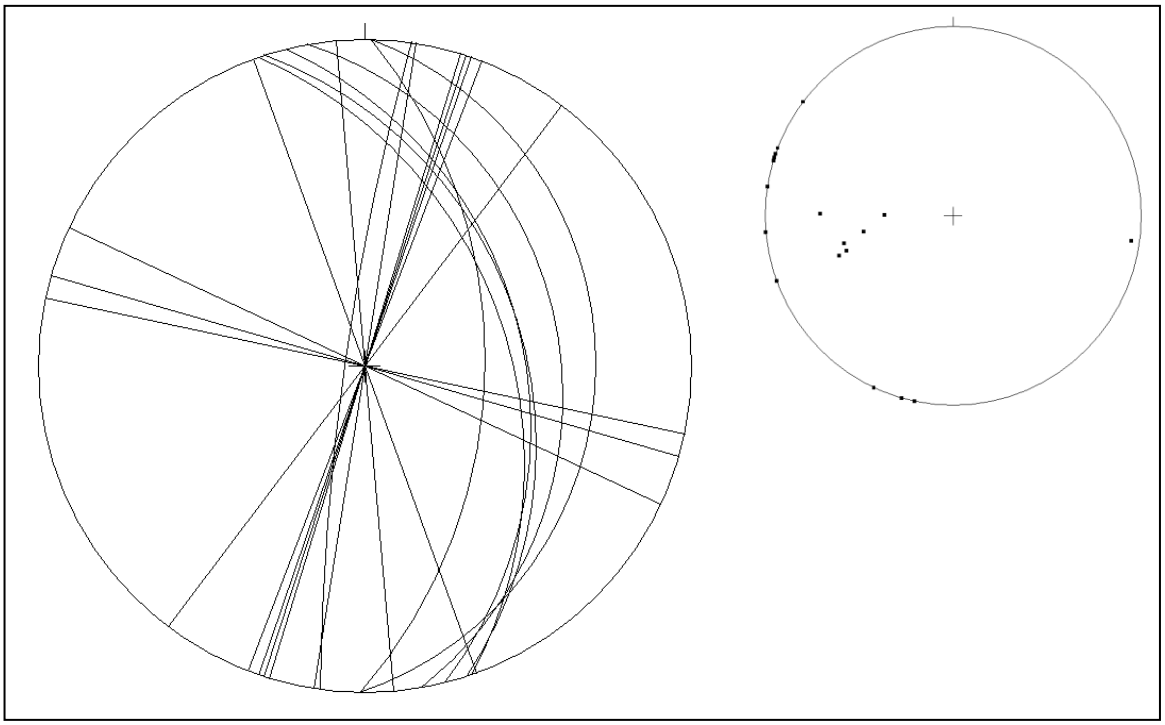

Fig. 4.2.4 Stereographic projection of veins from the Landsverk mapping area (planes, with summary poles)

There are 2 principle groups of veins in the Landsverk mapping area (Fig. 4.2.4); those orientated NNE-SSW dipping near-vertical, those orientated NNW-SSE and dipping east. NNE-SSW veins (despite dipping steeply) correlate closely with the fabric defined by gneisses in the region (Fig. 4.2.2). The difference in dip may be a function of exposure; apparently vertical structures may change at depth. It is likely that early hydrothermal fluids utilised these initial Agder phase structures as the only available pathways. NNW-SSE east-dipping veins correlate closely with the orientations of several pegmatites within the mapping area (Fig. 4.2.3). Late hydrothermal fluids/pegmatite melts probably utilised the recently formed (and therefore unfilled) discontinuities produced in the Dalane phase.

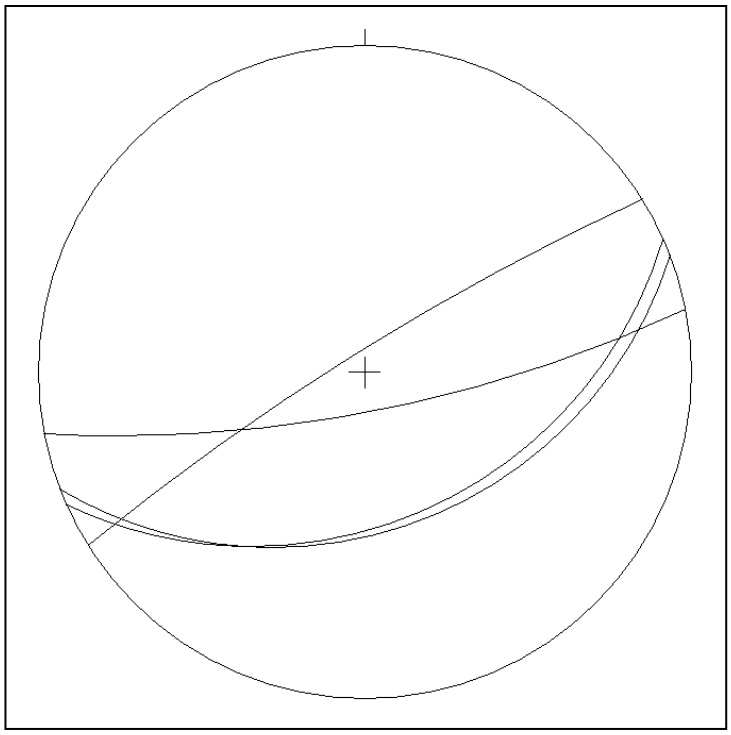

Fig. 4.2.5 Stereographic projection of joints from the Landsverk mapping area (planes)

There are limited examples of unmineralised discontinuities in the mapping area (Fig. 4.2.5); those that are observed strike approximately ENE-WSW and tend to dip steeply to the SE. The fact that they are not infilled by either hydrothermal minerals or pegmatite suggests that they post-date Sveconorwegian magmatism, and may represent extension during crustal relaxation.

From a single exposure (indicated on Fig. 4.2.1), a relative chronology for the region's structures can be suggested (Fig. 4.2.6). The oldest phase (**a**) is orientated NNE-SSW, suggesting NNE-SSW contraction or WNW-ESE extension. The structure may represent reidal shears associated with sinistral shearing during the Agder phase, 1050 – 980 Ma, which caused high pressure amphibolite metamorphism (Bingen et al., 2008; these may be evidenced by the localised examples of amphibolites exposed). This structure is post dated by a NE-SW structure (**b**), indicating NE-SW contraction or NW-SE extension, and may represent riedal shears associated with sinistral shearing during the Falkenberg phase, 980-970 Ma. These structures are most likely related to the Kristiansand-Porsgrunn Shear Zone, which dips to the southeast and is interpreted as a Sveconorwegian thrust zone reworked as an extensional detachment (Bingen et al., 2008). This thrusting has been associated with NW-

verging folds; the shears and fold hinges produced in this regime may act as pathways necessary for melt movement. The final observable phase (**c**) is orientated NNW-SSE, suggesting NNW-SSE contraction or ENE-WSW extension, and likely representing NW-SE contraction during the Dalane phase, 970 – 940 Ma. The fabrics observed as the latest phase may be representative of part of the gneiss dome generated during voluminous post-collisional magmatism (Bingen et al., 2008).

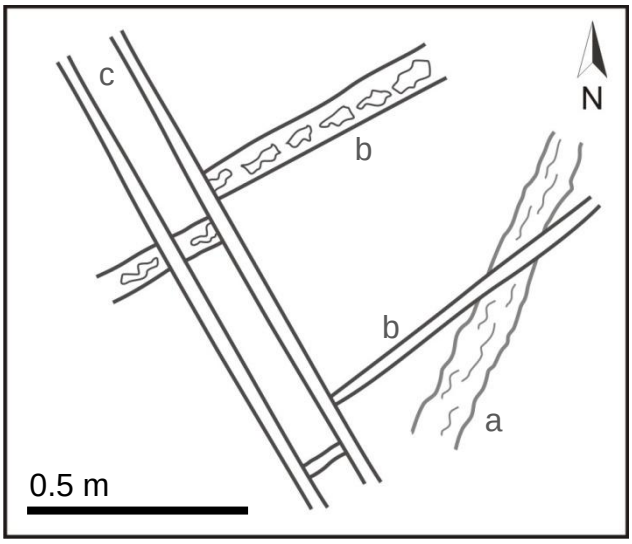

Fig. 4.2.6 Structural relationships in the Landsverk 1 mapping area, as indicated by meta-gabbro hosted granitic veins. **a** is a slightly altered and deformed fine grained granitic sheet, **b** a pegmatite sheet and **c** a quartz vein. Younging occurs from the meta-gabbro, to **a**, to **b**, to **c**

4.3 Whole-rock geochemistry

4.3.1 Major element geochemistry

The chemical composition and variation of the Evje-Iveland pegmatites was assessed in a variety of ways. Due to their very coarse crystal size, it is difficult to obtain a representative and volumetrically manageable sample. As a result, the method chosen was to sample the granitic border zone facies found at the periphery of the pegmatites. The assumption was made that this fine grained (0.5 – 1 cm) border zone represents the composition of the initial pegmatite melt. Figs. 4.3.1, 4.3.2 and 4.3.3 display whole rock data for all pegmatites, country rocks and granites studied, obtained by ICP-AES data (reported in APPENDIX 2).

In the pegmatites (Fig. 4.3.1) the following trends are demonstrated: an inversely proportional relationship between SiO_2 and Al_2O_3; a positive trend between Fe_2O_3 and TiO_2 (with Fe_2O_3 approximately an order of magnitude greater than TiO_2); little correlation between Na_2O and P_2O_5; positive correlation between Na_2O and CaO, with both negatively correlated with K_2O; MgO shows poor correlation with other plotted elements.

The country rocks (Fig. 4.3.2) are typically lacking in geochemical trends, but do display some correlation between Fe_2O_3 and TiO_2 (with Fe_2O_3 approximately twice as abundant as TiO_2), K_2O with P_2O_5 and MgO with CaO. Na_2O is generally consistent between all samples. The Høvringsvatnet granites (Fig. 4.3.3) show strong correlation between Fe_2O_3, MgO, CaO, TiO_2 and P_2O_5, and between SiO_2 and K_2O. Na_2O is consistent between all samples. In the medium grained syenomonzonite, a decrease in SiO_2 corresponds with an increase in Fe_2O_3, MgO, CaO, TiO_2 and P_2O_5.

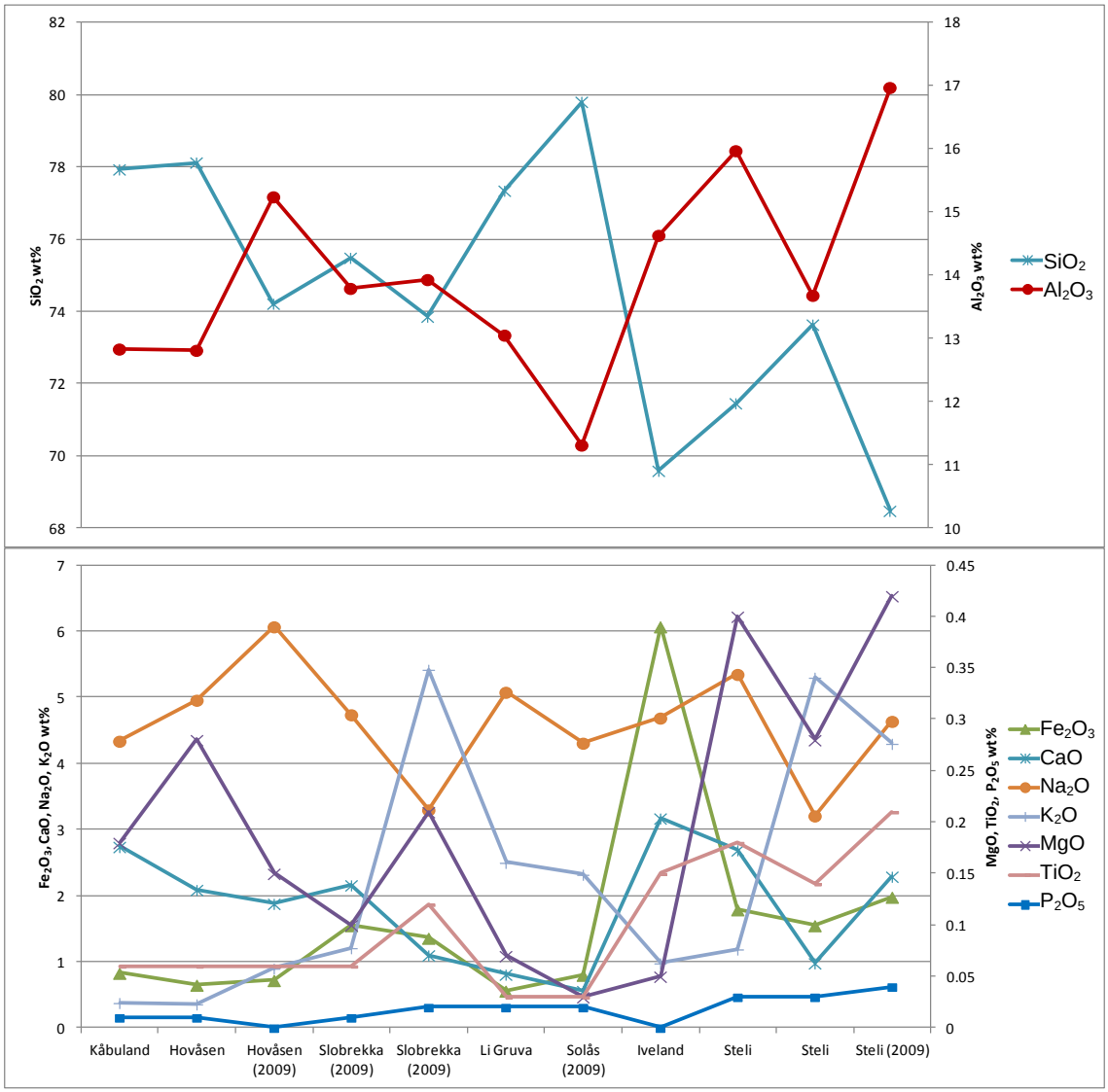

Fig. 4.3.1 Spider diagram showing whole rock compositions of pegmatites, based on ICP-AES data

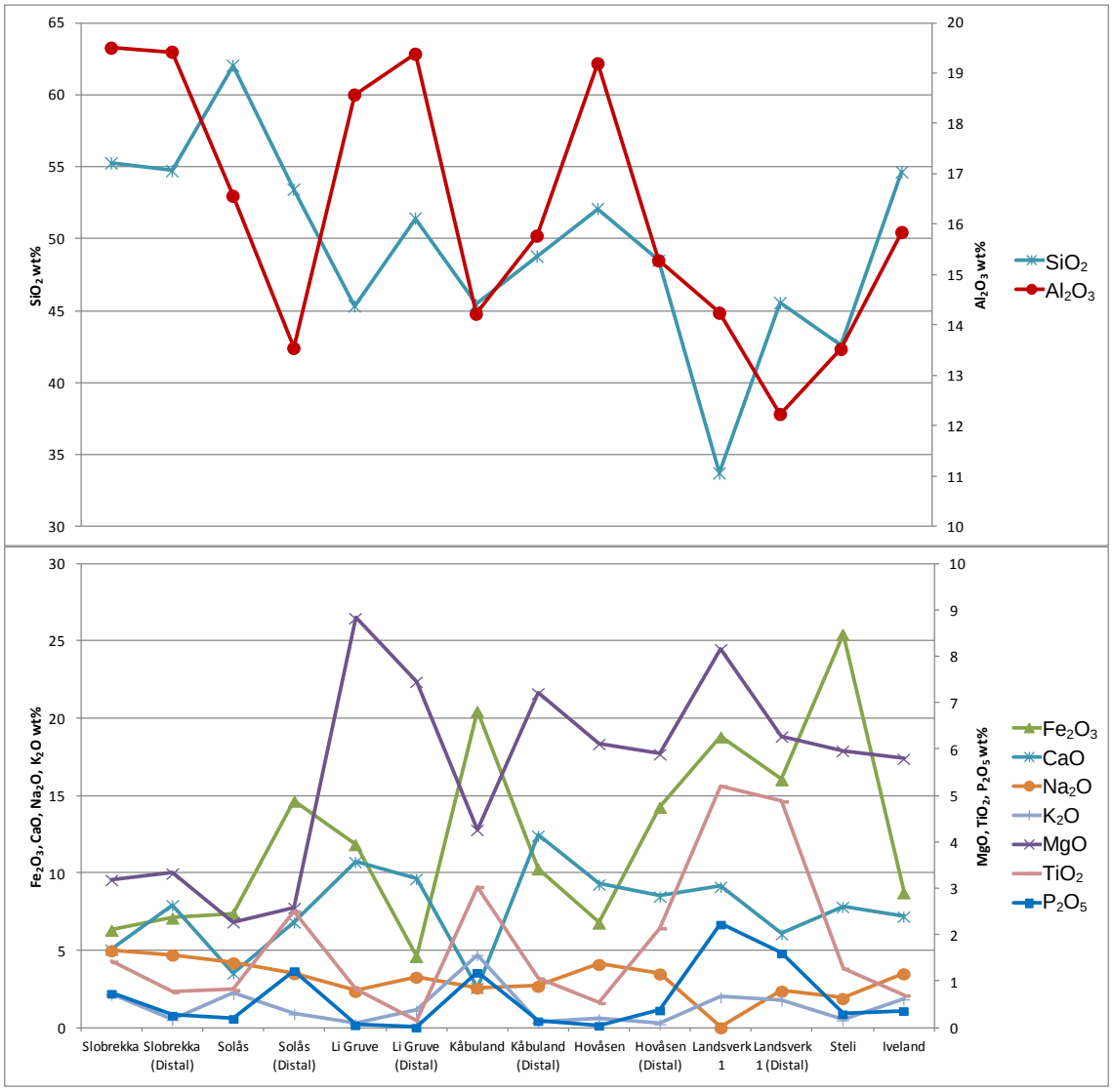

Fig. 4.3.2 Spider diagram showing whole rock compositions of pegmatite country rock, based on ICP-AES data

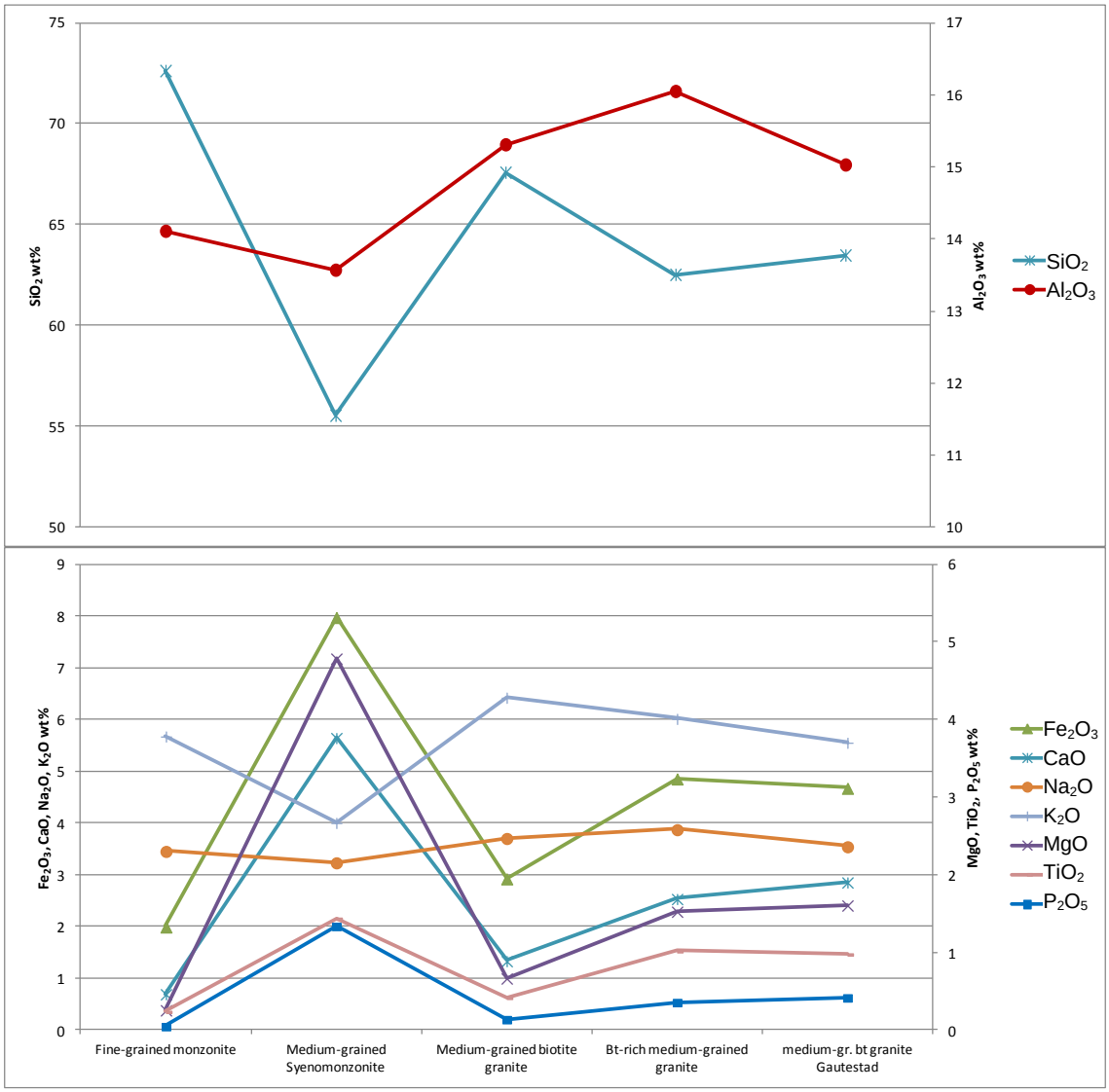

Fig. 4.3.3 Spider diagram showing whole rock compositions of Høvringsvatnet granite, based on ICP-AES data

Due to the dominance of SiO_2 in the geochemical compositions of the Evje-Iveland samples, traditional Harker diagrams are unsuitable due to the effect of 'closure' i.e. the introduction of false trends as a result of one constituent making up over half of the composition (Johansson and Wold, 1984; Rollinson, 1993). As such, elements are plotted against Fe_2O_3.

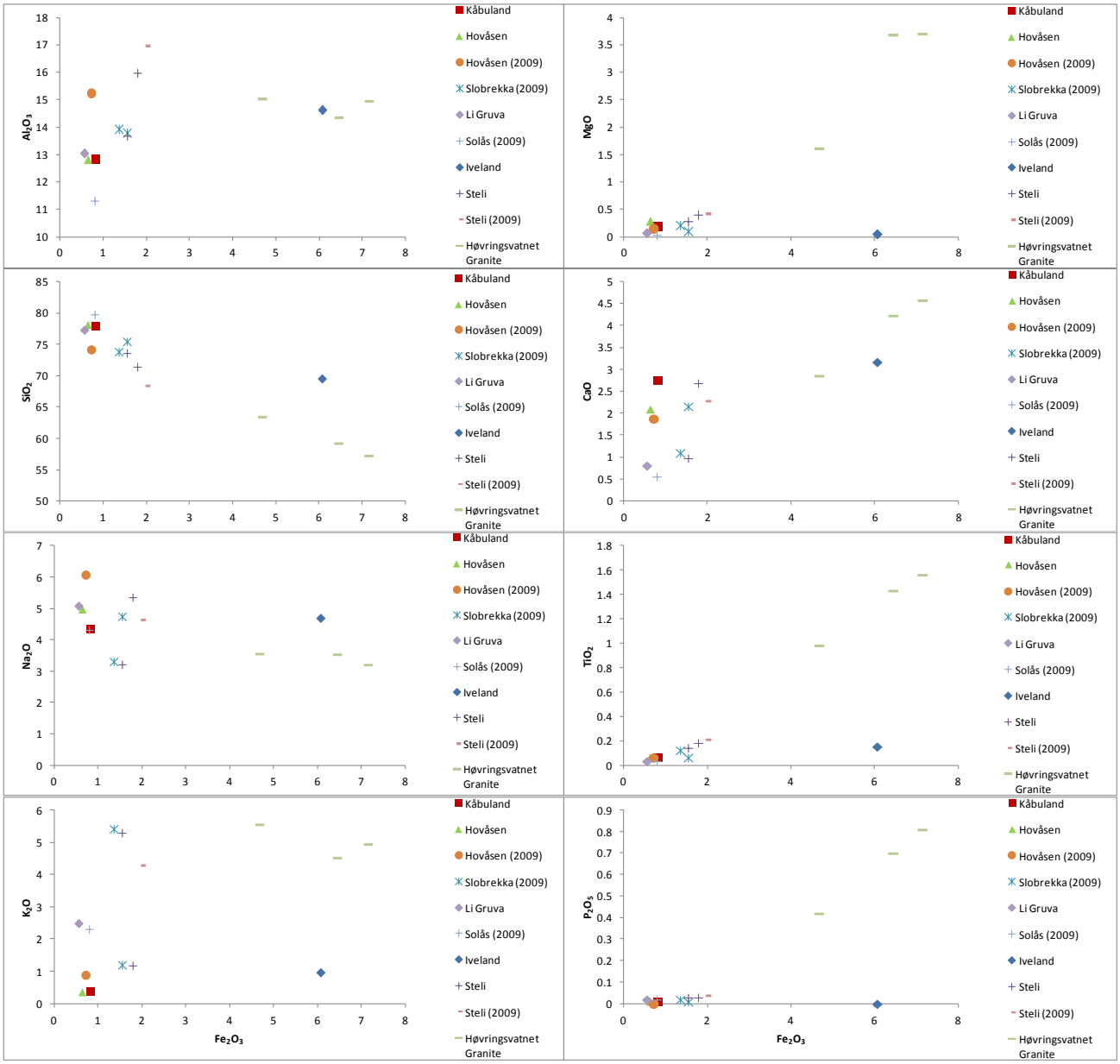

Fig. 4.3.4 Whole-rock variation diagrams for Fe_2O_3 (wt%) verses major element oxides (wt%) combining ICP-AES and ICP-MS whole-rock pegmatite data (as summarised in APPENDIX 2) taken from the Evje-Iveland pegmatite belt. The legend has been arranged from top to bottom, in order of increasing distance south from the Høvringsvatnet granite

From Fig. 4.3.4, the pegmatites show limited trends with each other or the Høvringsvatnet granite. There appears to be correlation between Fe_2O_3 and TiO_2 (this is likely an effect of Ti substituting for Fe) and Fe_2O_3 and SiO_2 (this is likely the effect of closure due to high levels of Si in the system). Na_2O, MgO and P_2O_5 remain at a relatively constant concentration. K_2O does not appear to show clear trends, but does show two populations of higher and lower K. The Høvringsvatnet granites do not appear to fit into the limited trends described by

the pegmatites forming primitive members of a fractionation series. Indeed for SiO_2, MgO, CaO, TiO_2 and P_2O_5, the granites form an entirely separate population, with no apparent geochemical relation.

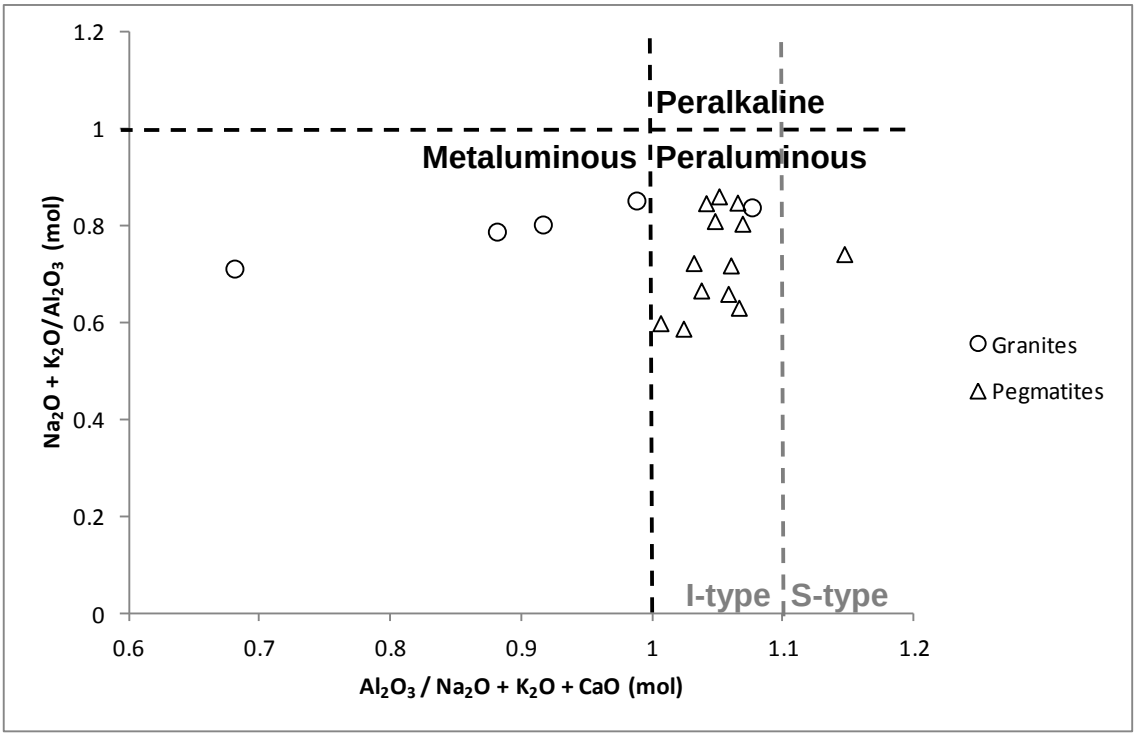

Fig. 4.3.5 Mol (Na_2O+ K_2O) / Al_2O_3 (Whalen et al., 1987) versus ASI (mol Al_2O_3/NaO+K_2O+Ca (e.g. Chappell and White, 2001) for pegmatites and Høvringsvatnet granites

From Fig. 4.3.5 (generated from the same ICP-AES whole rock data summarised in Fig. 4.3.4), the pegmatite wall rocks (excluding one sample) and the Høvringsvatnet granites all fall within the field typical of I-type granites, having an ASI (molar Al_2O_3/(Na_2O+K_2O+CaO)) < 1.1 (Chappell and White, 2001). The pegmatites can be described as weakly peraluminous, whereas the granites can be described as variably metaluminous, with one peraluminous sample (Frost et al., 2001). None of the samples display a peralkaline i.e A-type granitic signature.

4.3.2 Trace element geochemistry

Trace element data (as summarised in APPENDIX 2) are considered for whole-rock pegmatite compositions, country rock from the pegmatite contact, country rock distal to the pegmatite contact and the Høvringsvatnet granites (Figs. 4.3.6, 4.3.7 and 4.3.8 respectively). Initially, the raw ICP-MS data for selected

trace elements was normalised with respect to chondrite, as outlined by Rollinson (1993), and subsequently for Rare Earth Elements (REEs). It is highlighted that normalisation is required in order to eliminate the abundance variation between odd and evenly atomic numbered elements to better define relative trends, and to allow the fractionation of trace elements relative to chondrite to be identified. The data was normalised using the values for chondrite from McDonough and Sun (1995), and then used to produce a series of spidergrams for each sample 'type'.

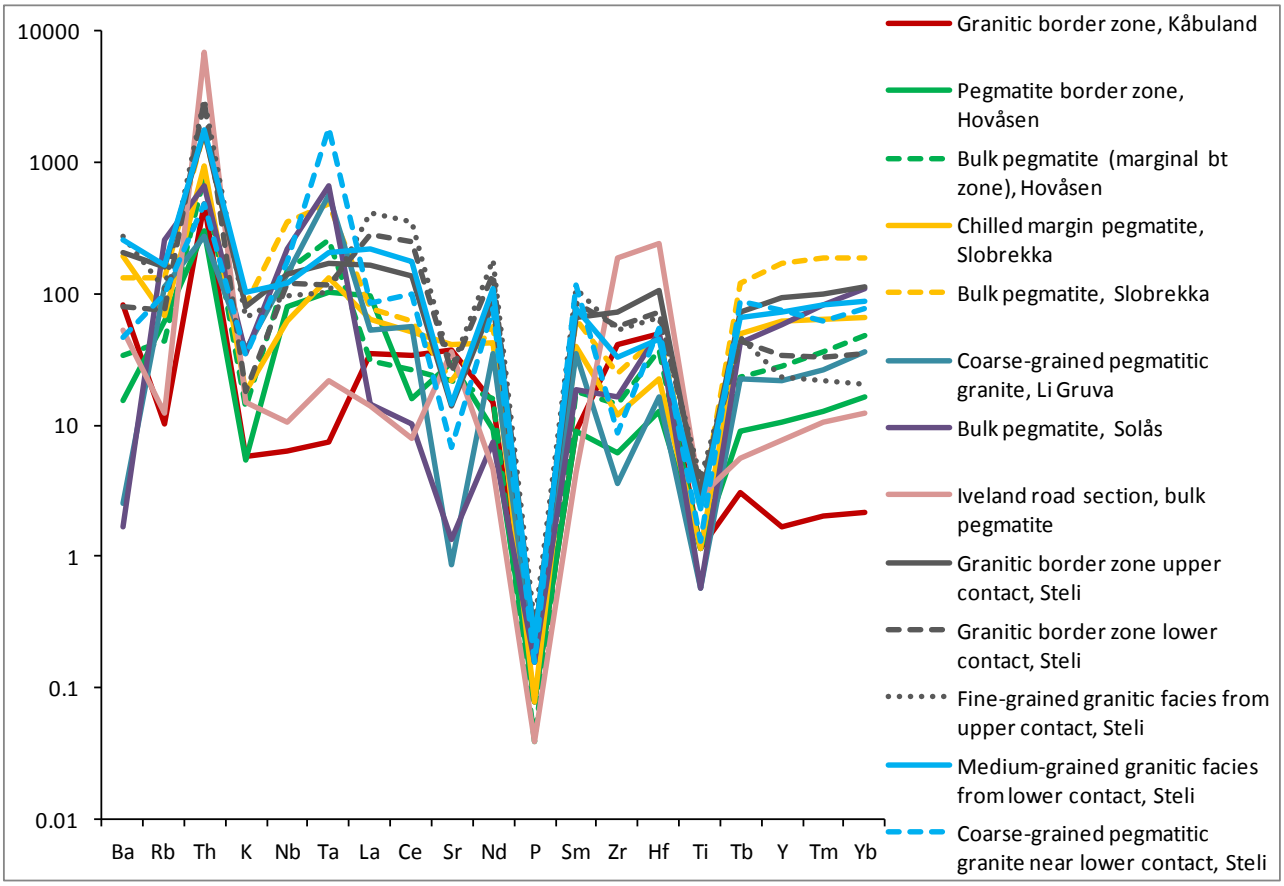

Fig. 4.3.6 Chondrite-normalised (McDonough and Sun, 1995) spider diagrams for pegmatites, based on ICP-AES data

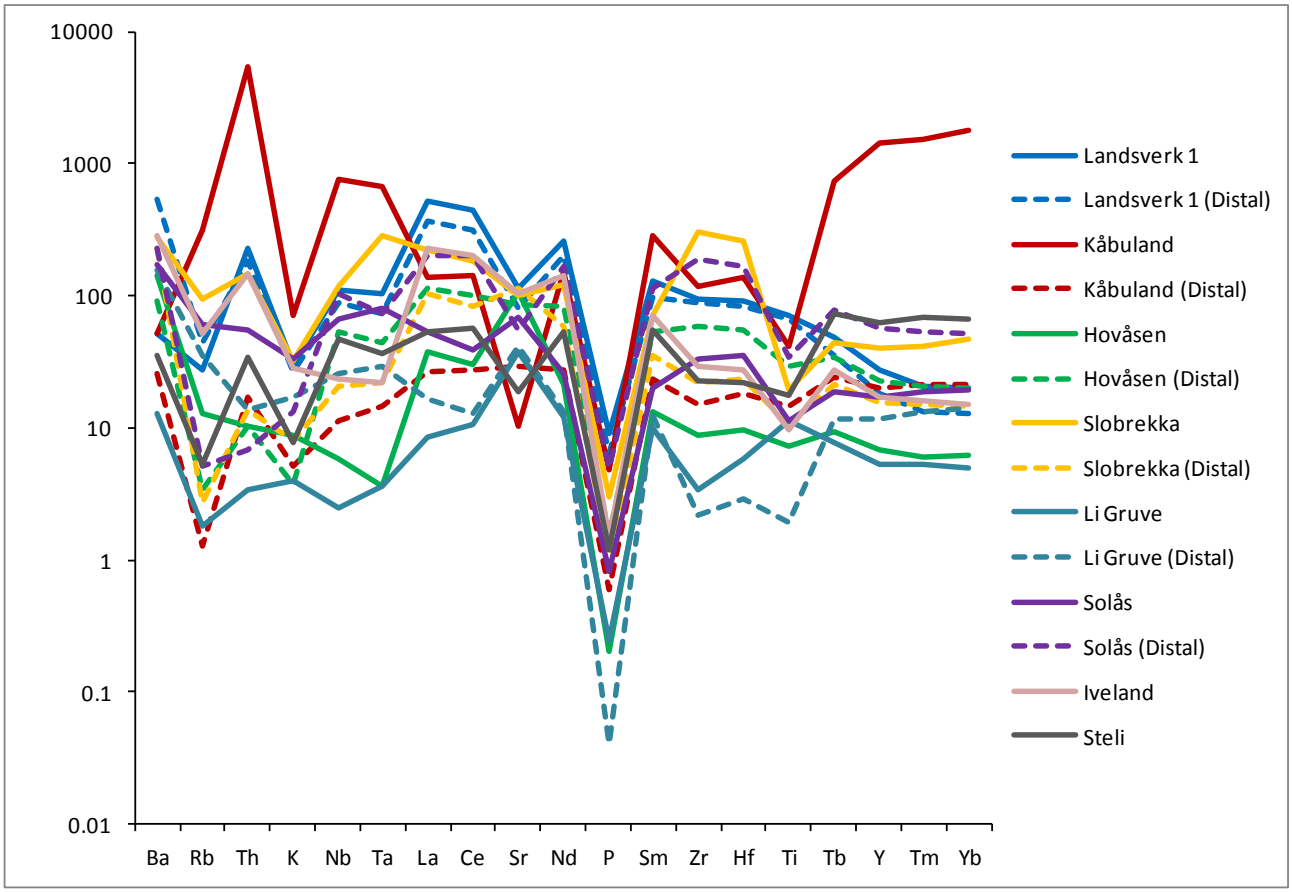

Fig. 4.3.7 Chondrite-normalised (McDonough and Sun, 1995) spider diagrams for country rocks, based on ICP-AES data

Fig. 4.3.8 Chondrite-normalised (McDonough and Sun, 1995) spider diagrams for Høvringsvatnet granites, based on ICP-AES data

The pegmatites are seen to have consistent peaks for Th, Ta, Nd, Hf and Tb, with relatively low levels of Rb, K, P and Zr. The Th, Nd and Tb peaks are shared with the country rocks, as are the Rb, K and P troughs (the country rocks also peak in Sm, and trough in Ti). The Høvringsvatnet granites have consistent peaks in Ba, Th, La, Nd and Tb, with decreased relative levels of Rb, K, Ta, Sr, P and Ti.

REE were utilised for additional trace element investigation. The relative proportion of LREEs to HREEs may be indicated by the La/Lu_N number; that produced when dividing normalised La concentrations by normalised Lu concentrations. Enrichment in LREEs produces a La/Lu_N greater than 1. Enrichment in HREEs produces a La/Lu_N less than 1. Eu anomalies are a common feature of REE plots, and may be quantified by comparing normalised Eu concentrations with the interpolated (and therefore expected) normalised value (Eu*) found between normalised values of Sm (Sm_N) and Gd (Gd_N). The value for Eu/Eu^*_N is thus calculated by dividing Eu_N by the square root of the

product of Sm_N and Gd_N. Values greater and less than 1 denote positive and negative anomalies, respectively (Rollinson, 1993).

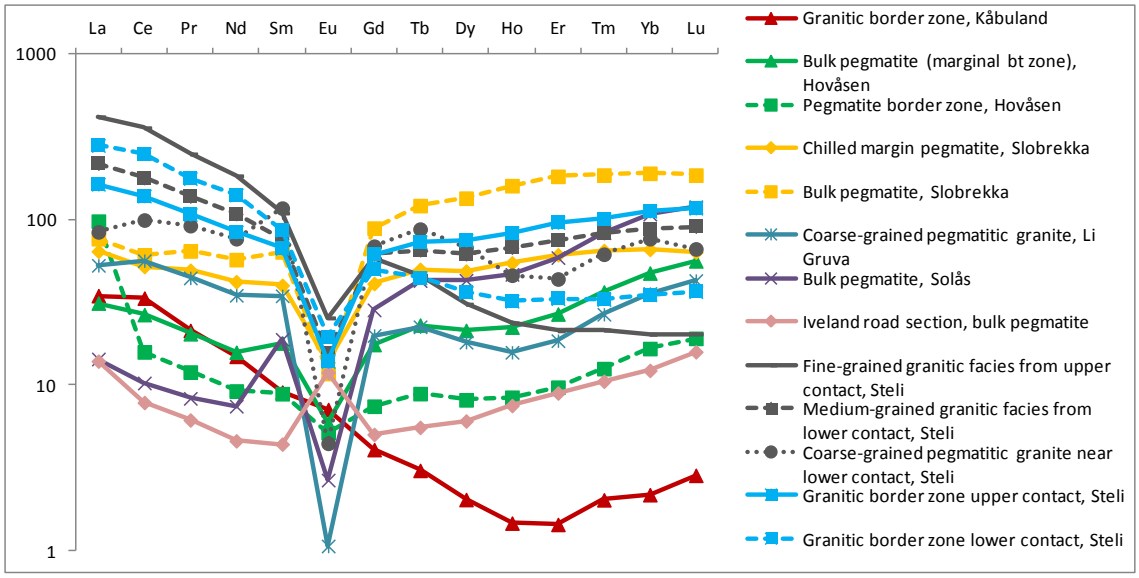

Fig. 4.3.9 Chondrite-normalised (McDonough and Sun, 1995) REE plots for whole rock (after wall facies) compositions of pegmatites

As an entire population (Fig. 4.3.9), the pegmatites appear to display little preferential enrichment in either LREEs or HREEs. However, this is a result of individual pegmatites tending to be enriched in either LREEs over HREEs (Kåbuland, Steli and Li Gruva have La/Lu_N = 12.2, 1.3 – 20.4 and 1.2 respectively), or enriched in HREEs over LREEs (Solås, Slobrekka, and Iveland have La/Lu_N = 0.1, 0.4 and 0.9 respectively). The Hovåsen pegmatite displays a compositional 'trough', with the LREE and HREE end members showing preferential enrichment. 12 of the 14 samples show strong negative Eu anomalies; only Kåbuland and Iveland show positive Eu anomalies.

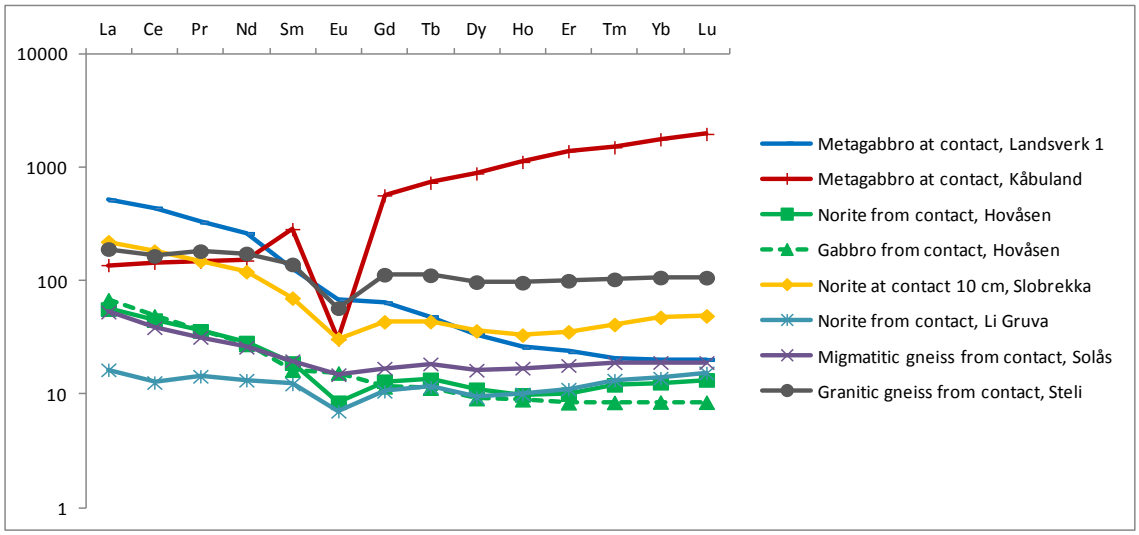

Fig. 4.3.10 Chondrite-normalised (McDonough and Sun, 1995) REE plots for country rocks at pegmatite contacts

From Fig. 4.3.10, country rocks close to pegmatite contacts are typically enriched in LREEs over HREEs, but this enrichment is less marked than for the granites (mean La/Lu_N = 6.0). In contrast, country rocks at the contact at Li Gruva show relatively flat patterns (La/Lu_N = 0.1) and those at Kåbuland are relatively enriched in HREEs (La/Lu_N = 25.5). Eu anomalies are generally negative, ranging from 0.82 in migmatite gneiss at Solås to a significant 0.08 in granitic gneiss at Kåbuland. However, gabbro (a predominantly plagioclase bearing rock) from Hovåsen displays a positive anomaly (1.13). There appears to be a compositional variation with regards to the LREEs, with the development of two 'groups'; Landsverk 1, Slobrekka, Steli and Kåbuland country rocks appear relatively LREE rich (100 – 400 sample/chondrite), with Hovåsen, Solås and Li Gruva country rocks appearing LREE deficient (approximately 50 sample/chondrite). HREEs typically vary between 10 and 100, with the metagabbro at Kåbuland at ~1000.

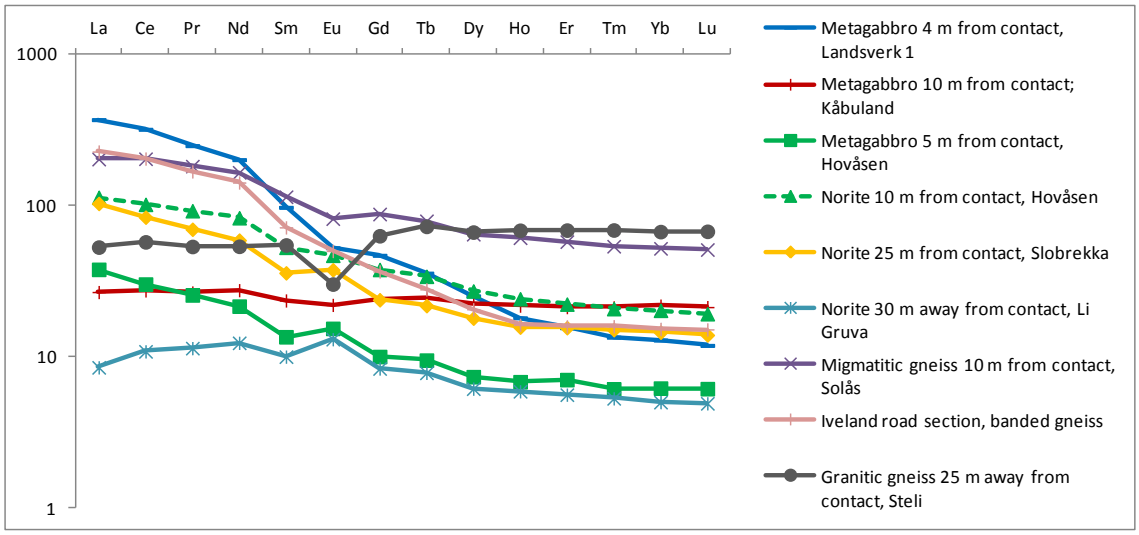

Fig. 4.3.11 Chondrite-normalised (McDonough and Sun, 1995) REE plots for country rocks distal to pegmatite contacts

The country rocks distal to the pegmatite contact are generally more enriched in LREEs over HREEs (La/Lu_N = 0.8 to 31.2), compared with the samples closer to the contact. The exception is the metagabbro at Kåbuland, which shows flat patterns, and the granitic gneiss at Steli, which shows an increased proportion of HREEs (Fig. 4.3.11). Eu anomalies are variable, with the Li Gruva norites and the Hovåsen metagabbros showing strong positive anomalies (Eu/Eu * = 1.44 and 1.39 respectively), and the Steli granitic gneiss showing a strong negative anomaly of 0.52. The remaining samples vary, with the Iveland gneiss having a negligible anomaly of 0.99.

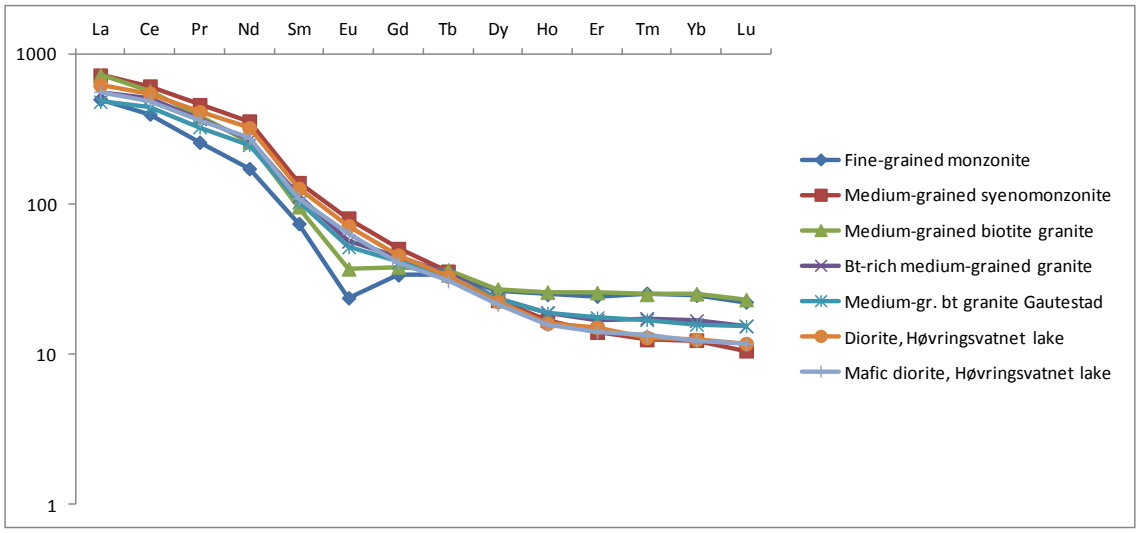

Fig. 4.3.12 Chondrite-normalised (McDonough and Sun, 1995) REE plots for the Høvringsvatnet granites

Fig. 4.3.12 shows chondrite-normalised REE abundances for a series of samples from the Høvringsvatnet granites. The granites are typically enriched in LREEs (La/Lu_N = 22.3 to 53.0), with little compositional variation between the granites. Negative Eu anomalies are essentially limited to a medium grained biotite granite (Eu/Eu * = 0.61) and a fine grained monzonite (Eu/Eu * = 0.48). The medium grained syenomonzonite shows the most difference between LREEs and HREEs, with the biotite rich medium-grained granite showing the least variation.

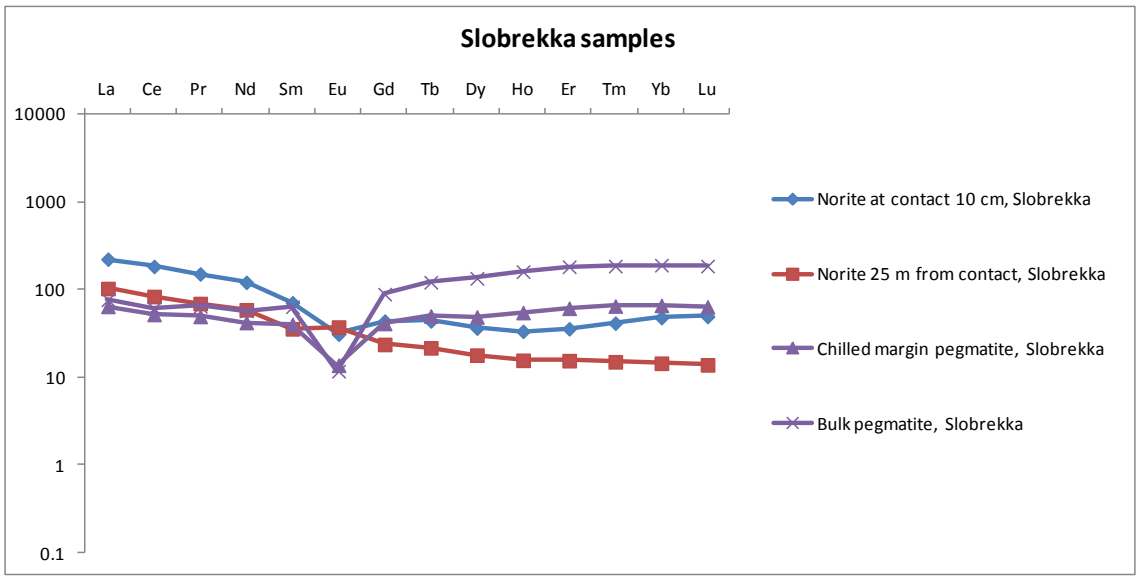

Fig. 4.3.13 Chondrite-normalised (McDonough and Sun, 1995) REE plots for Slobrekka samples

The lithologies associated with the Slobrekka pegmatite display an interesting evolution (Fig. 4.3.13). They appear to show progressive depletion of LREEs from the highest values in the country rock (specifically at the contact with the pegmatite) and the lowest values within the pegmatite, whereas the reverse is the case for the HREEs (pegmatite > contact > country rock).

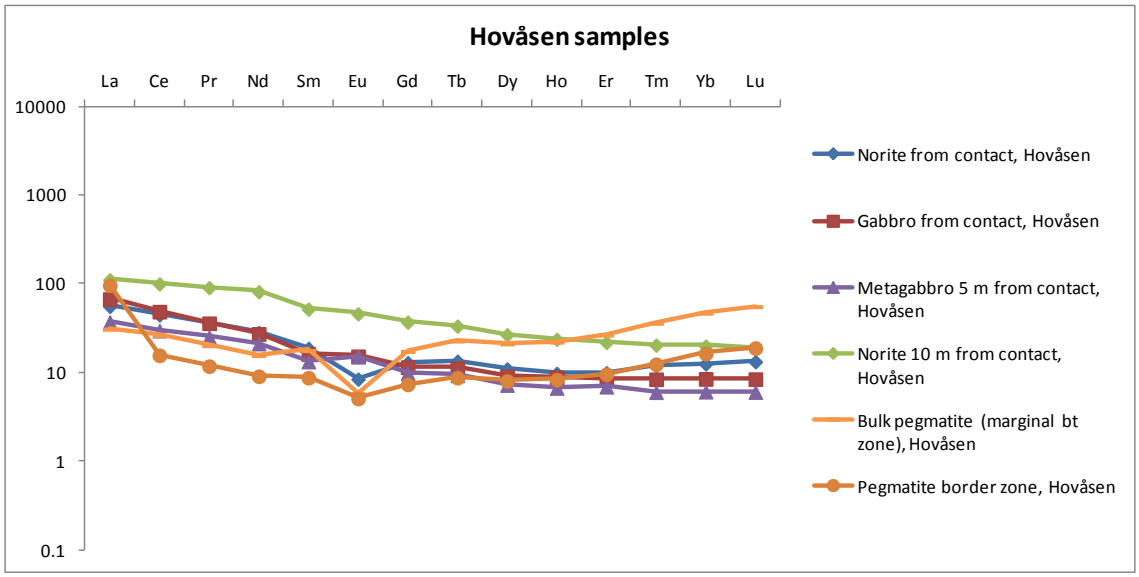

Fig. 4.3.14 Chondrite-normalised (McDonough and Sun, 1995) REE plots for Hovåsen samples

A similar effect occurs at Hovåsen; the country rock contains a greater amount of LREEs (which appear to increase with distance from the contact) than the pegmatite. The pegmatite shows a concave upwards pattern, centred about a negative Eu anomaly; the pegmatite typically contains less LREEs but more HREEs than the country and contact rock (Fig. 4.3.14).

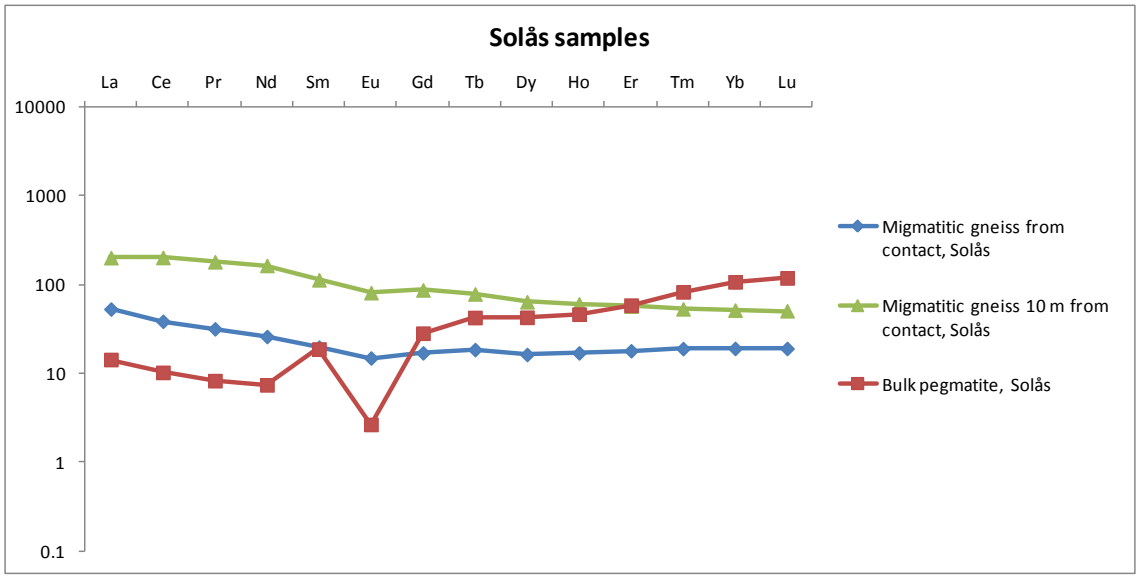

Fig. 4.3.15 Chondrite-normalised (McDonough and Sun, 1995) REE plots for Solås samples

The compositions of the proximal and distal country rocks at Solås are comparable in shape but not abundance with the contact material, consistently depleted in REEs (Fig. 4.3.15). Progressive reduction in abundance with atomic

weight within the gneiss correlates with increasing HREE abundance in the pegmatites.

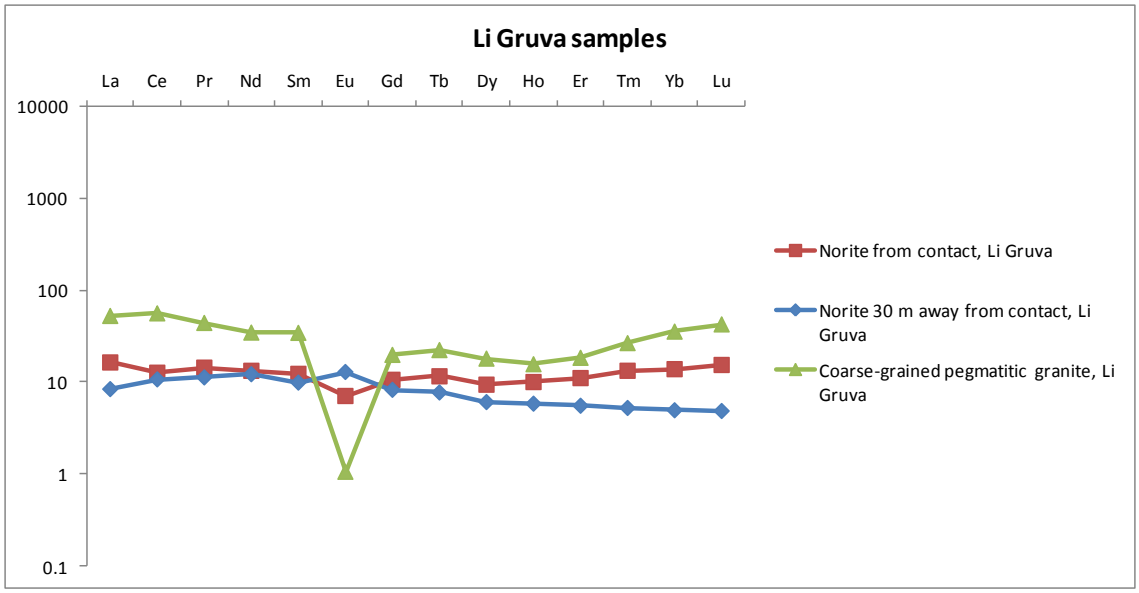

Fig. 4.3.16 Chondrite-normalised (McDonough and Sun, 1995) REE plots for Li Gruva samples

REE abundance increases from the distal host, through the contact zone and into the pegmatite, and may represent progressive fractionation/preferential partial melting leading to an eventual concentration of incompatible elements. The negativity of the Eu anomaly also progressively increases in magnitude. The pegmatite is generally enriched in LREEs over HREEs (Fig. 4.3.16).

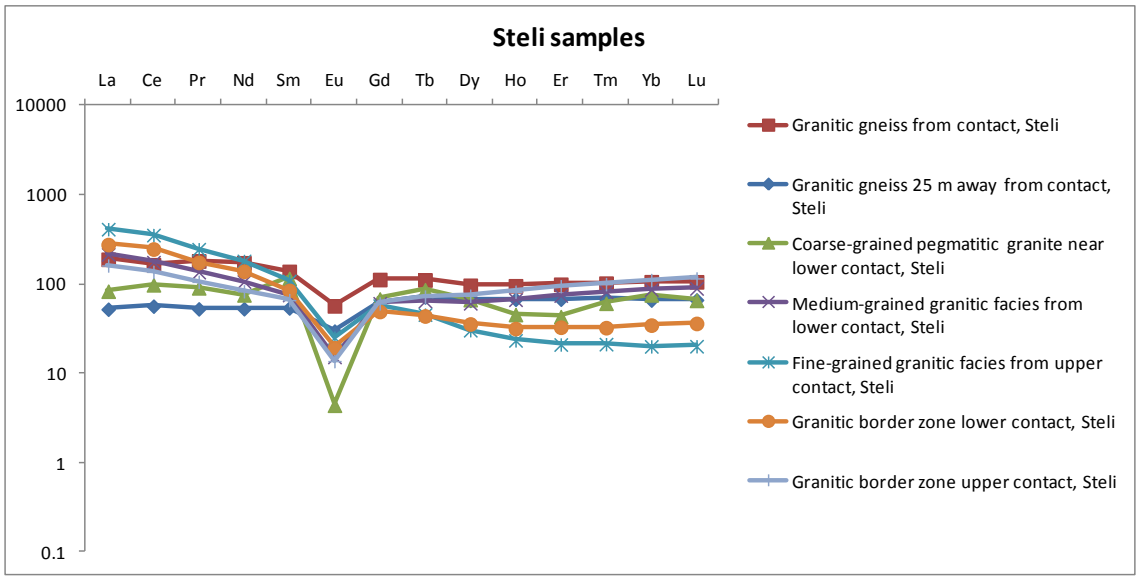

Fig. 4.3.17 Chondrite-normalised (McDonough and Sun, 1995) REE plots for Steli samples

All material from Steli shares a negative Eu anomaly (Fig. 4.3.17); this is more defined in the pegmatite than the host rock, and may have been enhanced due to partial melting or fractionation processes. However, the country rock at Steli actually appears to contain a higher abundance of REE than the contact and pegmatite material, particularly as atomic number increases.

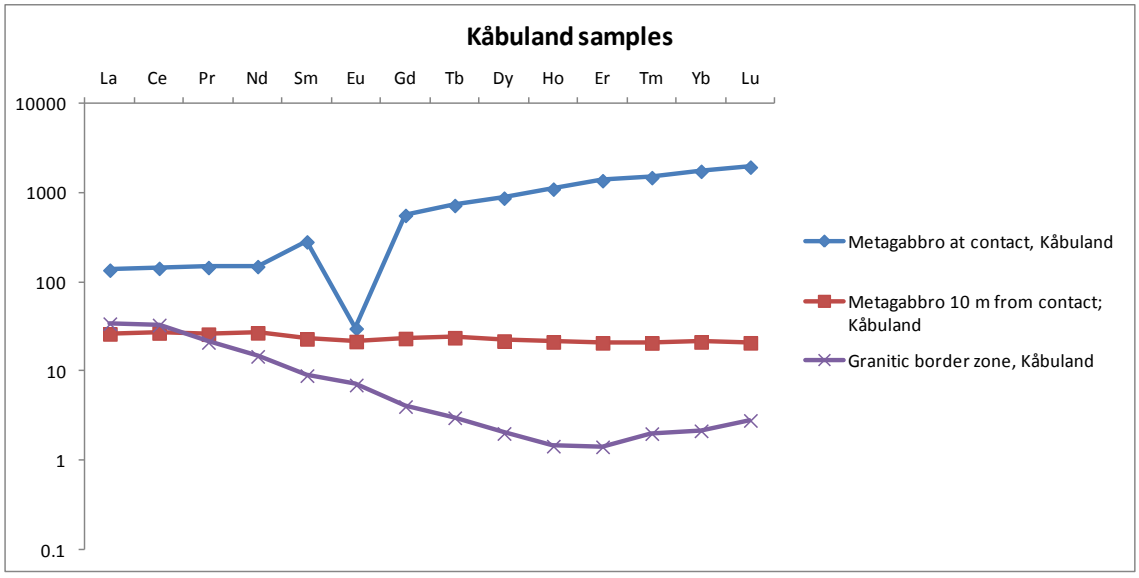

Fig. 4.3.18 Chondrite-normalised (McDonough and Sun, 1995) REE plots for Kåbuland samples

The Kåbuland pegmatite (Fig. 4.3.18) shows a surprising deficiency in overall REE abundance; it appears very primitive despite fairly common macroscopic REE mineralisation. LREEs are generally enriched over HREEs, and the Eu anomaly is slightly positive. With the host rock showing no preferential enrichment, trends or anomalies, it is the contact material which shows the greatest overall enrichment in REEs; an order of magnitude over the pegmatite material in LREEs, and two orders over the pegmatite in HREEs. The Eu anomaly in the contact material is significantly negative, potentially representing preferential melting and removal of plagioclase.

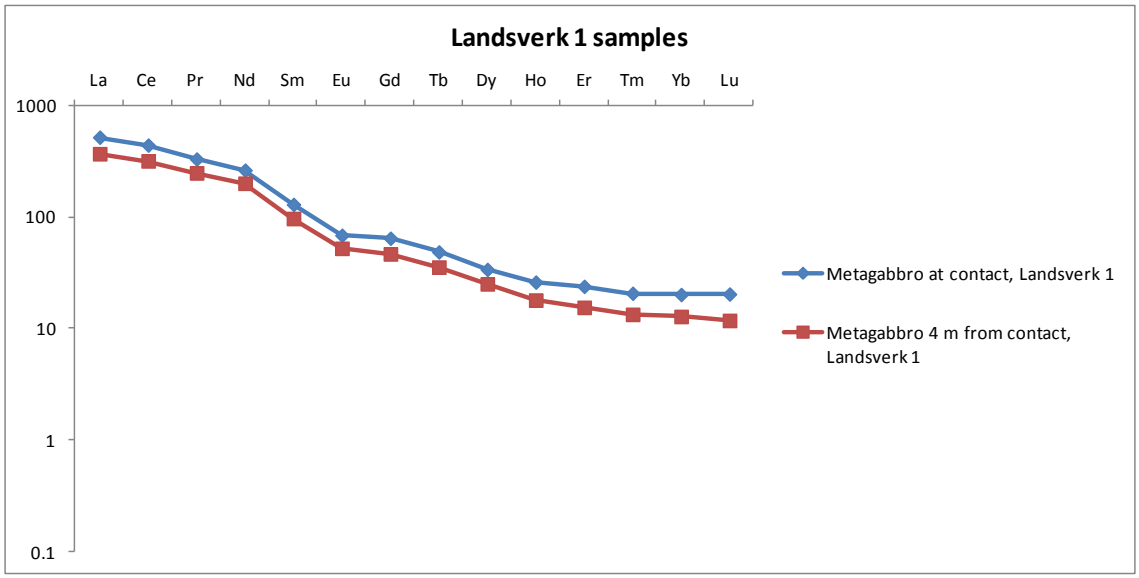

Fig. 4.3.19 Chondrite-normalised (McDonough and Sun, 1995) REE plots for Landsverk 1 samples

For Landsverk1, whilst no data was available for whole rock pegmatite compositions, it can be seen that the lithologies around the pegmatite are more enriched in LREEs over HREEs (Fig. 4.3.19); abundance decreases exponentially with atomic number. Contact material has slightly greater total REE abundance than country rock, but this difference becomes less marked as atomic number increases; partial melting may have concentrated lighter incompatible elements in the contact zone.

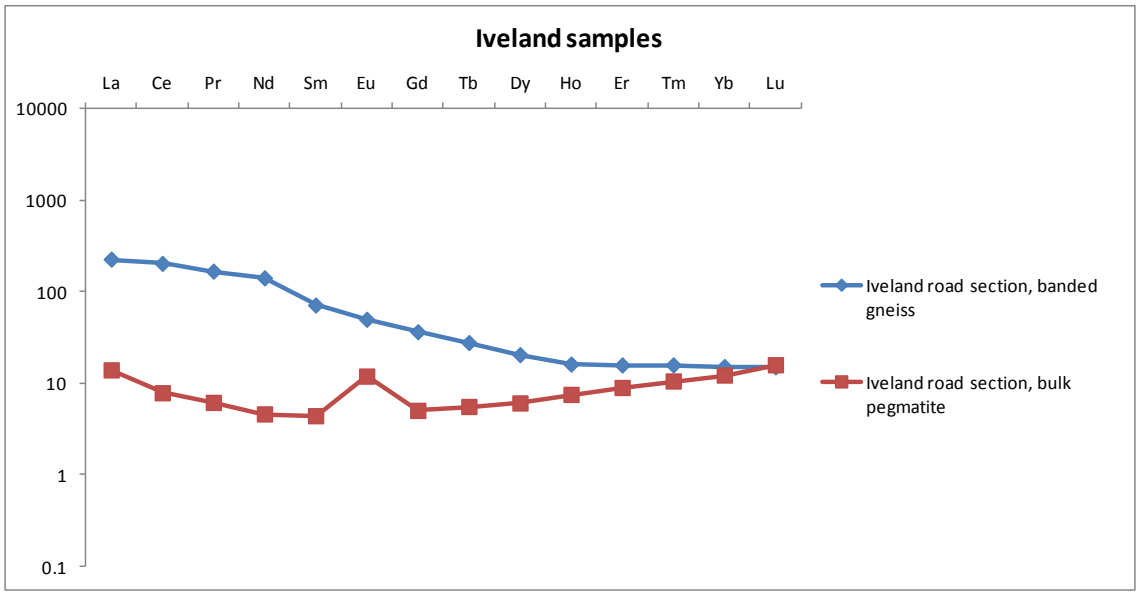

Fig. 4.3.20 Chondrite-normalised (McDonough and Sun, 1995) REE plots for Iveland samples

The Iveland pegmatite sample (Fig. 4.3.20) is greatly depleted in REEs compared to the host rocks; up to an order of magnitude in the LREEs. A strong positive Eu anomaly is present in the pegmatite material, and composition converges towards the HREEs. It is possible the dominant source for the pegmatite melt is not the Iveland material, but a more REE deficient mass. Upon intrusion, the Iveland country rock material undergoes partial melting and 'contaminates' the pegmatite melt with its most incompatible material i.e. HREEs. Geochemical modelling however does indicate that the Iveland country rock can produce a melt comparable in REE composition to the pegmatite; further investigation is required.

4.4 Mineral chemistry

4.4.1 K-feldspar

Fractionation indices (after Larsen, 2002) from pegmatitic K-feldspar (Fig. 4.4.1 after XRF analyses) indicate clear evolutionary trends, from a primitive phase (upper left) to a more evolved faction (lower right). The simplified fractionation graph (Sr against Rb) supports this (the proportion of Rb in the feldspar increases with fractionation due to its incompatible nature compared to Sr) (London, 2008). The conclusion that the pegmatites represent a progressively fractionated suite is therefore a reasonable one, and, when determining potential sources of the pegmatite melt, a logical step would be an attempt to relate degree of fractionation (i.e. magnitude of elemental ratio) with distance from the Høvringsvatnet granite (measured from the pegmatite to the centre of the granitic outcrop); the more evolved the pegmatite, the more distal it should be. This is discussed further in *Chapter 5.1.2*, utilising elemental ratios from the same XRF data set as Fig. 4.4.1.

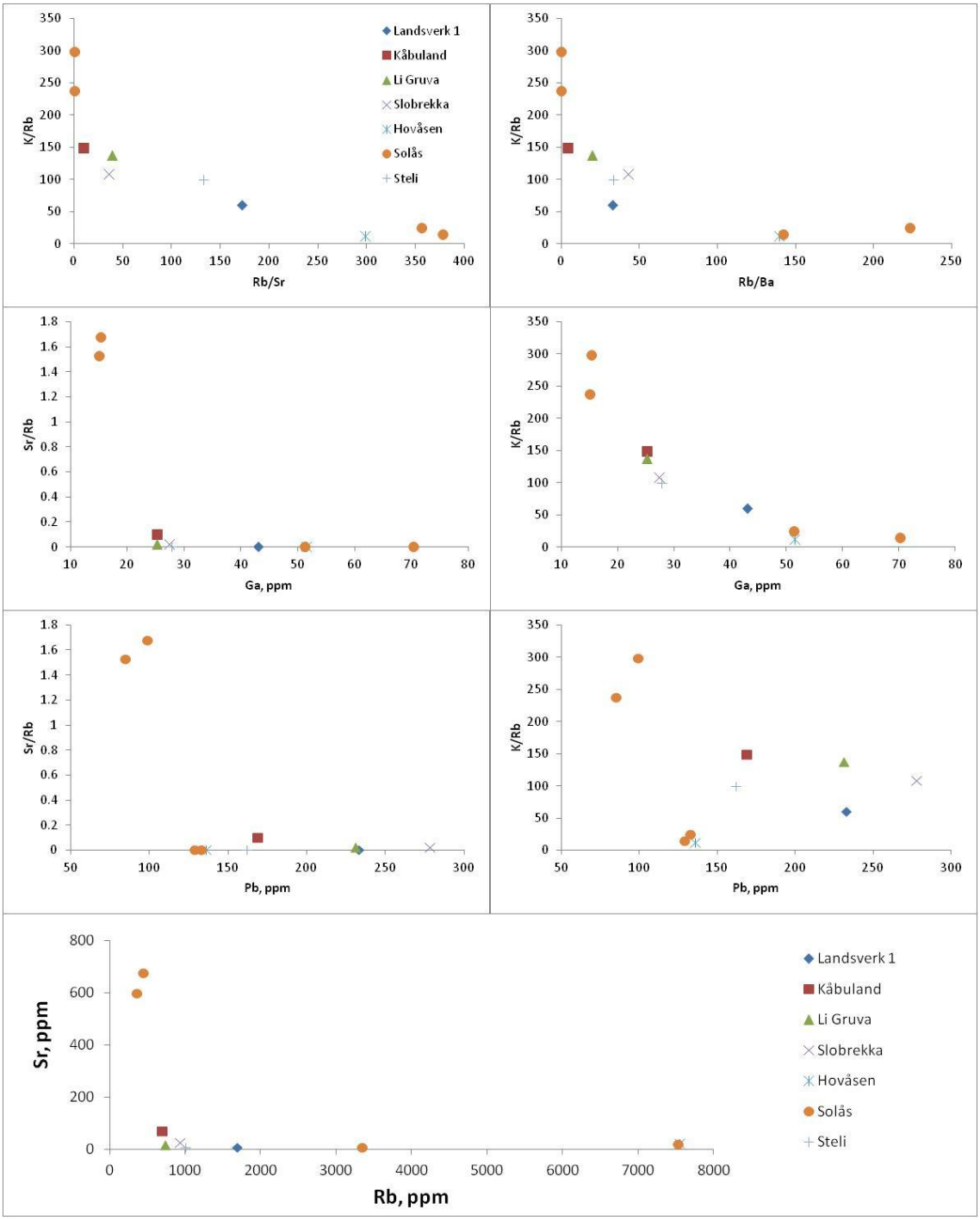

Fig. 4.4.1 Demonstration of evolutionary trends in pegmatitic K-feldspar

4.4.2 Trace element data for quartz from the Evje-Iveland pegmatites

LA-ICP-MS analyses were carried out to investigate the trace element compositions of both primary magmatic and secondary hydrothermal (the distinction is based initially on field observations) quartz. 47 samples in total, from a variety of zones within each of the seven pegmatites selected, were analysed for Al, Li, Be, B, Mn, Ge, Rb, Sr, Sb, Na, Al, P, K, Ca, Ti, Fe, Zn and Ga; data is summarised in APPENDIX 2. Figs. 4.4.2 to 4.4.10 are box whisker

diagrams for trace element content in pegmatite quartz. The blue boxes represent the middle 50% of the data, bounded by the upper and lower quartiles, with the mean marked as an internal black line. The whiskers demonstrate the range of the data. The vertical blue lines indicate LOD associated with the LA-ICP-MS analytical runs.

Data for Al is summarised in Fig. 4.4.2. The hydrothermal quartz crystal from Landsverk 1 (L1) contains the greatest range of Al values out of all pegmatitic quartz samples (0 – 835 ppm). Pegmatitic quartz from Landsverk 1 contains 170 ppm Al, which is also a relatively high value. Kåbuland quartz generally contains more Al than other pegmatite quartz and displays a small range of values. This may be a function of small sample population size, but as Hovåsen and Steli also display similar Al ranges, it is probably realistic. Solås and Steli contain the least Al (20 – 40 ppm), with generally little variation in concentration. Al content is dictated by the nature of the host quartz; magmatic quartz typically contains 100 – 400 ppm Al, with hydrothermal quartz containing 1000 – 5000 ppm (e.g. Götze, 2009). The quartz from the Evje-Iveland area contains an order of magnitude less Al than these quantities.

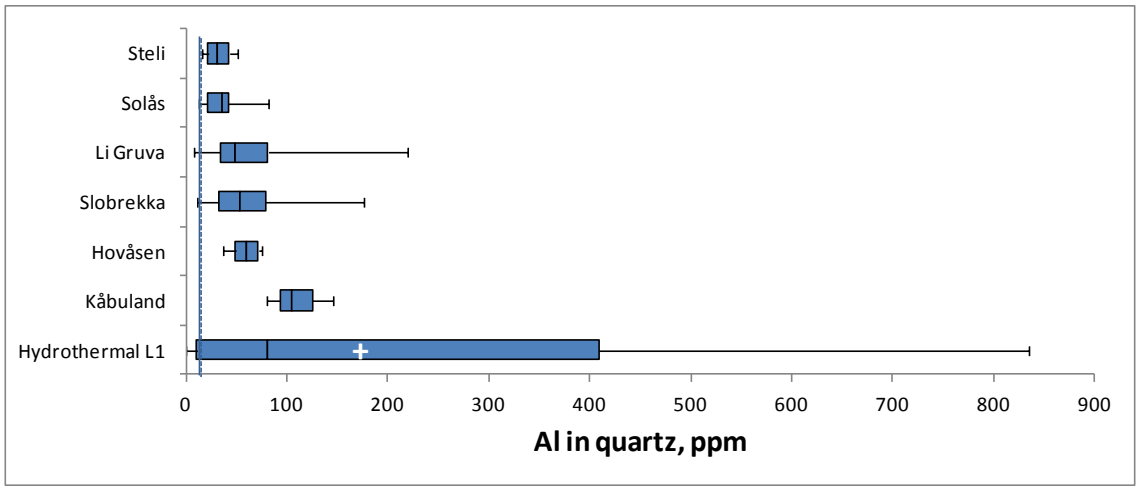

Fig. 4.4.2 Al in quartz from the Evje-Iveland pegmatites (pegmatite quartz from L1 denoted by white +)

Data for Ti is summarised in Fig. 4.4.3. Whereas quartz from the Landsverk 1 pegmatite contained the most Al, it is entirely devoid of Ti (in both hydrothermal and pegmatitic samples). A negative correlation between Al and Ti cannot be drawn however as Kåbuland, which also exhibited elevated Al content, contains

the greatest proportion of Ti (excepting one outlier; graphic quartz from the cupola of Li Gruva) and Steli, with amongst the least amount of Al, contains relatively little Ti . Indeed, Hovåsen excepted, Al and Ti appear to be directly proportional.

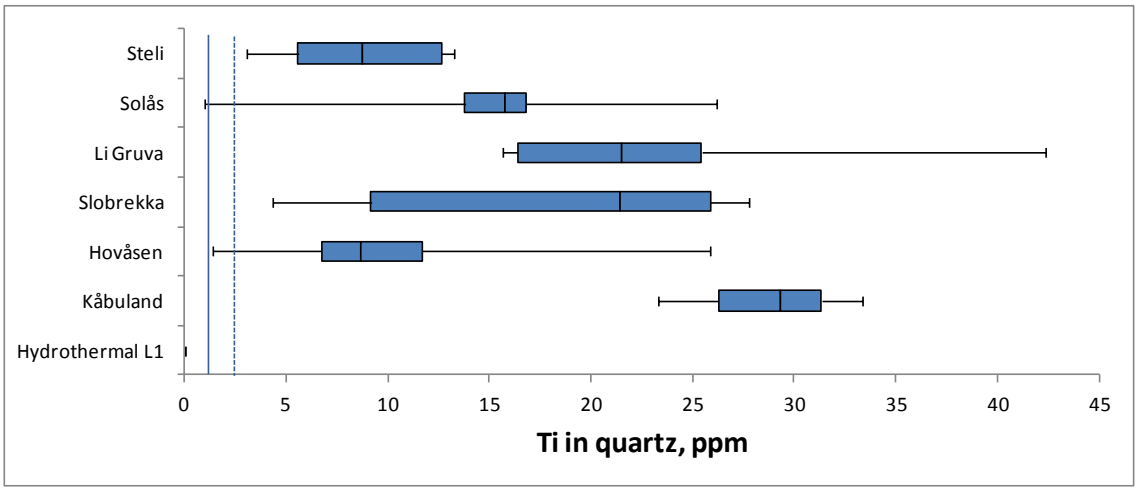

Fig. 4.4.3 Ti in quartz from the Evje-Iveland pegmatites

Data for Li is summarised in Fig. 4.4.4. As with Al, the hydrothermal quartz from Landsverk 1 displays the highest concentration and greatest range (0 – 62ppm). Pegmatitic Landsverk 1 quartz also contains a high concentration of Li (24 ppm). Hovåsen contains a relatively large Li component, with Solås and Slobrekka containing the least. Despite similar relative proportions of Al and Li in the Landsverk 1 and Solås pegmatites, the Kåbuland pegmatite contains a relatively reduced amount of Li compared to an elevated amount of Al. Both elements display a limited range in this pegmatite however.

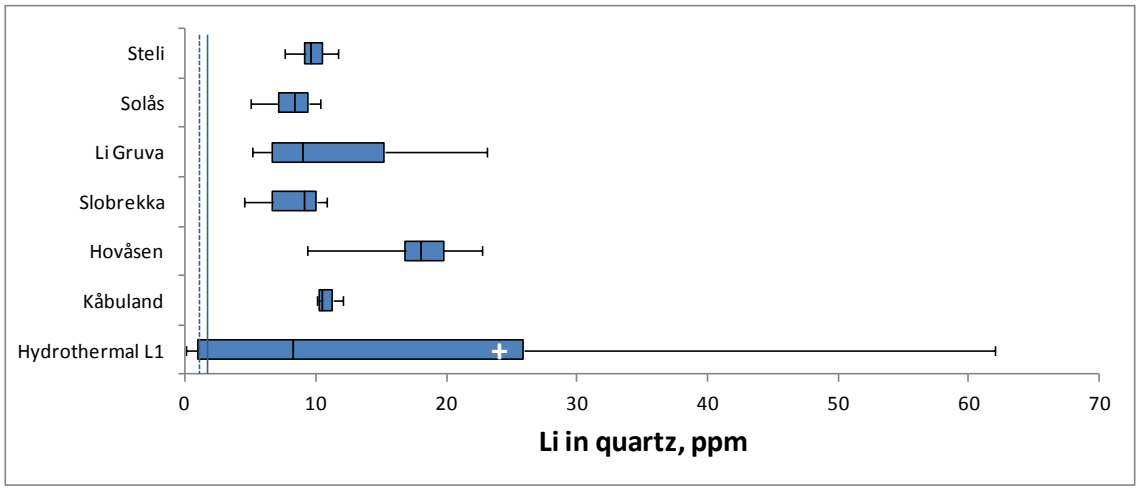

Fig. 4.4.4 Li in quartz from the Evje-Iveland pegmatites (pegmatite quartz from L1 denoted by white +)

Data for Ge is summarised in Fig. 4.4.5. Excepting the quartz from Landsverk 1, the majority of samples report Ge values above the detection limit. With typical values ranging from between 1 and 4 ppm, there is little variation in Ge content. However, the Steli, Li Gruva and Kåbuland pegmatites contain relatively little Ge, with little variation in concentration, whereas the Slobrekka, Hovåsen and in particular Solås pegmatites display a wide range in Ge.

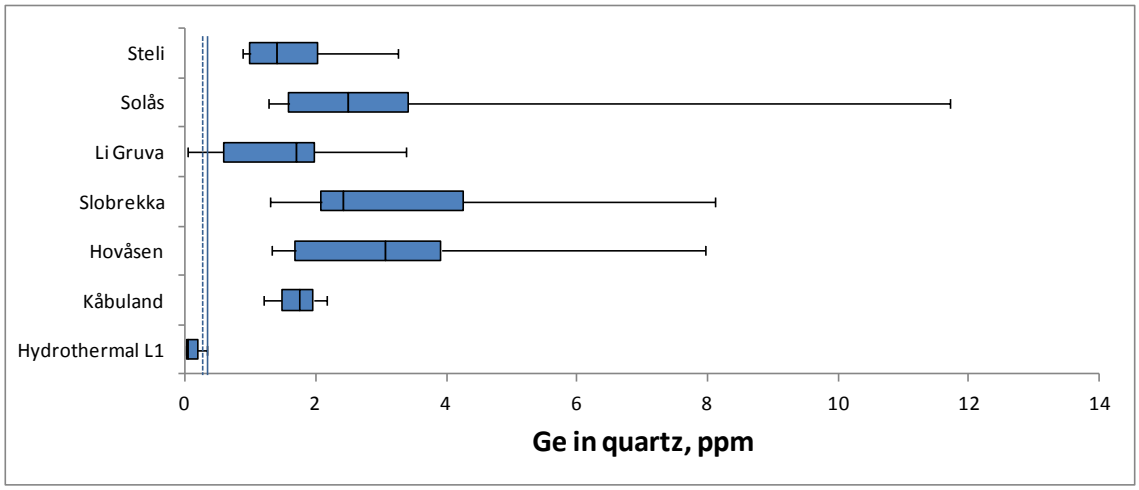

Fig. 4.4.5 Ge in quartz from the Evje-Iveland pegmatites (pegmatite quartz from L1 is 0.15 ppm)

Data for B is summarised in Fig. 4.4.6. The Li Gruva pegmatite contains the highest levels of B (0.5 – 3.5 ppm). The other pegmatites show little variation in B content, with typically between 0.5 and 1 ppm B. Landsverk 1 shows a large difference between hydrothermal and pegmatitic compositions, at 0.2 – 1.1 and 2.1 ppm respectively and, with Slobrekka, contains the least B.

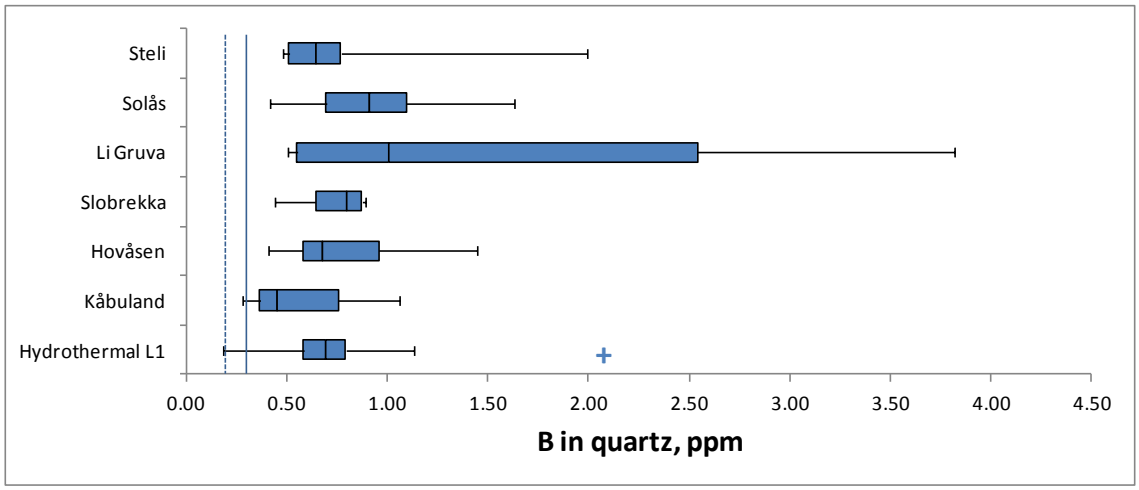

Fig. 4.4.6 B in quartz from the Evje-Iveland pegmatites (pegmatite quartz from L1 denoted by blue +)

Data for K is summarised in Fig. 4.4.7. The majority of data for K falls below detection limits. The main exceptions to this are pegmatitic quartz from Landsverk 1 which contains around 154 ppm and from Kåbuland which shows a range from 4.7 – 43.6 ppm.

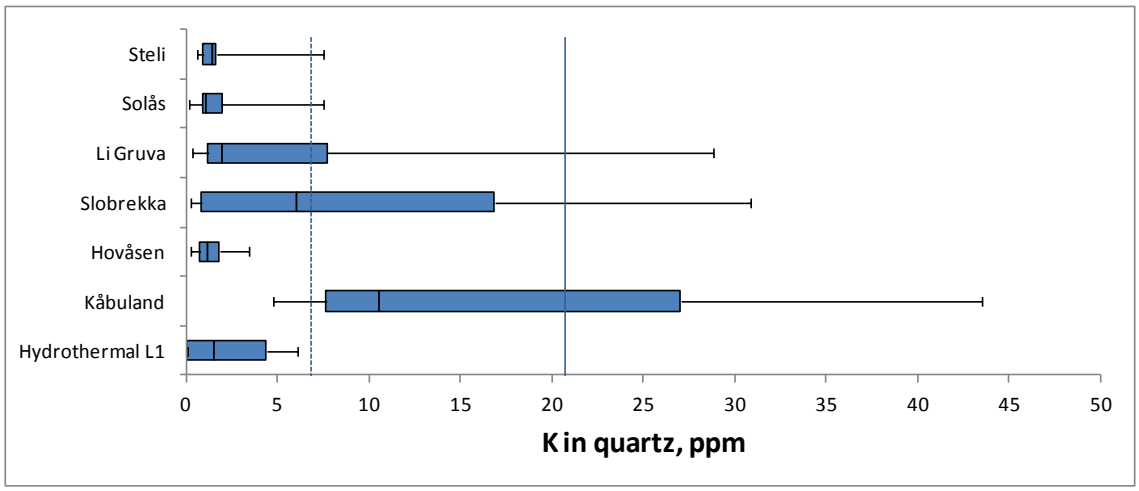

Fig. 4.4.7 K in quartz from the Evje-Iveland pegmatites (pegmatite quartz from L1 is 154 ppm)

Data for Be is summarised in Fig. 4.4.8. Whilst there is very little actual variation in the Be contents of the pegmatites, relatively Li Gruva quartz shows the highest concentrations of Be, with an upper value of 1.4 ppm. Quartz from Hovåsen and Kåbuland display elevated levels of Be, with the hydrothermal quartz from Landsverk 1 (the pegmatitic quartz contains 0.2 ppm Be) and samples from Steli and Solas containing relatively low Be. There appears to be

little correlation between Be and other elements, aside from high levels of both B and Be at Li Gruva.

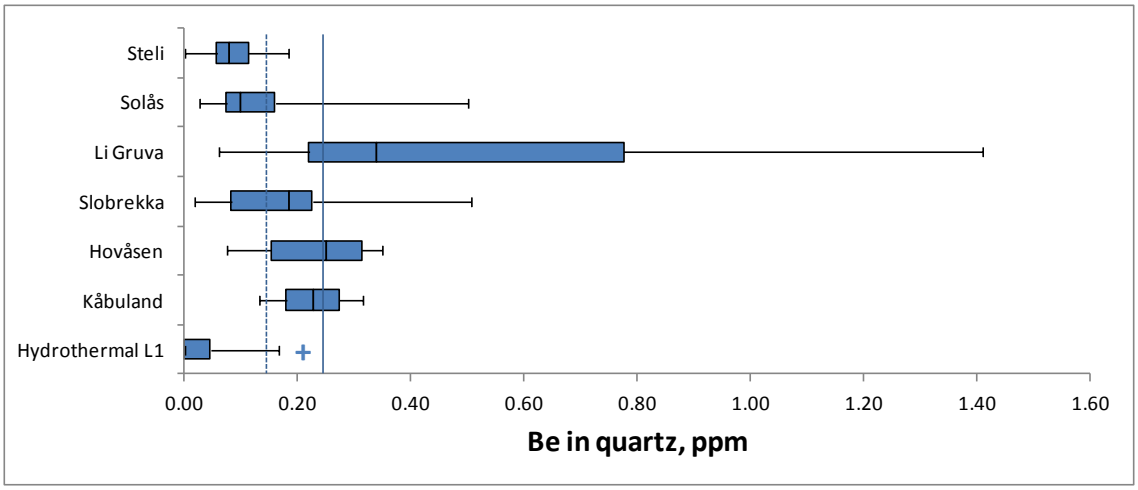

Fig. 4.4.8 Be in quartz from the Evje-Iveland pegmatites (pegmatite quartz from L1 denoted by blue +)

Data for Fe is summarised in Fig. 4.4.9. The pegmatites in the study area contain very little Fe, typically below 2 ppm. The exception is quartz from the Steli pegmatite, which has Fe values ranging from 3.0 to 13.3 ppm, and the cupola of the Li Gruva pegmatite at 13.2 ppm. There appears to be some limited correlation between the distribution of Fe and that of Ti (i.e. quartz from Kåbuland and Li Gruva contain more of these elements than Solås and Hovåsen, with Slobrekka plotting between). Quartz from Landsverk 1 (both hydrothermal and pegmatitic) contains limited values of Fe (below 1 ppm). Müller et al. (2012) caution the use of Fe as a genetic indicator due to its high rate of diffusion; potentially the elevated Fe levels in Steli and Li Gruva are simply a result of diffusion from a nearby Fe-rich mineral.

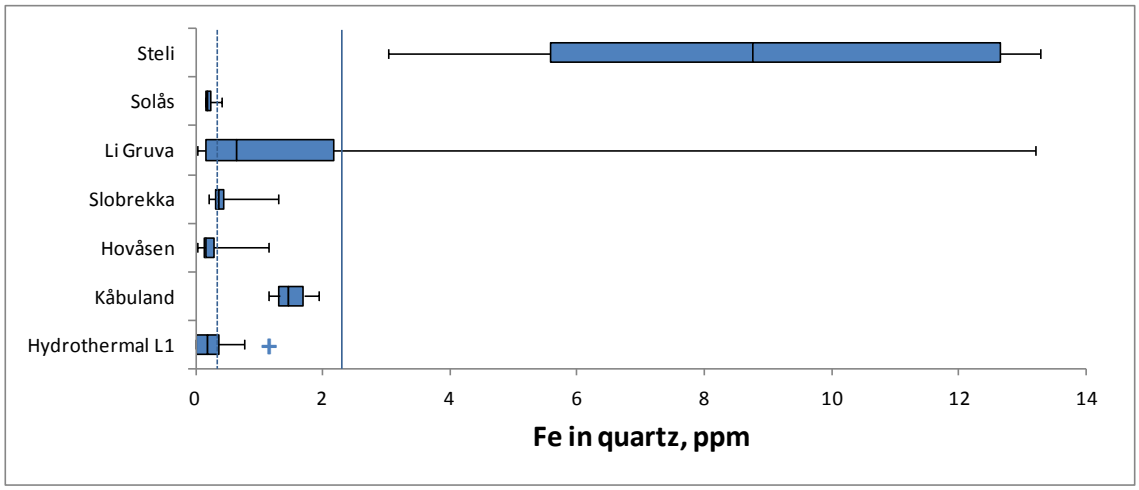

Fig. 4.4.9 Fe in quartz from the Evje-Iveland pegmatites (pegmatite quartz from L1 denoted by blue +)

Data for P is summarised in Fig. 4.4.10. The concentration of P within each pegmatite is relatively varied compared with other elements, although many values are close to or below detection limits. Kåbuland, Solås and Slobrekka show the highest average values. These three pegmatites appear to match the trends highlighted by other elements; Kåbuland contains a higher concentration of trace elements, Solås is relatively purer, and Slobrekka is between the two.

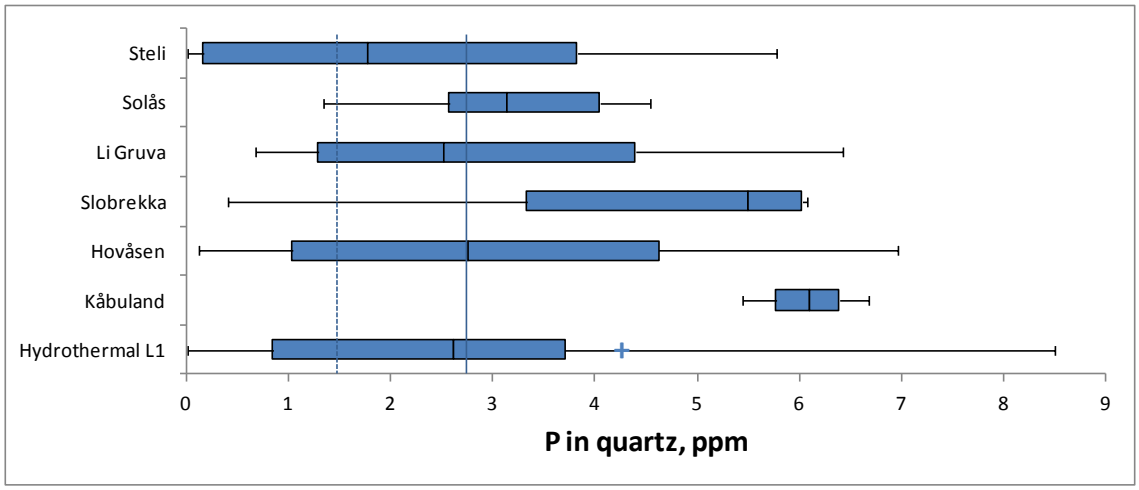

Fig. 4.4.10 P in quartz from the Evje-Iveland pegmatites (pegmatite quartz from L1 denoted by blue +)

The following bivariate plots have been generated for Al, Li, Ti and Ge (Fe, K, B and P fall consistently below LOD) for each pegmatite using the data synthesised above in an attempt to illustrate chemical trends, relationships, controls and spatial distribution. The higher of the LODs are included to indicate degree of confidence.

Figs. 4.4.11 to 4.4.18 demonstrate the typically positive correlation between Al and Li. The Al:Li ratio varies from approximately 2:1 at Steli and Solås to 10:1 at Li Gruva and Slobrekka i.e. there is little correlation between degree of evolution and Li content. The positive correlation is expected, as Li^{+} acts as a charge compensator for Al^{3+} when substituting for Si^{4+} in the quartz lattice. Kåbuland is unusual in that Al and Li show a negative correlation. Throughout the pegmatites, there doesn't appear to be a strong control on the Li content depending on position within the profile. However, at Hovåsen, core material does seem to be enriched or depleted in Li depending on the absence or presence respectively of beryl.

In an attempt to qualify the extent Li^{+} acts as a charge compensator for Al^{3+}, the 1:1 atomic ratio of Al to Li (calculated using the relative atomic mass of Al and Li; the line represents an equal number of atoms of each of the elements) is plotted for Figs. 4.4.11 to 4.4.18 and 4.4.36. If Al^{3+} favours Li^{+} as its charge compensator i.e. $Al^{3+} + Li^{+} = Si^{4+}$ is ideal, then the analyses should plot along this 1:1 atomic ratio. Perpendicular variation from the line toward either axis provides information on the extent that other charge compensators are present. This approach is also taken for Ti vs. Ge plots (Figs. 4.4.35 and 4.4.39), as although no substitutional relationship exists between Ti^{4+} and Ge^{4+}, the 1:1 atomic ratio is useful as it suggests which ion is typically favoured in the lattice.

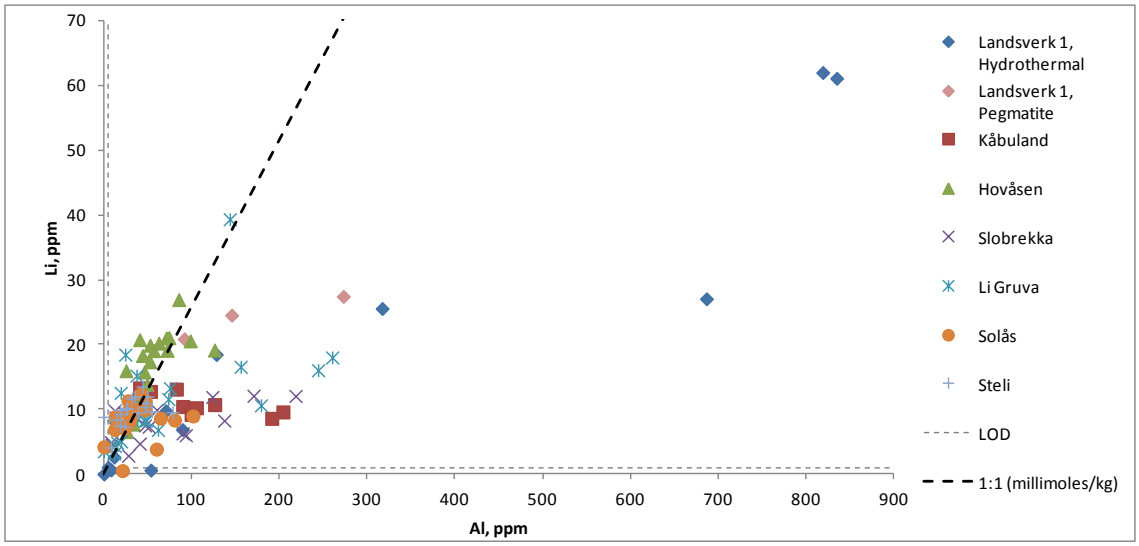

Fig. 4.4.11 Li versus Al for quartz from all pegmatites

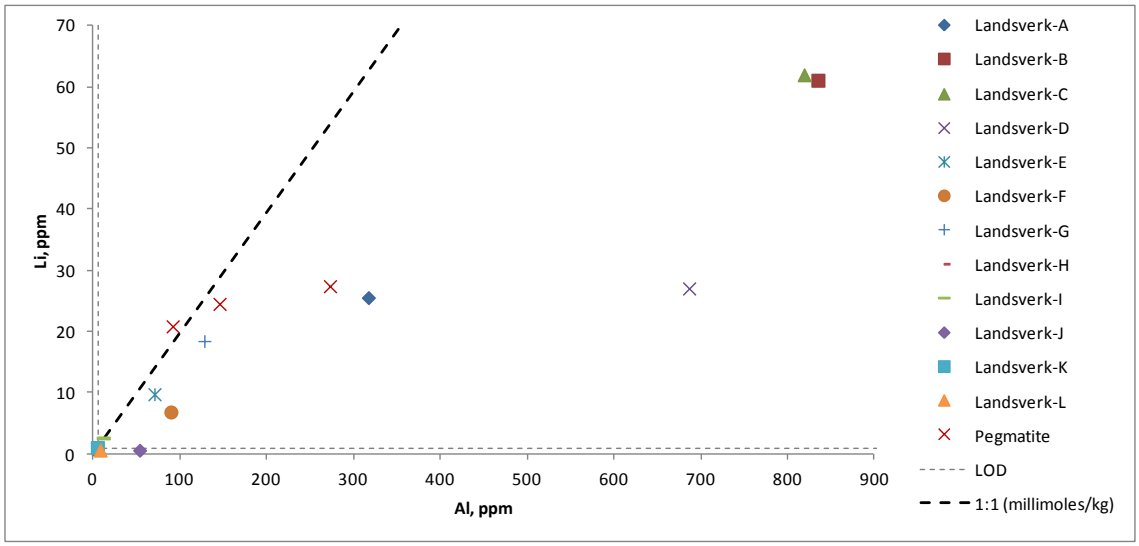

Fig. 4.4.12 Li versus Al for quartz from L1

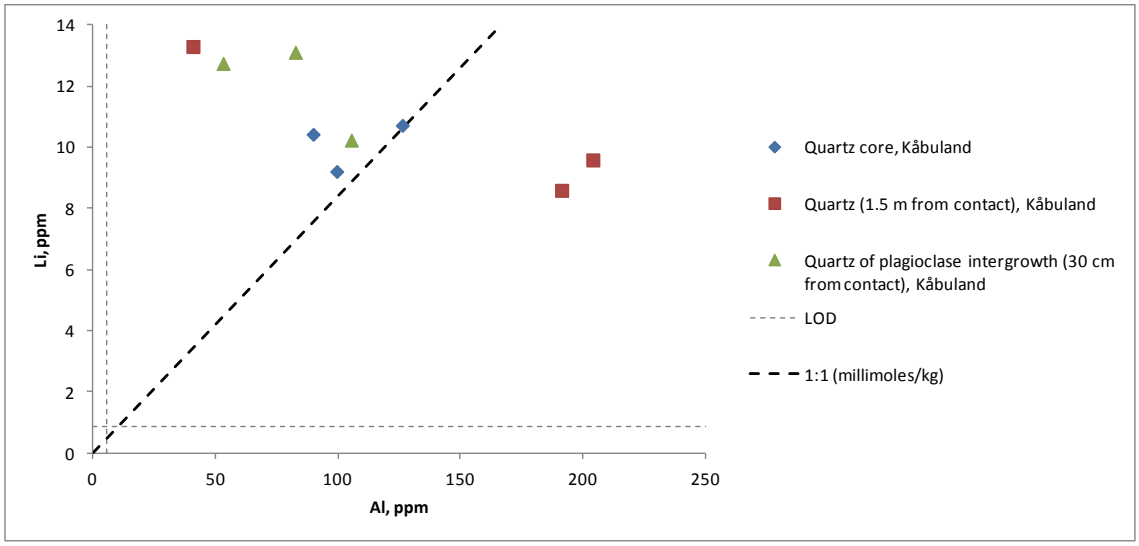

Fig. 4.4.13 Li versus Al for quartz from Kåbuland

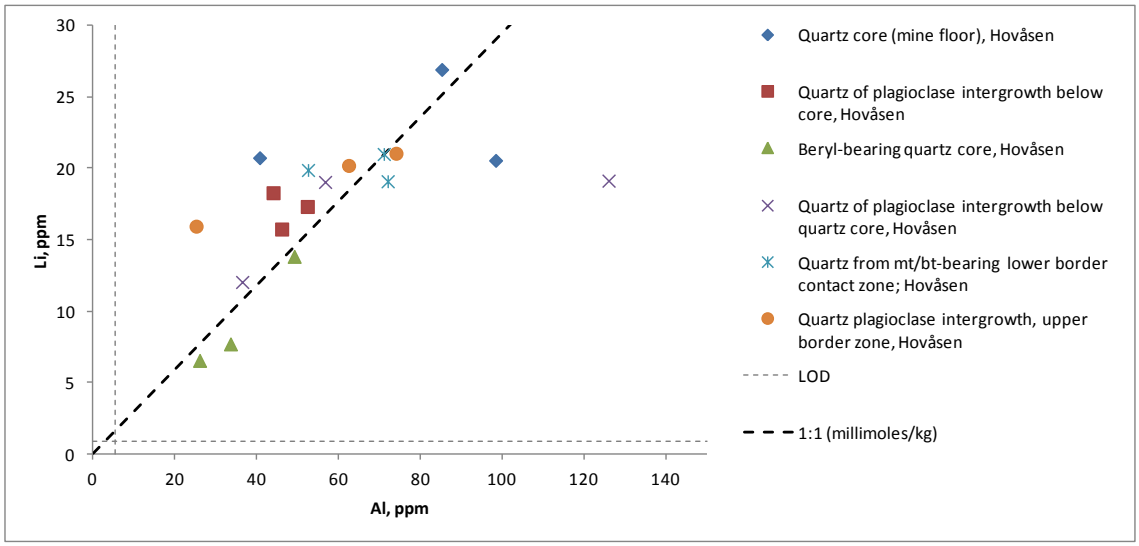

Fig. 4.4.14 Li versus Al for quartz from Hovåsen

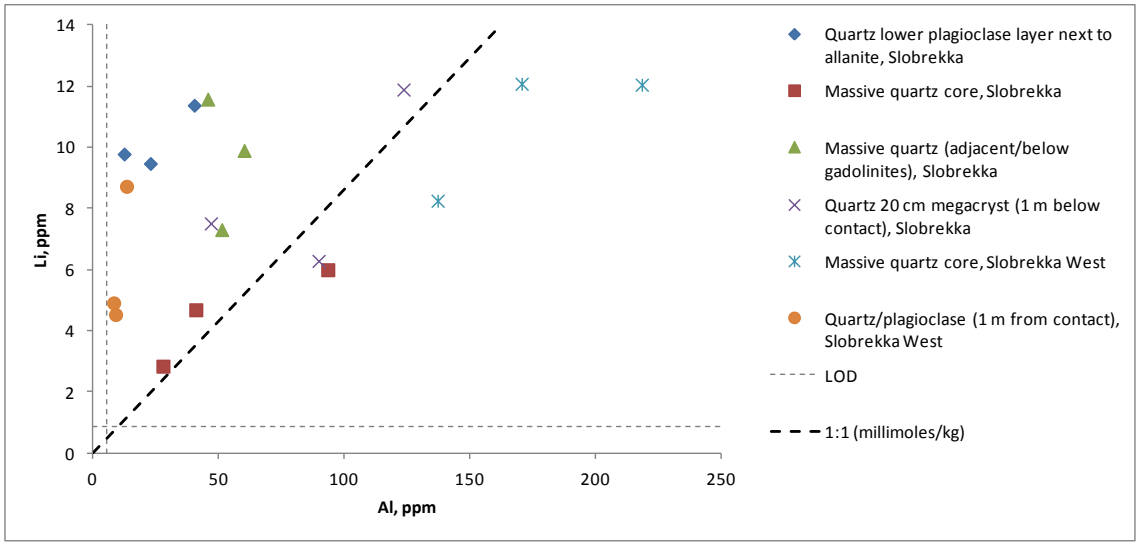

Fig. 4.4.15 Li versus Al for quartz from Slobrekka

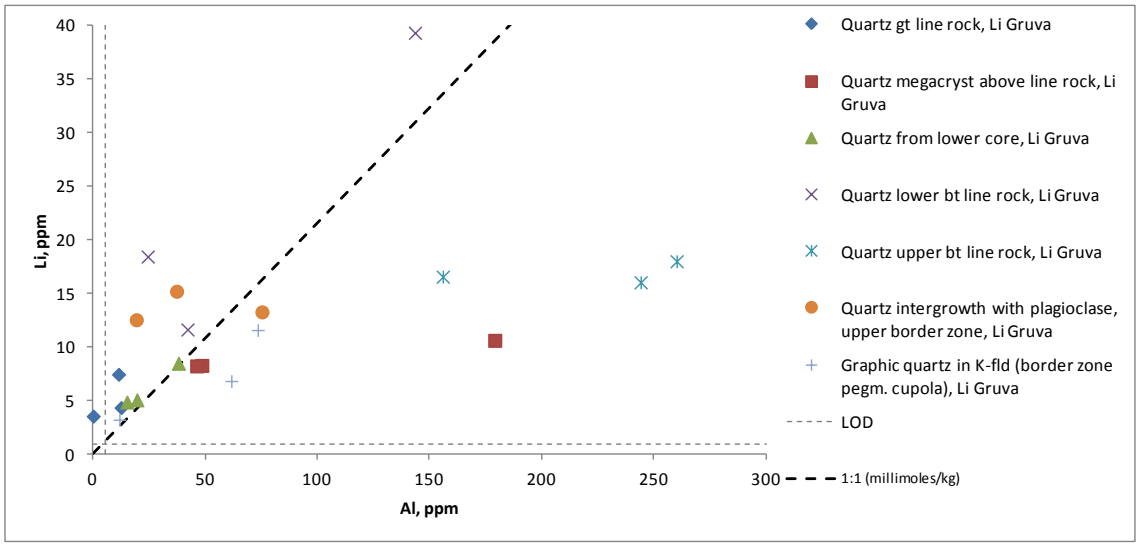

Fig. 4.4.16 Li versus Al for quartz from Li Gruva

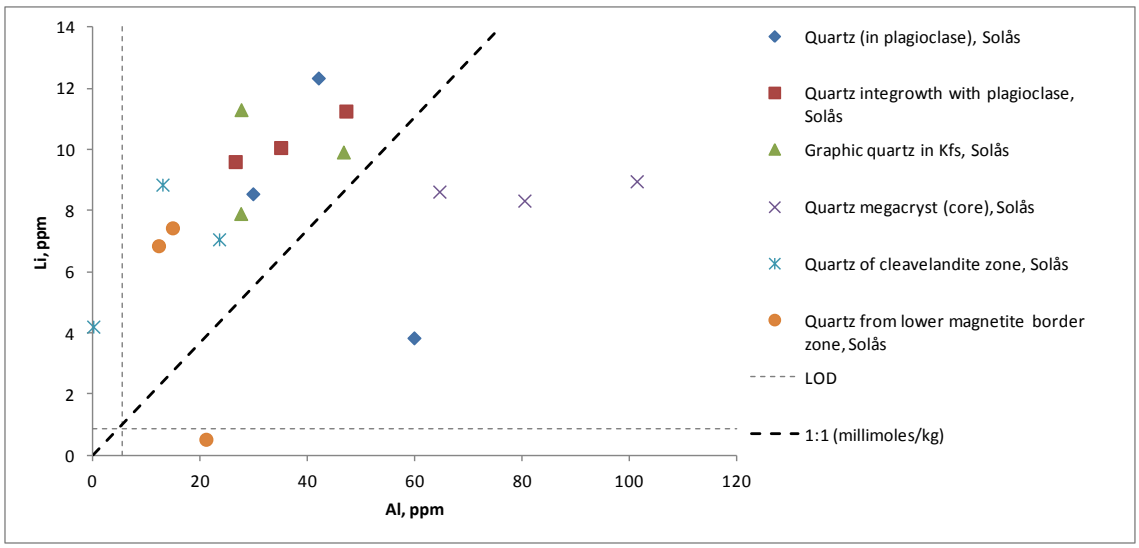

Fig. 4.4.17 Li versus Al for quartz from Solås

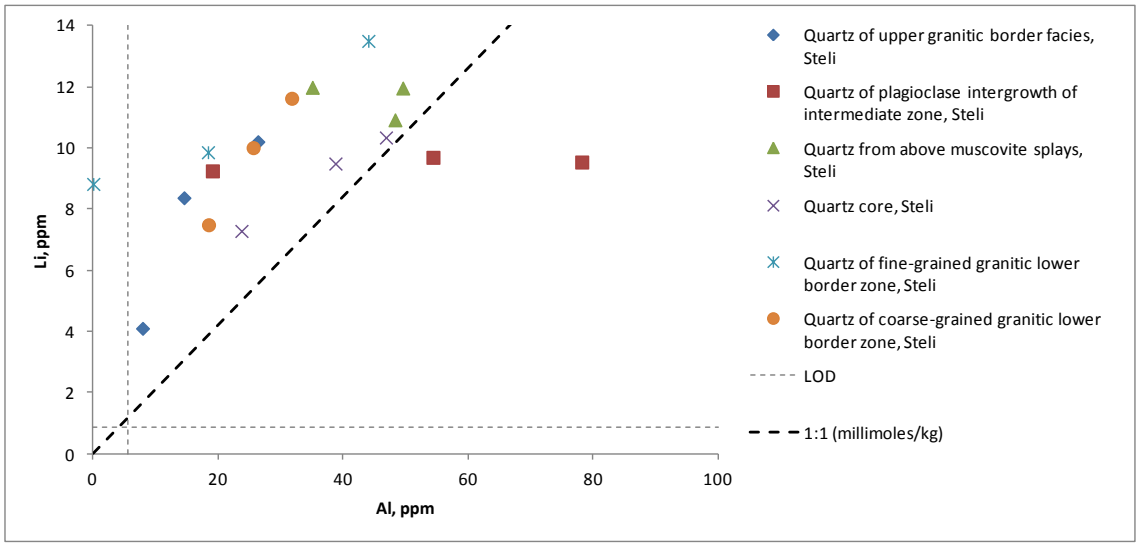

Fig. 4.4.18 Li versus Al for quartz from Steli

Figs. 4.4.19 to 4.4.26 demonstrate the typically positive correlation between Al and Ti. In magmatic quartz, there is a generally positive correlation between Ti and Al, with the exception of Steli which displays a strong negative correlation. Generally there appears to be little control on Ti content based on profile position. However, the beryl bearing quartz core of Hovåsen is enriched in Ti over the non-beryl core; the reverse is true for Li. The reverse is true for quartz associated with muscovite splays at Steli; potentially muscovite takes up Ti over Li, altering the trace elements available for incorporation in quartz. Notably, even the apparently 'pegmatitic' quartz from Landsverk 1 has been stripped of Ti, resembling more the hydrothermal material than the magmatic quartz.

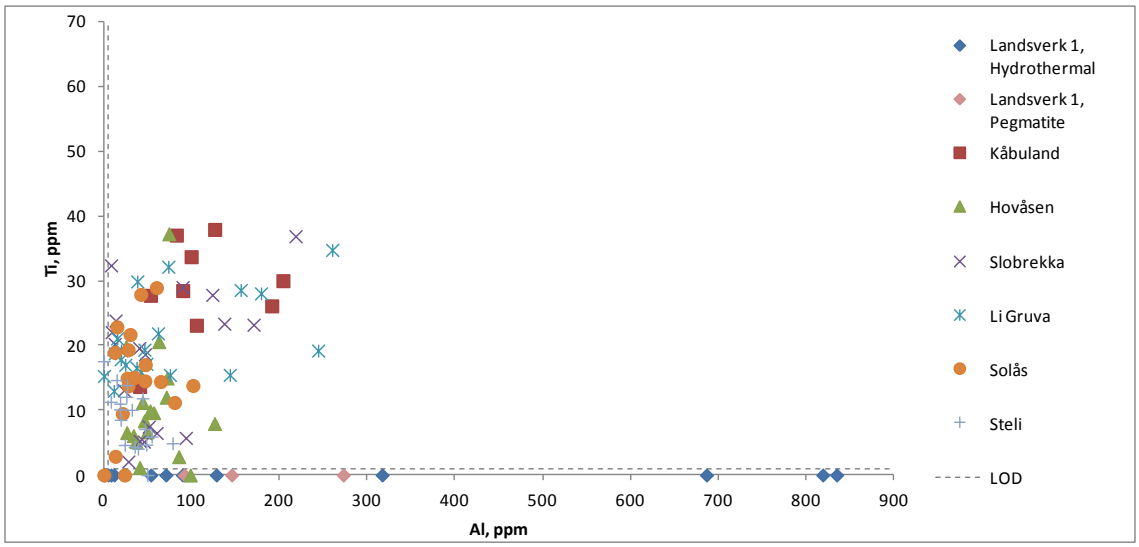

Fig. 4.4.19 Ti versus Al for quartz from each pegmatite

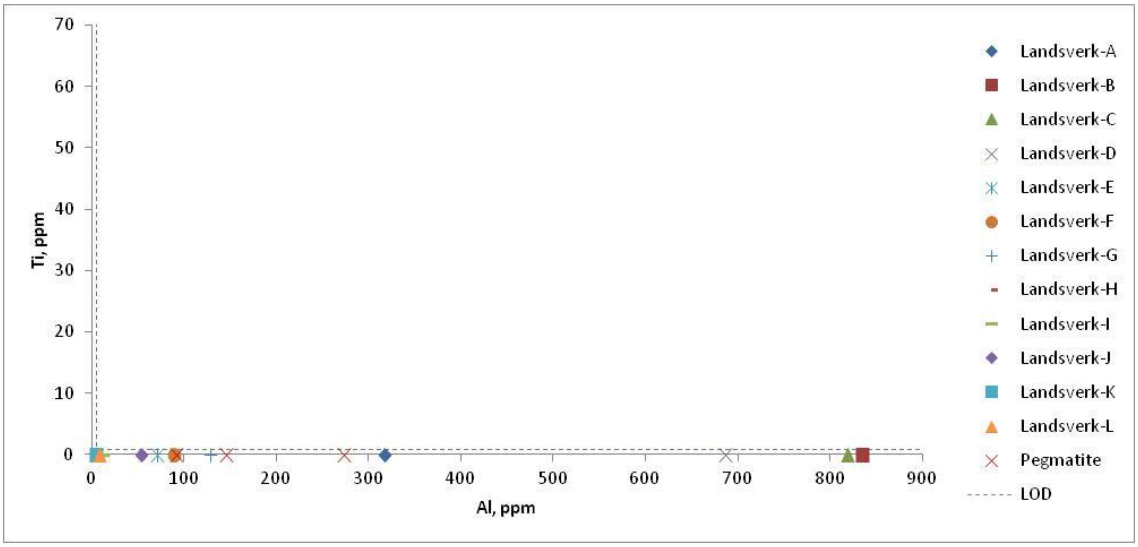

Fig. 4.4.20 Ti versus Al for quartz from L1

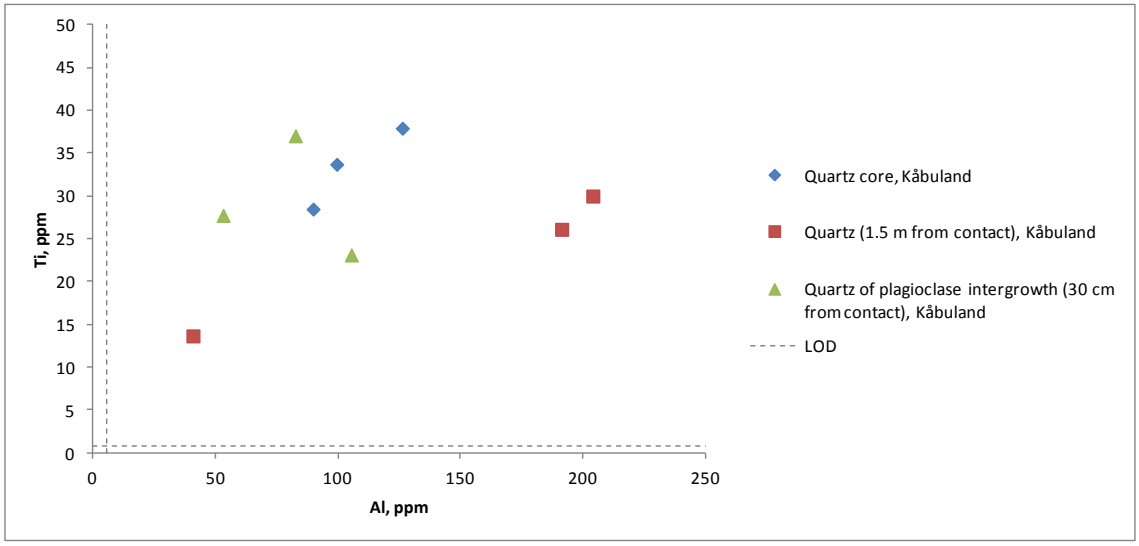

Fig. 4.4.21 Ti versus Al for quartz from Kåbuland

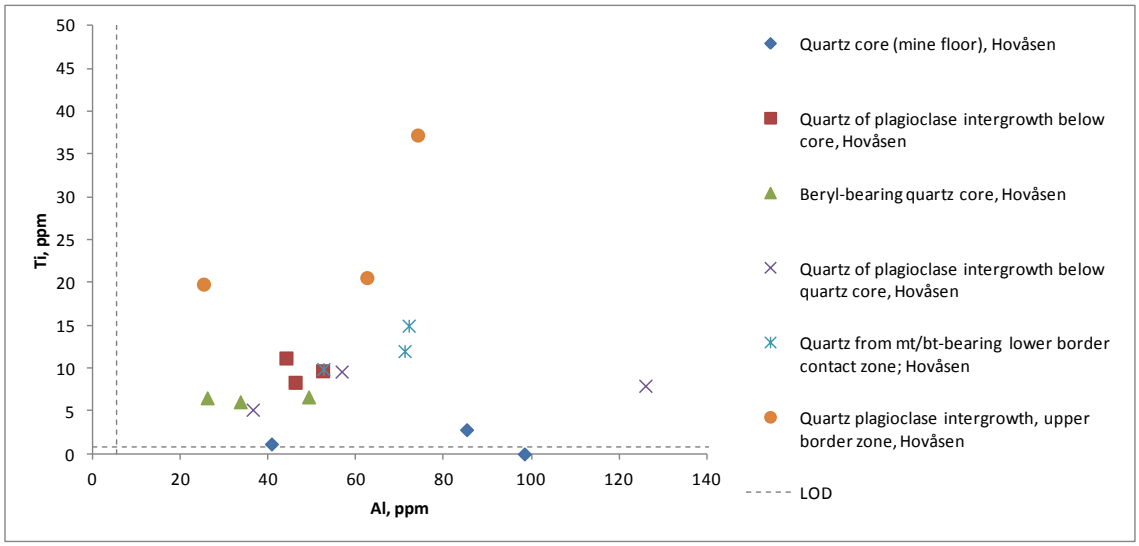

Fig. 4.4.22 Ti versus Al for quartz from Hovåsen

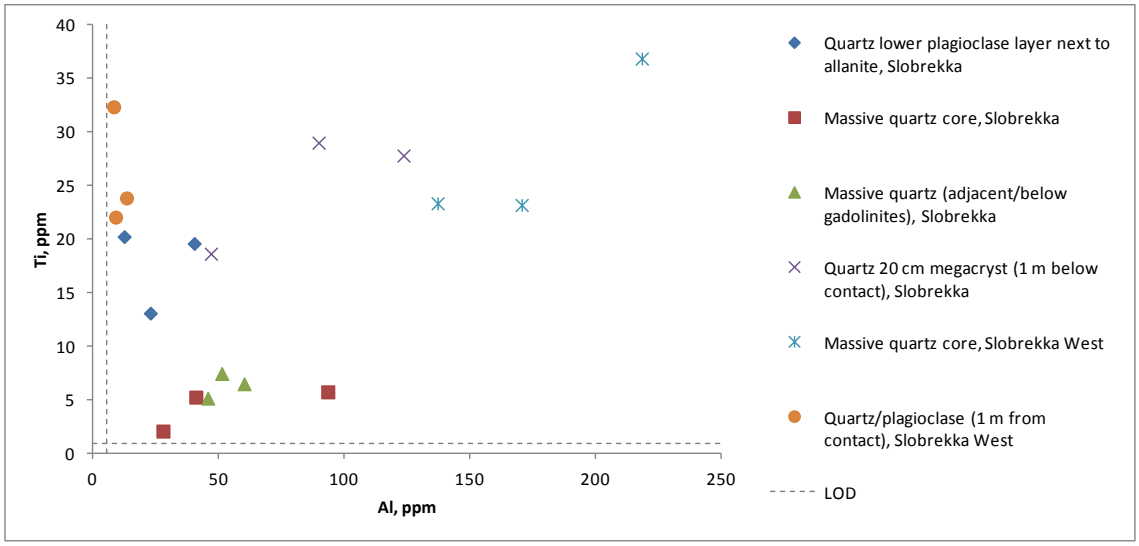

Fig. 4.4.23 Ti versus Al for quartz from Slobrekka

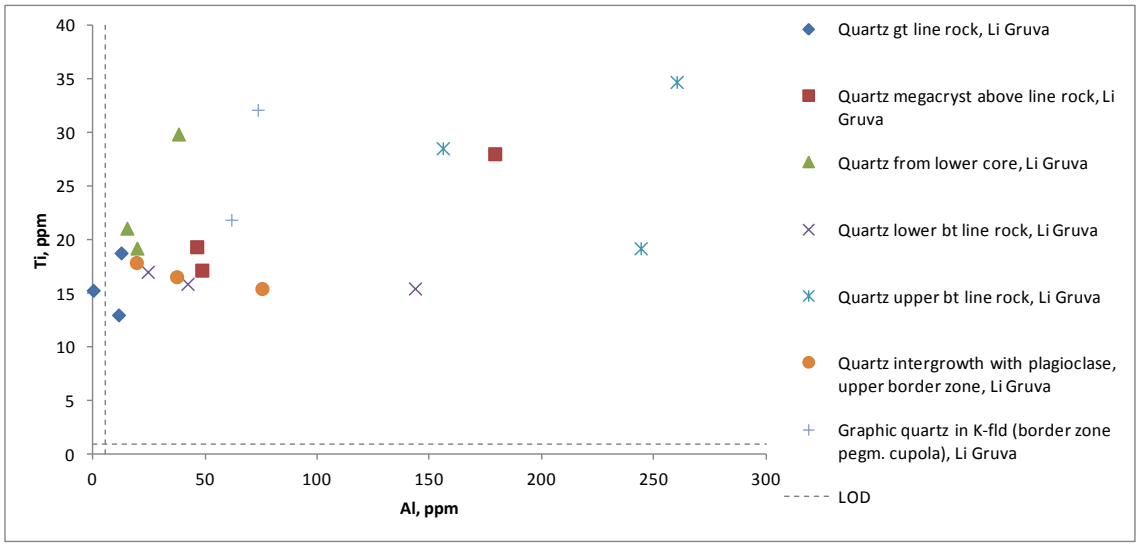

Fig. 4.4.24 Ti versus Al for quartz from Li Gruva

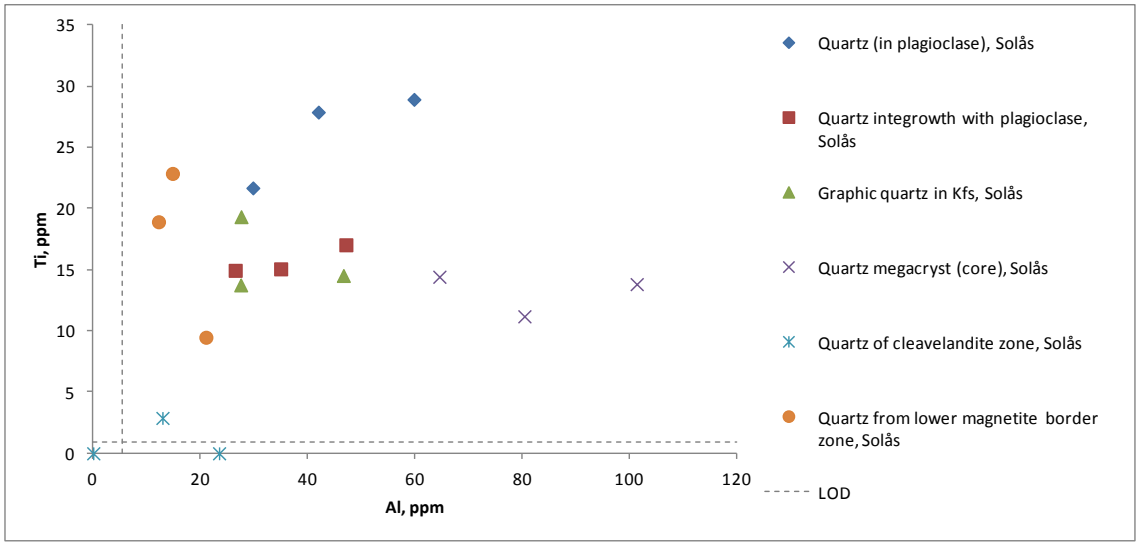

Fig. 4.4.25 Ti versus Al for quartz from Solås

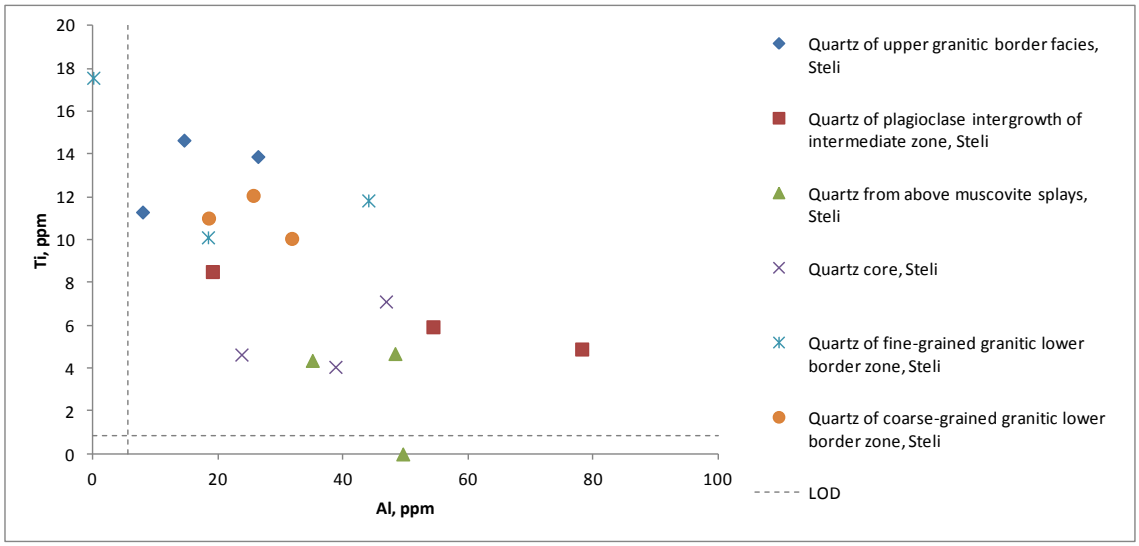

Fig. 4.4.26 Ti versus Al for quartz from Steli

Figs. 4.4.27 to 4.4.34 indicate that Ge follows a similar trend to Ti, in that it is relatively enriched in magmatic quartz, but essentially absent from hydrothermal quartz. Initial assessment appears to indicate that samples relatively low in Ti are high in Ge, and vice versa. Quartz of the upper granitic border facies at Steli, for example, is relatively low in Ge, but high in Ti. This makes sense, as quartz will accommodate either Ge or Ti in substitution for Si^{4+}, and it would be interesting to see if particular pegmatite zones/phases of crystallisation favour incorporation of Ti or Ge. Indeed, in Steli, Slobrekka and Hovåsen, the quartz core zones seem to be elevated in Ge, with border zones displaying elevated Ti; this relationship is supported by Fig. 4.4.35, which demonstrates an inverse correlation between Ti and Ge.

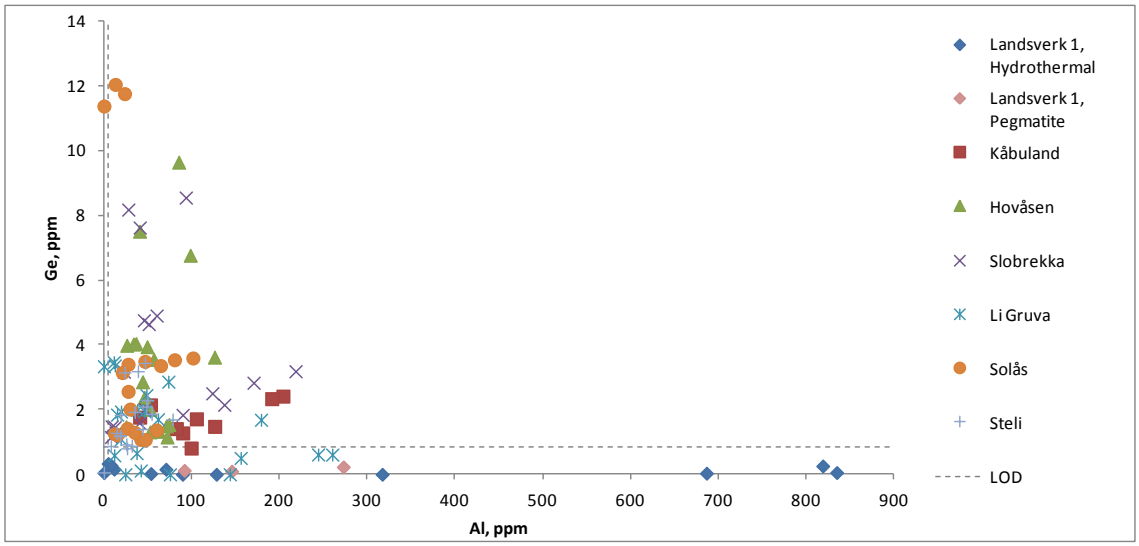

Fig. 4.4.27 Ge versus Al for quartz from each pegmatite

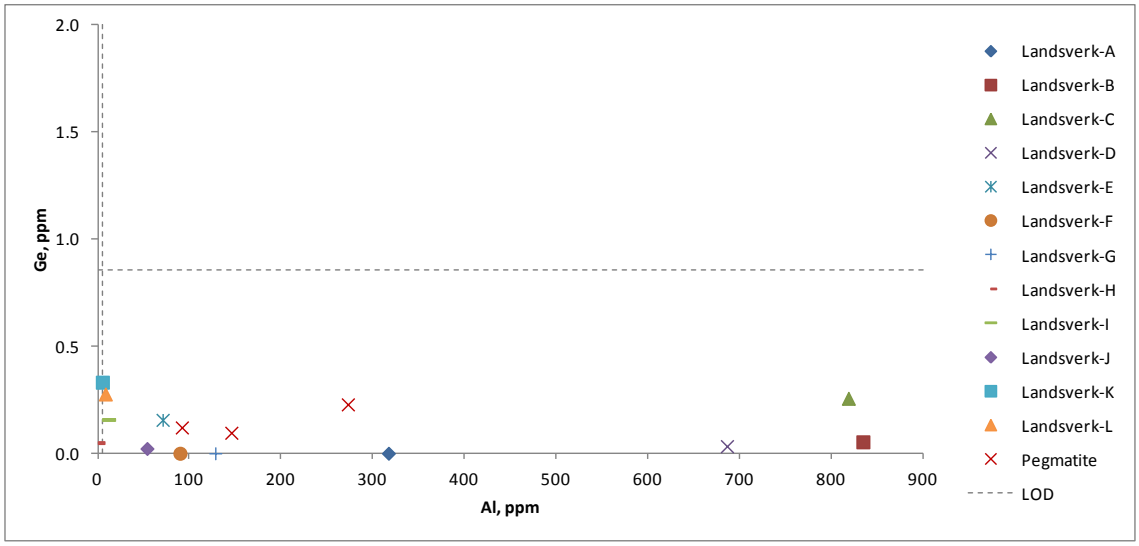

Fig. 4.4.28 Ge versus Al for quartz from Landsverk 1

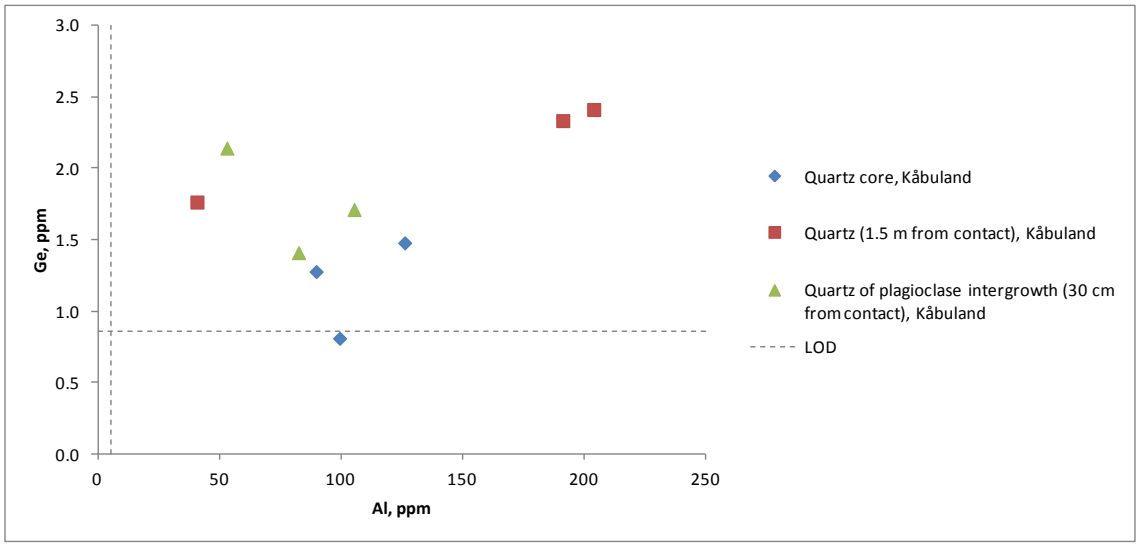

Fig. 4.4.29 Ge versus Al for quartz from Kåbuland

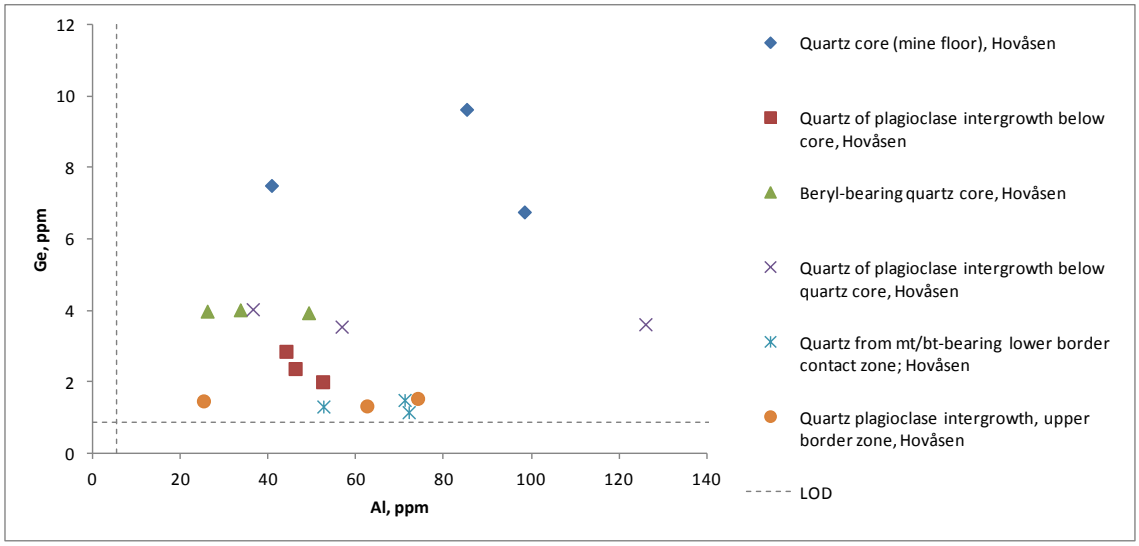

Fig. 4.4.30 Ge versus Al for quartz from Hovåsen

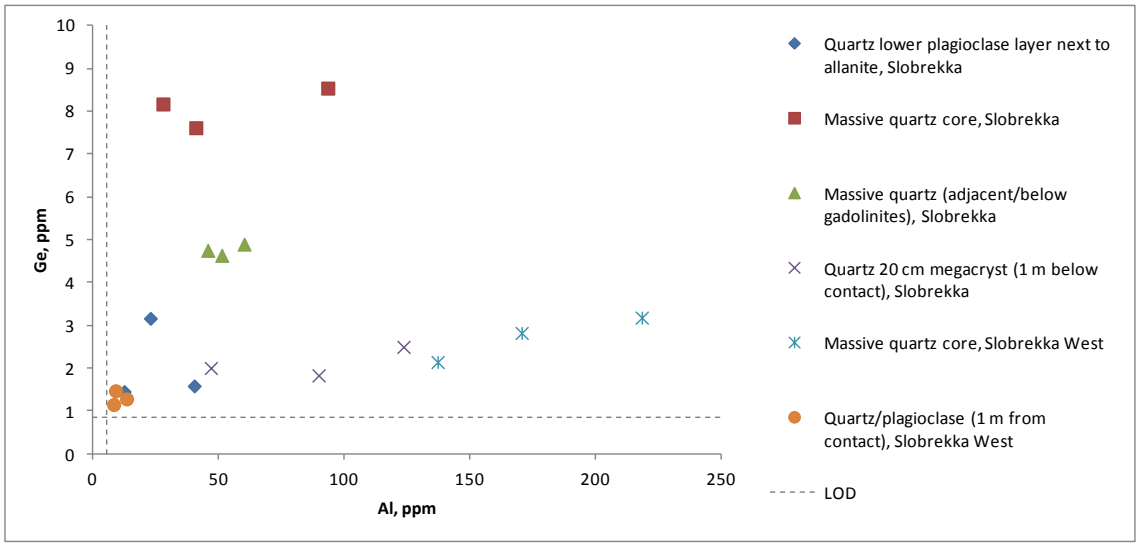

Fig. 4.4.31 Ge versus Al for quartz from Slobrekka

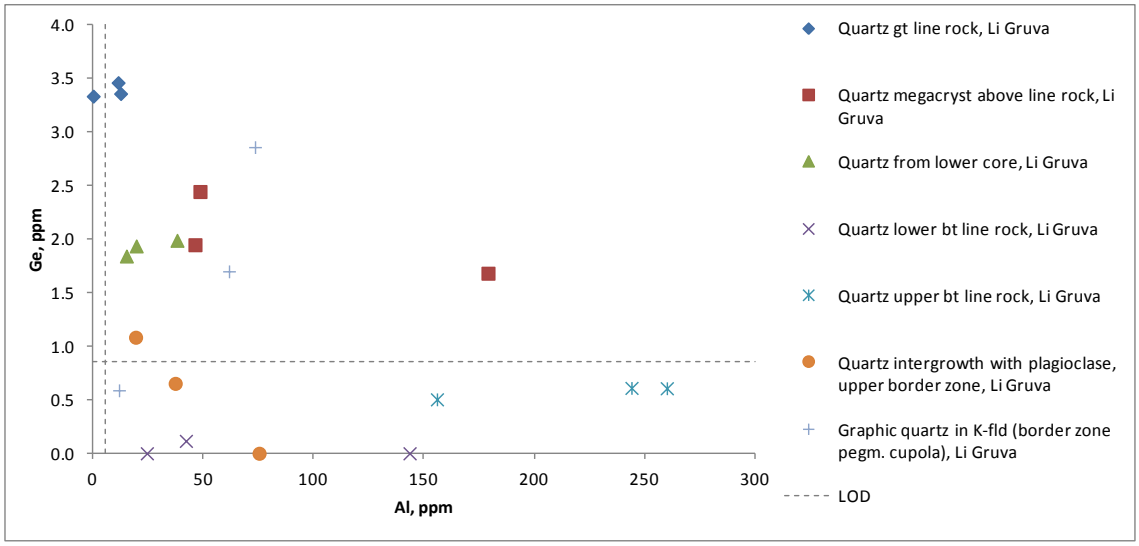

Fig. 4.4.32 Ge versus Al for quartz from Li Gruva

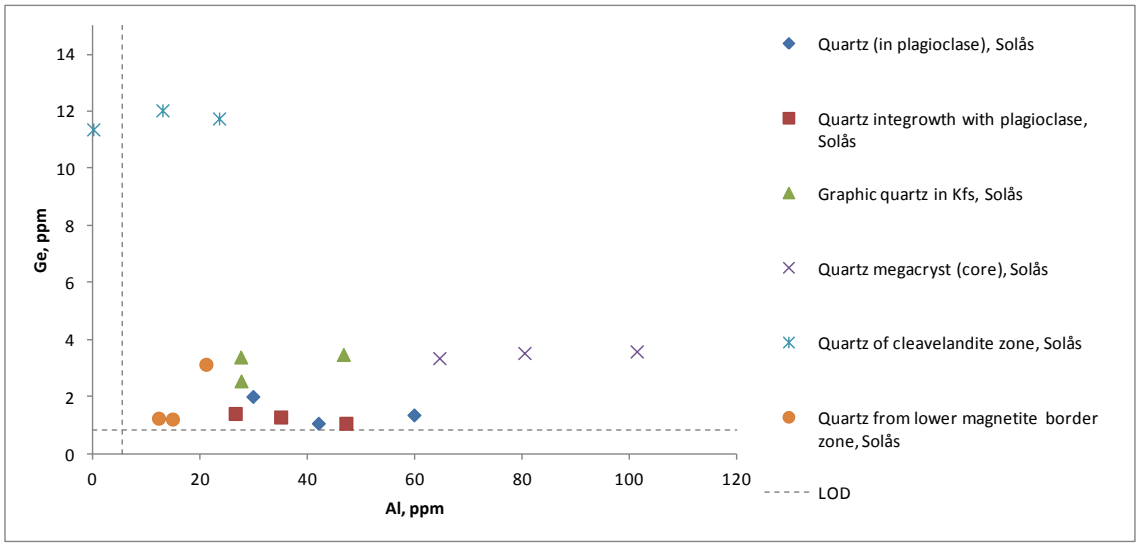

Fig. 4.4.33 Ge versus Al for quartz from Solås

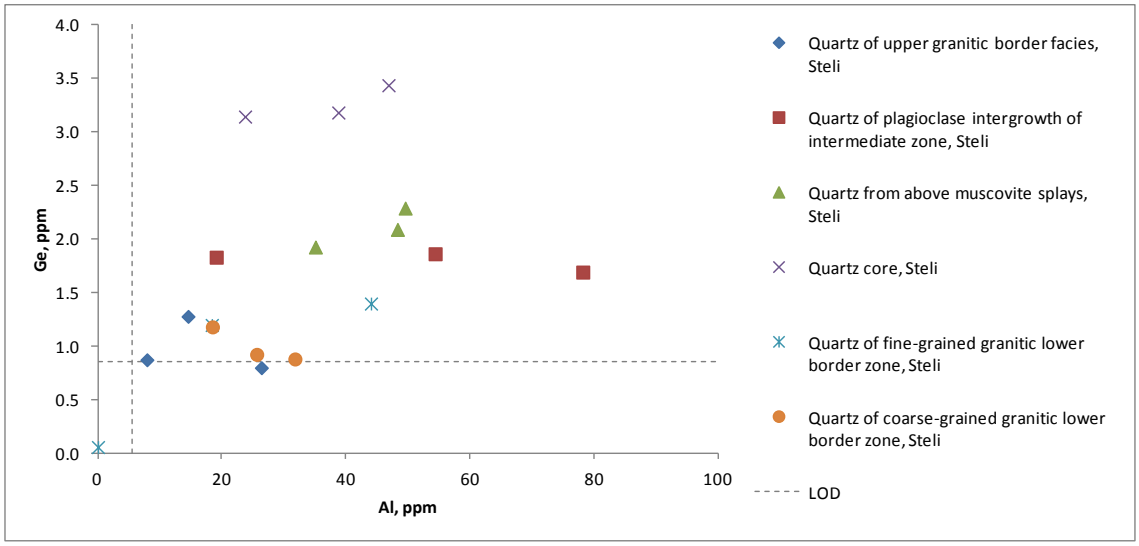

Fig. 4.4.34 Ge versus Al for quartz from Steli

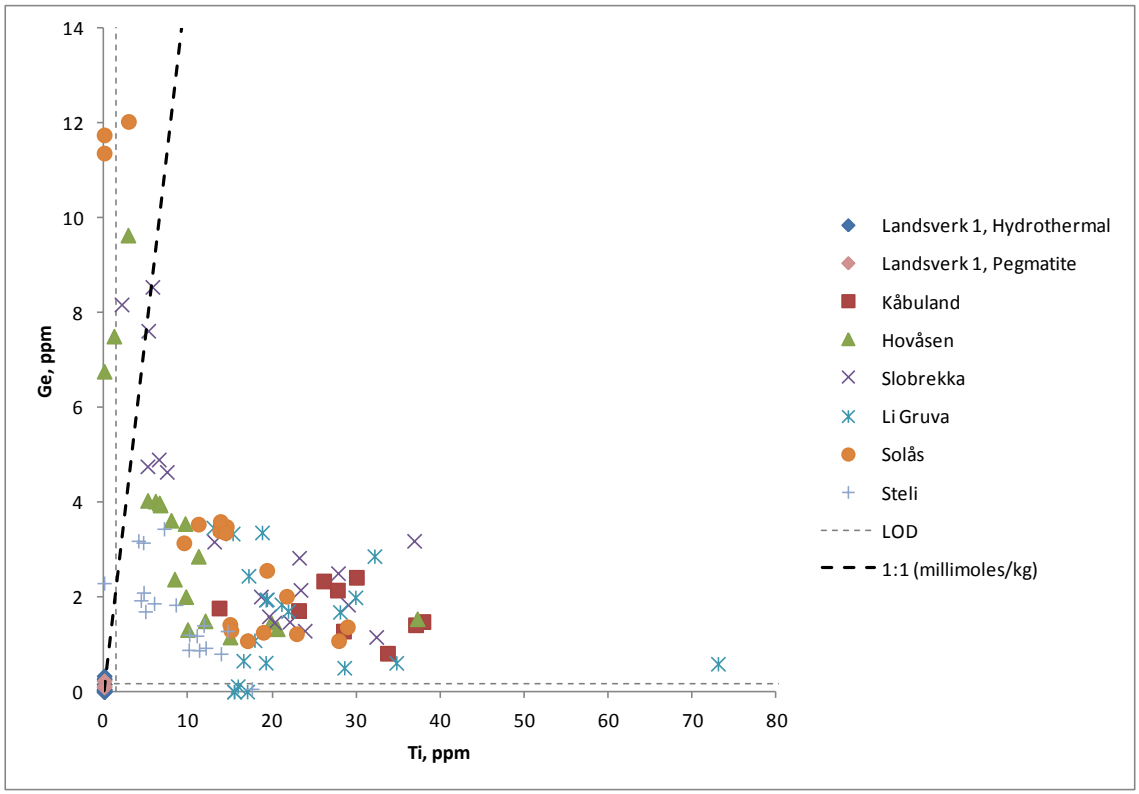

Fig. 4.4.35 Inverse relationship between Ti and Ge

4.4.3 Trace element data for quartz from the Landsverk pegmatites

57 samples from the pegmatites in the Landsverk region were analysed by LA-ICP-MS. The purpose of this exercise was to investigate the nature of the quartz surrounding the Landsverk 1 pegmatite. Due to limited exposure, quartz samples were taken predominantly from massive quartz pods, reminiscent of micro-cores, up to 1 m^3 in volume. The elements analysed for were Al, Li, Be, B, Mn, Ge, Rb, Sr, Sb, Na, Al, P, K, Ca, Ti, Fe, Zn and Ga; data is summarised in APPENDIX 2. The data was determined in two separate analytical runs; data falling below LOD has been omitted from mean calculations. The following bivariate plots (Figs. 4.4.36 to 4.4.39) contrast Li, Ti and Ge against Al to determine trace element trends in quartz. Points labelled 'Pegmatites' were observed in the field to represent unaltered pegmatites, and display a chemical signature similar to pegmatites elsewhere in the Evje-Iveland field. Points labelled 'Hydrothermal' were observed to display potential hydrothermal interaction, and contain an absence of Ge and Ti, as with Landsverk 1 quartz. Field observations were uncertain for points labelled 'Transition', which geochemically appear to correlate with primary pegmatite quartz over hydrothermal material. 'Vein' refers to the 1.5 m thick quartz vein orientated

161/54 E 300 m east of Landsverk 1 seen to contain pyrite and epidote; members of the hydrothermal mineral suite representative of overprinting at Landsverk 1.

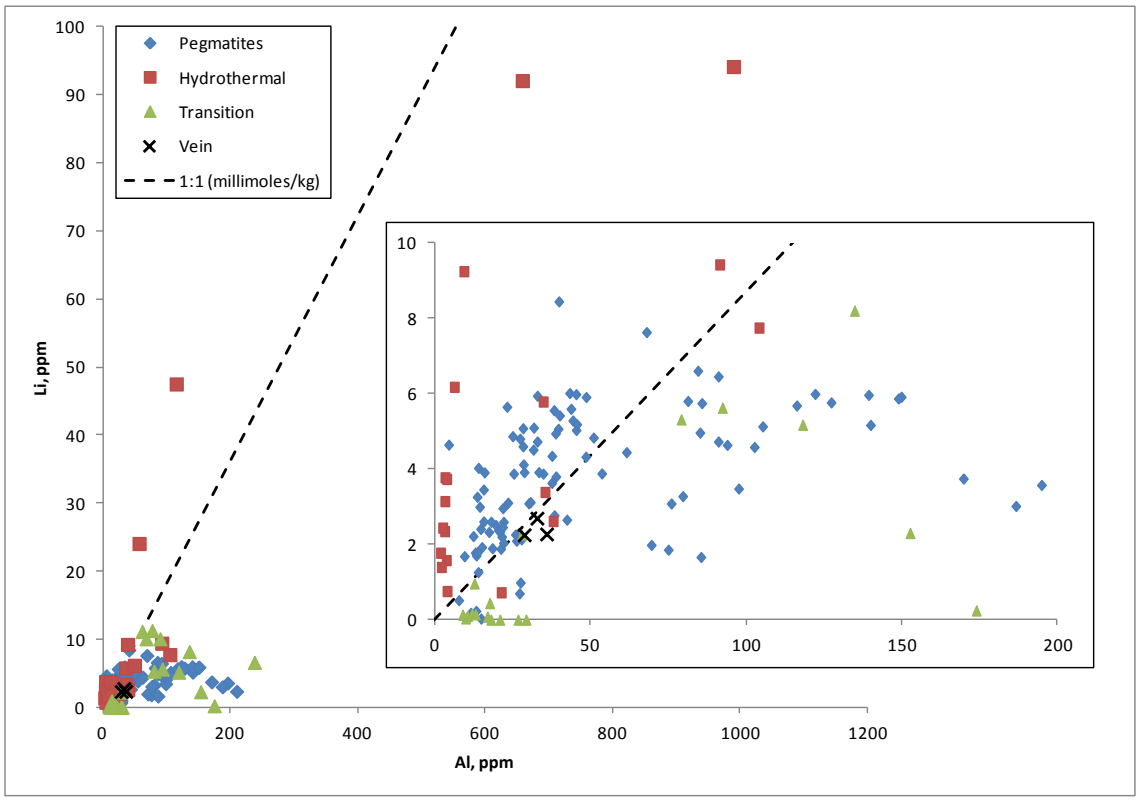

Fig. 4.4.36 Li versus Al for quartz from the Landsverk pegmatites

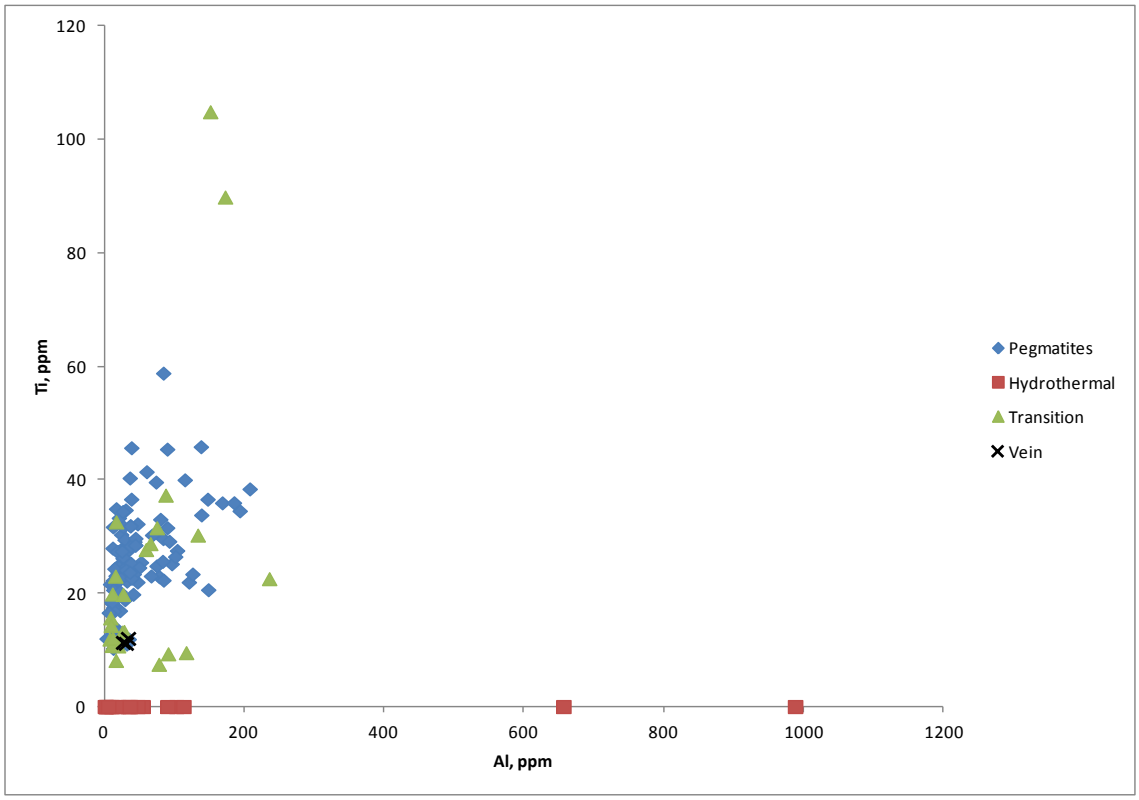

Fig. 4.4.37 Ti versus Al for quartz from the Landsverk pegmatites

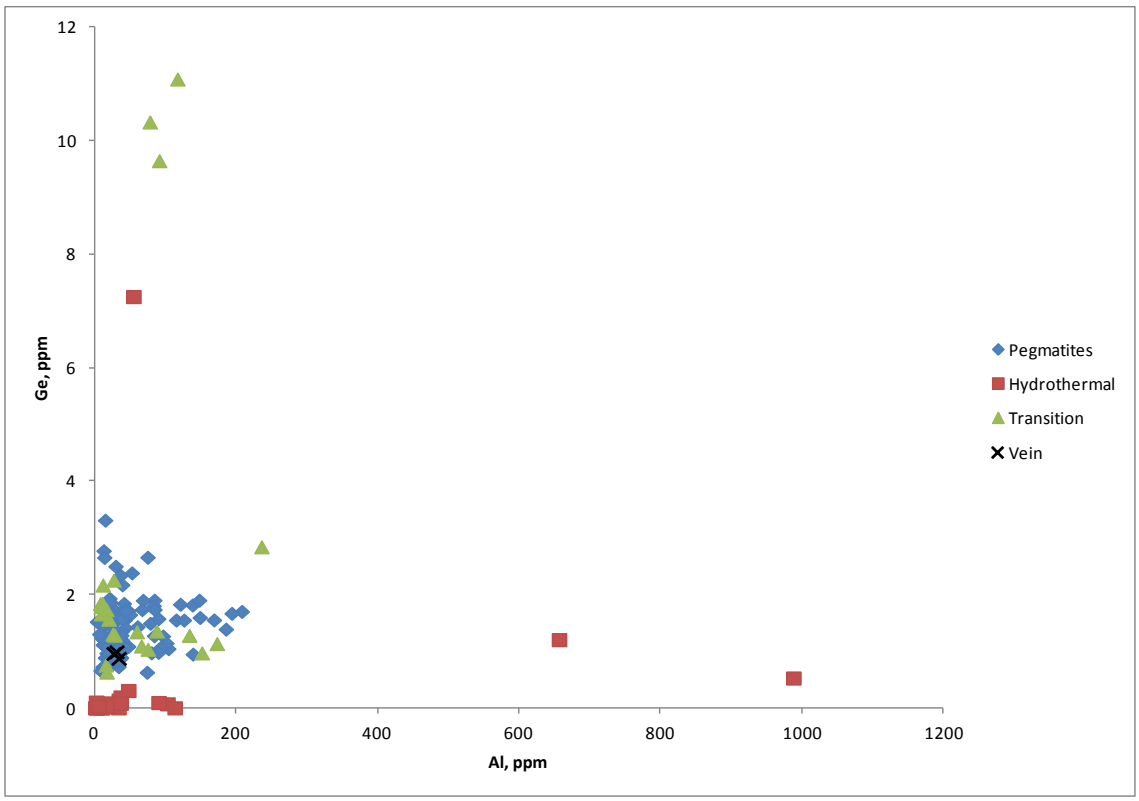

Fig. 4.4.38 Ge versus Al for quartz from the Landsverk pegmatites

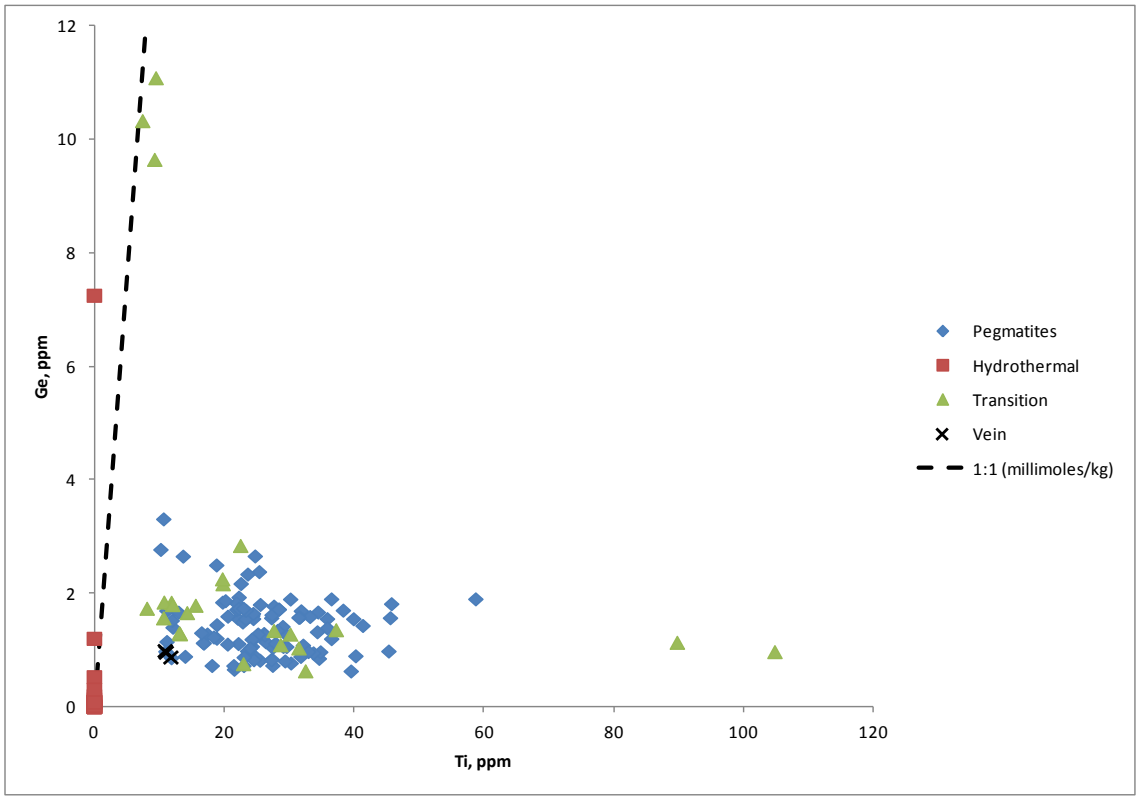

Fig. 4.4.39 Ge versus Ti for quartz from the Landsverk pegmatites

The concentrations of Al, Li, Ti and Ge from quartz sampled in the Landsverk 1 region were plotted onto the geological map produced for the area. Sample sites are indicated in Fig. 4.4.40. Figs. 4.4.41 to 4.4.44 display georeferenced symbols proportional in size to concentration bands, as indicated in the legend. As with quartz throughout the Evje-Iveland pegmatites, there is an approximate correlation between Al and Li, and an inverse relationship between Ti and Ge (demonstrated in Fig. 4.4.35). There appears to be no spatial (and therefore structural) control over the distribution of the elements.

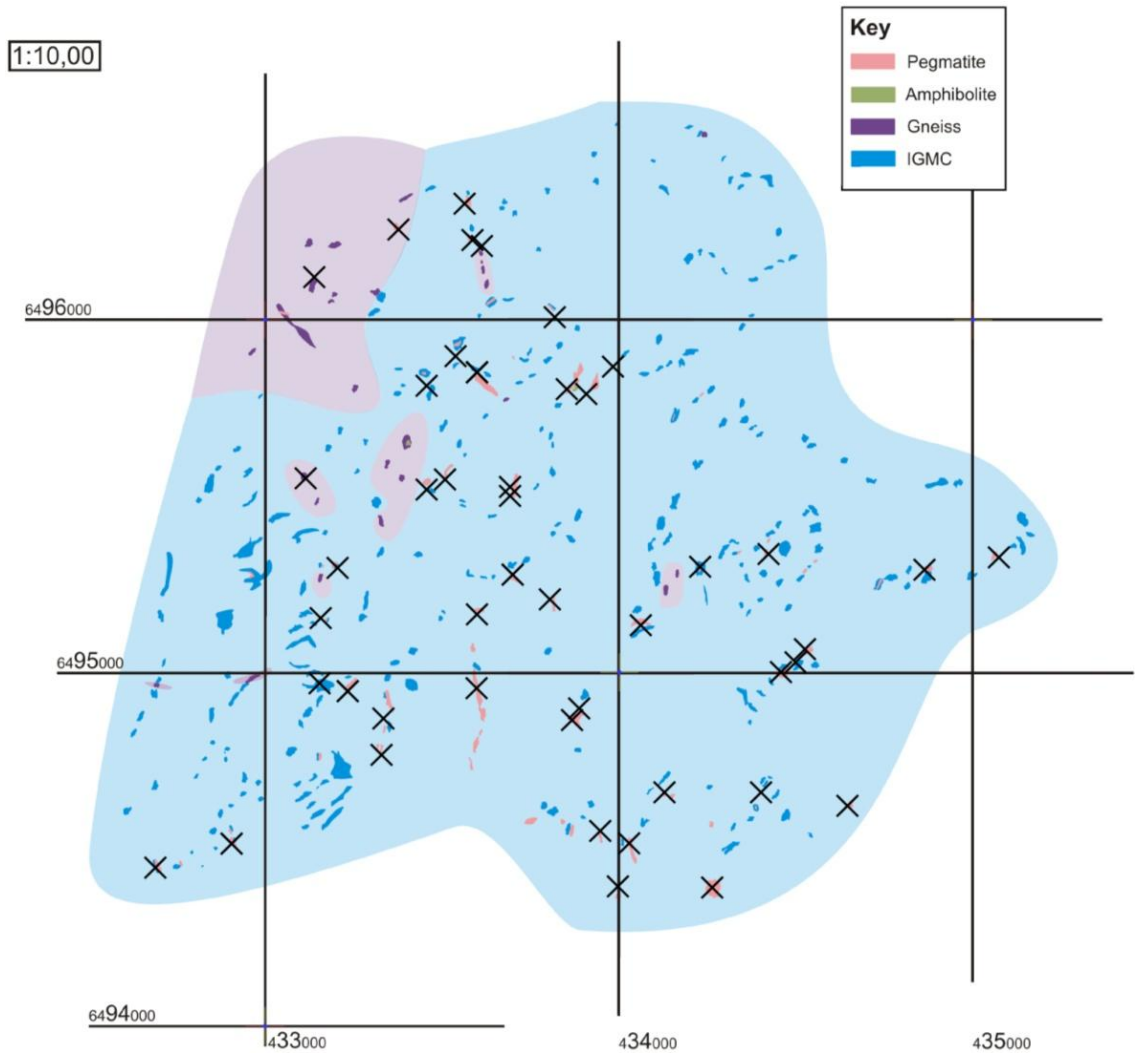

Fig. 4.4 40 Sample sites (X) for pegmatitic quartz in the area surrounding the Landsverk 1 pegmatite (gridlines are 1 km square)

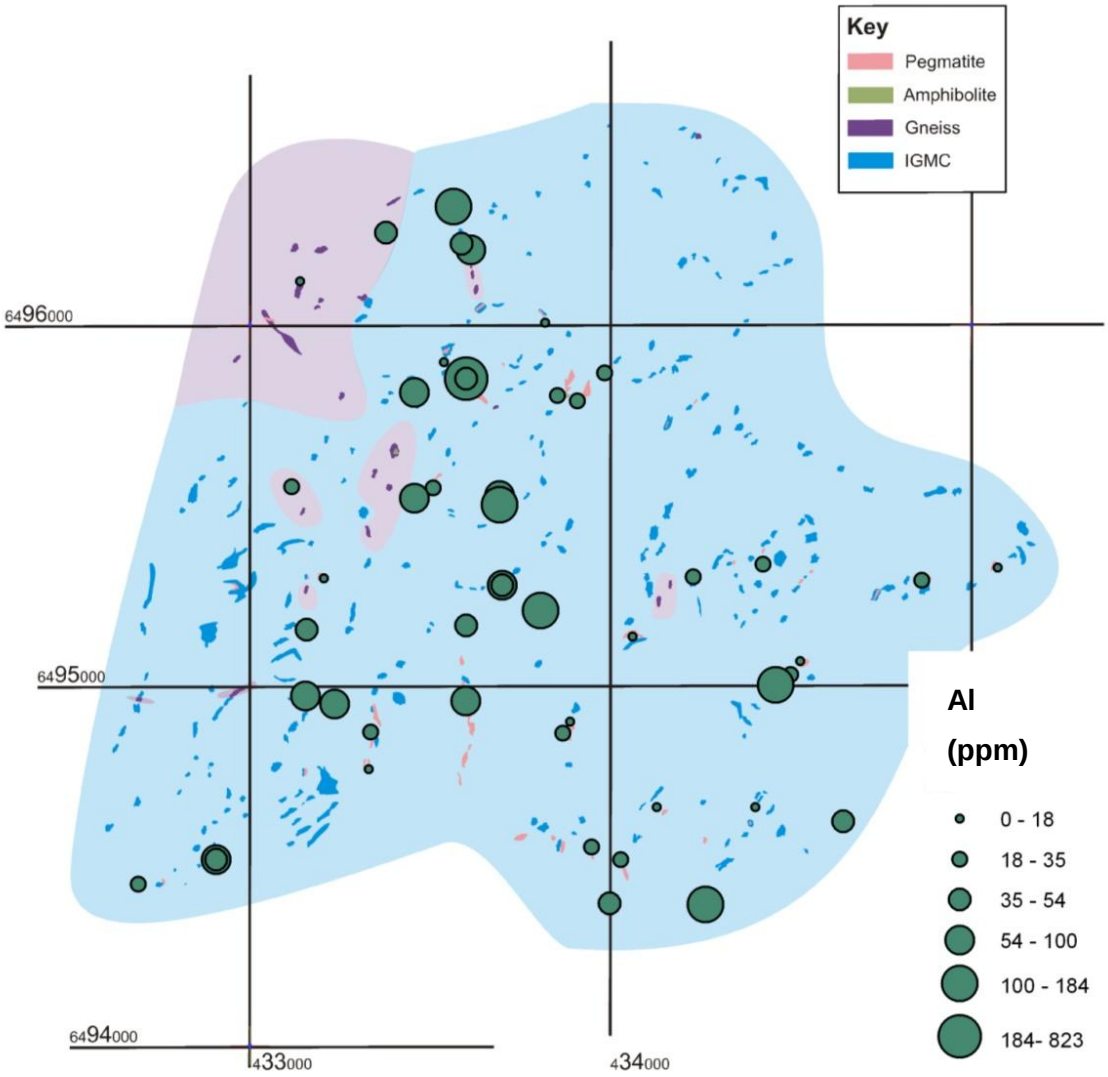

Fig. 4.4.41 Distribution of Al (ppm) in pegmatitic quartz in the area surrounding the Landsverk 1 pegmatite (gridlines are 1 km square)

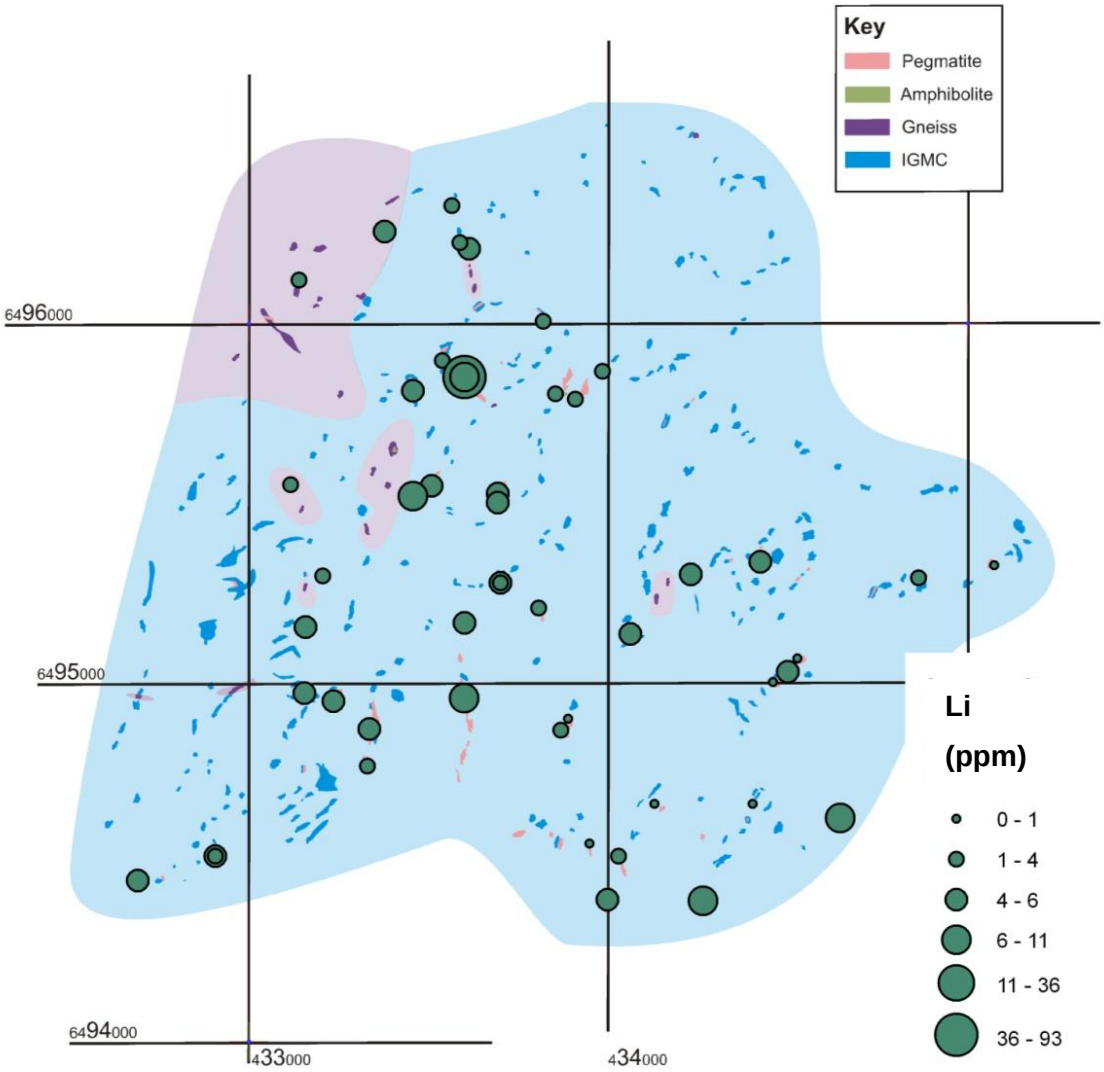

Fig. 4.4.42 Distribution of Li (ppm) in pegmatitic quartz in the area surrounding the Landsverk 1 pegmatite (gridlines are 1 km square)

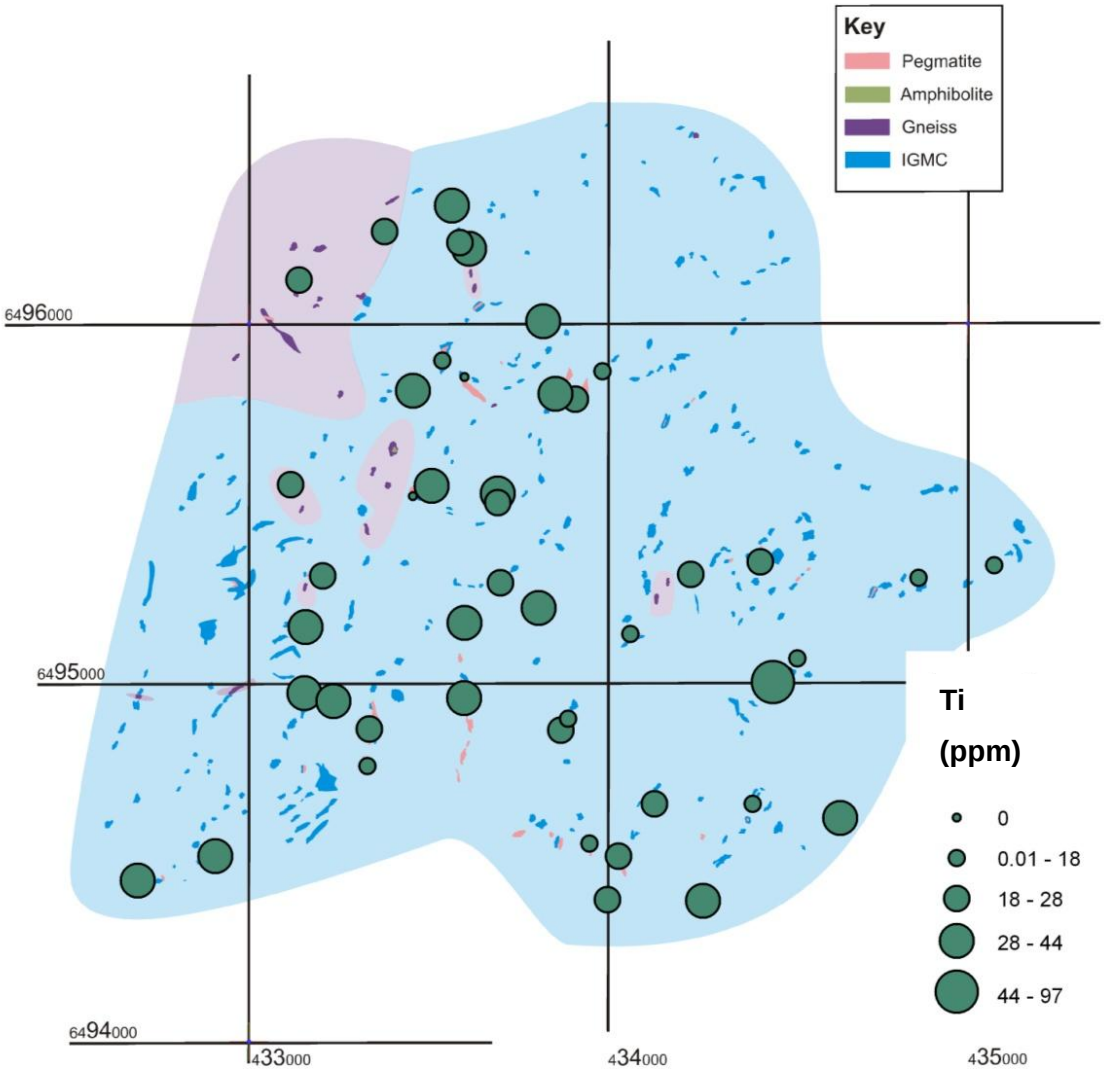

Fig. 4.4.43 Distribution of Ti (ppm) in pegmatitic quartz in the area surrounding the Landsverk 1 pegmatite (gridlines are 1 km square)

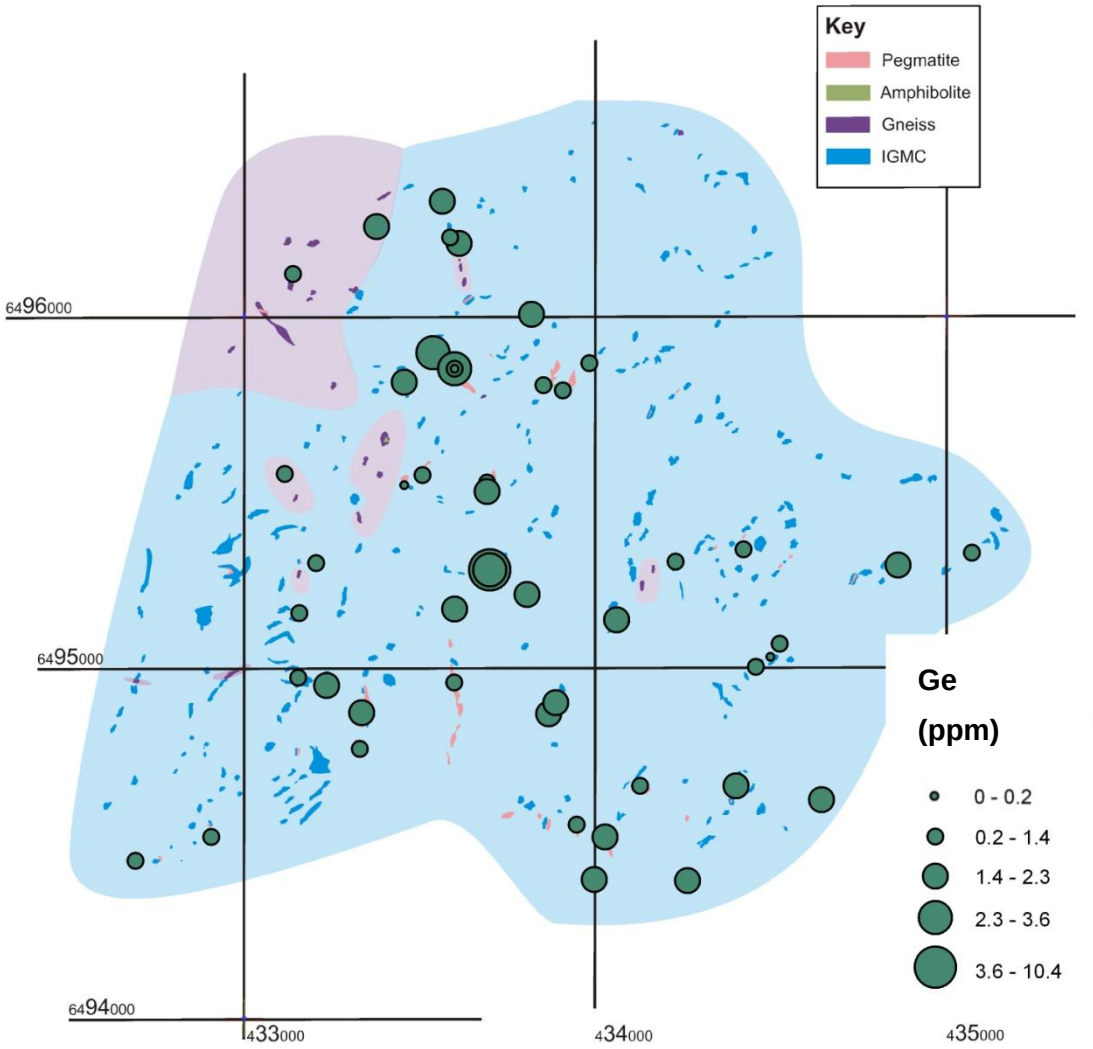

Fig. 4.4.44 Distribution of Ge (ppm) in pegmatitic quartz in the area surrounding the Landsverk 1 pegmatite (gridlines are 1 km square)

4.4.4 Micas

XRF data is presented to classify pegmatite micas in the scheme of Tischendorf et al. (2001) (as outlined in their Fig. '16'). Data for micas (both 'biotite' and 'muscovite') analysed by XRF are summarised compositionally in APPENDIX 2. Classification was based on the feal and mgli parameters of Tischendorf et al. (2001); Fe_{Total} + Mn + Ti – Al^{VI} and octahedral (Mg – Li) respectively, which were calculated using the methods of Tindle and Webb (1990). The results are demonstrated in Fig. 4.4.45, which indicates that the 'biotites' are predominantly magnesian sidero-phyllites, with the material from Steli containing increased Mg. The 'muscovites' are classified as zinnwaldite, essentially an Fe-rich lepidolite. This is unexpected, as the Evje-Iveland pegmatites are renowned for an absence of Li. Because the Li values were calculated based on SiO_2 and

MgO contents, it is likely to be overestimated; a reduction in Li would move the mica towards the ferroan muscovite field, which is perhaps more realistic.

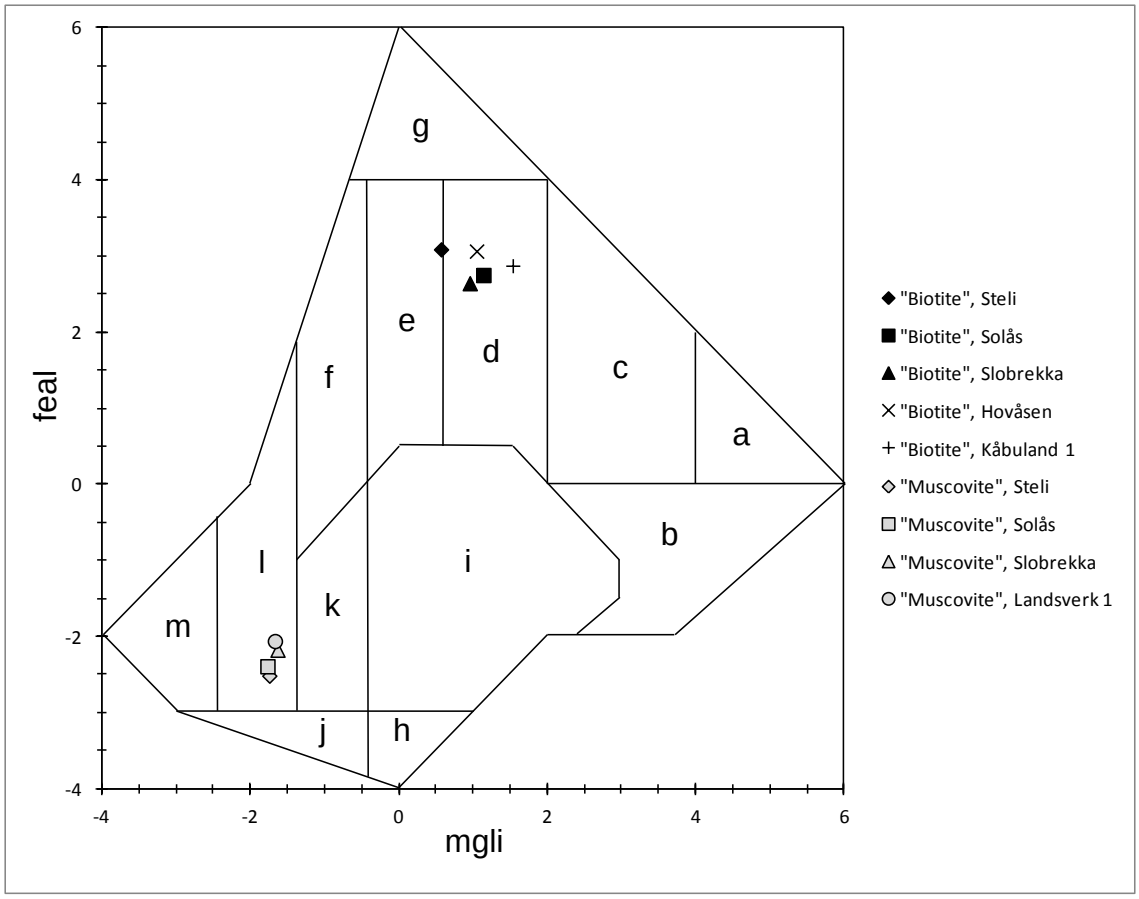

Fig. 4.4.45 Classification of Evje-Iveland micas using XRF compositional data, after Tischendorf et al. (2001) and Tindle and Webb (1990). a = phlogopite. b = aluminium phlogopite. c = ferroan phlogopite (Mg biotite). d = magnesian sidero-phyllite (Fe biotite). e = siderophyllite. f = lithian sidero-phyllite (proto-lithionite). g = annite. h = muscovite. i = ferroan muscovite (phengite). j = lithian muscovite. k = lithian ferroan muscovite (Li phengite). l = ferroan polylithionite (zinnwaldite). m = poly-lithionite (lepidolite).

4.5 Geothermometry

Wark and Watson (2006) demonstrated a correlation between the concentration of Ti in quartz (Qtz_{Ti}) and the temperature of crystallisation of the quartz, and in doing so developed the TitaniQ geothermometer, based on the substitution of Ti^{4+} for Si^{4+}, calibrated for quartz crystallised in the presence of rutile. Samples were microscopically assessed prior to analyses by LA-ICP-MS; rutile is present ubiquitously as needles (see *Chapter 4.6.1*), so the material qualifies as suitable for the application of the TitaniQ geothermometer below:

$$T\,(°C) = \frac{-3765}{\log(Qtz_{Ti}) - 5.69} - 273$$

As samples were taken in vertical profiles through the pegmatites (i.e. from the upper margin, progressively through the core, and from the lower margin) LA-ICP-MS data was utilised to generate temperature profiles (Fig. 4.5.1). It can be demonstrated that quartz crystallises at a higher temperature at pegmatite peripheries immediately after emplacement (~600°C), and progressively cools towards the core with further crystallisation (~450°C). Quartz from the L1 pegmatite contained Ti below LOD i.e. <0.75 ppm. 0.75 ppm produces a crystallisation temperature of less than 374°C, which suggests a formation temperature below that of the other Evje-Iveland pegmatites.

An attempt was made to relate temperature of crystallisation with quartz chemistry; at Slobrekka (Fig. 4.5.2) there appears to be a correlation between Al content and crystallisation temperature, but this is not strong, and is the only example.

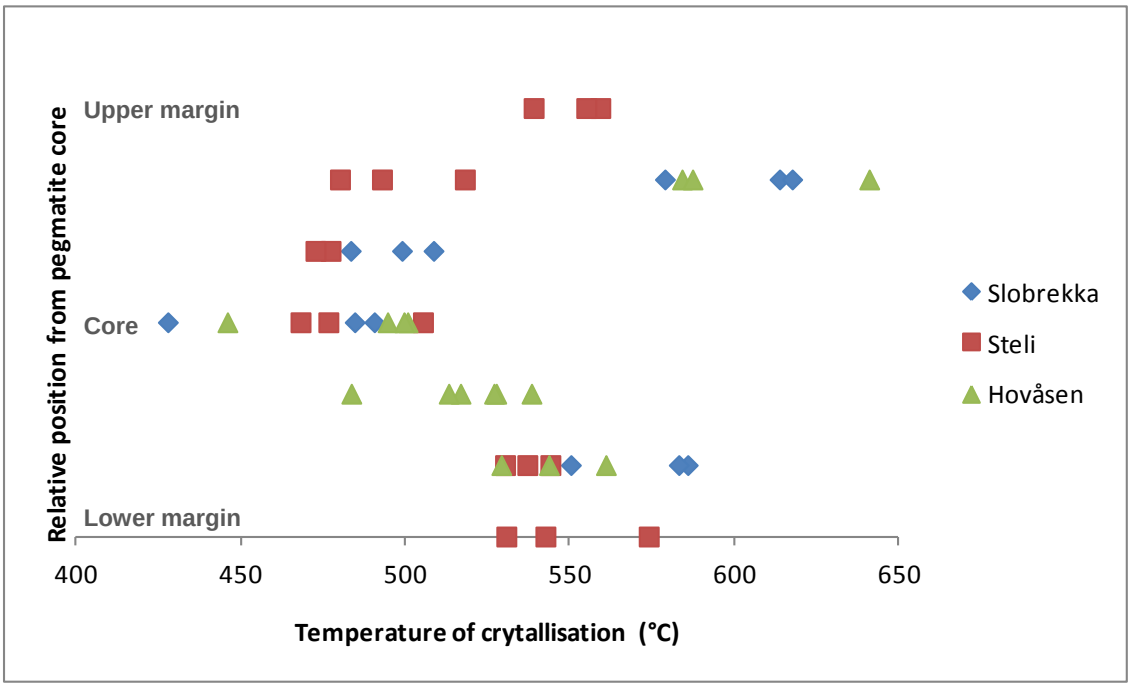

Fig. 4.5.1 Estimates of quartz crystallisation temperatures (as assessed using the TitaniQ method of Wark and Watson (2006)) in vertical sections through the Slobrekka, Steli and Hovåsen pegmatites, demonstrating symmetrical distribution

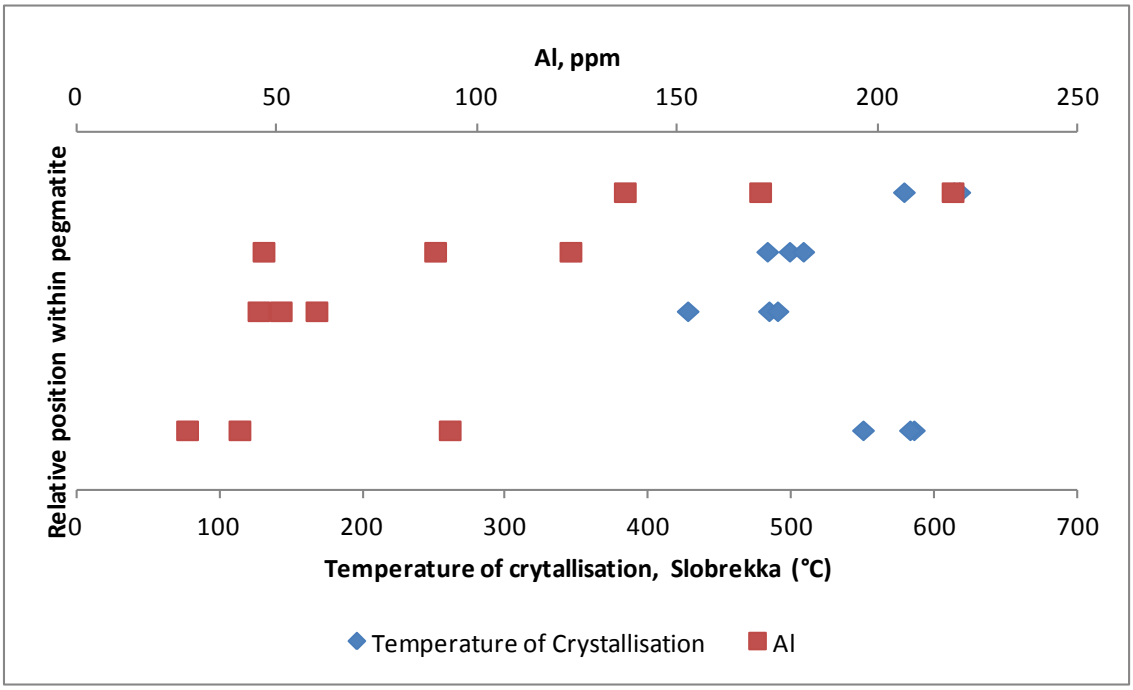

Fig. 4.5.2 Correlation between crystallisation temperature (as assessed using the TitaniQ method of Wark and Watson (2006)) and Al content of quartz in the Slobrekka pegmatite

4.6 SEM-CL assessment of mineralogical textures

4.6.1 Structures and inclusions in magmatic quartz

Quartz samples from the Landsverk 1, Kåbuland, Hovåsen, Slobrekka, Li Gruva, Solås and Steli pegmatites were imaged using cathodoluminescence in SEM (SEM-CL) to determine the various stages of quartz development present through textural and colour contrasts, following the method of Müller et al. (2008). The results are summarised in Table 4.6.1. In Table 4.6.1, pqtz represents primary quartz and sqtz represents secondary quartz overprinting primary quartz (with 1 denoting early and 6 late stage overprints, and the letter suffix denoting synchronous/chronologically indistinguishable events). - indicates a phase is not present.

pqtz

After Müller et al. (2008), this material is the primary magmatic quartz (likely to have initially crystallised as β-quartz, after the temperatures in **Chapter 4.5**), formed initially upon crystallisation of quartz material directly from the pegmatite melt; it is abundant, massive, featureless and of mid-grey luminosity (right side of Fig. 4.6.1) – typically the brightest quartz phase.

sqtz1a

A texture present typically in material from the wall zone but also within the core of the pegmatite, sqtz1a appears as a network of darker quartz in the pqtz. Potentially, the texture represents a migration of defects and/or trace elements from the quartz lattice, forming a series of pure cores and element-rich rims. The nuclei which form as a result of the network are approximately 10 μm in diameter (Fig. 4.6.2). Alternatively, the texture may be related to late-kinematic emplacement and represent quasi-recrystallisation.

sqtz1b

sqtz1b is extremely similar in nature and morphology to sqtz1a, but the nuclei appear on a 100 μm scale. Sqtz1b appears to be crosscut by later quartz generations in a manner comparable to sqtz1a, so the two are interpreted to be synchronous.

sqtz1c

sqtz1c is manifested as diffuse overprinting (often forming wavefronts) of darker zones within pqtz, and is cut by sqtz2. Quartz of lower luminescence typically contains fewer defects than brighter quartz and for energetic reasons tends to replace defect-rich quartz by grain-boundary migration (e.g. Müller et al., 2002a). This results in a type of progressive zoning representing the steps of boundary migration. Sqtz1c is only observed in those samples from the wall zone of the pegmatite (Fig. 4.6.1).

sqtz1d

sqtz1d is present as approximately 5 µm specks of low luminosity quartz hosted in pqtz (Fig. 4.6.1).

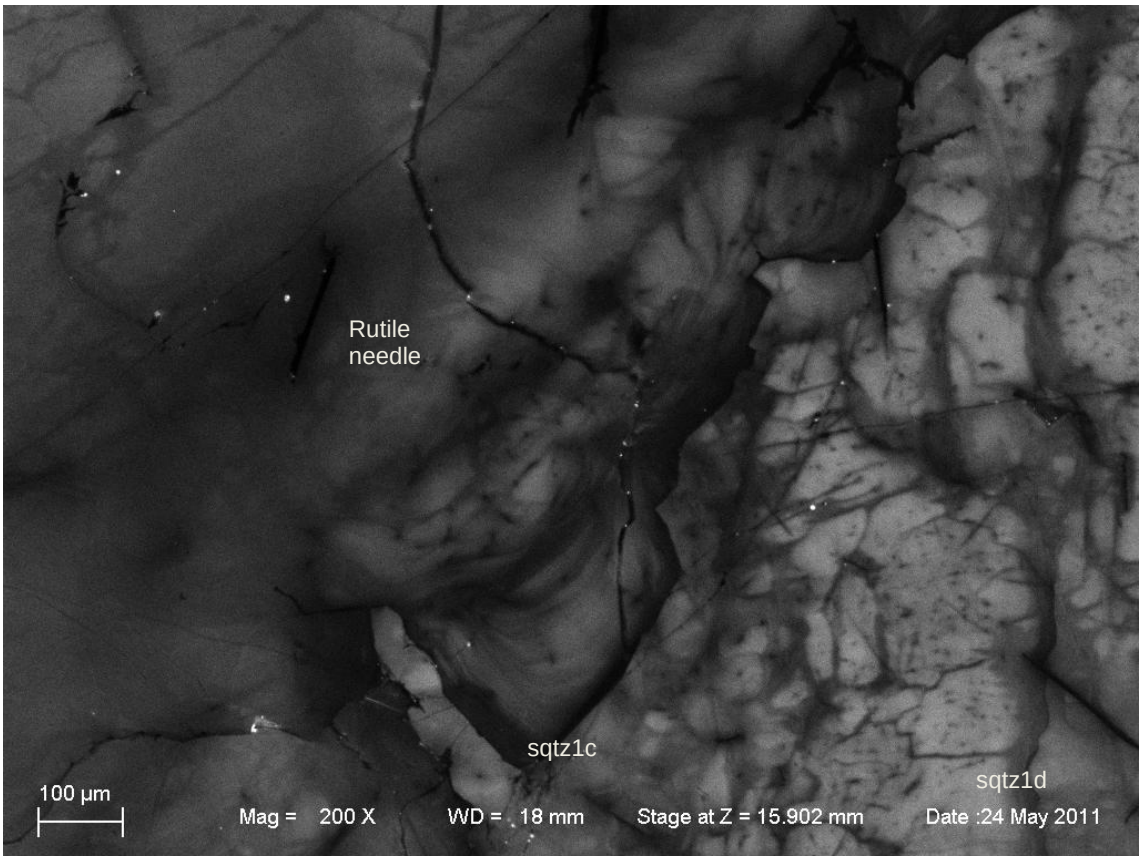

Fig. 4.6.1 CL-SEM image of quartz from Li Gruva wall zone (100910-01), showing a variety of quartz phases; pqtz on the right side (mid grey), sqtz1c, sqtz1d and sqtz5a (with limited sqtz2a)

sqtz2a

The second generation of secondary quartz, sqtz2a is likely to represent a complete massive replacement of pqtz, forming preferentially orientated fingers

branching from healed cracks with emanating stringers (which may appear quite diffuse; this orientation may reflect crystallographic axes) (see Fig. 4.6.2). These stringers may coalesce to form the massive replacement zones. Luminescence is mid/dark grey, with a central black core (see sqtz5a).

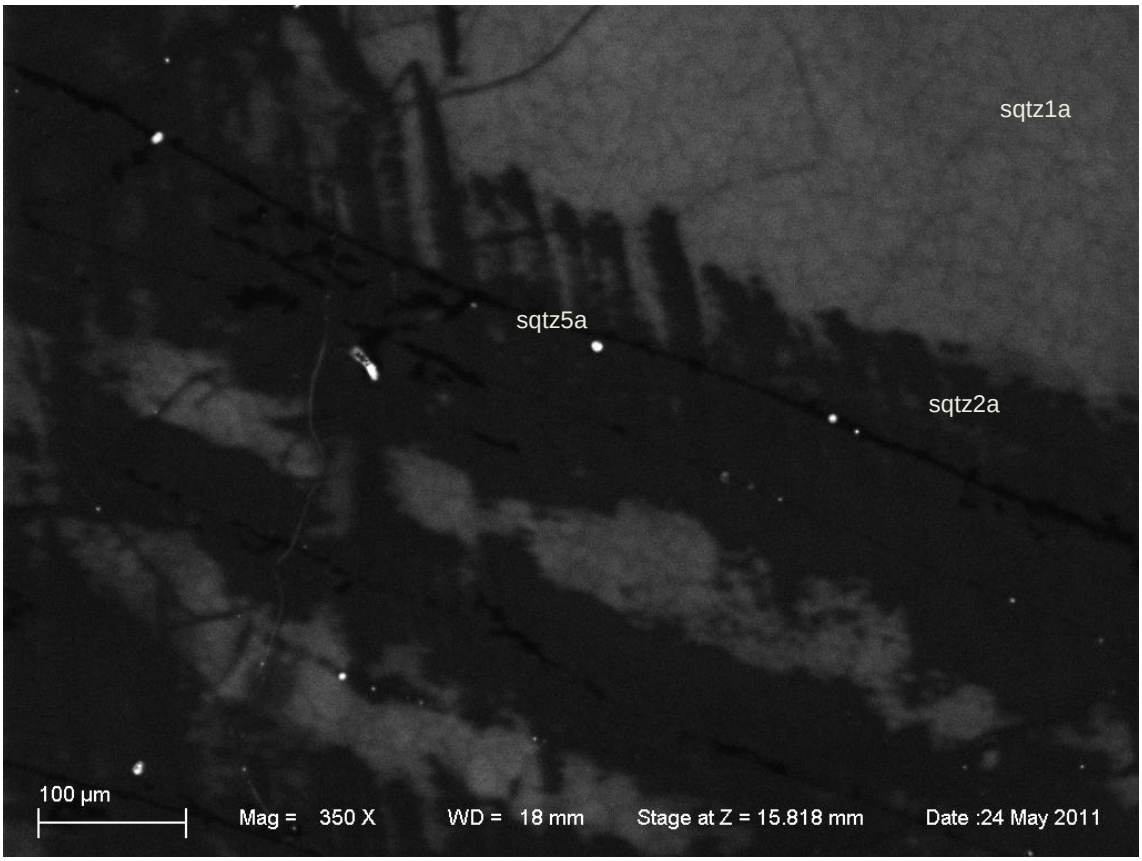

Fig. 4.6.2 CL-SEM image of quartz from Solås wall zone (080910-05), showing an overprinting sequence; pqtz (mid grey), sqtz1a, sqtz2a and sqtz5a. sqtz2a varies between defined stringers and massive replacement, dependant on level of diffusion/amalgamation

sqtz2b

sqtz2b is extremely similar to sqtz2b (i.e. mid-gray masses of replacement quartz, locally forming stringers). Its classification is based on the difference between sqtz5a and sqtz5b; sqtz2a is overprinted by sqtz5a, and sqtz2b is overprinted by sqtz5b.

sqtz2c

sqtz2c (Fig. 4.6.3) overprints pqtz and is overprinted by sqtz5. This domain is less defined and often on a smaller scale to other sqtz2 phases, has a slightly

brighter luminescence and is similar in morphology to healed cracks. Locally, sqtz2c diffuses to form massive replacements.

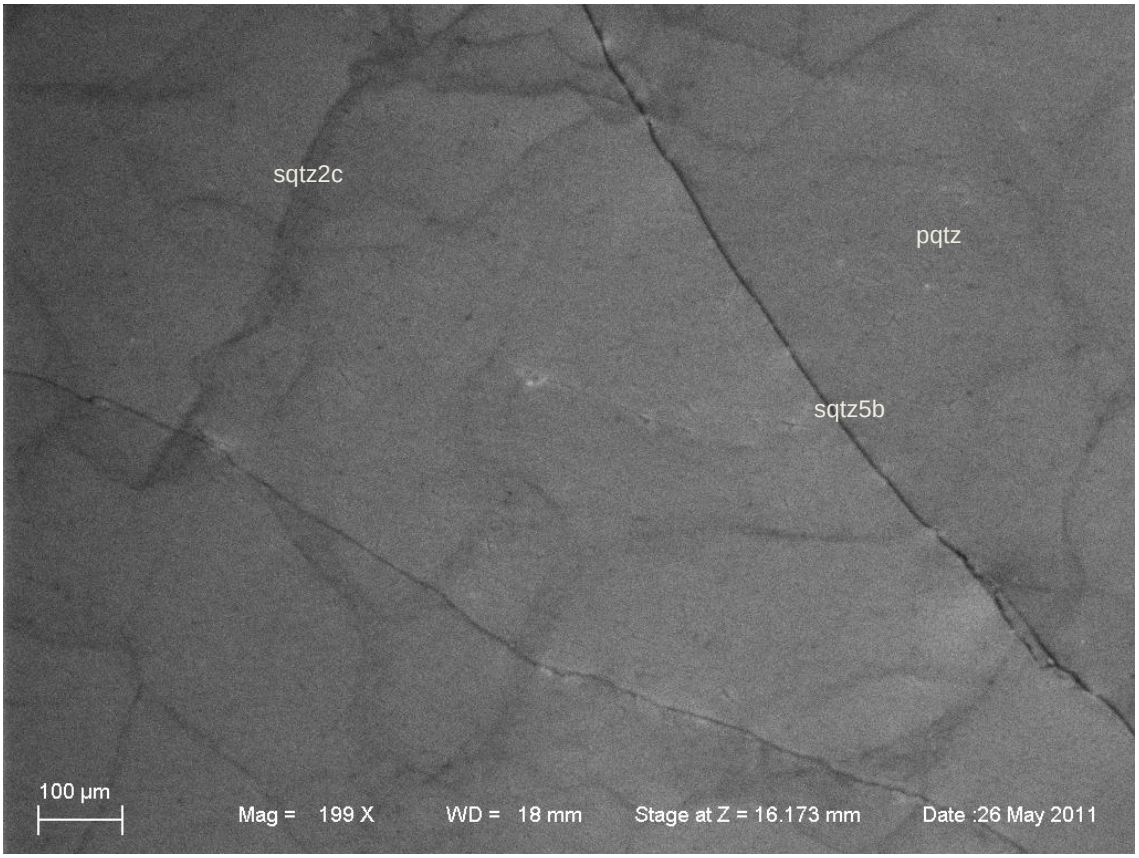

Fig. 4.6.3 CL-SEM image of quartz from Kåbuland core zone (130910-01), indicating fracture fill and an overprinting sequence of pqtz overprinted by sqtz2c, which is overprinted by sqtz5b

sqtz3

The third generation of secondary quartz, sqtz2a is typically a replacement often associated with sqtz4, manifested as massive and complete replacement (presumably of sqtz2). Luminescence is dark grey.

sqtz4

The fourth generation of secondary quartz, sqtz4 post dates sqtz3 but is often in close association with it; sqtz3 may act as a favourable chemical pathway. The very high luminescence intensity in sqtz4 (appearing white; Fig. 4.6.4) may be due to this zone having once been a fluid pathway. The bright CL indicates a high defect density in sqtz4 (increased trace elements) or damage to the quartz structure such as that caused by radioactive fluids moving along existing cracks (Botis et al., 2005).

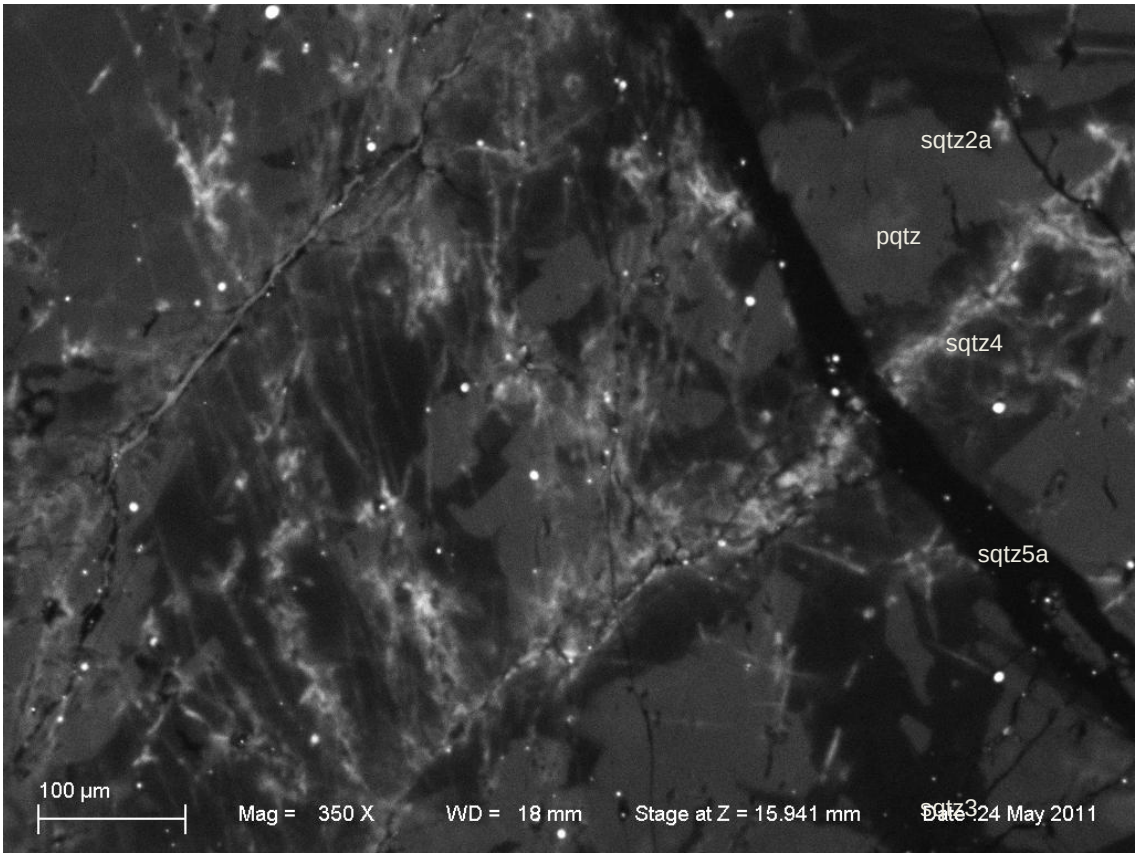

Fig. 4.6.4 CL-SEM image of quartz from Solås core (080910-04), indicating an overprinting sequence; pqtz (mid grey), sqtz2a (mid/dark grey), sqtz3 (dark grey), sqtz4 (white) and sqtz5a (black, with white fluid inclusions). sqtz2a is present as massive replacements

sqtz5a

The fifth generation of secondary quartz, sqtz5a is of a very low luminescence (near black; Fig. 4.6.4) and overprints all previous phases. It contains a high proportion of fluid inclusions. Particularly apparent in the wall facies of Solås, sqtz5a material appears to follow cracks in a manner similar to sqtz2a, making them darker at the centre with an increased proportion of fluid inclusions. It appears that these microfractures are ultimately healed by sqtz5a. These final overprinting 'veins' may represent final water vestiges (which remain as the melt crystallises) escaping along microfractures.

sqtz5b

sqtz5b is similar to sqtz5a in that it has very low luminescence and overprints all previous phases, forming the healed cores of the pathways utilised by fluids which formed sqtz2. It differs from sqtz5a in that it has an almost complete lack

of fluid inclusions, which suggests a different fluid was responsible for its (and sqtz2b's) formation.

sqtz6

The apparently final phase of quartz growth is uncommon, forming discrete regions which show diffusional zoning but no other features (Fig. 4.6.5). This zoning is reminiscent of sqtz1d, but is not overprinted by any other domain i.e. it forms as a final stage.

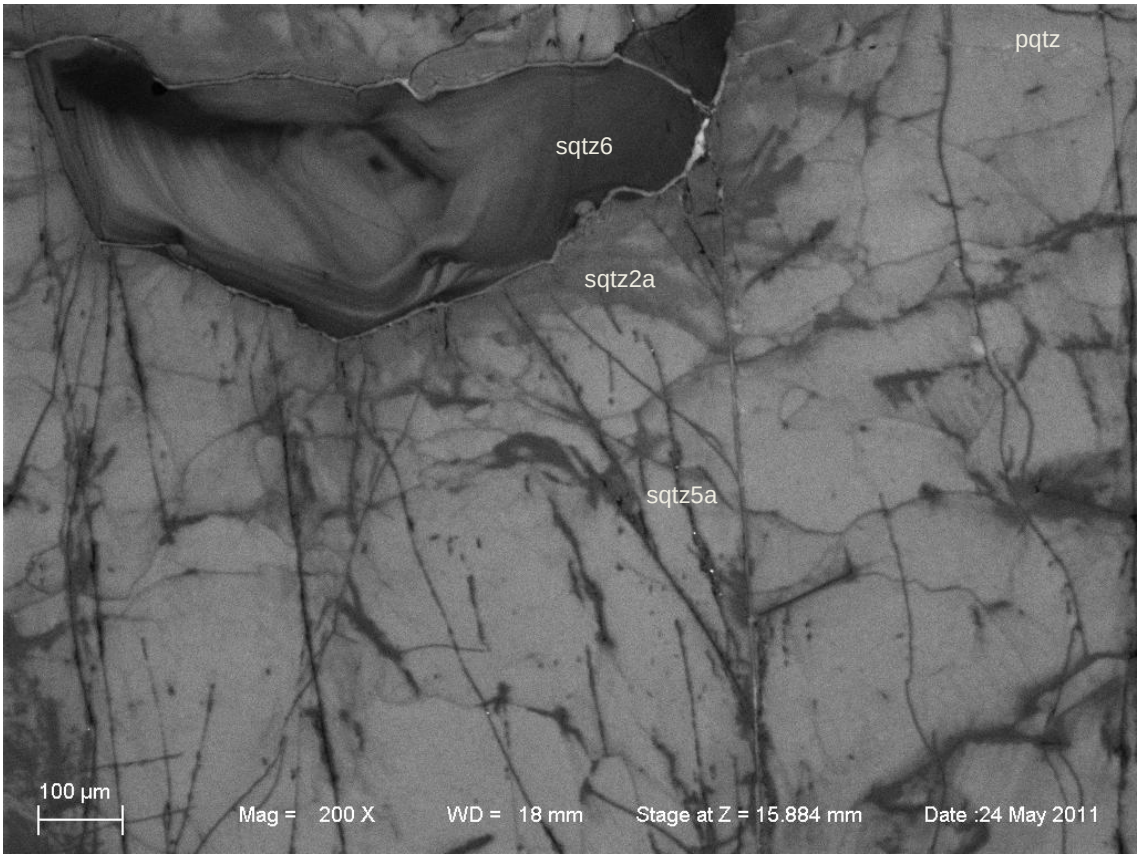

Fig. 4.6.5 CL-SEM image of quartz from Steli wall zone (080910-29), indicating an overprinting sequence; pqtz (mid grey), sqtz2a (mid/dark grey, fractured controlled but not defined), sqtz5a (black, with localised white fluid inclusions) and sqtz6, displaying diffusional zoning.

It is apparent that pqtz, sqtz2a and sqtz5a are phases common to all quartz samples. Sqtz3 and sqtz4 appear only in core material from Solås, with sqtz1b, sqtz2b, sqtz5b and sqtz6 unique to wall zone material at Steli.

All samples contain 50 µm needles of rutile (with a width to length ratio of approximately 1:100). These were not typically visible in CL (as they were often

transacted perpendicular to the c-axis, forming nanometre scale non-luminescent circular cross sections), but were apparent in transmitted light due to a large contrast in optical relief between the needles and host quartz. Their presence suggests that the host pegmatite has undergone some degree of retrograde metamorphism. The reason for this may be that as the pegmatite system re-equilibrated, Ti became unstable within the quartz lattice and was exsolved, forming needles of rutile; essentially, exsolution of rutile needles results from cooling or decompression of Ti-rich quartz (e.g., Adachi et al. 2010). This is theoretical however; there is no CL variation around the needles which may indicate Ti migration towards the sites of rutile growths. It may be possible that these needles are incorporated into ablation sites as they are essentially impossible to avoid, potentially increasing the Ti content of the analysis. However, the Ti comprising the needles is not external to the system i.e. it results from a chemical reordering, rather than a compositional change. As such, and as needle size was consistent throughout the samples, the Ti content values are assumed to be 'real'.

Interestingly, one sample from the Hovåsen wall zone (110910-05) shows regular linear zones of a phase similar in luminosity to sqtz2 (Fig. 4.6.6). These structures, which are also visible in BSE images, look reminiscent of extremely dense fluid inclusion trails (as evidenced by sporadic white inclusions).

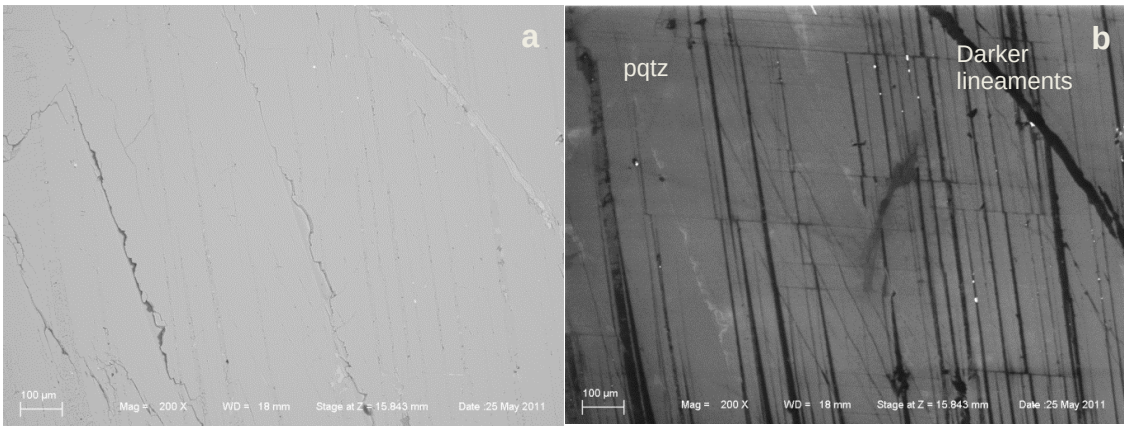

Fig. 4.6.6 BSE (a) and CL (b) image of quartz from part of the Hovåsen wall zone (110910-05), showing linear features (low luminosity, localised fluid inclusion trails) within primary quartz.

It was revealed during petrographic assessment of the thick sections produced for O isotope analysis (*Chapter 3.2.4*), that the pegmatite quartz hosts fluid

inclusions (Figs. 4.6.7 and 4.6.8). The majority of the inclusions are two-phase liquid and vapour, which vary in size from 5 – 15 μm. The inclusions typically define trails or fracture infills rather than being present on crystal growth surfaces, suggesting that they are secondary (or, realistically, pseudo-secondary) in nature (e.g. Van den Kerkhof and Hein, 2001; Wilkinson, 2001). Locally, larger inclusions exist (up to 30 μm in diameter) and are generally not in trails, so are therefore most likely to be primary. Critically it was noted that, across the pegmatites, core quartz contains fluid inclusions larger in both abundance and size than that of marginal quartz.

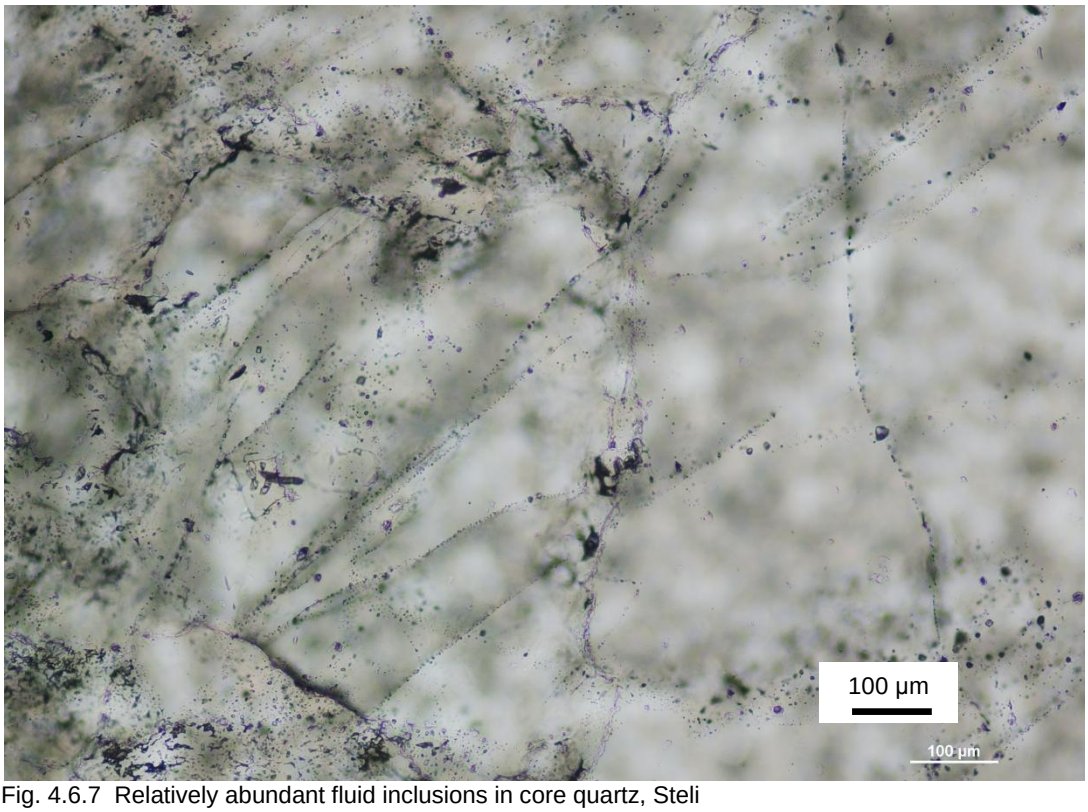

Fig. 4.6.7 Relatively abundant fluid inclusions in core quartz, Steli

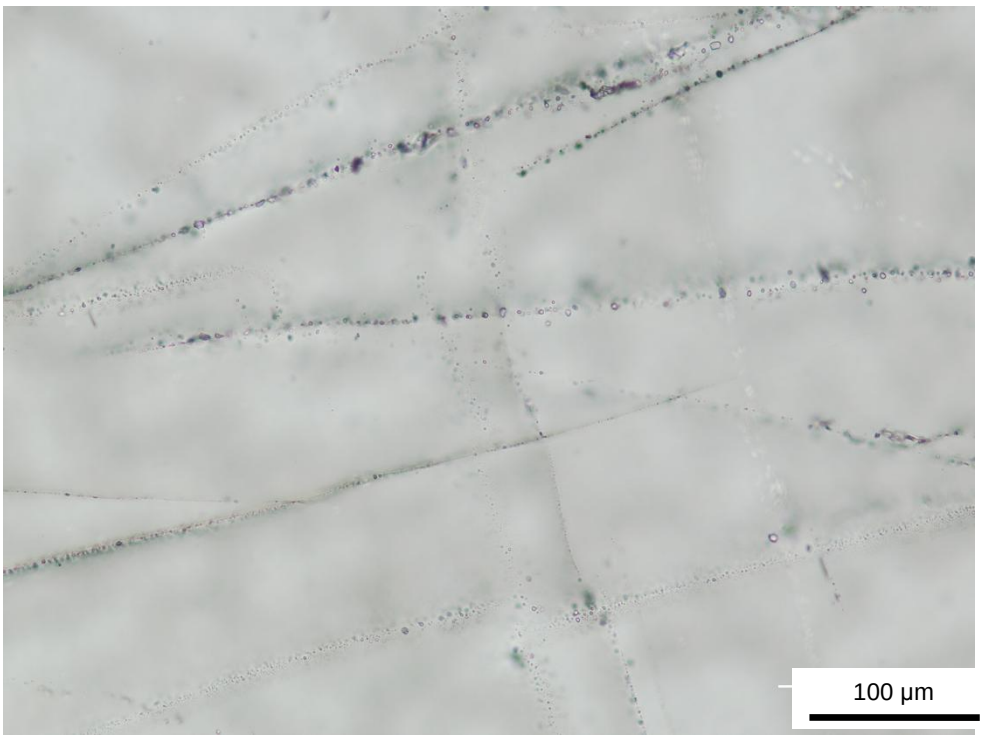

Fig. 4.6.7 Relatively scarce fluid inclusions in border zone quartz, Steli

Table 4.6.1 Summary of quartz phases in samples assessed by SEM-CL

Pegmatite	Zone	pqtz	sqtz1a	sqtz1b	sqtz1c	sqtz1d	sqtz2a	sqtz2b	sqtz2c	sqtz3	sqtz4	sqtz5a	sqtz5b	sqtz6
Landsverk	Inter	25%	-	-	-	-	65%	-	-	-	1%	9%	-	-
Kåbuland	Core	65%	10%	10%	-	-	-	-	10%	-	-	-	5%	-
	Outer	15%	50%	-	-	-	-	25%	-	-	3%	-	7%	-
Hovåsen	Core	5%	25%	-	-	-	30%	30%	-	-	-	5%	5%	-
	Outer	70%	-	-	5%	-	-	20%	-	-	-	-	5%	-
Slobrekka	Core	10%	60%	-	-	-	-	25%	-	-	-	v slight	5%	-
	Outer	20%	30%	-	-	20%	25%	-	-	-	-	5%	-	-
Li Gruva	Core	60%	-	-	-	-	30%	-	-	-	-	10%	-	-
	Outer	42%	-	-	3%	20%	29%	-	-	-	1%	5%	-	-
Solås	Core	13%	-	-	-	-	35%	-	-	35%	12%	5%	-	-
	Outer	77%	0%	-	-	-	20%	-	-	-	-	3%	-	-
Steli	Core	60%	5%	-	-	-	30%	-	-	-	-	5%	-	-
	Outer	43%	-	3%	-	-	40%	5%	-	-	-	5%	2%	2%

4.6.2 Textures in hydrothermal quartz

Fig. 4.6.8 Scan of a thick section of a hydrothermal quartz crystal from Landsverk 1, with corresponding CL-SEM image. The rounded rectangles indicate regions containing LA-ICP-MS ablation sites

From Figs. 4.6.8 and 4.6.9, it is clear that hydrothermal quartz (such as that from Landsverk 1) is texturally very different to magmatic quartz. Landsverk 1 was selected for further investigation as, after field observations, it displayed the most extensive overprint. Based around a massive core, the hydrothermal crystal shows complex, in part oscillatory zoning in CL, with irregular and discordant features at the peripheries. Additionally, a late and extremely dark (black in these images) phase is present throughout the crystal, displaying a large fluid inclusion content, which clearly overprints existing quartz structures (Fig. 4.6.9). Interestingly, this dark overprinting phase seems mostly developed within a particularly bright zone, of which there are small relicts on its margins

(marked **a** on Fig. 4.6.9). This replacement phenomenon is repeated in a narrower zone (marked **b** on Fig. 4.6.9).

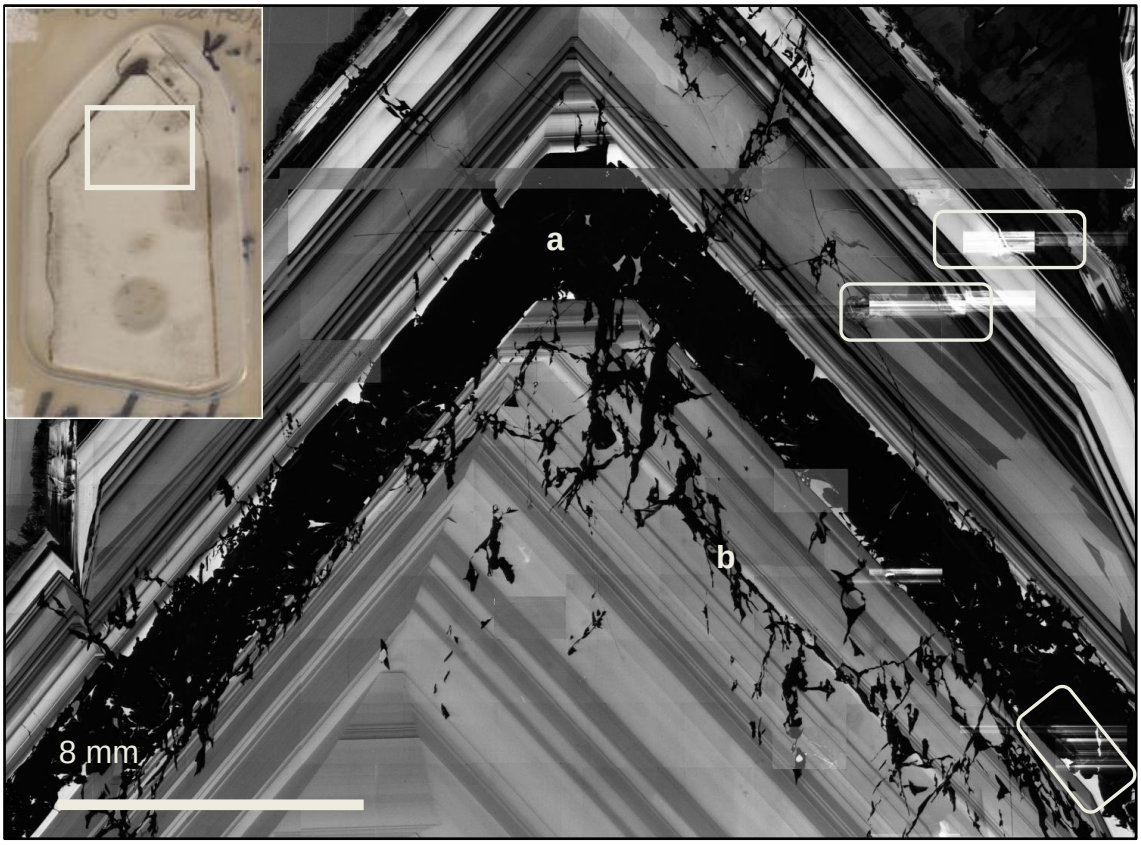

Fig. 4.6.9 Enlarged CL-SEM image of the hydrothermal quartz crystal from Landsverk 1, with a late stage overprinting event (limited to previously bright zones) at **a** and **b**. The rounded rectangles mark LA-ICP-MS ablation sites

4.3.3 Correlating CL domains with trace element chemistry

Preliminary work has been undertaken to better understand the chemical controls on CL signal in different quartz domains. EPMA mapping was performed on the entire Landsverk 1 hydrothermal quartz crystal for Fe (Fe^{2+} quenches luminescence), Mg (Mg^{2+} promotes luminescence) and Al. Fe and Mg fell below LOD, which, whilst prohibitive for providing chemical conclusions, demonstrates that the colour variation observed in the CL-SEM images is likely to be 'real' and compositionally dependant, rather than accentuated by Fe^{2+} and Mg^{2+}. Fig. 4.6.10 displays the Al results relative to the CL-SEM image. The upper region shows very little variation in Al content; this may result from the Al in this region being present below the detection limit of the EPMA (this is reinforced by LA-ICP-MS data; the lower portion of the crystal contains over 800

ppm, whilst the upper portion contains as little as 4 ppm Al). It is equally possible that the rhythmic zoning observed here is simply not controlled by Al.

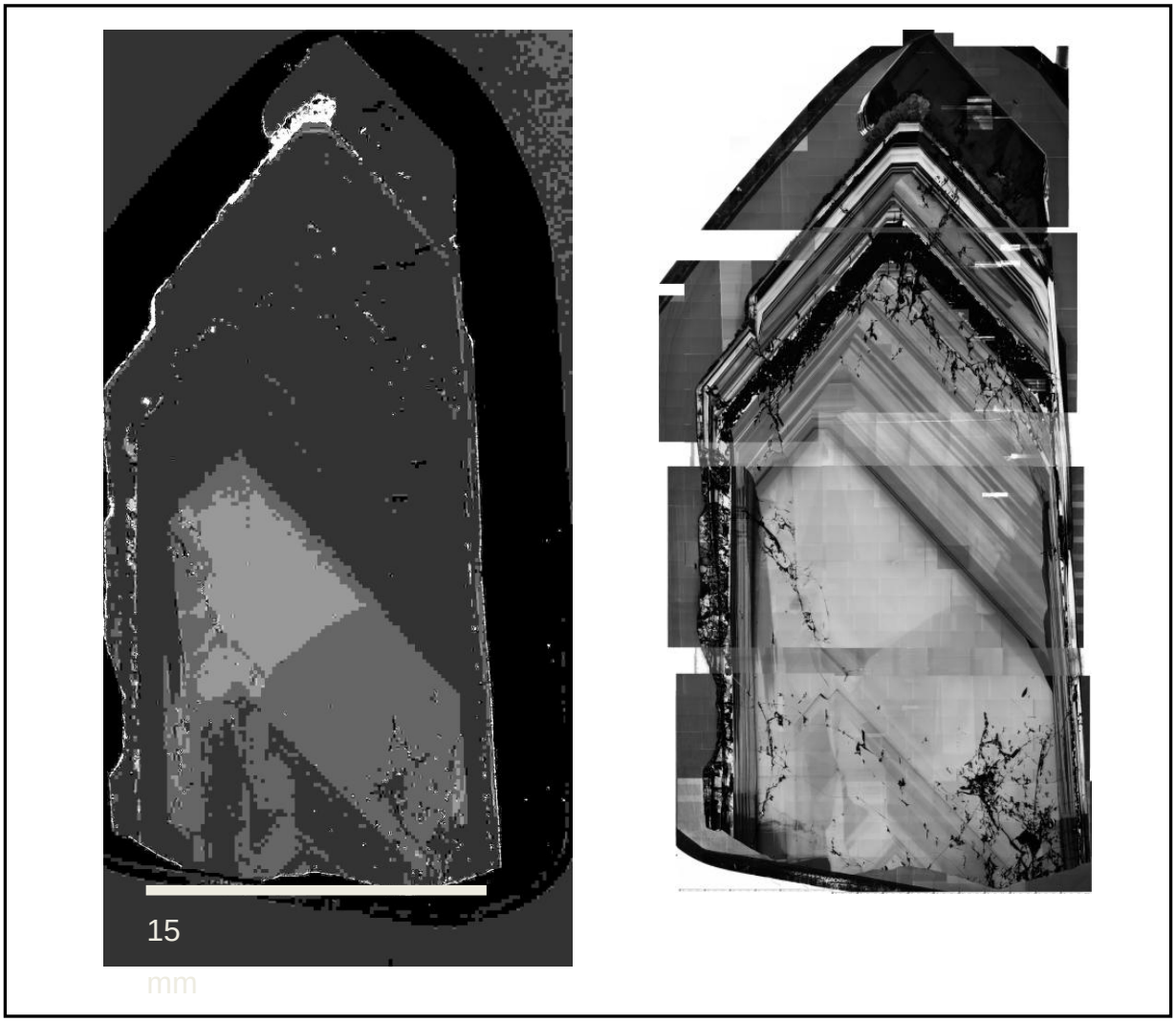

Fig. 4.6.10 X-ray element map for Al in a hydrothermal quartz crystal from Landsverk 1, with corresponding CL-SEM image

However, in the core region of the crystal, there is a clear correlation between Al and CL-SEM zoning; a greater Al content produces a brighter CL response (light grey). A reduced Al content produces a mid-grey CL response, with a very reduced Al content producing a dark grey/black CL response. This suggests that Al may be an important compositional element initially (as the core develops) but other elements are taken up preferentially with Al not available in later hydrothermal fluids.

4.7 Oxygen isotope geochemistry

Data is presented for oxygen isotope analyses in Fig. 4.7.1 and summarised in Table 4.7.1. As discussed in *Chapter 3.2.4*, quartz was taken from previously analysed thick sections of quartz from outer and core zones from the Solås and Steli pegmatites, and from the base and tip of the Landsverk 1 hydrothermal crystal (see Fig. 3.2.4 for exact positions of 'base' and 'tip' sections) to investigate the $\delta^{18}O$ signature of quartz and characterize the nature of the fluids responsible for its crystallization. The four samples from the pegmatites are seen to display consistent $\delta^{18}O$ values of between 8 and 9‰, which is typical of granites (6 – 10‰, e.g. Hoefs, 1997). The hydrothermal quartz from Landsverk 1 displays large variation, from -8.98 to 11.74‰. This variation can be bracketed into distinct $\delta^{18}O$ populations, representing distinct fluids, which correspond closely with particular CL zones (see Figs. 4.7.1 and 4.7.10 and *Chapters 5.2.2* and *5.2.3* for further discussion).

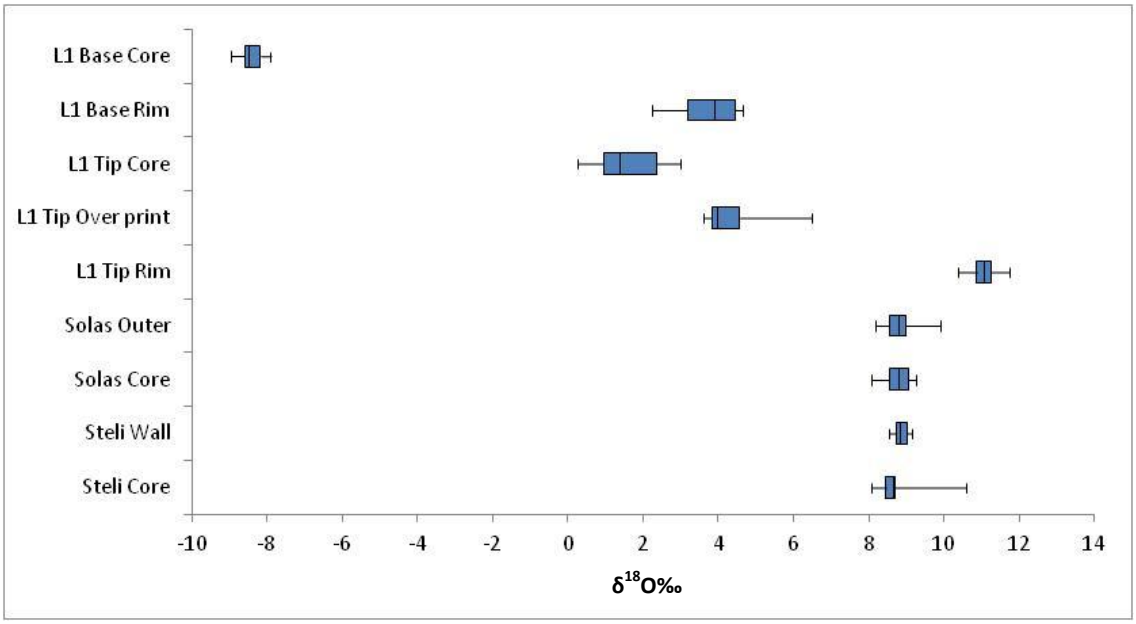

Fig 4.7.1 Summary of $\delta^{18}O$ values for the quartz samples analysed for O-isotopes

Table 4.7.1 Numerical summary of $\delta^{18}O$ values for the quartz samples analysed for O-isotopes

Zone	Steli	Solås	Landsverk 1
Core	8.56 (s.d. 0.20)	8.77 (s.d. 0.32)	
Outer	8.85 (s.d. 0.19)	8.76 (s.d. 0.29)	
Base			-8.39 (s.d. 0.28) 3.69 (s.d. 0.92)
Tip			1.55 (s.d. 0.83) 4.17 (s.d. 0.51) 11.03(s.d. 0.40)

4.7.1 Steli

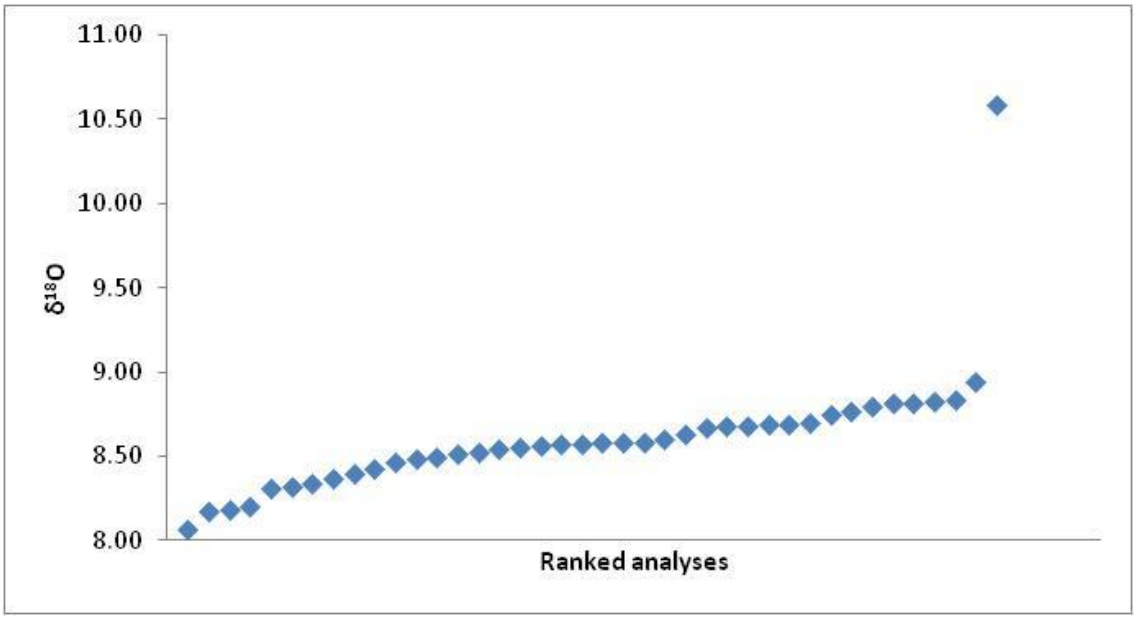

Fig. 4.7.2 Summary of $\delta^{18}O$ values for the Steli pegmatite core zone

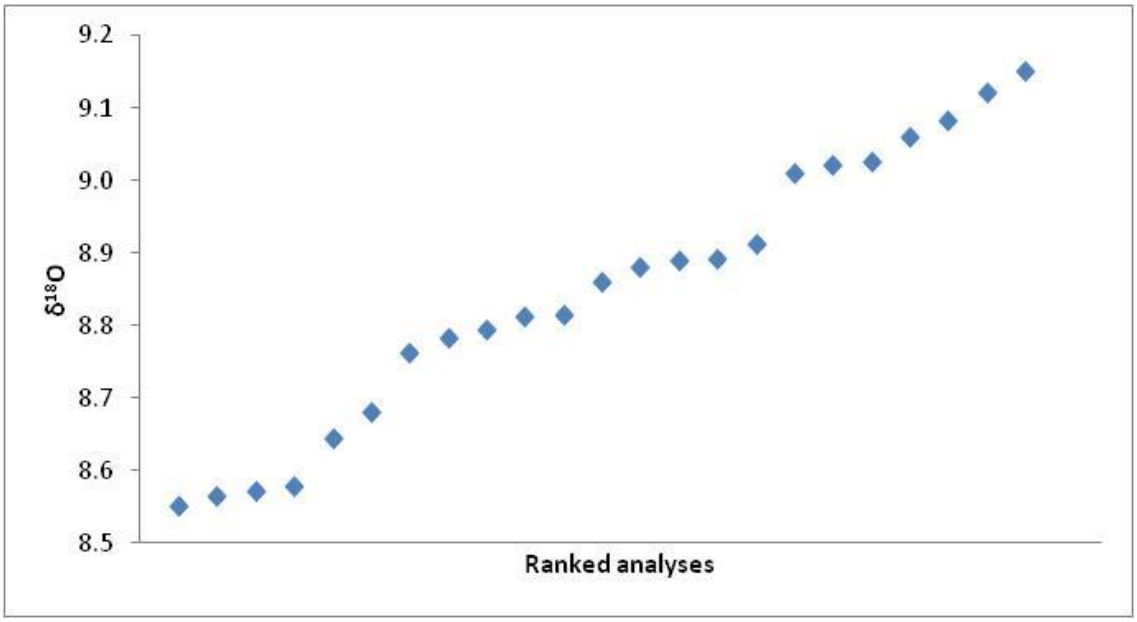

Fig. 4.7.3 Summary of $\delta^{18}O$ values for the Steli pegmatite outer zone

The Steli core zone (excluding the outlier of 10.58) had an average $\delta^{18}O$ value of 8.56‰, with a standard deviation of 0.20. The Steli outer zone had an average $\delta^{18}O$ value of 8.85‰, with a standard deviation of 0.19.

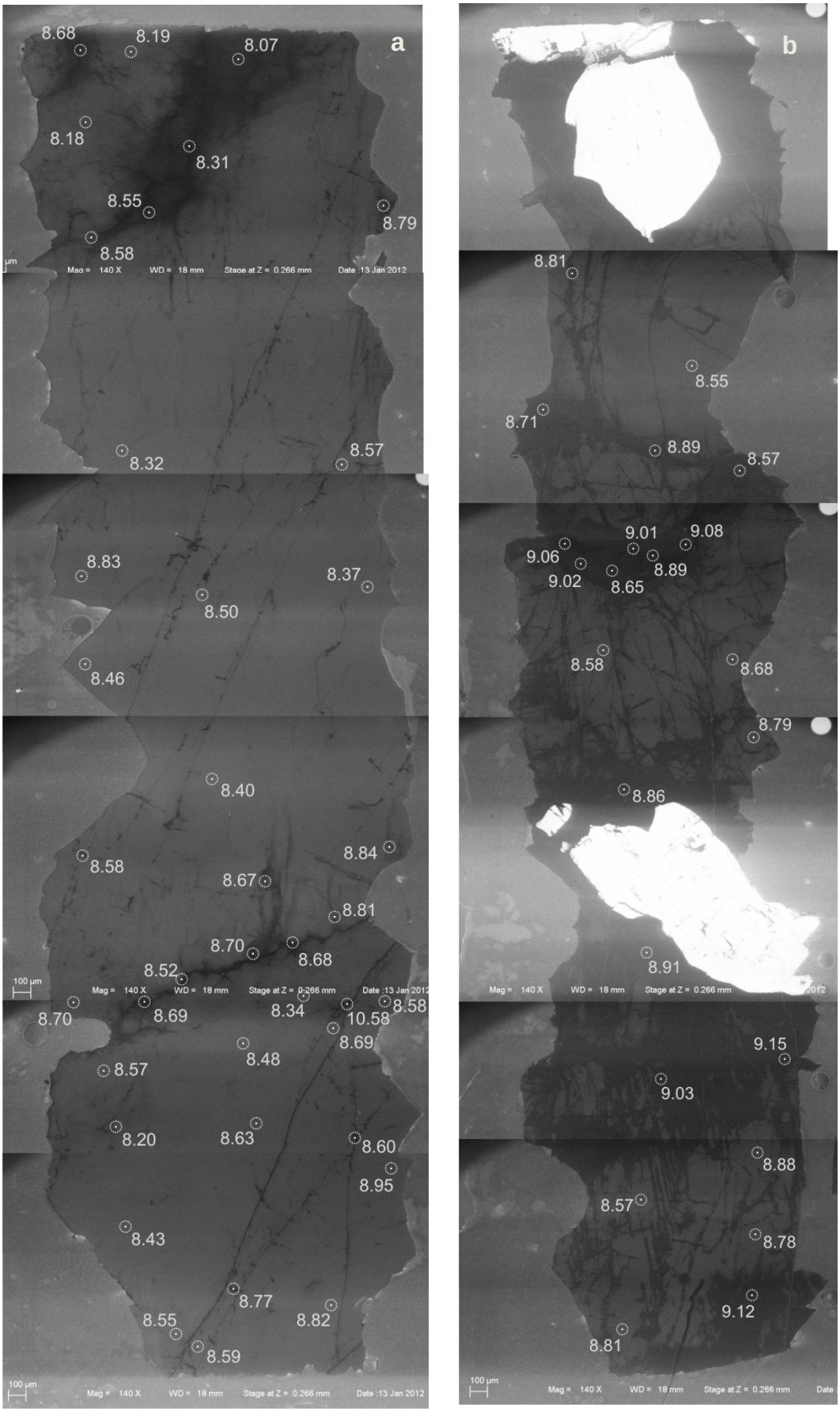

Fig. 4.7.4 Distribution of $\delta^{18}O$ values for the Steli pegmatite core (a) and wall (b) zones

4.7.2 Solås

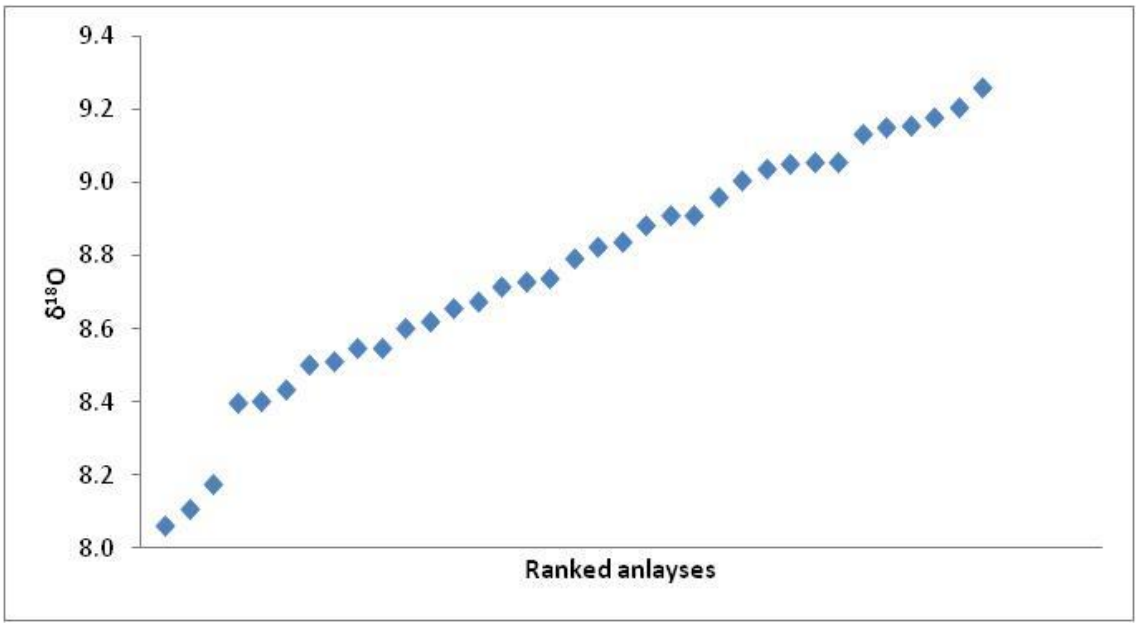

Fig. 4.7.5 Summary of $\delta^{18}O$ values for the Solås pegmatite core zone

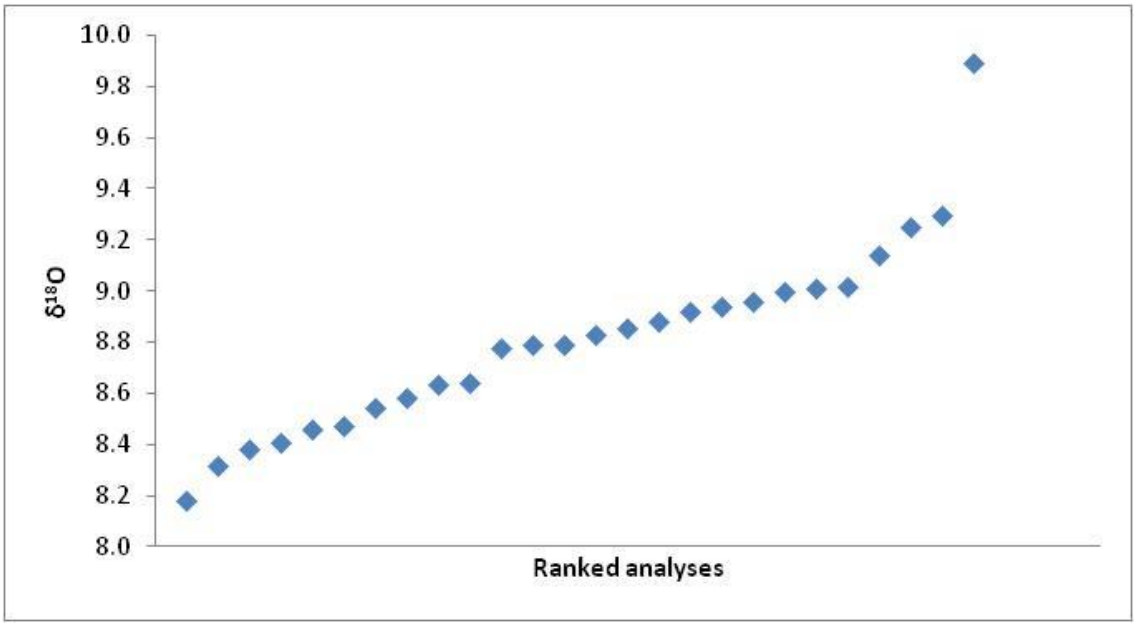

Fig. 4.7.6 Summary of $\delta^{18}O$ values for the Solås pegmatite outer zone

The Solås core zone had an average $\delta^{18}O$ value of 8.77‰, with a standard deviation of 0.32. The Solås core zone (excluding an outlier of 9.89‰) had an average $\delta^{18}O$ value of 8.76‰, with a standard deviation of 0.29.

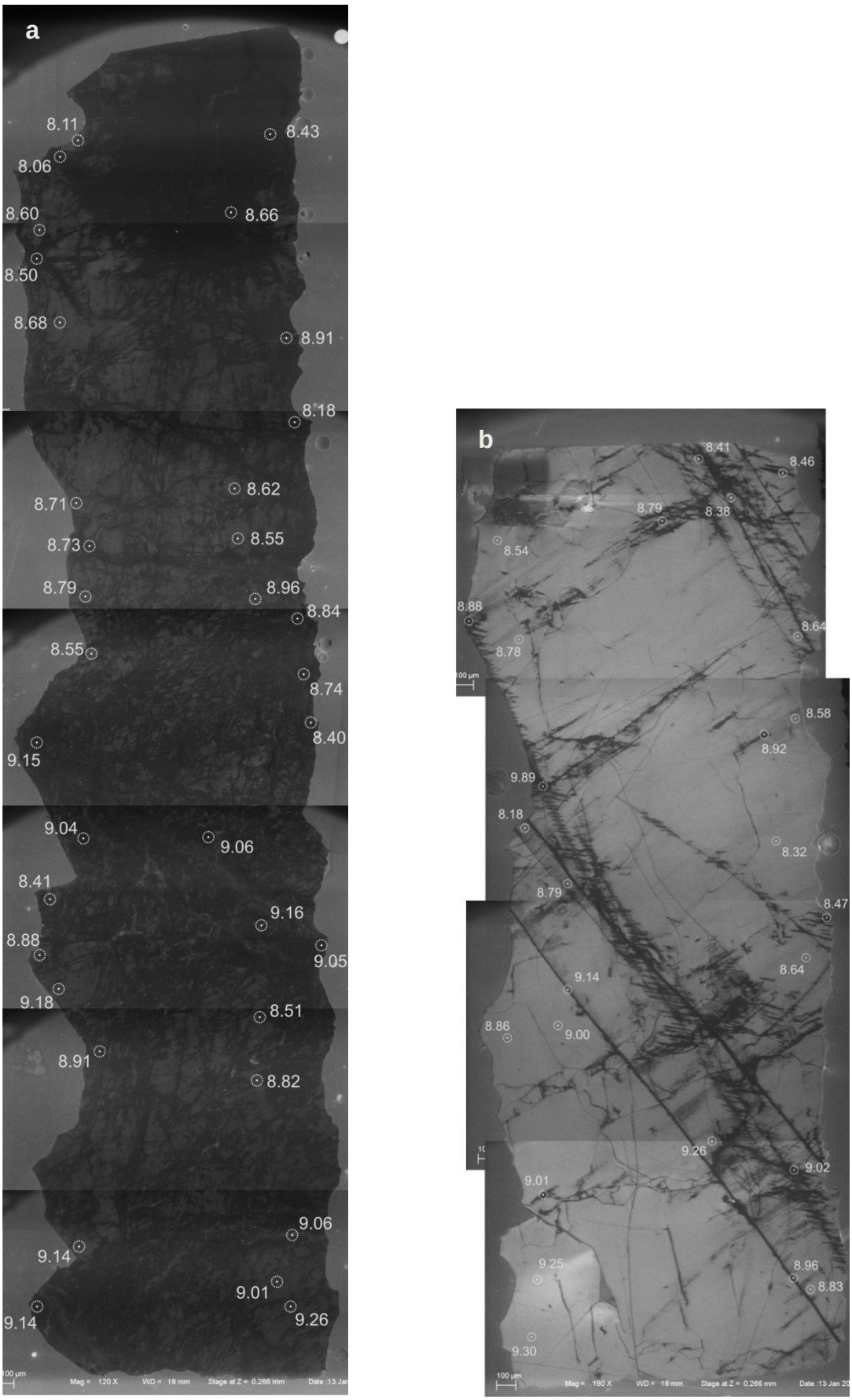

Fig. 4.7.7 Distribution of $\delta^{18}O$ values for the Solås pegmatite core (a) and wall (b) zones

4.7.3 Landsverk 1

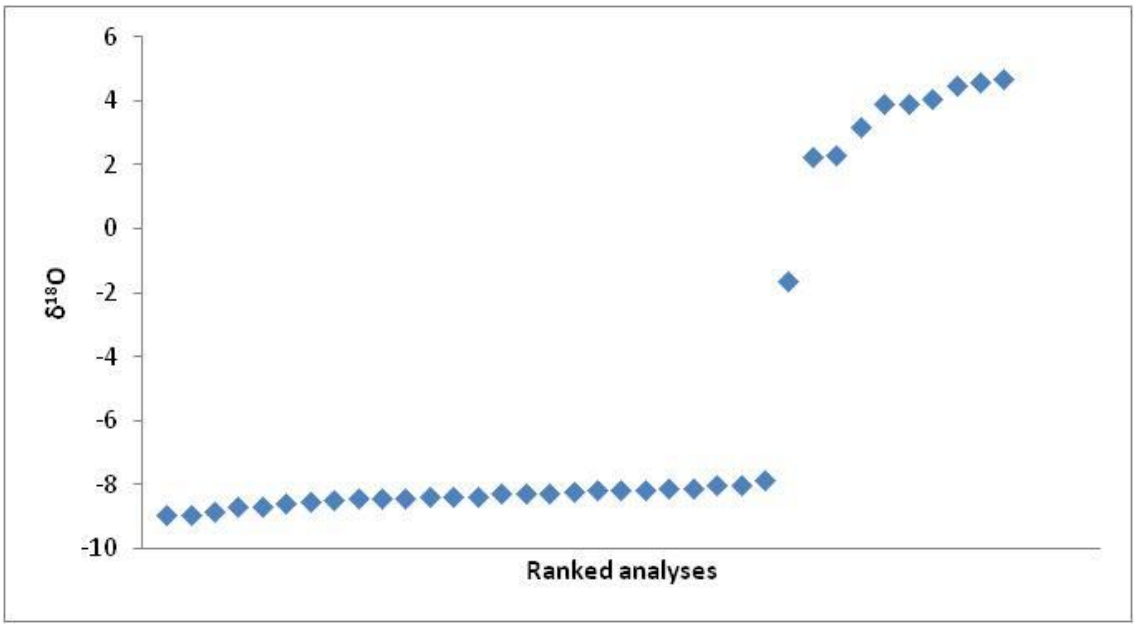

Fig. 4.7.8 Summary of $\delta^{18}O$ values for the Landsverk 1 quartz crystal base

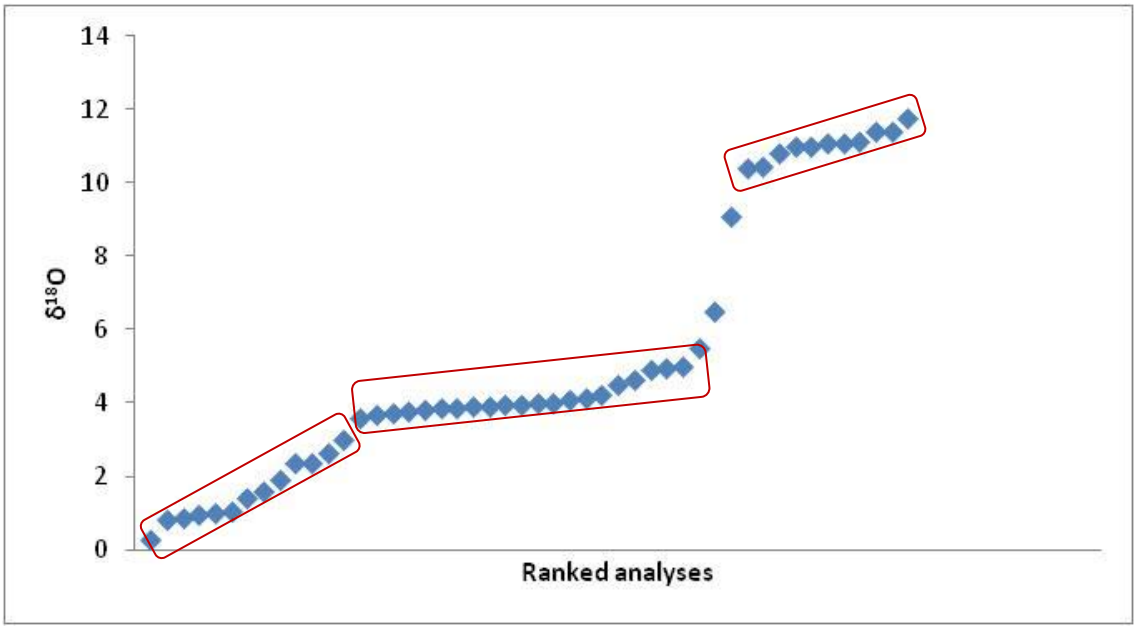

Fig. 4.7.9 Summary of $\delta^{18}O$ values for the Landsverk 1 quartz crystal tip

The base of the Landsverk 1 crystal (excluding outlier of -1.63) had two distinct average $\delta^{18}O$ values of -8.39 and 3.69‰, with standard deviations of 0.28 and 0.92 respectively. The tip of the Landsverk 1 crystal (excluding outliers of 9.09 and 6.50‰) had three distinct average $\delta^{18}O$ values of 1.55‰, 4.17‰ and 11.03‰, with standard deviations of 0.83, 0.51 and 0.40 respectively.

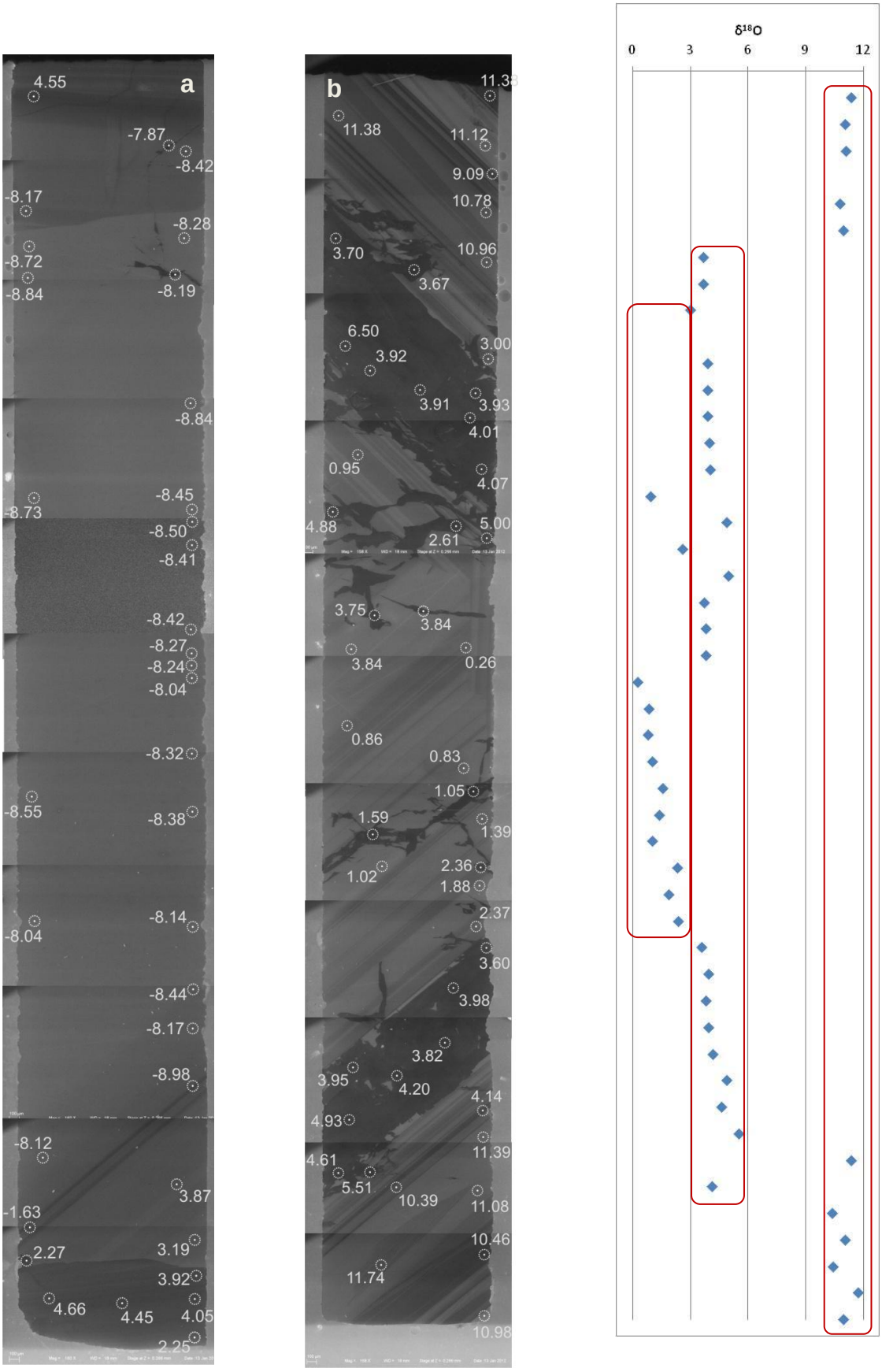

Fig. 4.7.10 Distribution of $\delta^{18}O$ values for the Landsverk 1 quartz crystal base (a) and tip (b) with associated (approximate) positon of analysis points in the tip (three $\delta^{18}O$ suites correlate with those of Fig. 4.7.9, with two outliers excluded)

4.8 U-Pb geochronology

Geochronology was required for this study to investigate the genetic link between the Høvringsvatnet granites and the pegmatites of the Evje-Iveland field, specifically to test the hypothesis that there is a significant age discrepancy between the granites and the pegmatites. Differing U-Pb ages produced from zircons from each unit would contribute towards this assertion. Table 4.8.1 summaries data from this study (Figs. 4.8.1 to 4.8.6) and from the literature. The ages produced for the granites in the current study have a much tighter range, an associated error an order of magnitude lower than published ages, and are considerably older than previously measured. Pegmatite ages vary considerably (both between different pegmatite units and from ages in the literature), but cluster at approximately 910 Ma. The dates provided by Seydoux (2011) are U-Pb ages from monazites. The variation in ages produced for the pegmatites (Fig. 4.8.4) in the current study likely arises from the metamict nature of the zircons, which leads to a flood of common Pb during analysis and a less precise age determination (Figs. 4.8.5 and 4.8.6). However, the relatively lower precision (compared to measured granite ages) of the Steli and Slobrekka ages (± 7.5 and 48 Ma respectively) obtained in the current study display a lower error than some published ages (e.g. Andersen et al., 2002; Pederson, 1981), so are included for consideration. Additionally, the granites appeared to contain only one generation of zircons, whereas the pegmatites where observed to contain limited examples of older i.e. more than 1 Ga zircons (Fig. 4.8.4); these are likely inherited zircons.

Table 4.8.1 Ages of the Høvringsvatnet granites and the Evje-Iveland pegmatites from this study and from literature

Body	Source	Age (Ma)	Error (± Ma)
Høvringsvatnet granites	This study	982.9	3.6
		982.8	4.5
		979.7	3.8
	Andersen et al. (2002)	971	+63/-34
	Pederson and Konnerup-Madsen (1994)	945	53
	Pederson (1981)	900	53
Steli	Anne-Magali Seydoux (pers. comm.)	938	5
Mølland (E-I pegmatite)		912	12
Landsverk 1		855	5
Steli		904	5
E-I pegmatites	Scherer et al. (2001)	910.5	1.6
	Andersen (2001)	909	5
	Boudin and Deutsch (1970)	901	20
Steli	This study	891.6	7.5
Slobrekka		876	48

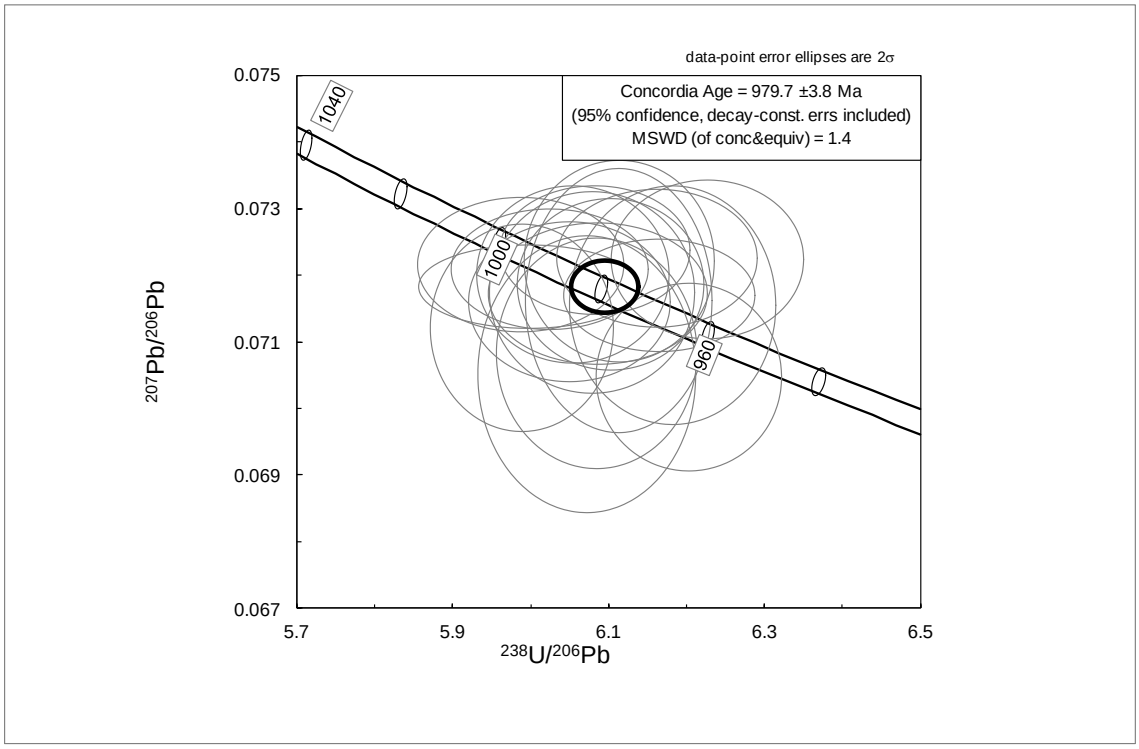

Fig. 4.8.1 Concordia age for the Høvringsvatnet granite (syenomonzonite)

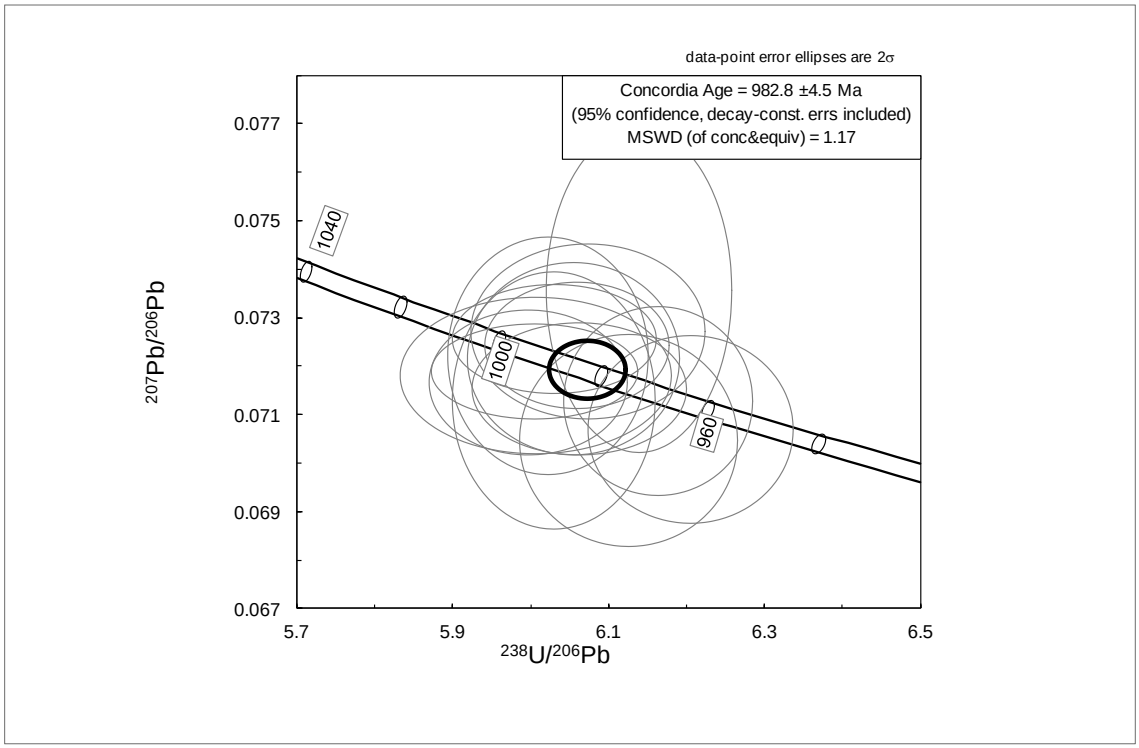

Fig. 4.8.2 Concordia age for the Høvringsvatnet granite (biotite granite)

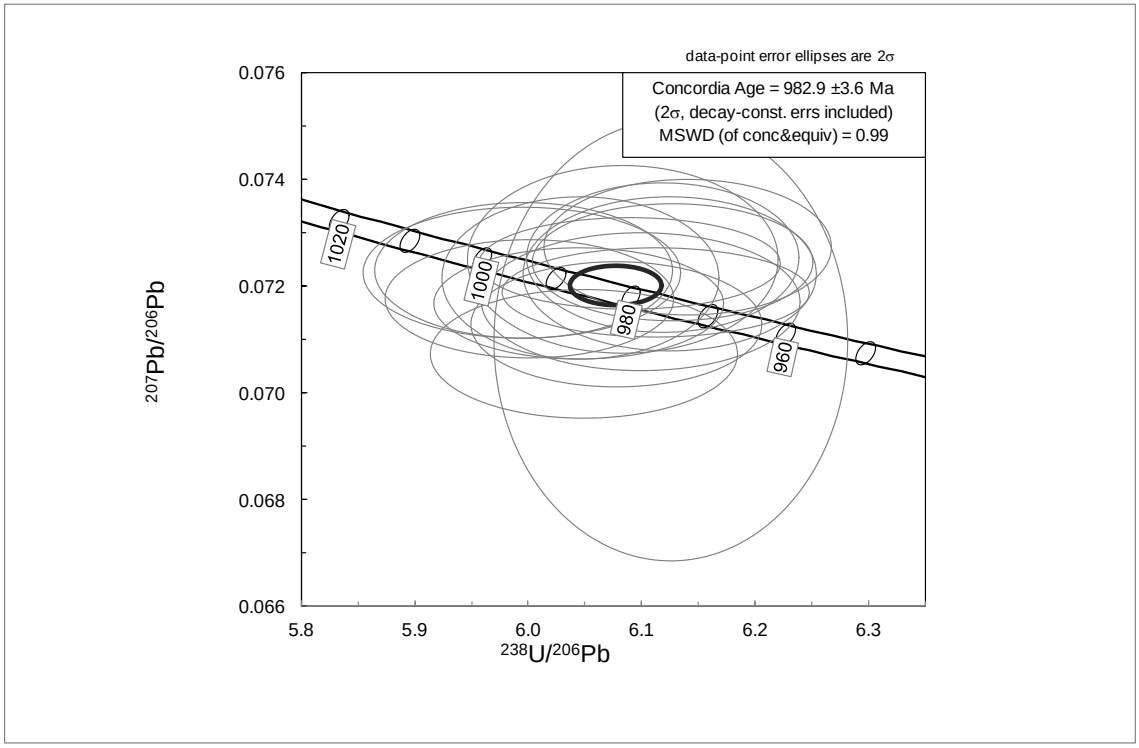

Fig. 4.8.3 Concordia age for the Høvringsvatnet granite (biotite rich granite)

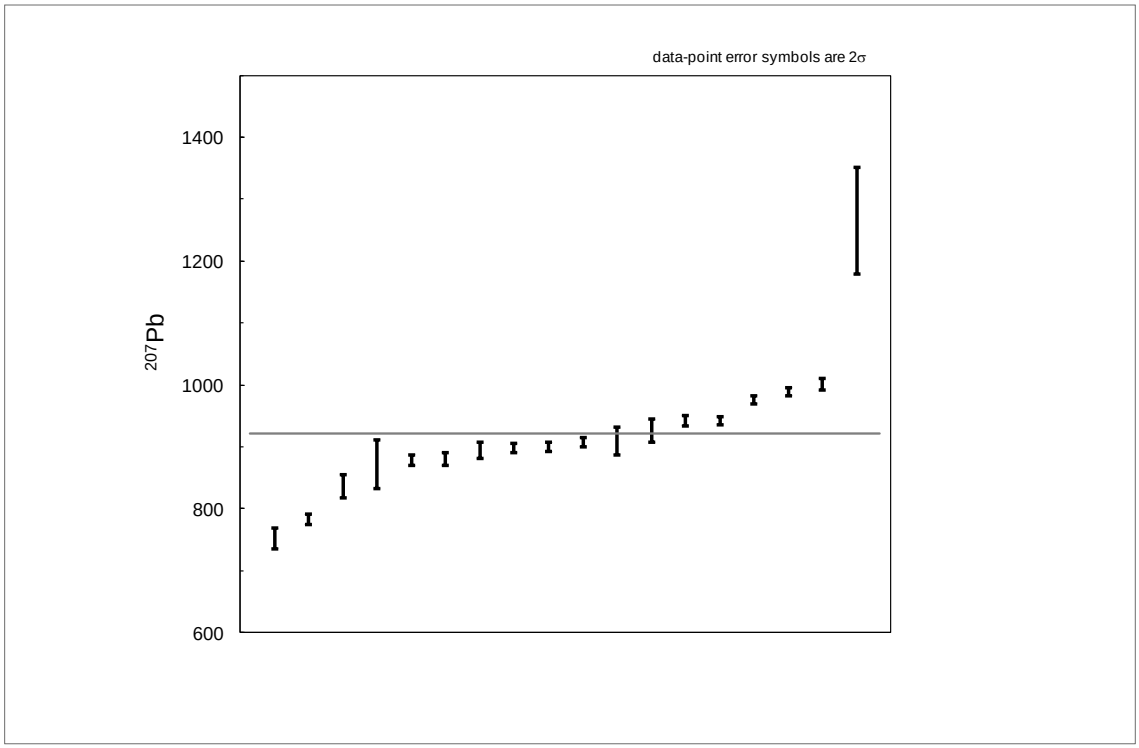

Fig. 4.8.4 Average ^{207}Pb age distributions for pegmatite zircons. Suggested age ~915 Ma

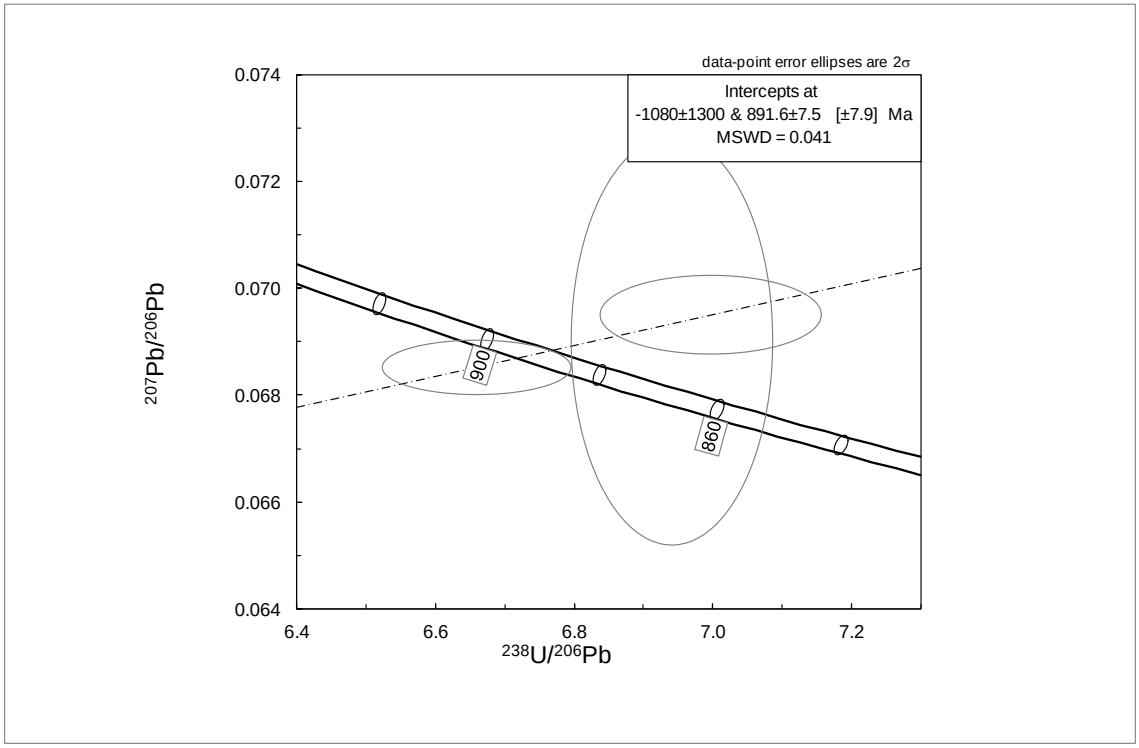

Fig. 4.8.5 Concordia age for the Steli pegmatite (dubious quality due to low number of ellipses)

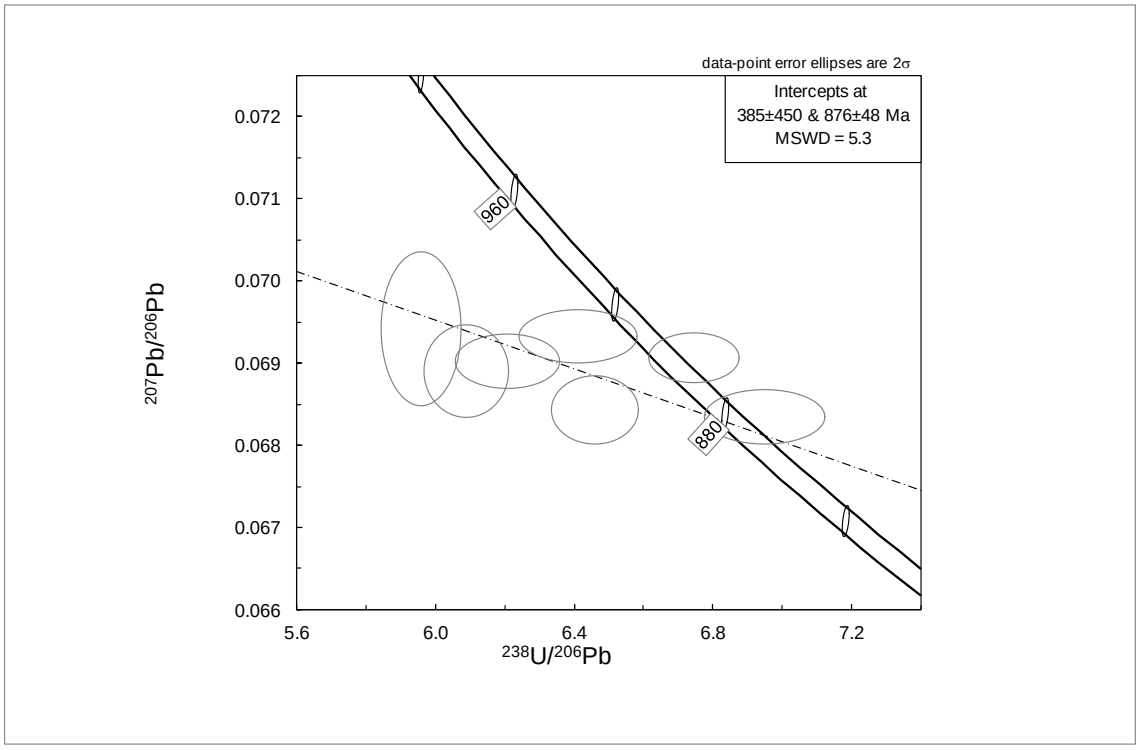

Fig. 4.8.6 Concordia age for the Slobrekka pegmatite (dubious quality due to low number of ellipses)

5. DISCUSSION

To develop exploration models for HPQ it is vital to first understand the nature and genesis of existing deposits. The aim of the current study of the Evje-Iveland pegmatites was therefore to develop criteria necessary for the prediction and location of naturally occurring quartz of a sufficiently high purity for use in a range of vital and growing industrial applications. The classification and genesis of the pegmatites is first discussed, and then the nature and origin of HPQ in the Evje-Iveland pegmatite field.

5.1 Pegmatite genesis

5.1.1 Classification of the Evje-Iveland pegmatites

Based on the genetic component classification scheme of Černý and Ercit (2005), the studied pegmatites of the Evje-Iveland belt fall in to the REL class, and typically the REL-REE subclass. They can be further classified (using the petrogenetic family component of Černý and Ercit's 2005 scheme) as belonging to the NYF family, variably containing columbite, fergusonite, gadolinite, polycrase, xenotime, allanite and thortveitite. Interestingly, they contain almost no fluorine, with F-bearing minerals (e.g. topaz) being restricted to replacement units which comprise <10 vol% of the pegmatite body, and which form in <10% of the pegmatites in the field. The REL class of pegmatites are considered to form by differentiation of granitic melts at intermediate to shallow emplacement depths, with the REL-REE subclass purportedly from post to anorogenic granites in typically extensional settings (Černý and Ercit, 2005); this generalisation is in conflict with initial hypotheses (**Chapter 1.2**), and will be discussed further. NYF pegmatites are sub- to metaluminous A- to I-types, with an $\delta^{18}O$ single maximum of approximately 8‰ (Černý, 1991a); this matches the characteristics of the Evje-Iveland pegmatites in Fig. 4.3.5 and the O-isotope data of Fig. 4.7.1.

A major issue with the 2005 scheme is the necessity for consideration of the tectonic histories and settings of the pegmatites, which is not always possible. As such, classification is influenced by mineralogy, which is utilised when defining the 'Type' subset. Without investigations into specific geological

histories, the more readily applicable classification of petrogenetic family (NYF or LCT) is obviously favourable, highlighting the difficulties encountered when utilising Černý and Ercit's class system (2005); the implied tectonic setting cannot necessarily be corroborated. Table 5.1.2 attempts to define the extent of evolution (associated with the class system).

Table 5.1.1 Summary of the classification of the studied pegmatites

Pegmatite	**CLASS**	**Subclass**	Type
Landsverk 1	RARE-ELEMENT (REL)	REL-REE	allanite-monazite/euxenite
Kåbuland	RARE-ELEMENT (REL)	REL-REE	allanite-monazite
Hovåsen	MUSCOVITE – RARE-ELEMENT (MSREL)	MSREL-REE	n/a
Slobrekka	RARE-ELEMENT (REL)	REL-REE	gadolinite
Li Gruva	RARE-ELEMENT (REL)/ABYSSAL (AB)	REL-REE	euxenite
Solås	RARE-ELEMENT (REL)	REL-REE	allanite-monazite
Steli	RARE-ELEMENT (REL) transitional to MUSCOVITE – RARE-ELEMENT (MSREL)	REL-REE to MSREL-REE	allanite-monazite

Table 5.1.2 Schematic indicating the degree of evolution based upon pegmatite classification (and by definition mineral assemblage)

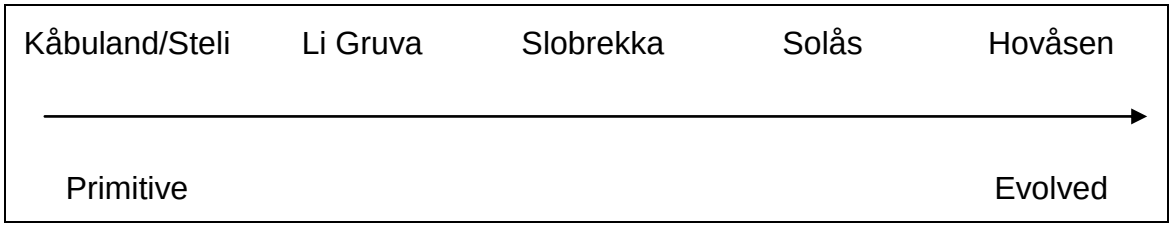

5.1.2 Geochemical constraints on the genesis and evolution of the pegmatite melts

Despite not having defined the source of the Evje-Iveland pegmatites, studies performed by Larsen et al. (2000 and 2004) identified two controls on the trace element composition of quartz in the Evje-Iveland pegmatites; spatial distribution north-south (analogous to position in relation to the granite) and

degree of fractionation (represented by the Rb, Pb and Ga contents of K-feldspar).

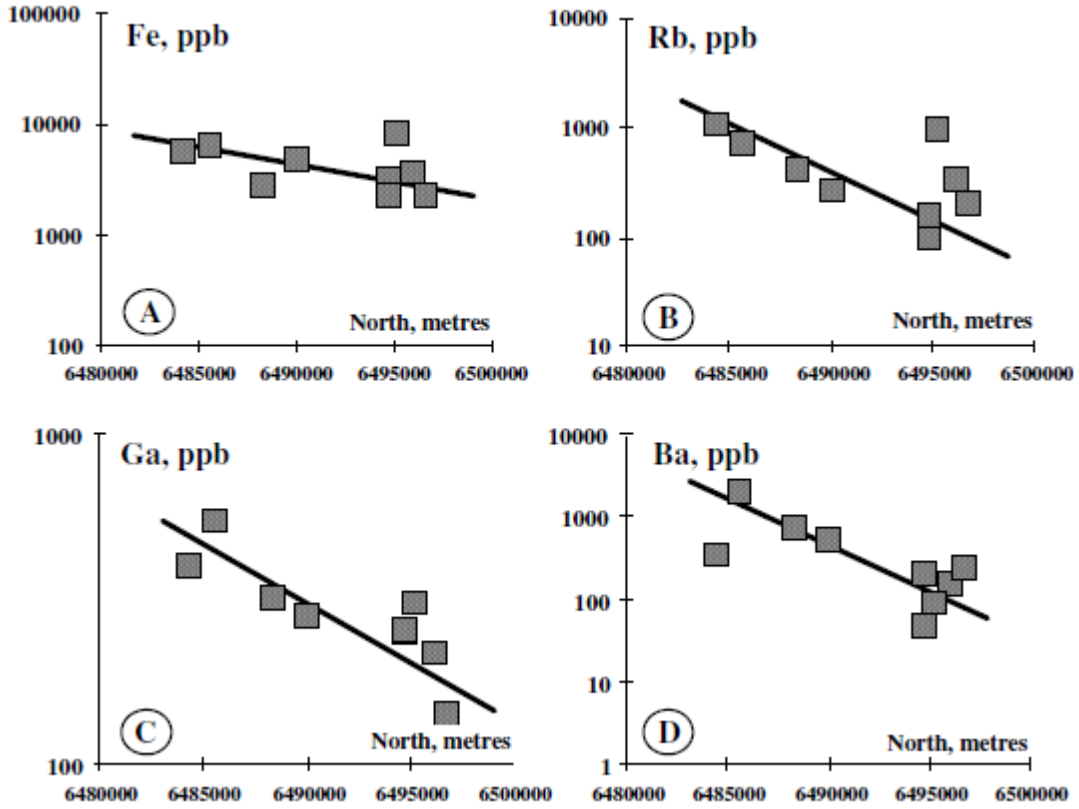

Fig. 5.1.1 Concentrations of structural impurities in quartz from the intermediate-zone of granite pegmatites at Evje-Iveland in a profile running from south to north in the studied area (Larsen et al., 2000)

From the data in Fig. 5.1.1 the trace element content of pegmatitic quartz decreases towards the north i.e. with increasing proximity to the Høvringsvatnet granite. The interpretation was that more highly differentiated pegmatites are further from their source and contain quartz with higher concentrations of trace elements; “an igneous melt becomes progressively more saturated with incompatible elements as differentiation proceeds” (Larsen et al., 2000). A potential parallel conclusion therefore is that less fractionated pegmatites occurred closest to Høvringsvatnet granite. Critically, Al was excluded from this study, which seems surprising considering it is one of the most abundant trace elements present in the quartz of this study.

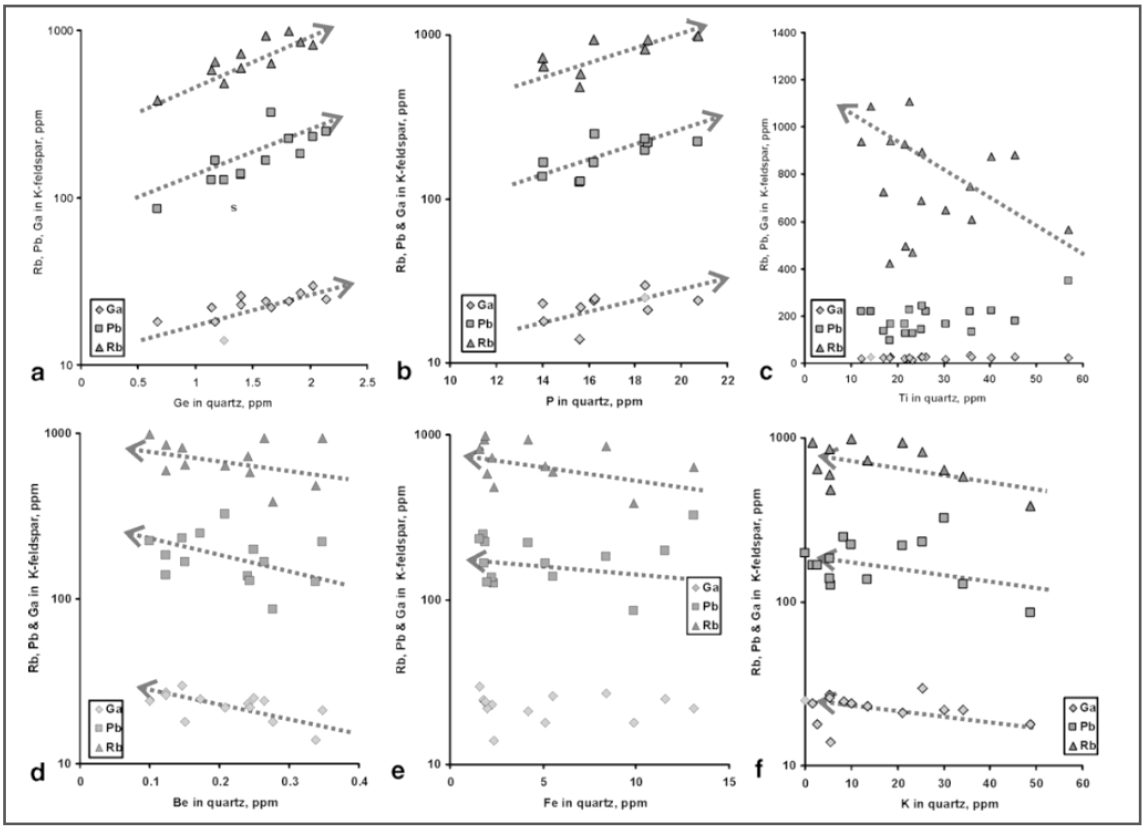

Fig. 5.1.2 Absolute concentration of Ge, P, Ti, Be, Fe, K, Al and Li in quartz compared to the concentration of three incompatible elements in granitic K-feldspar (Rb, Pb and Ga). All samples are from the Evje pegmatite field. Arrows define the direction of igneous differentiation (Larsen et al., 2004)

Subsequent investigation of the Evje-Iveland pegmatites (Larsen et al., 2004) (demonstrated in Fig. 5.1.2) indicates how trace element content is affected by progressive fractionation, where fractionation is marked by an increasing concentration of Rb, Pb and Ga in K-feldspar. Larsen et al. (2004) report how Ge and P increase with fractionation, whereas Be, Fe, K (and, vaguely, Ti) decrease with fractionation. Initially, the data appears to provide conflicting information about how the degree of fractionation affects trace element distribution in quartz, some elements increasing and others decreasing. Instead, the graphs provide evidence that certain elements were compatible in the quartz lattice. For example, Ge and P are most abundant in quartz from more fractionated pegmatites, with Be, Fe and K most abundant in quartz from less fractionated pegmatites. Rather than revealing overall trace element behaviours, this indicates that Ge and P are incompatible in quartz, remaining in the melt as it fractionates, whereas Be, Fe and K (and Ti) are compatible and partition into mineral phases (i.e. the quartz lattice) whilst the melt is still

juvenile. This is why the Ge/Ti of quartz is deemed a strong indicator of melt fractionation.

Despite the apparent clarity of the trends in Fig. 5.1.2, there are some perceived issues with the data. Each data point represents chemical information from one pegmatite, but not one sample site. From each sample “locality”, four samples were collected; two of quartz and two of K-feldspar “in close proximity” (Larsen et al., 2004). The inherent flaw in this method is that the two minerals potentially formed in quite different environments and at different times.

As there appeared to be issues with Larsen et al.’s (2000 and 2004) data sets, and because the Høvringsvatnet granite would seem to be such an obvious source for melts to form the pegmatites, it was deemed necessary to reassess the hypothesis that the pegmatites represent fractionated equivalents of the melts which formed the Høvringsvatnet granite. If this were the case then it would not be unreasonable to observe some spatial control over pegmatite composition. Simmons (2007) for example proposed that relatively juvenile pegmatites would form closest to the granites (as the melt has had little time to fractionate) with more evolved pegmatites further away from the granites, fractionating en route. This is referred to as regional zonation, and occurs in a large variety of pegmatite fields (Agomor et al., 1987; Malló et al., 1995; Norton and Redden, 1995). In Evje-Iveland however, neither trace element content (initially proposed by Müller and Ihlen, 2011) nor degree of fractionation (as indicated by Figs. 5.1.3 and 5.1.4 respectively) showed strong correlation or spatial relationships with distance to the granite complex. Indeed, the data emphasises the large variation within quartz from a single pegmatite, how unrepresentative singular samples must be and therefore the importance of sampling well constrained materials.

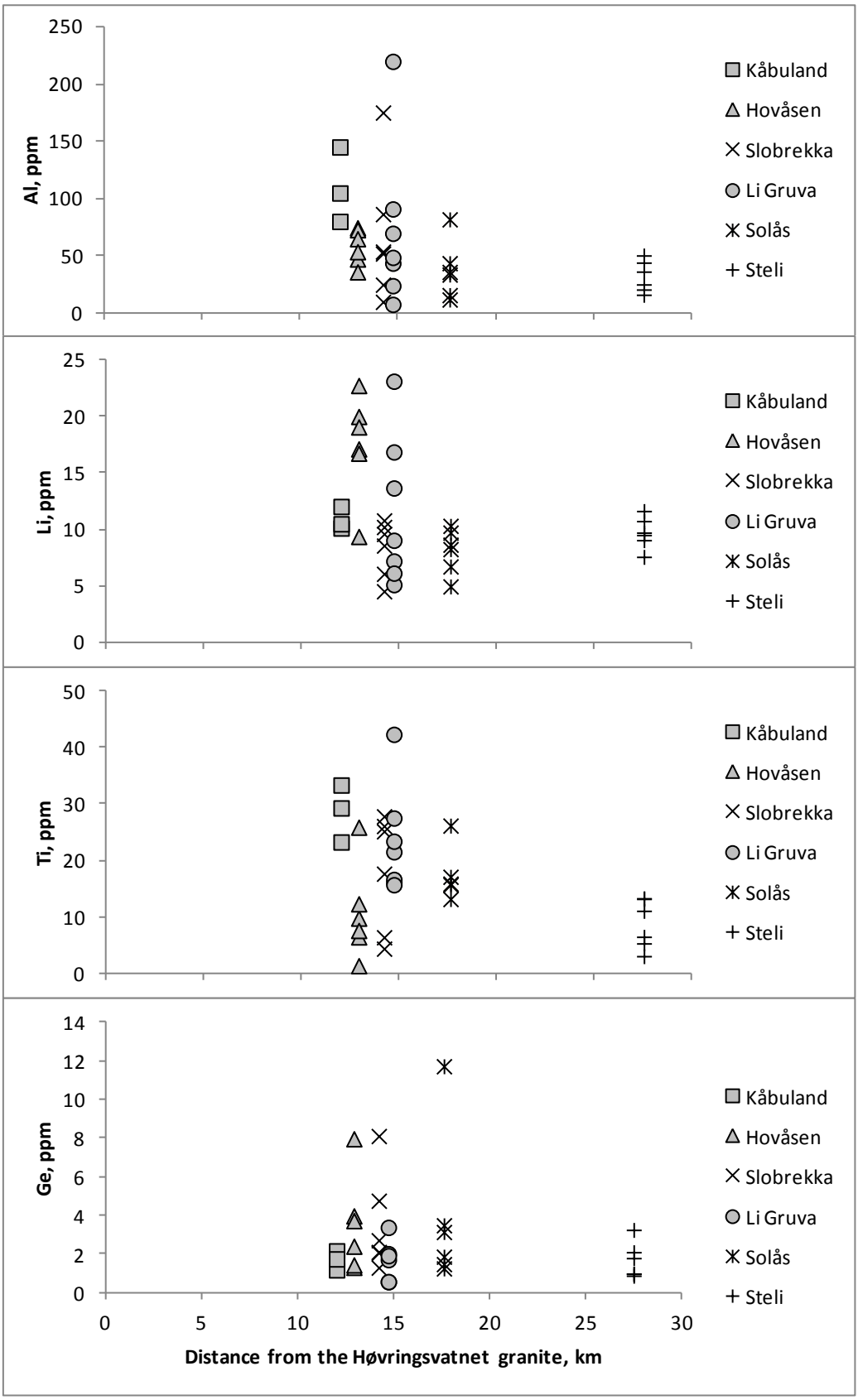

Fig. 5.1.3 Concentrations of structural impurities in quartz from the Evje-Iveland pegmatites, related to spatial distribution

The similarity in the distribution of Al and Li in quartz is almost certainly because Al^{3+} and Li^{+} together form a classic coupled substitution for Si^{4+}. Ge appears to form an opposing distribution, marking a graduation between coupled (Al^{3+} and Li^{+}) and simple (Ge^{4+}) substitutions. This data set fails to display the spatial control over trace element content reported by Larsen et al. (2000 and 2004). This undermines, to some extent, the notion that the pegmatites represent more fractionated equivalents of the Høvringsvatnet granites.

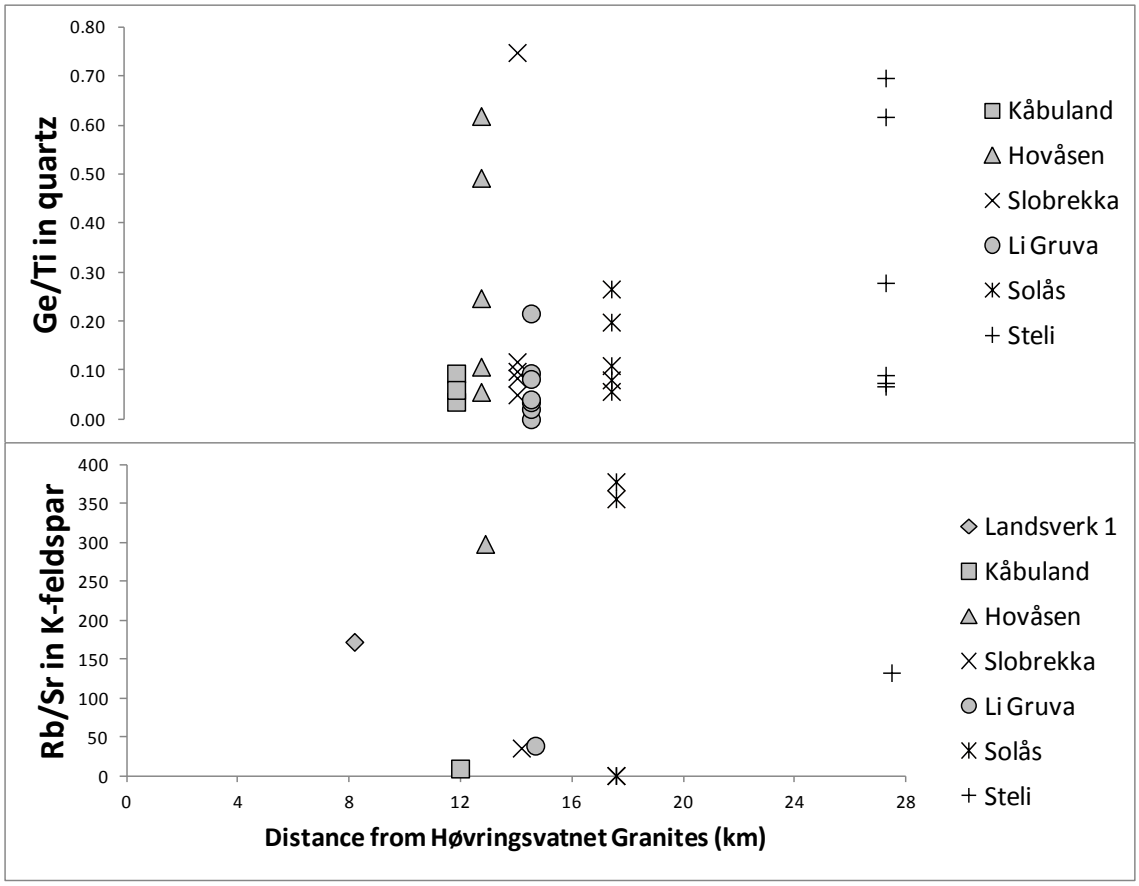

Fig. 5.1.4 Distance from Høvringsvatnet granites verses degree of fraction of the Evje-Iveland pegmatites inferred from Ge/T in quartz (above) and Rb/Sr in K-feldspar (below)

This assertion is supported by data in Fig. 5.1.5; there is little correlation between indicators of fractionation in quartz, feldspar or from relative degree of pegmatite evolution. Fig. 5.1.6 suggests that currently utilised fractionation indicators are perhaps not as robust as initially thought, as there is little correlation between Ge/Ti in quartz, and the classic methods of element distribution in K-feldspar.

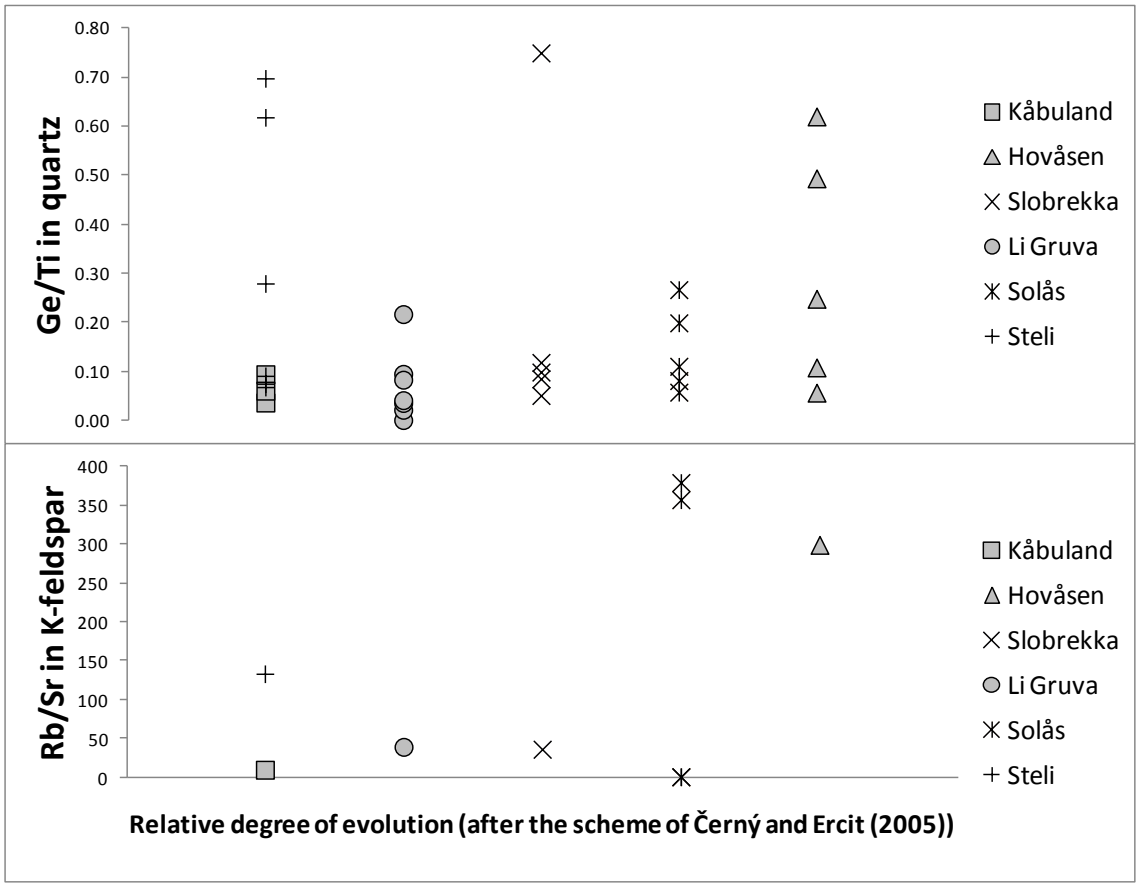

Fig. 5.1.5 Graphs of degree of evolution of the Evje-Iveland pegmatites (inferred from Ge/Ti in quartz and Rb/Sr in K-feldspar) related to relative fractionation, after Černý and Ercit (2005) (see Table 5.1.2)

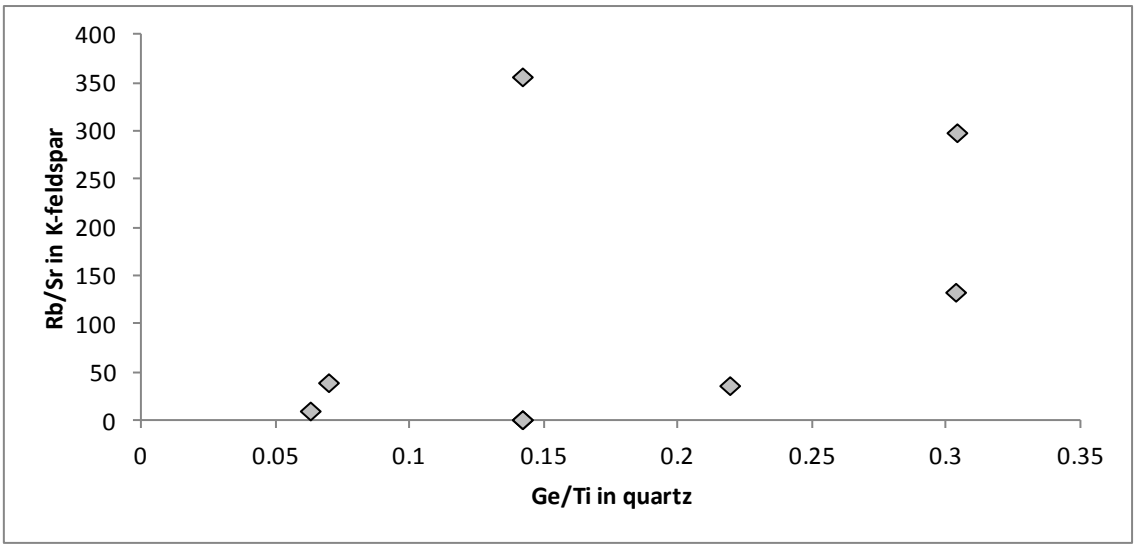

Fig. 5.1.6 Correlations between different indicators of the degree of fraction of the Evje-Iveland pegmatites

5.1.3 Geochronological constraints on the timing of pegmatite emplacement

Previous dating of the Høvringsvatnet granites provided a range of ages; 900±53 Ma (Rb-Sr whole-rock, monzonitic sheets,) and 945±53 Ma (Rb-Sr whole-rock, granite) from Pederson (1981), and 971+63/-34 Ma (U-Pb zircon)

from Andersen et al. (2002) respectively. Despite the large errors associated with each age, they place the granites in close chronological proximity to the pegmatites, which have been dated by Scherer et al. (2001), Andersen (2001) and Boudin and Deutsch (1970) at 910.5±1.6 Ma (U-Pb upper Concordia age), 909±5 Ma and 901±20 Ma ($^{207}Pb/^{206}Pb$), respectively. This correlation is likely to have led to the apparent assumption that the Evje-Iveland pegmatites are genetically related to the Høvringsvatnet granites.

U-Pb zircon dating in the current study has produced ages for three samples from the granites, at 979.7±3.8 (syenomonzonite), 982.8±4.5 and 982.9±3.6 Ma (biotite granites). These ages not only display a much lower (an order of magnitude lower) error than previous ages, but are in much better initial correlation with each other, whilst maintaining the precedent that the monzonite facies postdates the biotite granite. The age data demonstrates that the Høvringsvatnet granites were emplaced in the closing stages of the Agder phase of the SNO (Bingen et al., 2008b), at a time of peak regional medium pressure metamorphism (M1) with associated syn-collisional plutonism. Alternatively, the Høvringsvatnet granites may be an early result of regional decompression which occurred after M1 metamorphism. The pegmatites appear to have been emplaced in the closing stages of the Dalane phase, at a time of general crustal relaxation and gravitational collapse, and a slowing in exhumation rates by 920 Ma (Bingen et al., 2008b).

The new ages serve to put approximately 70 Ma between the Høvringsvatnet granites and literature ages for the Evje-Iveland pegmatites (Fig. 5.1.7). This is an unfeasibly long time for a granitic melt to persist and to continually fractionate whilst not producing any field evidence of intermediary stages. Excluding the Høvringsvatnet granite complex (the varying facies of which appear to be broadly synchronous, based on field exposure and the produced dates) and the pegmatites (which appear approximately 70 Ma after the granites) there are no other granitic expressions in the region; no other plutons, no plugs, no dikes, no sills, no magmatic or pyroclastic evidence.

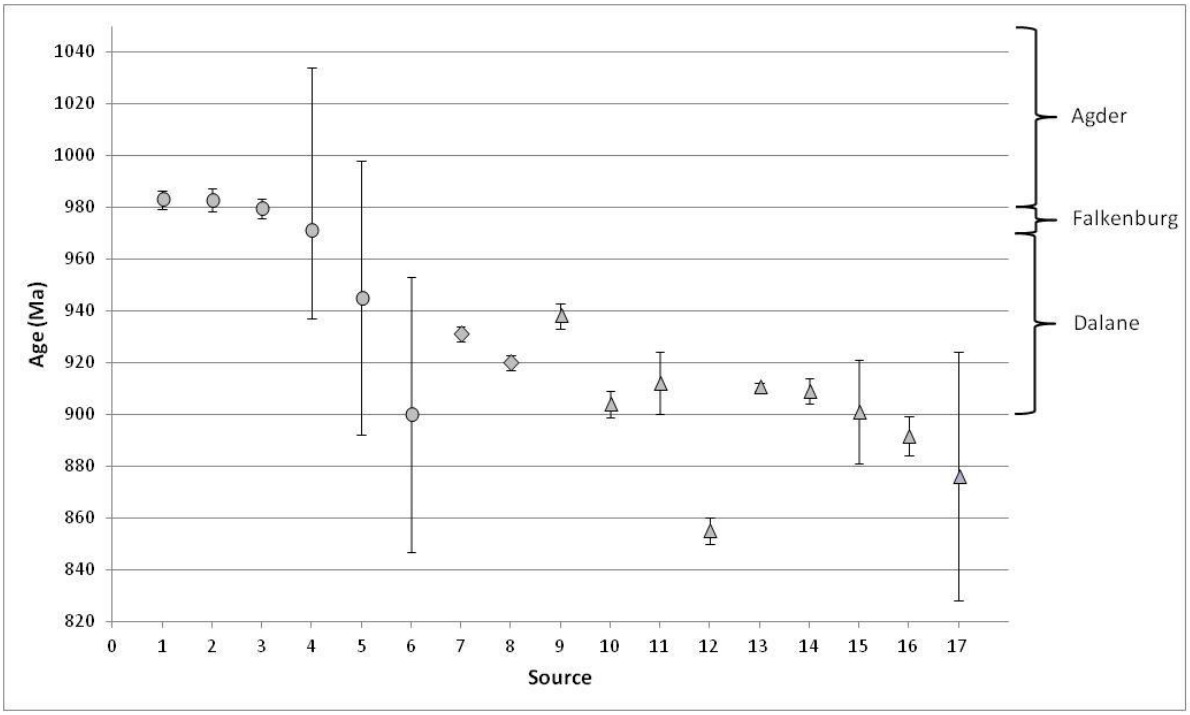

Fig. 5.1.7 Geochronology of the Evje-Iveland province. Circular markers represent the Høvringsvatnet granites, diamond markers the Rogaland Anorthosite complex and triangular markers pegmatites from Evje-Iveland. 1, 2 & 3: this study. 4: Andersen et al. (2002), 5: Pedersen and Konnerup-Madsen (1994), 6: Pederson (1981), 7 & 8: Schärer et al. (1996; emplacement of the anorthosite complex and the ilmentite norite of the Tellnes deposit respectively), 9, 10, 11 & 12: Anne-Magali Seydoux, personal communication (2011, from Steli, Steli, Mølland and Landsverk 1 pegmatites respectively), 13: Scherer et al. (2001), 14: Andersen (2001), 15. Boudin and Deutsch (1970), 16 &17: this study (Steli and Slobrekka pegmatites respectively)

The lack of additional granitic phases in the pegmatite field suggests that the Høvringsvatnet granite is limited spatially to the northeast of the area; a southerly extension of the granites at depth is deemed unlikely from the Bouguer anomaly map (Fig. 5.1.8), which indicates a marked contrast between the signal provided by the granite complex and the pegmatite field. The pegmatites are situated on a strong positive anomaly indicating the presence of high density rocks i.e. fundamentally different underlying rocks to those below the Høvringsvatnet granites.

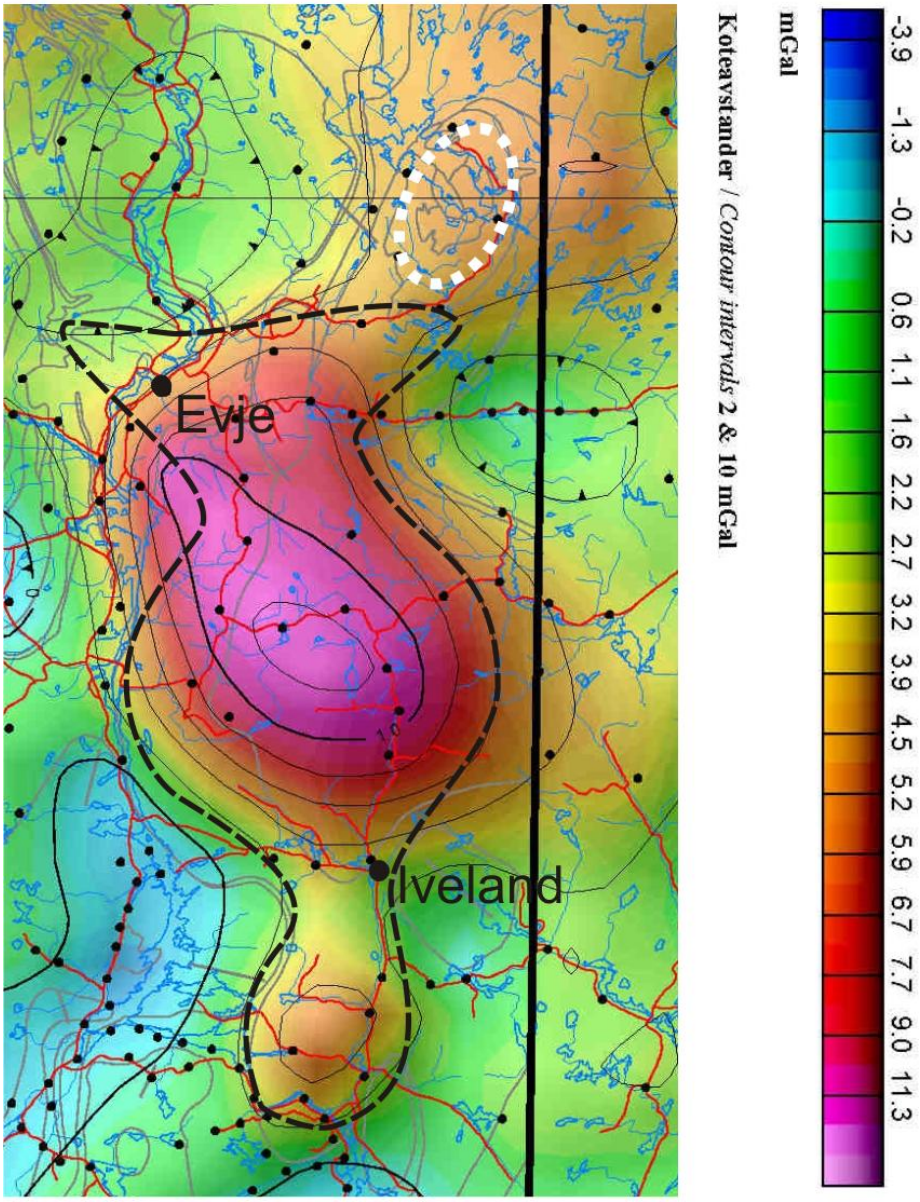

Fig. 5.1.8 Bouguer anomaly map of the Evje-Iveland pegmatite field showing a marked contrast in response density between the pegmatite field (black dashes) and the Høvringsvatnet granite (white dots). From Gellein (2007)

If the Høvringsvatnet granites did not supply melts to produce the pegmatites, then the question arises as to the source and the mechanism to produce the Evje-Iveland pegmatites. Andersen et al. (2006) report near-juvenile Hf isotope compositions in magmatic protoliths from the deep crust. Underplating is thought to have contributed towards 1.0 – 0.92 Ga anorogenic magmatism, which formed the Rogaland Igneous Province, less than 90 km to the southwest of the Evje-Iveland field area, which is most notable for the Rogaland anorthosite-mangerite-charnockite (AMC) complex (e.g. Duchesne et al., 1999;

Schärer et al., 1996). The underplating would have been early Sveconorwegian in age, preceding melting by ca. 50 Ma. Schiellerup et al. (2000) report a lower continental crust-derived source for the AMC. They suggest that Sveconorwegian ramp tectonics (such as those discussed by Andersson et al., 1996) caused the intrusion of crustal tongues into the mantle, which subsequently underwent partial melting. The work of Andersson et al. (1996) describes a large gravity and seismic anomaly indicating a large Moho offset. They propose that “this offset is related to Sveconorwegian crustal underthrusting” and that granitic melts (e.g. the pegmatites of Evje-Iveland) “could have formed by anatexis of mid-crustal rocks downthrusted to greater depths” in the vicinity of the observed Moho irregularity. Bingen et al. (2008b) refer to crustal thinning occurring in the Dalane Phase of the SNO, which may have induced further melting.

The most intense phase of metamorphism induced by the emplacement of the Rogaland AMC complex was that of a thermal aureole, with associated temperatures of up to 900°C (Jansen et al., 1985; Wilmart and Duchesne, 1987) and pressures of up to 5 kbar (Vander Auwera and Longhi, 1994). Critically, this emplacement occurred between 932±3 and 920±3 Ma (Schärer et al., 1996), with ‘ultra-high temperature metamorphism’ (up to 1050°) occurring at 927±5/922±5 Ma (Tobi et al., 1985); approximately the time that the pegmatites begin to appear (Fig. 5.1.7).

It is proposed therefore that, as demonstrated at Iveland (Fig. 4.1.1), basement country rock (variably gneisses or IGMC) in the region has undergone anatexis, and it is this partial melt product which is responsible for forming the pegmatites. The underplating associated with the Rogaland AMC metamorphism may be the heat source necessary to induce partial melting of country rocks. Whalen (1983) suggests most I-types form by re-melting of material produced by underplating of continental crust. The majority of the units present in the IGMC (i.e. meta-igneous bodies) would be suitable candidates for generating potential pegmatite-forming melts.

It must be noted however that Bingen et al. (2008a) suggest that this metamorphism was spatially limited to west of a clinopyroxene isograd, which runs NNW-SSE approximately 50 km to the west of the Evje-Iveland pegmatite field. However, high grade metamorphism is thought to have occurred in Southern Telemark during the gravitational collapse of the late Sveco-Norwegian orogeny c. 913 to 907±7 Ma (the Dalane phase, Bingen et al., 2008b), which may have produced/contributed the heat and/or fluxes necessary to induce partial melting. Only one pegmatite age does not support this theory; 938±5 Ma from Steli. However, an alternate age from Steli is 904±5 Ma, which correlates closely with Scherer et al.'s (2001) age of 910.5±1.6 Ma, with Andersen's (2001) age of 909±5 Ma and with the age of the Mølland pegmatite of 912±12 Ma (Anne-Magali Seydoux, pers. comm., 2011); approximately 2 km north of the Solås pegmatite (Bjørlykke, 1935)). It also overlaps with the pegmatite age of 891.6±7.5 Ma produced by the current study. It is possible that this early age (which essentially postdates the Rogaland AMC complex), which is from monazite, represents material inherited from country rocks; for example, Bingen *et al*. (2008a) provide monazite ages of 947±5 Ma, potentially representative of an event between the M1 and M2 events of Tobi et al. (1985).

5.1.3 Pegmatite genesis by partial melting of country rocks

From the discussion above, it is proposed that anatexis of Evje-Iveland country rocks (such as that observed at Iveland; Fig. 4.1.1) generated the melts which ultimately formed the pegmatites. With respect to pegmatite melt production there is little evidence of in situ melting of country rocks adjacent to pegmatites, other than at Iveland (and, to some extent, Slobrekka). Pegmatite contacts are often characterised by deflected cleavage (i.e. the host rock was ductile upon pegmatite emplacement), hydration of amphibole to biotite and, locally, included components of country rock xenoliths (which aren't always consistent with adjacent host rock). This suggests that pegmatite melts have undergone transportation away from their source, with feeder structures unexposed or sheared out during final orogenesis. Additionally, there is a significant discrepancy in HREE signature between the Evje-Iveland pegmatites and their country rock (*Chapter 4.3.2*). For these reasons, it may be difficult to reconcile the compositions of particular host rocks with that of their pegmatites; the

source may be present at depth rather than adjacent to the pegmatites. As the Iveland pegmatite displays conspicuous evidence of in situ melting, the composition of country rock from this locality is assumed as a 'protolith' for melt production in the following modelling of partial melting, which was performed to investigate the geochemical potential for pegmatite melts to form purely by anatexis of country rock.

Melt production was modelled for six pegmatites using batch melting principles as described by Rollinson (1993), whereby a melt is produced which is "continually reacting and re-equilibrating with the solid residue at the site of melting until mechanical conditions allow it to escape as a single 'batch' of magma". This melting mechanism was favoured over fractional melting as at Iveland melt was seen to remain in situ; evidently, the rheologically critical melt percentage (RCMP, suggested as 15%, 20 – 25% and 20 – 35% (Clemens and Vielzuf, 1987; Vigneresse et al., 1996; Arzi, 1978 respectively)) locally prevented partial melts from escaping immediately. Additionally, the underplating/crustal tongue mechanisms suggested above imply relatively deep melt conditions, which allow for a certain degree of equilibration. Melt element compositions (C_L) were calculated using the expression:

$$C_L = \frac{C_O}{D_{RS} + F(1 - D_{RS})}$$

where C_O is the element concentration in the unmelted source, D_{RS} is the bulk partition coefficient for the residual solid and F is the weight fraction of the melt produced. Utilised partition coefficients were arithmetic means of those provided for dacitic/rhyolitic melts (as the pegmatites are >63% wt SiO_2) in Rollinson (1993); see Table 5.1.3.

Table 5.1.3 References for coefficients utilised in partial melting modelling

Mineral	Utilised References
Biotite	Arth, 1976; Pearce and Norry, 1979; Nash and Crecraft, 1985; Mahood and Hildreath, 1983
Garnet	Arth, 1976; Irving and Frey, 1978
Plagioclase	Arth, 1976; Pearce and Norry, 1979; Nash and Crecraft, 1985
K-feldspar	Pearce and Norry, 1979; Nash and Crecraft, 1985; Mahood and Hildreath, 1983
Apatite	Pearce and Norry, 1979; Fujimaki, 1986
Zircon	Mahood and Hildreath, 1983; Fujimaki, 1986
Allanite	Mahood and Hildreath, 1983; Brooks et al. 1981

Modelling was performed for Sr and Rb and REEs, to match a theoretical 'Melt' composition generated from a particular 'Source' (initially the Iveland country rock) to a 'Target' (taken as the composition of the pegmatite border facies, interpreted to be representative of initial melts) (Fig. 5.1.9). The 'Melt' was generated by adjusting degree of partial melting, and remaining proportions of the minerals summarised in Table 5.1.3.

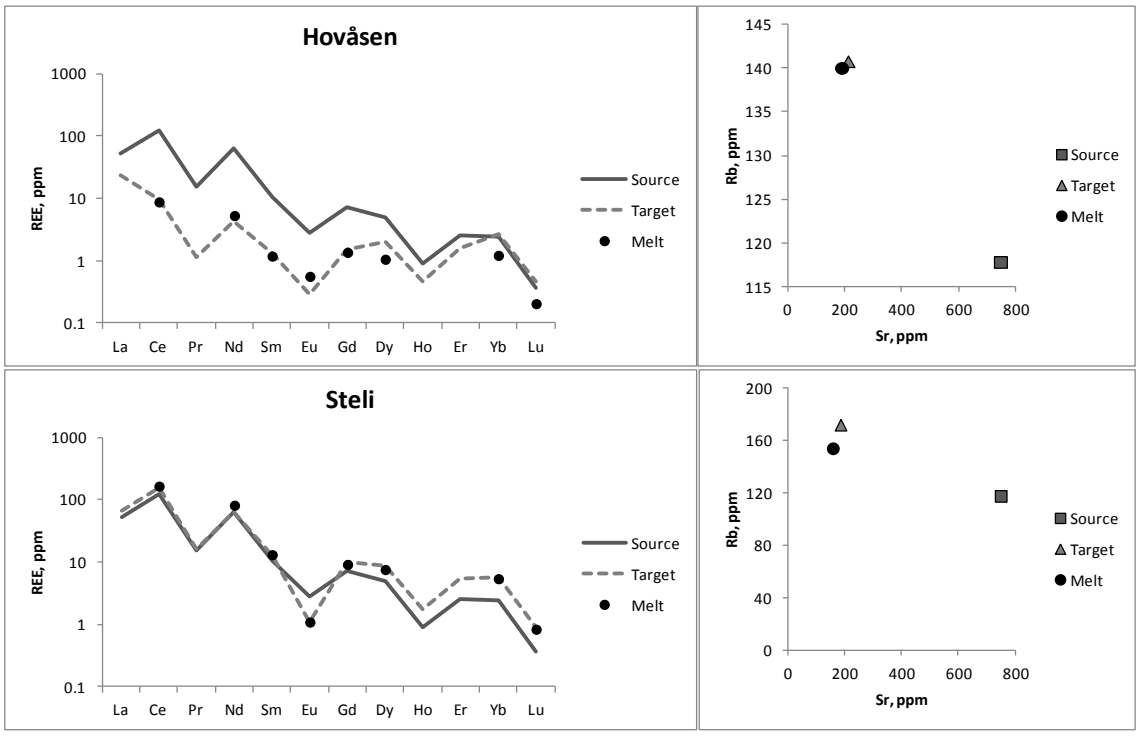

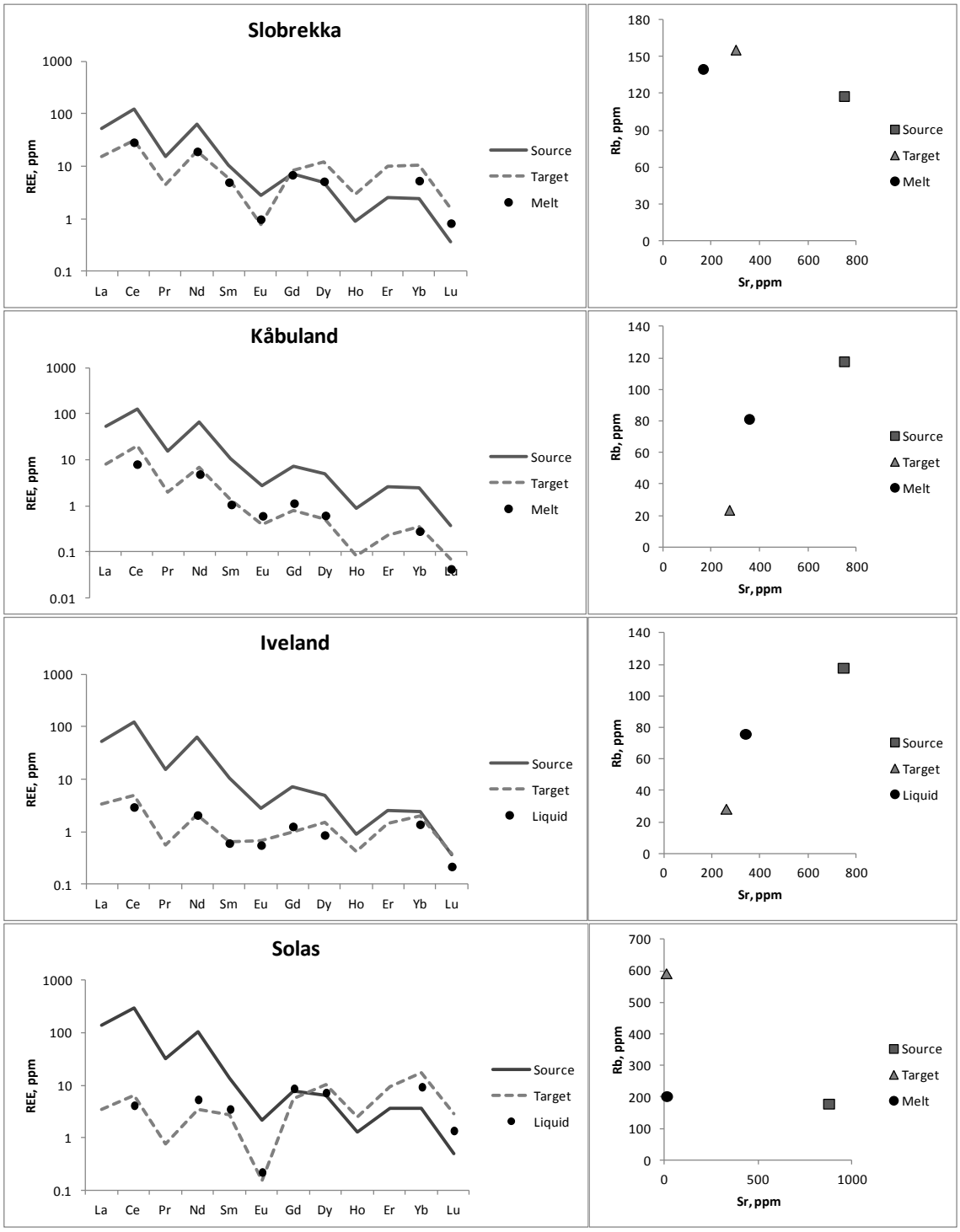

Fig. 5.1.9 Geochemical modelling for batch partial melting of Iveland country rocks to produce the composition of wall rock facies of the pegmatites, using partition coefficients listed in Table 5.1.3

Hovåsen

REE modelling appears relatively successful for partial melting at Hovåsen. The model requires 20% melt production, with 43% plagioclase, 30% K-feldspar, 16% biotite, 10% apatite, 1% allanite and no garnet or zircon remaining in the residue.

Steli

The REE model generated requires 20% melt to be produced, with 60% plagioclase, 25% K-feldspar, 14% biotite, 1% apatite, 1% allanite and no garnet or zircon remaining in the residue.

Slobrekka

*S*uccessful REE modelling at Slobrekka required 15% partial melting, and 43% plagioclase, 43% K-feldspar, 13% biotite, 1% apatite and no garnet, allanite or zircon to remain in the residue.

Kåbuland

The REE model generated requires 15% melt to be produced and 20% plagioclase, 15% K-feldspar, 43% biotite, 10% apatite, 10% garnet, 1% allanite and 1% zircon to remain in the residue. The Eu anomaly is quite minor.

Iveland

With compositional trends which converge towards the HREEs (akin to Hovåsen) and a negligible Eu anomaly, the pegmatitic melt at Iveland can be successfully modelled for REEs with 30% melting (approximately that observed in the field) and 25% plagioclase, 15% K-feldspar, 51% biotite, 5% apatite, 4% allanite and no garnet or zircon remaining in source. This is a relatively high apatite concentration and there is a total absence of zircon (further similarities with the Hovåsen pegmatite).

Solås

Excepting the end members of the HREEs, REE modelling for the Solås pegmatite was relatively successful. Based on 20% melt production, the remaining minerals are 30% plagioclase, 10% K-feldspar, 10% biotite, 1% apatite, 0.1% garnet, 1% allanite and no zircon.

Geochemical modelling was successful for the majority of pegmatites, with theoretical REE and Rb/Sr levels correlating closely with measured whole rock values from the border zone. At Kåbuland and Iveland, REE levels could be reproduced, but a sufficiently low Rb level could not be produced in the

modelling. A possible reason for this is the partitioning behaviour of Rb between granitic melts and aqueous fluids. During crystallisation, granitic melts become progressively enriched in incompatible fluxes (including water) and, as reported by London (2009), this flux rich boundary precedes the crystallisation front i.e. CZR. It is the concentrated presence of these fluxes (which actually represent a very small proportion of overall pegmatite melt volume) which allows the undercooling and limited nucleation believed necessary for pegmatite genesis. The fluid may re-equilibrate with the newly formed crystals, and as Rb partitions preferentially into an aqueous fluid over a granitic melt (Bai et al., 1999), the Rb content of the rind is therefore less than that modelled by a system which only accounts for two phases (melt/crystal, rather than fluid/melt). The correct Rb and Sr content for Solås could not be reconciled.

An important possible complicating factor in the modelling is that the 'Target' composition was provided by the granitic material of the pegmatite border zones as these were interpreted to represent the composition of initial melts. This assumption has previously been questioned by London (2008), after the work of Jolliff et al. (1992), on the basis that their compositions are strongly peraluminous and therefore unrealistic, with large "constitutional variability". However, Jolliff et al. (1992) based their observations on the compositions of pegmatite wall zones; a coarser grained, internal and therefore later variant of the border zone. Additionally, the original study was based on one particular region of a much larger and varied single pegmatite field. Other pegmatites from other locations may well have different characteristics due to the possibility of "substantially different source terranes". It is this variation in source that could be responsible for the potentially unique peraluminosity in the Jolliff et al. (1992) study; the pegmatites in this study display a weak peraluminous signature (Fig. 4.3.5).

In summary, geochemical modelling indicates that it is possible to produce melts geochemically similar to pegmatite compositions. Melt material from Iveland basement gneisses can be modelled to a similar composition to that of the Hovåsen, Steli, Slobrekka, Kåbuland, Iveland and, for REEs, Solås pegmatites. Partial melting of appropriate country rock allows the production

and agglomeration of melt. The melt may then crystallise in situ, or will reach its RCMP and escape the melt region. The Evje-Iveland pegmatite field may represent a single threshold escape from the single melt source, multiple escapes from a single source or, most likely, multiple melt episodes from multiple (potentially unexposed) sources (which include Iveland). This model is simple as the partial melting may be in situ; only a heat source (and limited transport) is required (e.g. Martin and De Vito, 2005; Simmons et al., 1996).

5.2 Formation of high purity quartz

5.2.1 Field and geochemical evidence for spatial control on the formation of pegmatitic and high purity quartz

In order to predict the occurrence of HPQ in pegmatites, pegmatitic quartz in Evje-Iveland was investigated. The distribution of sufficiently pure material within the field and within individual pegmatites was characterised, prior to defining its formation mechanism. The concept of spatial distribution in quartz chemistry has already been demonstrated to be nonexistent and mapping and sampling of the Landsverk area indicates that there are no distribution trends within those particular pegmatites over the trace element content of quartz pods (*Chapter 4.4.3*; Figs. 4.4.44 to 4.4.47). As discussed in *Chapter 5.1.1*, there is no control over degree of fractionation or trace element content based on pegmatite position relative to the Høvringsvatnet granite (e.g. Figs. 5.1.3 and 5.1.4).

With regards to the hydrothermal event which is seen to brecciate and overprint existing rocks at Landsverk 1 (removing Ti and promoting Al), as discussed in **Chapter 4.2** a 1.5 m thick quartz vein orientated 161/54 E and 300 m east of Landsverk 1 was seen to contain minerals representative of the hydrothermal suite present within the pegmatite (Table 4.1.3). This may represent a feeder structure responsible for the later hydrothermal event, considering its concordant alignment with the pegmatite. Indeed, Figs. 4.4.39 to 4.4.42 indicate that, despite containing limited Ti (and hence different to the Ti-barren hydrothermal quartz identified previously e.g. Fig. 4.4.6) the vein is consistently amongst the purest quartz sampled in the Landsverk region.

Studies of the Froland pegmatite field, some 30 km to the east, indicate that there is not only a consistency in trace element concentration in quartz between pegmatites, but also within individual pegmatites across internal zonation (Müller et al., 2008; Müller and Ihlen, 2011). They report variation in quartz of typically 34 – 44 ppm, 6 – 10 ppm, 4 – 8 ppm and 0.9 – 1.8 ppm for Al, Li, Ti and Ge, respectively. Due to the precise nature of the selective sampling campaign performed during this investigation, the position of quartz material could be plotted within a pegmatite profile, thereby mapping trace element concentrations throughout the body. Fig. 5.2.1 indicates that not only is there considerably more variation in Al concentration in the Evje-Iveland pegmatites than those in Froland, but that there is no apparent preference for Al or Li to be concentrated in a particular zone. In contrast, Ti (Fig. 5.2.2) appears to be concentrated in quartz in the margins of pegmatites, with Ge concentrated in the cores (displaying the inverse relationship demonstrated previously e.g. Fig. 4.4.38). The fact that Ti is concentrated in the border zones (i.e. the first quartz to crystallise in the pegmatites) indicates that Ti is more compatible than Ge, which remains in the melt until the final stages of crystallisation (as discussed in association with Fig. 5.1.2). That Ti is more compatible than Ge is demonstrated by Figs. 4.4.35 and 4.4.39; in the vast majority of analysed quartz, Ti occurs over Ge. It also implies that the hydrothermal event at Landsverk 1 may have actively removed Ti from system, as Ti favours the mineral phase over the liquid (Fig. 4.4.6). The event which stripped Ti from the quartz does not appear to have affected Fe (Fig 4.4.11; this is unusual as Ti^{4+} and Fe^{4+} act as common substitutions), whilst seemingly promoting Al (Fig. 4.4.5).

Additionally, Figs. 4.4.11 to 4.4.18 and 4.4.36 display the relative dominance of Li^{+} as a charge compensator to Al^{3+} when substituting for Si^{4+}. At Hovåsen and Steli, quartz contains a greater proportion of Li than is perhaps to be expected. Quartz from Slobrekka and Solås also demonstrates a general relative enrichment in Li, except that core quartz demonstrates relative Li depletion. Quartz in Li Gruva contains heterogeneous Li:Al, whereas Kåbuland and Landsverk 1 contain quartz with relatively elevated Al levels. The general implication is that later (i.e. core and hydrothermal) quartz contains diminished Li relative to Al. H^{+} may start to feature as an alternative charge compensator to

Li^+ due to increased water concentrations during the crystallisation of quartz in these core/hydrothermal environments.

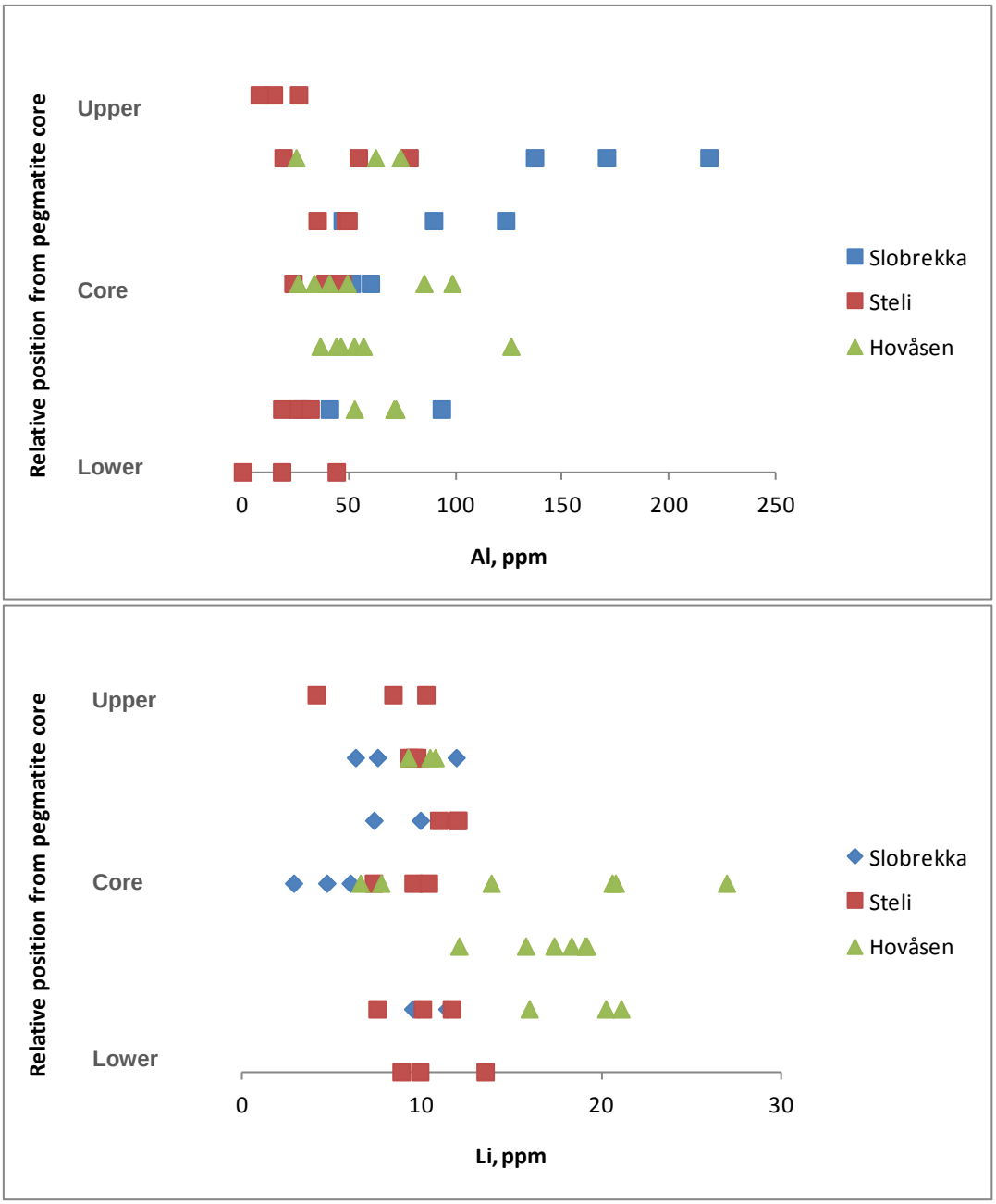

Fig. 5.2.1 Concentration of Al and Li in pegmatitic quartz through pegmatite profiles, for Slobrekka, Steli and Hovåsen

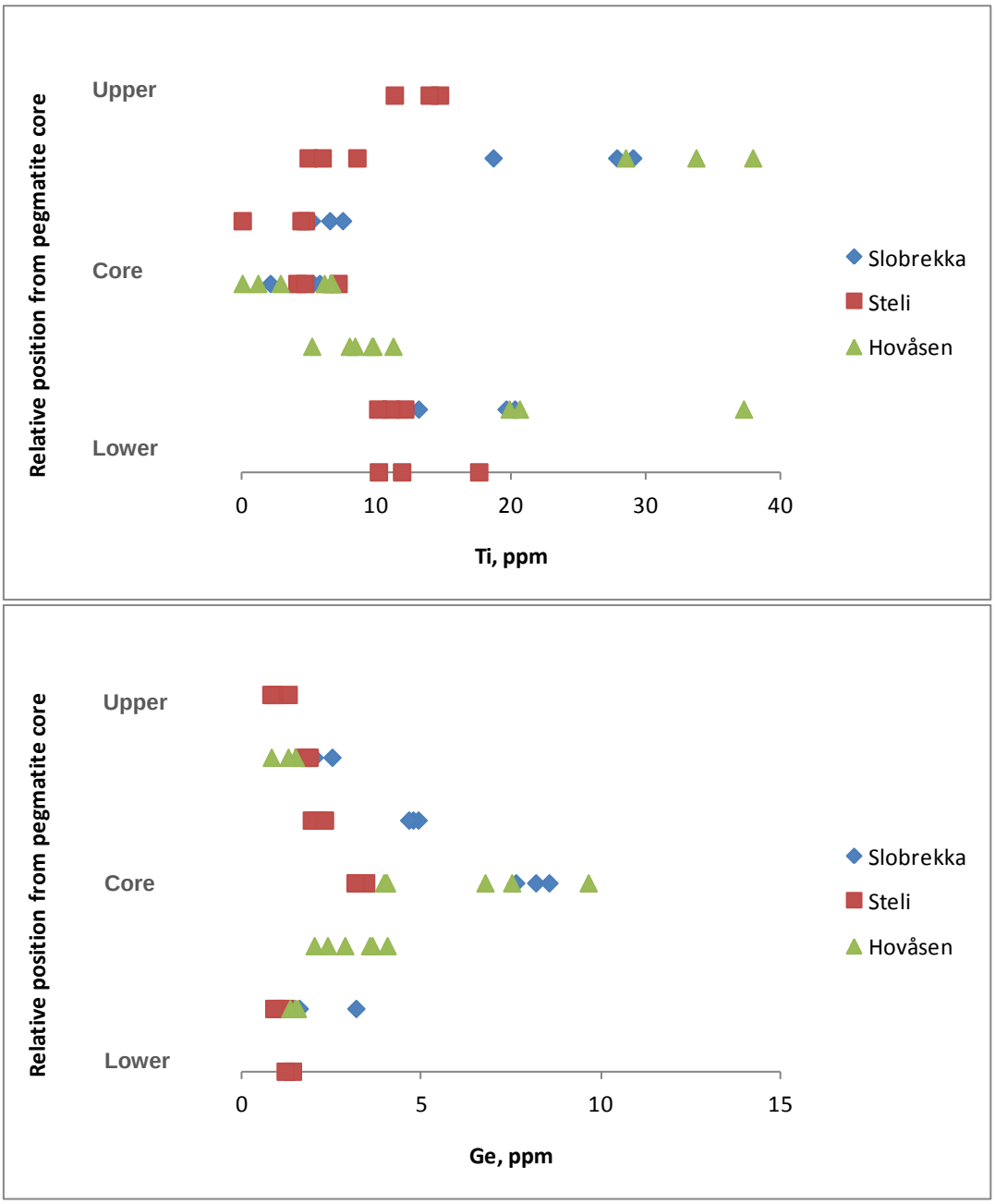

Fig. 5.2.2 Concentration of Ti and Ge in pegmatitic quartz through pegmatite profiles, for Slobrekka, Steli and Hovåsen

In essence, there appears to be no consistency in primary pegmatitic quartz composition between pegmatites, within individual pegmatites (excepting Ti and Ge), or indeed within single samples. This is in contrast to the proximal Froland pegmatites, which are variably associated with the SNO and syngenetic with respect to the emplacement of the Herefoss granite pluton (Müller et al., 2008; Müller and Ihlen, 2011). The trace element content of primary pegmatitic quartz from the Evje-Iveland pegmatites is seemingly too unpredictable to allow for reliable exploration recommendations (as initially suggested by Müller and

Ihlen, 2011), making the region unsuitable as a potential site of HPQ extraction. Tanner et al. (2013) report huge variation in quartz characteristics (e.g. chemistry, isotope signatures) caused by oscillatory zoning, down to the 30 μm level; the compositional variation in quartz demonstrated by CL-SEM (**Chapter 4.6**) indicates that same is likely true for material from the Evje-Iveland. If detection limit issues can be overcome, perhaps bulk digest methods are more appropriate than in situ beam techniques for determining overall trace element content to compensate for this microscale variation.

This heterogeneity of trace element content in primary pegmatitic quartz is also present in the Borborema pegmatites, northeast Brazil (Beurlen et al., 2011). Beurlen et al.'s study reports that in non-Li bearing pegmatites (comparable to those of Evje-Iveland) the Al, Li, and Ge concentrations in quartz from all zones remain at the same level as the border and wall zones, and indicates that Ti concentrations are lower in core quartz (<3 ppm) over quartz from the border and wall zones (7 – 25 ppm; Beurlen et al., 2011). Excluding Ge, this is in fine agreement with the trace element distribution observed in primary pegmatite quartz from Evje-Iveland. Additionally, the conclusion of Beurlen et al. (2011) that trace element signatures relate to degree of fractionation, and that the Evje-Iveland pegmatites' position relative to the Høvringsvatnet granite has no bearing on trace element concentration in pegmatite quartz, support the previous conclusion that there is no genetic link between granite and pegmatite at Evje-Iveland.

5.2.2 Evidence for variations in fluid composition and quartz purity from cathodoluminescence imaging

Having determined that the variation of trace element concentrations in primary pegmatitic quartz is too great to constitute HPQ, and the trace element levels too high (Fig. 5.2.1 demonstrates that pegmatite quartz typically contains greater than 50 ppm Al alone), SEM-CL and LA-IC-MS data from the hydrothermally overprinted material at Landsverk was assessed. Diverse and preferential replacement of quartz was documented in a hydrothermal quartz crystal (e.g. Fig. 4.6.9), and the chemistry of this quartz was seen to differ from primary pegmatitic quartz (e.g. Figs. 4.4.5 to 4.4.8). LA-ICP-MS of the

hydrothermal quartz (Fig. 5.2.3) attempted to relate specific CL domains with a geochemical signature, but a combination of spatial reconciliation issues (i.e. accurately targeting a CL domain with an optical laser camera) combined with sub-beam width variations in quartz composition (e.g. Fig. 4.6.9, Tanner et al., 2013) meant that this was essentially impossible; ablation sites invariably incorporated a variety of quartz zones and hence chemistries (as demonstrated in Fig. 5.2.4, which represents ablation sites I and J).

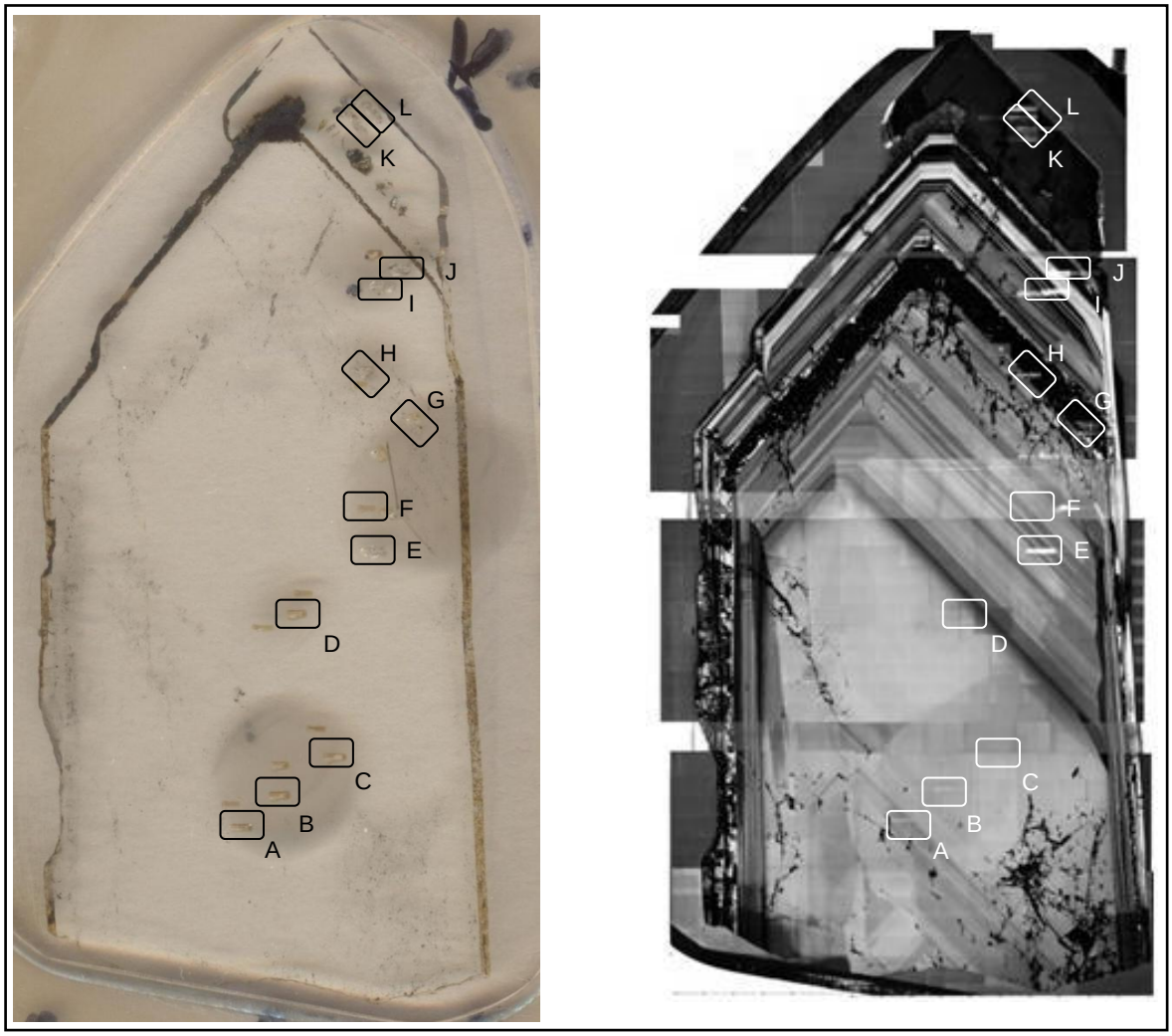

Fig. 5.2.3 Ablation sites in the Landsverk 1 hydrothermal quartz crystal

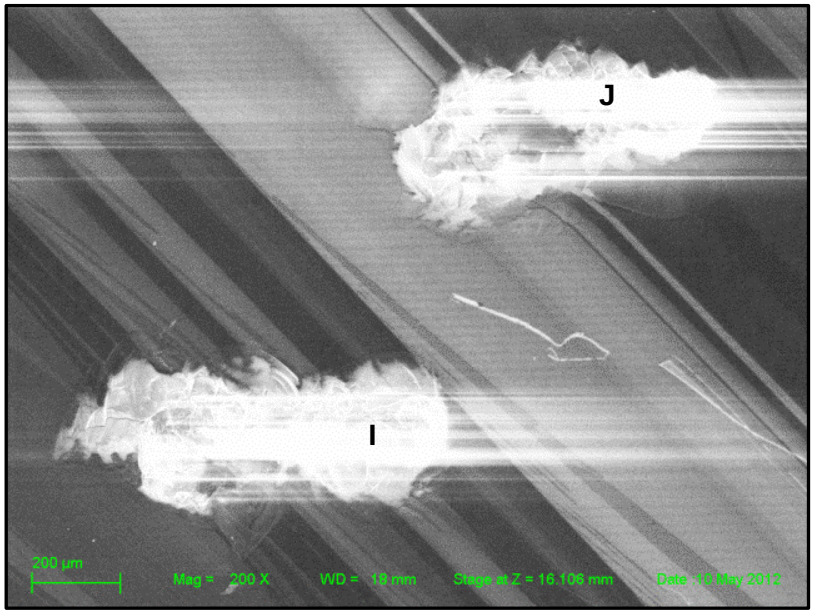

Fig. 5.2.4 Ablation sites for analyses **I** and **J** in the Landsverk 1 hydrothermal quartz crystal. Craters cross-cut quartz zones due to low spatial resolution of LA-ICP-MS

In spite of this spatial reconciliation issue, some geochemical trends can be identified. The core of the hydrothermal quartz crystal (and hence, the early fluids) contains the most trace elements, with the margins of the crystal containing less (Fig. 5.2.5). The majority of the quartz analysed in the hydrothermal crystal actually is no purer than magmatic quartz from other pegmatites (Solås and Steli are included as comparison and as this was quartz analysed for O isotopes). However, three sites did contain less than 50 ppm impurities (the HPQ threshold, as identified by Harben, 2002); H, I and K. Site L and the potential Landsverk feeder vein contained close to the threshold (both 52 ppm) and material from the margin of the Solås and Steli pegmatites contained less than 50 ppm.

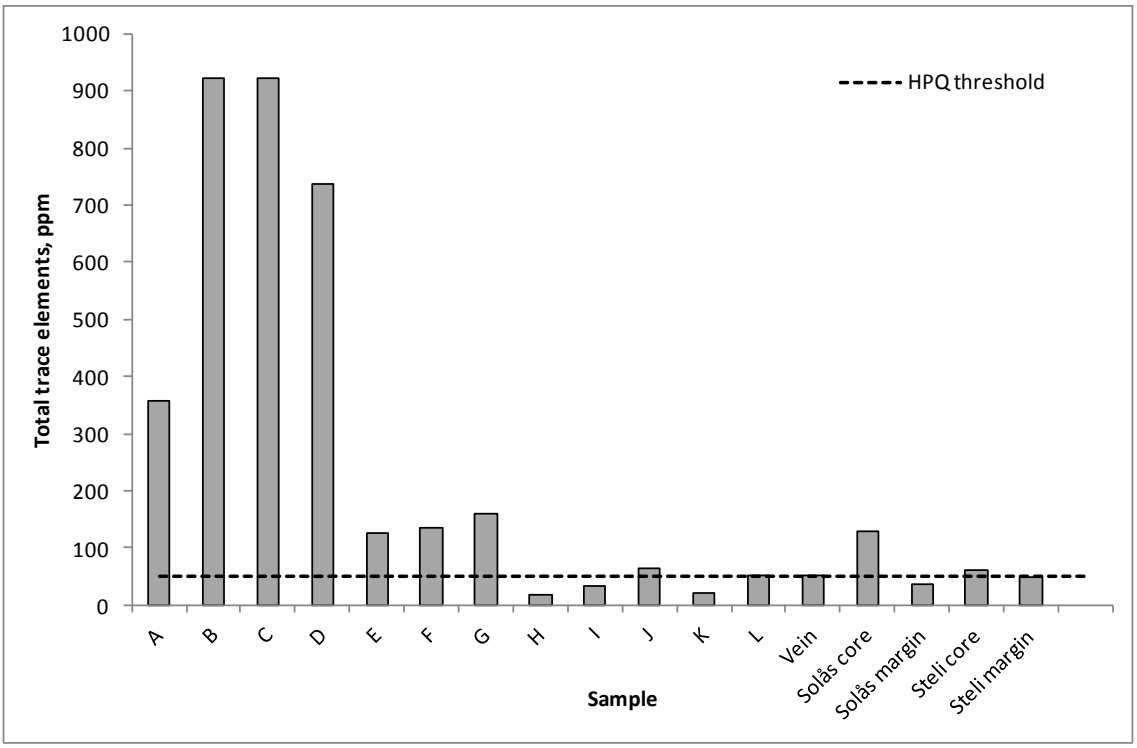

Fig. 5.2.5 Total trace element content in quartz from the Landsverk 1 hydrothermal crystal (A to L), the potential feeder vein east of Landsverk 1 and core and marginal quartz from the Solås and Steli pegmatites

Individual chemical profiling (Fig. 5.2.6) indicates that Al makes up the vast majority of impurities in the analysed quartz; quartz which can be classed as high purity consistently displayed reduced concentrations of Al. Al and Li concentrations correlate, and quartz from the Landsverk pegmatite displays an absence of Ti, with Ge typically below LOD. The potential feeder vein contains relatively elevated Ti levels. Site H displays the lowest proportion of trace elements (18 ppm); Fig. 5.2.7 indicates that the ablation falls entirely within the darkest CL phase previously identified as a late stage overprint; it is this overprint (e.g. Fig. 4.6.9) that displays the highest purity. Sites I and K (Figs. 5.2.3, 5.2.4 and 5.2.7) also occur in relatively dark quartz. That the margins of the Solås and Steli pegmatites contain HPQ is likely coincidental, as this feature is not repeated for all pegmatites (e.g. Fig. 5.2.1).

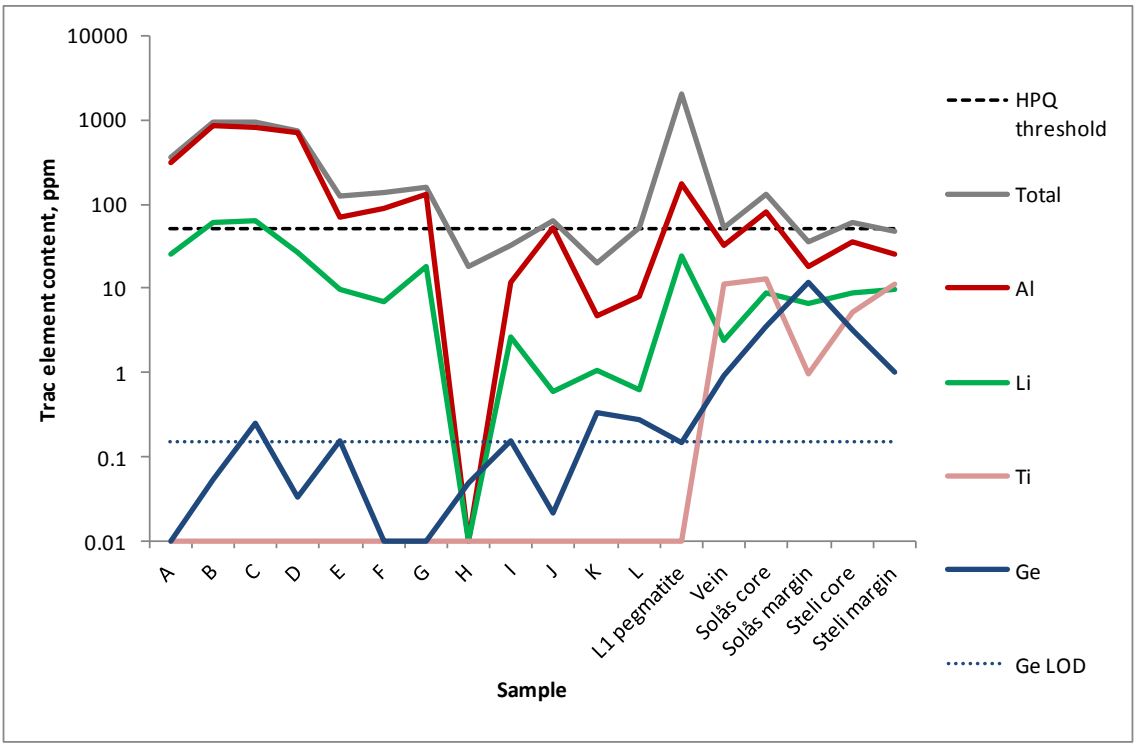

Fig. 5.2.6 Total trace element content in quartz from the Landsverk 1 hydrothermal crystal (A to L), pegmatitic quartz from Landsverk 1, the potential feeder vein east of Landsverk 1 and core and marginal quartz from the Solås and Steli pegmatites. All elements determined fall significantly above LOD except Ge, which has LOD displayed

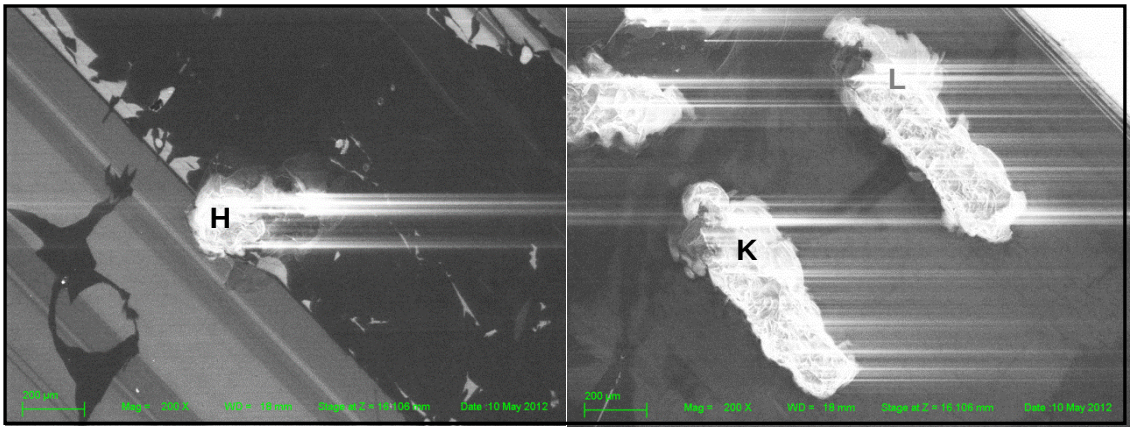

Fig. 5.2.7 Ablation sites for analyses **H**, **K** and **L** in the Landsverk 1 hydrothermal quartz crystal

5.2.3 O isotope constraints on the source of high purity quartz-forming fluids

Initial assessment of O isotope data (summarised in Table 4.7.1) indicates that the magmatic quartz i.e. that of the Steli and Solås pegmatites typically has a much higher $\delta^{18}O$ signature than that of hydrothermal quartz i.e. that of the Landsverk 1 pegmatite quartz (approximately 9‰ and 1 to 5‰ respectively). This immediately indicates that magmatic quartz has a magmatic fluid source (granitic fluids typically displaying $\delta^{18}O$ values of 6 to 10‰; Hoefs, 1997), whilst

quartz originally interpreted to be hydrothermal in nature does indeed display lower values (the base of the Landsverk 1 crystal displays an average value of -8.39‰).

The consistency of the $\delta^{18}O$ values in the magmatic quartz material is also significant, with only one population of values being formed in each case which has a low standard deviation. Additionally, there is little difference between $\delta^{18}O$ values in the core and outer zones of the pegmatites. This suggests that the fluid responsible for magmatic quartz is from either a single source and that once crystallisation initiates, the pegmatites essentially represent a closed system with no fluid recharge, or, more likely (as fluid recharge is realistically necessary to maintain volume), a continuous flow of magmatic waters through the system via a mostly closed melt conduit. Values are essentially identical at Solås (potentially a result of the chemistry involved in the development of the cleavelandite zone), but at Steli, the core zone shows a lower $\delta^{18}O$ value than the outer zone. This may suggest an increasing involvement of non-magmatic fluids during crystallization of the central core, as alluded to by the geothermometry of **Chapter 4.5**. The hydrothermal quartz of the Landsverk 1 crystal, by comparison, shows various fluid signatures and therefore generations. This can be seen mathematically by the differing means of Table 4.7.1, but is clearer in Figs. 4.7.1 and 4.7.10.

In the base of the Landsverk 1 crystal, taken from the core of the crystal, two isotope signatures are clearly present; a meteoric phase with a mean $\delta^{18}O$ value of -8.39‰ which makes up the majority of the crystal, and a more magmatic phase with a mean $\delta^{18}O$ value of 3.69‰. Study of Fig. 5.2.8 (effectively a synthesis of the data presented in Fig. 4.7.10) suggests that this elevated $\delta^{18}O$ material is late stage, as it makes up the boundaries of the crystal, and may represent late fluids (initially magmatic in nature) which have subsequently interacted with ^{18}O depleted meteoric-hydrothermal fluids under subsolidus conditions (Hoefs, 1997).

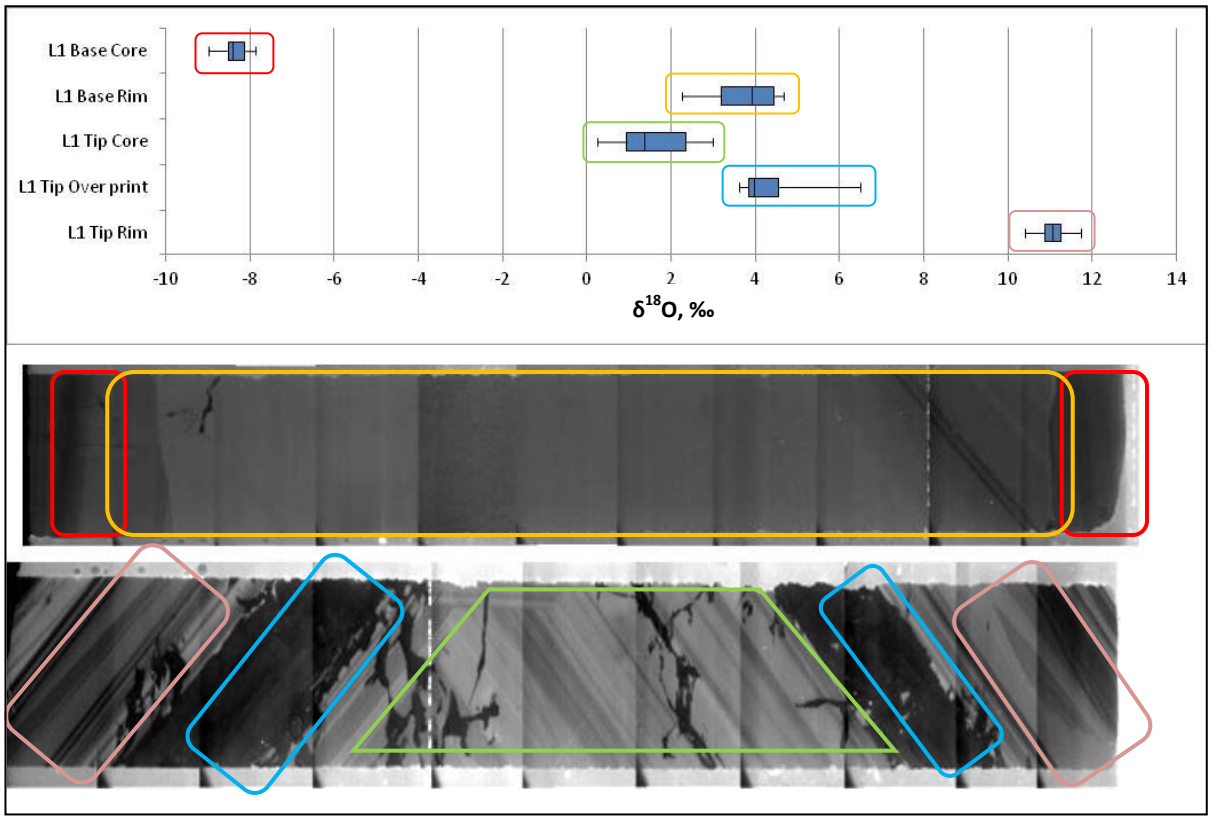

Fig. 5.2.8 Correlation of discrete $\delta^{18}O$ population values with particular CL domains

The tip of the crystal, which of course represents late stage crystallization and therefore fluid composition, again shows distinct $\delta^{18}O$-defined populations. These include a low $\delta^{18}O$ suite (mean $\delta^{18}O$ value of 1.55‰, and less than 3.00‰), which, upon comparison to CL imagery (Fig. 5.2.1), make up the centre of the tip, an elevated $\delta^{18}O$ suite (mean $\delta^{18}O$ value of 11.03‰) which makes up the periphery of the tip, and an intermediary $\delta^{18}O$ suite with a mean $\delta^{18}O$ value of 4.17‰. This material makes up a phase of extremely low luminosity which appears to overprint and indeed replace all other domains and must therefore represent the final generation of fluid influx. This progression indicates an initial meteoric-hydrothermal-magmatic fluid being superseded by a magmatic fluid, before finally being replaced by a mixed phase meteoric fluid. Indeed, this final phase is similar in $\delta^{18}O$ signature to the final phase of the quartz in the base of the Landsverk crystal; 4.17‰ (s.d. 0.51) and 3.69‰ (s.d. 0.92) respectively.

The analysis points which fall between O isotope populations (as plotted in Figs. 4.7.8 and 4.7.9) are not included in calculating the mean $\delta^{18}O$ values of the distinct suites, but are important to note as they may represent a transitional

fluid phase generated as initially hydrothermal-meteoric waters mix with more magmatic waters, increasing the positivity of the $\delta^{18}O$ signature.

5. 3 Synthesis

5.3.1 Formation of the Evje-Iveland pegmatites

From the lack of additional granitic phases, the lack of spatial control on pegmatite characteristics with distance from the granite (e.g. degree of fraction, geochemistry), the significant age discrepancy (70 Ma) between the Høvringsvatnet granites and the Evje-Iveland pegmatites and the possibility for the Evje-Iveland pegmatites to have formed by partial melting of country rock gneisses and metagabbros (hypotheses 1, 2 and 3 respectively), it is unlikely that the Evje-Iveland pegmatites represent evolved equivalents of the Høvringsvatnet granites.

Instead, an alternative model for the generation of the melts responsible for the Evje-Iveland pegmatites is proposed; partial melting of country rocks. This model is simple as the partial melting (as demonstrated at Iveland in Fig. 4.1.1) can be in situ; only a heat source is required. A potential candidate for this heat source is the large thermal gradient induced by the emplacement of the Rogaland Igneous Province. The formation model is summarised in Fig. 6.1.1. The primary event of the SNO (1140 – 900 Ma) was the Agder phase (1050 – 980 Ma), which caused tectonic imbrication of the Telemark, Bamble and Idefjord terranes and crustal thickening (Fig. 6.1.1a); continued thickening during the Falkenbeg phase (980 – 970 Ma) induced high grade metamorphism and magmatism in the lower crust (Bingen et al., 2008b); the Høvringsvatnet granite, dated by this study at approximately 983 Ma (Fig. 6.1.1b). Crustal thinning, underplating and/or crustal tongues occurred during the post-orogenic and extensional Dalane phase (970 – 900 Ma; Bingen et al., 2008b) forming the Rogaland Igneous Province (RIP), most notable for the Rogaland anorthosite-mangerite-charnockite (AMC) complex at approximately 930 Ma (Duchesne et al., 1999, Schärer et al., 1996); the heat source chronologically and spatially suitable to induce partial melting in Evje-Iveland country rocks which

demonstrate field evidence and a geochemical potential to produce the Evje-Iveland pegmatite field (Fig. 6.1.1c).

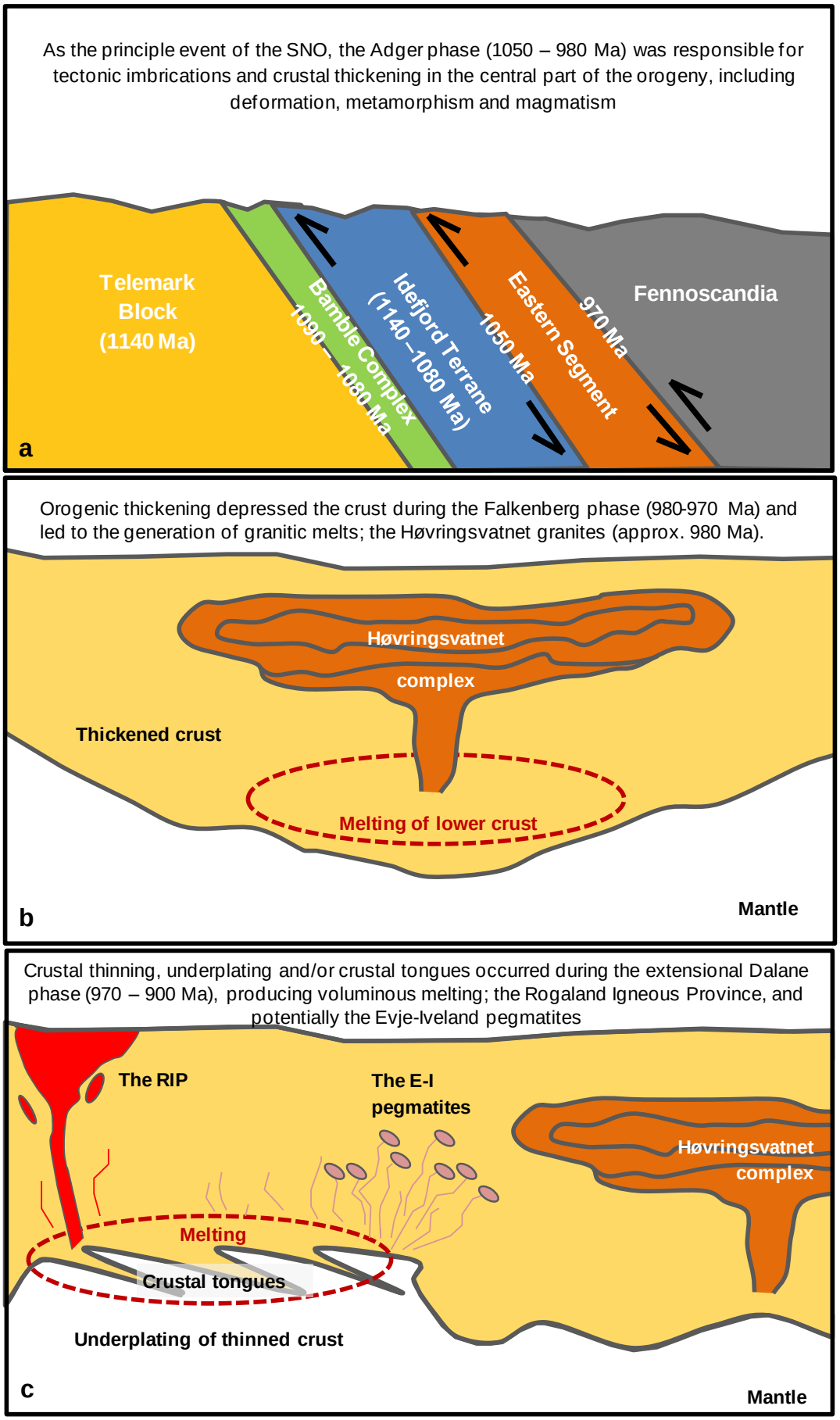

Fig. 6.1.1 Crustal evolution and potential formation mechanisms for the Evje-Iveland pegmatites (colour schemes after Fig. 2.1.3 and Bingen et al., 2008b)

5.3.2 Formation of HPQ in the Evje-Iveland pegmatites

The following synthesis of results will emphasise that there is little spatial or internal consistency in the trace element content of pegmatite quartz (hypothesis 4) whilst describing a mechanism for the formation of HPQ via secondary hydrothermal processes in pegmatites (Fig. 6.1.2; hypothesis 5).

The melts produced by anatexis of country rocks during the crustal thinning, underplating and tonguing (Fig. 6.1.1) underwent varying degrees of transport from the site of melting; limited at Iveland, as melting appears to have been in situ, and potentially significant elsewhere in the pegmatite field. The pegmatites are generally concordant with country rock metamorphic foliation and appear to have been plastically accommodated, there is no thermo-metamorphic aureole within the host and there is a lack of a chilled margin within the pegmatites, so there is likely a low temperature contrast between host rock and pegmatite melt. The pegmatites are intruded as lenses ranging in size from 10s of cm to 10s of m, and crystallisation initiates with a fine grained granitic border zone (Fig. 6.1.2a).Temperatures are likely in the region of 600° C (after TitaniQ (Wark and Watson, 2006)). The line rocks present at Li Gruva, ubiquitous USTs and the progressive occurrence of CZR are likely to indicate that volatiles are present in the system and that undercooling has occurred. This causes rapid crystallisation with limited nucleation opportunities, inducing internal zoning and the initiation of megacrystal growth (Fig. 6.1.2b).

Cooling continues as the lens crystallises inwards, to approximately 450° C in the core of the pegmatite. Opinions differ as to the water content of pegmatite melts. If low, the melt becomes too viscous (London, 2014) to maintain feeding the system (which also causes a reduction in temperature). If high, the melt becomes progressively water saturated (Thomas and Davidson, 2012) and therefore contains reduced mineral constituents to continue pegmatite crystallisation (note: the assemblage of hydrous minerals expected from a high water content is not present, and whole rock LOI is ~1%). Either way, as there is no evidence for collapse structures within the pegmatites, hydrostatic pressure must be preserved until crystallisation of the pegmatite is complete.

There is therefore an issue with volume within the pegmatite in the final stages of crystallisation as the melt vestiges alone cannot keep filling the space; the core cannot represent frozen almost-pure silica melts, as no such melts are known to exist in nature, possibly apart from transient silica gels (Williamson et al., 2002). Rather, Si bearing waters must be added to the system which maintain hydrostatic pressure and crystallise the final homogenous core component (significant increase in fluid inclusions in core quartz compared to marginal quartz; extensive CL variation in pegmatite quartz; lower crystallisation temperatures; apparent dominance of H^+ over Li^+). That pegmatite quartz displays consistent O-isotope signatures ($\delta^{18}O$ values of 8.5 to 9 ‰) suggests that this is generally magmatically derived water, likely produced during the partial melting episode responsible for the initial pegmatite melts. This late water is not incorporated into pegmatite minerals (the absence of sufficient hydrous minerals prohibit this), and, via crystal boundary migration, is likely expelled into the surrounding country rock, hydrating surrounding country rock minerals (Fig. 6.1.2b).

As there is apparently little control over either the composition of pegmatite melt source or the throughput of later waters, there is demonstrably little consistency in the trace element content of pegmatite quartz. This variation occurs between pegmatites and also within individual bodies, often at levels above the high purity threshold, which unfortunately makes the primary pegmatites of the Evje-Iveland field unsuitable as a source of HPQ.

However, as demonstrated by in situ beam techniques and CL imaging, HPQ is present in the Evje-Iveland field; the Landsverk 1 pegmatite has been subjected to a hydrothermal overprint, brecciating the primary pegmatite minerals, growing new hydrothermal quartz crystals and selectively recrystallising quartz to a higher purity (Fig. 6.1.2c). The event most likely involved a multistage injection of significantly cooler meteoric/metamorphic waters (3 distinct O-isotope signatures, typically lighter than the primary signature, relating to 3 different stages of crystal growth as defined by CL), potentially derived from retrograde metamorphism of country rocks during post-orogenic relaxation. A TitaniQ temperature (Wark and Watson, 2006) utilising 0 ppm Ti (i.e. the composition of

hydrothermal quartz from Landsverk 1) is 374°C; this is a realistic temperature (e.g. Michard, 1989). The overprinting event likely occurs later than initial pegmatite crystallisation and after significant cooling, under brittle rather than ductile conditions (as evidenced by the brecciation of primary pegmatite minerals, and the association with regular, subvertical and pyrite/epidote bearing feeder structures). This later hydrothermal event is the probable cause of the distinctly younger date produced for the Landsverk 1 pegmatite (Fig. 5.1.7). Several workers report that “fluid-aided alternation” (Williams et al., 2011) and “fluid-assisted recrystallisation” (Didier et al., 2013) of monazite may reset its age; in the case of Landsverk 1 by approximately 50 Ma.

As such, using the Evje-Iveland pegmatites as a proxy, it is proposed that HPQ in pegmatites is generated by secondary processes at the magmatic/hydrothermal transition i.e. an overprinting hydrothermal event, which may occur significantly after pegmatite crystallisation. The purification appears to be focussed along a particular zone within the quartz crystal (Fig. 4.6.9); whether this is a physical or chemical preference is uncertain. What is also unclear is whether the overprinting quartz is a replacement unit preferentially solubilising existing quartz, and therefore whether this overprint is hydrothermally derived or from internally remobilised quartz (consisting solely of silica and low levels of trace elements), or whether purification arises from solid state grain boundary migration whereby quartz with fewer defects replaces quartz with more defects. Müller et al. (2002b) refer to this process as neocrystallisation; deformation of the crystal lattice causing remobilisation of lattice defects (i.e. trace element) and purification of quartz. However, a distinct $\delta^{18}O$ value of the phase with lowest trace element concentrations perhaps favours an externally derived source of silica.

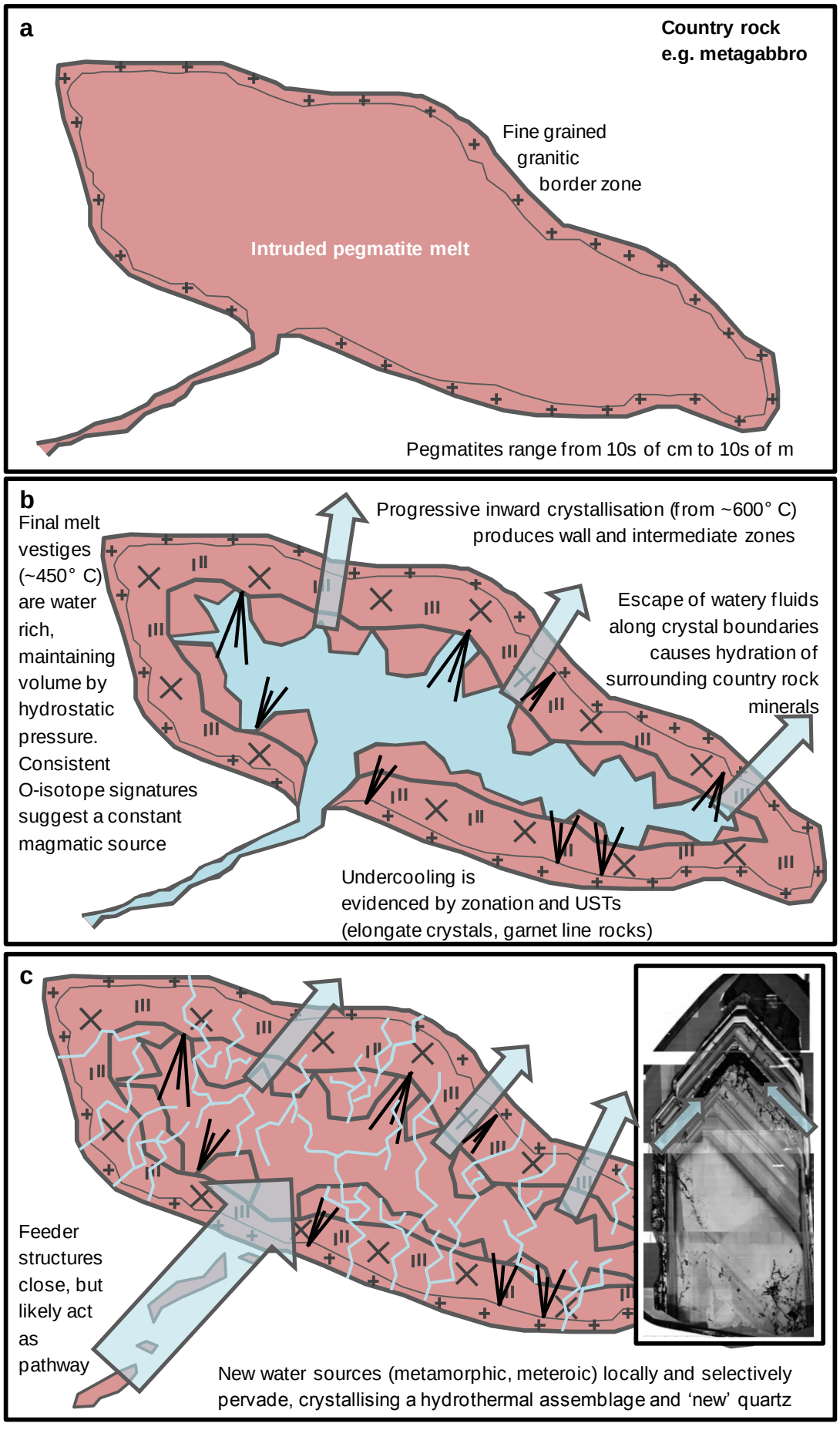

Fig. 6.1.2 Potential genetic model for a hypothetical HPQ bearing Evje-Iveland pegmatite

5.3.3 Implications for exploration tools

That the traditional genetic link between parental granite and pegmatite has been severed for the pegmatite field of Evje-Iveland expands exploration options for pegmatites not only as sources of quartz, but also for gems, feldspar, mica and 'critical' metals. It has been demonstrated that the Evje-Iveland pegmatites are more likely to have formed from partial melting of country rock, subsequently with variable degrees of transport, so exploration areas for pegmatite-hosted commodities (at least, as indicated by this study, HPQ) needn't be limited to regions around granitic plutons.

Additionally, based on the mechanisms of HPQ formation identified in the Evje-Iveland pegmatites, several suggestions may be made to facilitate the identification of potential HPQ resources once an area of interest has been defined. Exclusively amongst the pegmatites investigated, the structure of the Landsverk 1 pegmatite was disrupted and brecciated by the event likely responsible for the generation of HPQ. It would appear, therefore, that there is clear field evidence for the formation of hydrothermal, and possibly high purity, quartz in pegmatites. Selective sampling of replacement quartz and euhedral hydrothermal crystals is recommended, with the generation of representative thick sections.

SEM-CL imaging of quartz is a quick and readily available method of determining relative total trace element abundance prior to detailed compositional analysis. An exploration company must evaluate the relative merits of an O isotope SIMS campaign in characterising a quartz deposit. In the case of the Landsverk 1 pegmatite, quartz of the highest purity had a distinct O isotope signature (a mean $\delta^{18}O$ value of 4.17‰); potentially, 'high purity' quartz could be identified by this distinct isotopic signature. Actual compositional data for quartz is vital for deposit definition however, and therefore trace element determination by LA-ICP-MS, whilst costly both financially and in time, is inevitable. The exploration team must weigh up multiple factors (such as availability and suitability of analytical equipment; cost of analyses; process time) when deciding on the best method for characterising a potential deposit.

5.3.4 Assessment of techniques

Despite efforts to avoid shortcomings, naturally all investigations suffer from limitations in both approach and application of techniques. The following section discusses issues identified during the course of this study, and attempts to assess the degree of their impact.

The complex and micro-scale textures identified in quartz by CL techniques (*Chapters 4.6.1* and *4.6.2*) reveal a multi-stage evolution of hydrothermal quartz in pegmatites, with huge chemical variation. This has been encountered by previous workers (e.g. Tanner et al., 2013). These deviations in quartz characteristics lead to difficulties in the spatial reconciliation of CL domains with ablation (and hence analyses) points, as the laser could only be aimed with an optical camera, through which the quartz appeared entirely homogenous. This was a fairly serious factor, as revealing phase relationships (such as the apparently preferential overprinting of a previously bright phase by a subsequent dark phase illustrated in Fig. 4.6.9) could not be interrogated. Indeed, the relationship between O isotope signature and CL domain was so clearly constrained as a result of a thorough and systematic, rather than targeted, analytical approach.

The 2006 method of TitaniQ (Wark and Watson) as an estimation of temperature of crystallisation in quartz has been both updated by more recent Ti-in-quartz geothermometry techniques (e.g. Thomas et al., 2010) and reassessed by Huang and Audétat (2012). These new techniques, whilst no doubt an improvement on the original work, include pressure as a variable, for which no independent assessment can be made for the Evje-Iveland pegmatites. Wark and Watson's 2006 method is calibrated at 10 kbar which is not unreasonable for the regime (amphibolite facies metamorphism is ubiquitous in the Evje-Iveland region), and as pressure cannot be constrained, seems a viable starting point for indicative thermometry, producing realistic temperatures consistent between pegmatites (e.g. Colombo et al. (2012) cite crystallisation temperatures of 522° C). Indeed, the technique has been utilised as recently as 2013 (by Vasyukuva et al. and Hoffman et al.). Al-geothermometry in quartz (e.g. Dennen et al., 1970) is already fraught with

greater difficulties than TitaniQ, as more variables control the uptake of Al in quartz (e.g., fluid/melt chemistry, temperature, growth rates and pH; Botis and Pan, 2009). It must be noted that Huang and Audétat (2012) report Ti correlates with Al and Li in studied quartz; this is not the case for quartz of the Evje-Iveland pegmatites (Figs. 5.2.1 and 5.2.2), which may indicate limitations even in recent refinements.

Issues with the representability of bulk pegmatite composition from fine grained border zones has been discussed previously (*Chapter 5.1.3*). Due to the likely small thermal contrast between country rock and pegmatite, the border zones are unlikely to represent a chilled margin. However, it does represent the first crystallised portion of the pegmatite melt, and as such (short of sampling tonnes of pegmatite) is the best estimation of whole rock pegmatite available.

Finally, it is considered how representative the hydrothermal quartz crystal taken from a vug in the Landsverk 1 pegmatite is of large scale processes, and how accurately its chemistry represents the mineralising fluid. The author regrets that more hydrothermal material was not investigated, but time was a major limitation in the scope of the project, and curtailed the possibility of extensive CL-SEM, LA-ICP-MS and O isotope campaigns. The processes identified in the Landsverk 1 crystal are undeniably present, and the mechanisms proposed in *Chapter 5.3.2* may be useful to inform future investigations.

6. CONCLUSIONS

6.1 Thesis Summary

The formation mechanisms of HPQ in pegmatites is currently poorly constrained. The purpose of this study was to determine the source and evolution of the Evje-Iveland pegmatites (whether they represent evolved equivalents of the Høvringsvatnet granites or the products of low degrees of partial melting of local country rocks) and the controls on pegmatitic quartz purity to inform exploration procedures for this burgeoning commodity.

It is demonstrated that there is no spatial control on pegmatite characteristics (neither degree of fractionation nor quartz chemistry) with distance from the Høvringsvatnet granite. Additionally, it is shown that there is a significant (70 Ma) chronological inconsistency between the granites (982.9±3.9 to 979.7±3.8 Ma) and the Evje-Iveland pegmatites (e.g. 910.5±1.6 Ma). The absence of granitic phases aside from the Høvringsvatnet granites and the pegmatites suggests the granite is not extensive at depth. There is clear field evidence of in situ partial melting of country rocks occurring at Iveland, and that this melt material contributed directly to the pegmatites. Using the country rock at Iveland as a source, geochemical modelling demonstrates that it is possible to generate a theoretical melt comparable in composition to that of each of the pegmatites studied purely by partial melting. It is proposed that, rather than representing a highly evolved component of the Høvringsvatnet granite, the Evje-Iveland pegmatites were instead formed by late-Sveconorwegian partial melting of local country rock at depth, induced by the crustal thinning/underplating/crustal tongue model proposed to induce melts which ultimately formed the nearby Rogalnd Igneous Province.

Quartz geochemistry demonstrates that there is little consistency in trace element content either within individual pegmatites or between different pegmatite bodies, which makes the Evje-Iveland field unsuitable as a potential source of high purity primary quartz. However, certain pegmatites contain brecciated feldspar and replacement quartz, interpreted to be of ‘hydrothermal’ origin. From LA-ICP-MS analyses, hydrothermal quartz generally shows trace element contents below 50 ppm, so may classify as HPQ despite elevated Al

and Li with respect to magmatic quartz. The absence of Ti is likely indicative of a relatively low temperature of formation. Specific quartz domains identified by SEM-CL are characterised by specific $\delta^{18}O$ signatures; magmatic quartz shows $\delta^{18}O$ of 8 to 9‰, typical of granite quartz, whereas late stage, low trace element zones in hydrothermal quartz show $\delta^{18}O$ values -8 to 11‰, from variably meteoric and magmatic fluids. As such, it is proposed that HPQ in the Evje-Iveland pegmatites was generated by secondary processes involving relatively low temperature, externally derived hydrothermal fluids, rather than as a result of the formation of the pegmatite bodies themselves.

It has been demonstrated that an associated granite is not necessary for the generation of pegmatites, so exploration areas for pegmatite-hosted HPQ (and, indeed, other commodities) needn't be limited to regions around plutons. Exploration may be facilitated by field observations of pervasive hydrothermal events, and the occurrence of HPQ documented by a combination of CL-SEM imaging, O isotope campaigns and LA-ICP-MS analyses.

6.2 Recommendations for future studies: progress beyond the state-of-the-art

Having identified limitations present in this study, several avenues of further investigation are recommended, which go some way to address the issues identified in *Chapter 5.3.3*.

To attempt to resolve the issues of ablation positioning in quartz domains identified under CL, a CL bolt on viewer for the laser ablation apparatus would allow accurately defined in situ point analyses for quartz of particular interest, allowing interrogation of specific CL domains for their related chemistry, and by inference the mineralising fluid. This would facilitate characterisation of the various fluid phases, the nature of the preferential quartz replacement and the potential linking of components of the hydrothermal assemblage at Landsverk 1 with CL phases based on their chemistry. However, even with the newly provided excellent spatial resolution, given the scale of the variations of some of these quartz zones (10s of µms), the size of ablation craters (75 µm) and the

trace nature of the elements within the quartz, material sufficient in volume for elements to be detected perhaps could not be obtained.

Constraints on the pressure of the pegmatite system would allow for a ratification of the TitaniQ geothermometry. Numerous equilbria exchange thermometers and barometers exist from which to estimate temperature and pressure from pairs of minerals typically involving garnet and another (e.g. hornblende, clinopyroxene, feldspar+mica) as summarised by Spear (1993). However, these are typically designed to provide PT estimations for peak metamorphism in metamorphic rocks, which is unsuitable for the Evje-Iveland pegmatites as they form some 100 Ma after metamorphism. The minerals themselves may not even be compositionally suitable for this method, as London (2014) reports that the compositions of garnet and biotite in pegmatites "tend to deviate substantially from the calibrated values for Fe-Mg exchange". Several authors (e.g. Morgan and London, 1999; London et al., 2012) have made use of the ternary feldspar system (Ab-An-Or) to estimate crystallisation temperatures in the pegmatites, and this would require extensive electron microprobe analyses of phase proportions.

Rather, a detailed fluid inclusion investigation would be preferred in order to assess trapping temperatures in order to corroborate the geothermometry summarised in **Chapter 4.5**. Additionally, laser analyses of fluid inclusions could be used to assess the composition of the mineralising fluid (e.g. Günter et al., 1998; Seydoux, pers. comm.), which, when combined with CL domaining, improved spatial control over in situ trace element analyses and O isotope studies, would allow near-complete characterisation of the fluids responsible for the formation of HPQ in pegmatites.

As described in **Chapter 4.8**, difficulties arose in accurately dating the pegmatite zircons using U-Pb; a robust technique usually, but not when the material is metamict. Other studies have successfully acquired U-Pb ages from whole rock (Jercinovic et al., 2008) and from monazites (e.g. Seydoux-Guillame et al., 2002) of which there are plenty in the pegmatites; Seydoux-Guillame et al. (2013) even investigated material from Evje-Iveland. This would assist in

discovering whether the anatexis observed at Iveland represents a single continuous melting episode or progressive melting with multiple emplacement events.

REFERENCES

http://acmelab.com/pdfs/Acme_Price_Brochure.pdf AcmeLabs, price brochure. Accessed September 2012.

ADACHI, T., HOKADA, T., OSANAI, Y., TOYOSHIMA, T., BABA, S. & NAKANO, N. 2010. Titanium behaviour in quartz during retrograde hydration: Occurrence of rutile exsolution and implications for metamorphic processes in the Sør Rondane Mountains, East Antartica. *Polar Science*, **3**, 222-234.

AGOMOR, A.K., GORDIYENKO, V.V. & LAZERENKOV, V.G. 1987. Regional mineralogical and geochemical zoning of a pegmatite field in southern Ghana. *International Geology Review*, **29**, 151-159.

ANDERSEN, M. 2001. The genesis and crystallisation of RE pegmatites from Evje-Iveland pegmatite field, South Norway. *M.Sc. thesis*, *Copenhagen University*.

ANDERSEN, T. & MUNZ, I.A. 1995. Radiogenic whole-rock lead in Precambrian metasedimentary gneisses from South Norway: evidence of Sveconorwegian LILE mobility. *Norsk Geologisk Tidsskrift*, **75**, 156-168.

ANDERSEN, T., ANDRESEN, A. & SYLVESTER, A.G. 2002. Timing of late- to post-tectonic Sveconorwegian granitic magmatism in South Norway. *NGU-Bull*, **440**, 5-18.

ANDERSEN, T., GRIFFIN, W.L., JACKSON, S.E., KNUDSEN, T.L. & PEARSON, N.J. 2004a. Mid-Proterozoic magmatic arc evolution at the southwest margin of the Baltic shield. *Lithos*, **73**, 289-318.

ANDERSEN, T., LAAJOKI, K. & SAEED, A. 2004b. Age, provenance and tectonostratigraphic status of the Mesoproterozoic Blefjell quartzite, Telemark sector, southern Norway. *Precambrian Research*, **135**, 217-244.

ANDERSEN, T., GRIFFIN, W.L. & SYLVESTER, A.G. 2007. Sveconorwegian crustal underplating in southwestern Fennoscandia: LAM-ICPMS U-Pb and Lu-Hf isotope evidence from granites and gneisses in Telemark, southern Norway. *Lithos*, **93**, 273-287.

ANDERSON, E.M. 1936. The dynamics of the formation of cone-sheets, ring-dykes and cauldron subsidence. *Proceedings of the Royal Society of Edinburgh*, **56**, 128-157.

ANDERSSON, M., LIE, J.E. & HUSEBYE, E.S. 1996. Tectonice setting of post-orogenic granites within SW Fennoscandia based on deep seismic and gravity data. *Terra Nova*, **8**, 558-566.

ANDRÉASSON, P.G. & RODHE, A. 1994: Ductile and brittle deformation within the Protogine Zone, southern Sweden: a discussion. *Geologiska Föreningens i Stockholm Förhandlingar*, **116**, 115-117.

http://www.arcgis.com/home/webmap/viewer.html?useExisting=1 ArcGIS, My Map. Accessed March 2012

ARTH, J.G. 1976. Behaviour of trace elements during magmatic process – a summary of theoretical models and their applications. *J. Res. U.S. Geol. Surv*., **4**, 41-47.

ARZI, A.A. 1978. Critical phenomena in the rheology of partially melted rocks. *Tectonophysics,* **44**, 173-178.

BARTH, T.F.W. 1947: The nickeliferous Iveland-Evje amphibolite and its relation. *Norges Geologiske Undersøkelse*, **168**, 71 pp.

BEURLEN, H., MÜLLER, A, SILVA, D. & DA SILVA, M.R.R. 2011. Petrogenetic significance of LA-ICP-MS trace-element data on quartz from the Borborema Pegmatite Province, northeast Brazil. *Mineralogical Magazine*, **75**, 2703-2719.

BINGEN, B. 1998. Geochemistry of Sveconorwegian augen gneisses from SW Norway at the amphibolite-granulite facies transition. *Norwegian Journal of Geology*, **69**, 177-189.

BINGEN, B., BIRKELAND, A., NORDGULEN, Ø. & SIGMOND, E.M.O. 2001. Correlation of supracrustal sequences and origin of terranes in the Sveconorwegian orogen of SW Scandinavia: SIMS data on zircon in clastic metasediments. *Precambrian Research*, **108**, 293-318.

BINGEN, B., SKÅR, Ø., MARKER, M., SIGMOND, E.M.O., NORDGULEN, Ø., RAGNHILDSTVEIT, J., MANSFELD, J., TUCKER, R.D. & LIÉGEOIS, J-P. 2005. Timing of continental building in the Sveconorwegian orogen, SW Scandinavia. *Norwegian Journal of Geology*, **85**, 87-116.

BINGEN, B., STEIN, H.J., BOGAERTS, M., BOLLE, O. & MANSFELD, J. 2006. Molybdenite Re-Os dating constrains gravitational collapse of the Sveconorwegian orogen, SW Scandinavia. *Lithos*, **87**, 328-346.

BINGEN, B., DAVIS, W.J., HAMILTON, M.A., ENGVIK, A.K., STEIN, H.J., SKÅR, Ø. & NORDGULEN, Ø. 2008a. Geochronology of high-grade metamorphism in the Sveconorwegian belt, S. Norway: U-Pb, Th-Pb and Re-Os data. *Norwegian Journal of Geology*, **88**, 13-42.

BINGEN, B., NORDGULEN, Ø. & VIOLA, G. 2008b. A four-phase model for the Sveconorwegian orogeny, SW Scandinavia. *Norwegian Journal of Geology*, **88**, 43-72.

BINGEN, B. & VAN BREMEN, O. 1998. Tectonic regimes and terrane boundaries in the high-grade Sveconorwegian belt of SW Norway, inferred from U-Pb zircon geochronology and geochemical signature of augen gneiss suites. *Journal of the Geological Society, London*, **155**, 143-154.

BJØRLYKKE, H. 1935. The mineral paragenesis and classification of the granite pegmatites of Iveland, Setesdal, southern Norway. *Norsk Geologisk Tidsskrift*, **14**, 211-310.

BJØRLYKKE, H. 1937. The granite pegmatites of Southern Norway. *Journal of the Mineralogical Society of America*, **22**, 241-255.

BOOS, M.F. 1954. Genesis of Precambrian granitic pegmatites in the Denver Mountain Parks Area, Colorado. *Bulletin of the Geological Society of America*, **65**, 115-142.

BOTIS, S., NOKHRIN, S.M., PAN, Y., XU, Y. & BONLI, T. 2005. Natural radiation-induced damage in quartz. I. Correlations between cathodoluminescence colours and paramagnetic effects. *Canadian Mineralogist*, **43**, 1565-1580.

BOTIS, S & PAN, Y. 2009. Theoretical calculation of $[AlO_4/M^+]^0$ defects in quartz and crystal-chemical controls on the uptake of Al. *Mineralogical Magazine*, **73**, 537-550.

BOUDIN A. & DEUTSCH S. 1970. Geochronology: Recent Development in the Lutetium-176/Hafnium-176 Dating Method. *Science*, **168**, 1219-1220.

BRICKWOOD, J.D. 1986. The geology and mineralogy of some Fe-Cu-Ni sulphide deposits in the Bamble area, Norway. *Norsk Geologisk Tidsskrift*, 66, 189–208.

BROOKS, C.K., HENDERSON, P. & RONSBO, J.G. 1981. Rare earth element partitioning between allanite and glass in the obsidian of Sandy Braes, northern Ireland. *Mineralogical Magazine*, **44**, 157-160.

BRUECKNER, H.K. 2009. Subduction of continental crust, the origin of post-orogenic granitoids (and anothosites?) and the evolution of Fennoscandia. *Journal of the Geological Society*, **166**, 753-762.

BUDDINGTON, A.F. 1959. Granite emplacement with special reference to North America. *Geological Society America Bulletin*, **70**, 671-747.

BUSHEV, A.G. & KOPLUS, A.V. 1980. Rare-earth pegmatites of the granulite facies of metamorphism. *International Geology Review*, **22**, 221-232.

CAMERON, E.N., JAHNS, R.H., MCNAIR, A.H. & PAGE, L.R. 1949. *Internal structure of grantic pegmatites*. Economic Geology Monograph 2, pp.115.

ČERNÝ, P.T. 1991a. Fertile granites of Precambrian rare-element pegmatite fields: is geochemistry controlled by tectonic setting or source lithologies? *Precambrian Research*, **51**, 429-468.

ČERNÝ, P.T. 1991b. Rare-element Granitic Pegmatites. Part 1: Anatomy and Internal Evolution of Pegmatite Deposits. *Geoscience Canada*, **18**, 49-67.

ČERNÝ, P.T. & ERCIT, T.S. 2005. The classification of granitic pegmatites revisited. *The Canadian Mineralogist*, **43**, 2005-2026.

ČERNÝ, P.T., LONDON, D. & NOVÁK, M. 2012. Granitic Pegmatites as Reflections of Their Sources. *Elements*, **8**, 289-294.

CHAPPEL, B.W. & WHITE, A.J.R. 1974. Two contrasting granite types. *Pacific Geology*, **8**, 173-174.

CHAPPEL, B.W. & WHITE, A.J.R. 2001. Two contrasting granite types: 25 years later. *Australian Journal of Earth Sciences*, **48**, 489-499.

CLEMENS, J.D. & VIELZEUF, D. 1987. Constraints on melting and magma production in the crust. *Earth and Planetary Science Letters,* **86**, 287-306.

COLOMBO, F., SFRAGULLA, J. & GONZÁLES DEL TÁNAGO, J. 2012. The garnet-phosphate buffer in peraluminous granitic magmas: a case study from

pegmatites of the Pocho District, Córdoba, Argentina. *Canadian Mineralogist*, **50**, 1555-1571.

COSCA, M.A., MEZGER, K. & ESSENE, E.J. 1998. The Baltica-Laurentia connection: Sveconorwegian (Grenvillian) metamorphism, cooling, and unroofing in the Bamble Sector, Norway. *The Journal of Geology*, **106**, 539-552.

DEER, W.A., HOWIE, R.A. & ZUSSMAN, J. 1966. *An introduction to the rock-forming minerals*. Longman, London, pp. 528.

DENNEN, W., BLACKBURN, W. & QUESADA, A. 1970. Aluminium in quartz as a geothermometer. *Contributions to Mineralogy and Petrology*, **27**, 332-342.

DIDIER, A., BOSSE, V., BOULVAIS, P., BOULOTON, J., PAQUETTE, J.-L., MONTEL, J.-M. & DEVIDAL, J.-L. 2013. Disturbamce versus preservation of U-Th-Pb ages in monazite during fluid-rock interaction: textural, chemical and isotopic in situ study in microgranites (Velay Dome, France). *Contributions to Mineralogy and Petrology*, **165**, 1051-1072.

DUCHESNE, J.C., LIEGEOIS, J.P.M VANDER AUWERA, J. & LONGHI, J. 1999. The crustal tongue melting model and the origin of massive anorthosites. *Terra Nova*, **11**, 100-105.

http://www.earth-policy.org/indicators/c47 Earth Policy Institute 2013. With 1995-1999 data from Worldwatch Institute, Signposts 2004, CD-ROM (Washington, DC: 2005); 2000 data from Prometheus Institute, "23rd Annual Data Collection - Final," PVNews, vol. 26, no. 4 (April 2007), pp. 8-9; 2001-2006 from Prometheus Institute and Greentech Media, "25th Annual Data Collection Results: PV Production Explodes in 2008," PVNews, vol. 28, no. 4 (April 2009), pp. 15-18; 2007-2012 based on Shyam Mehta, GTM Research, e-mail to J. Matthew Roney, EPI, 30 July 2013. Accessed September 2013.

EBBING, J., AFEWORK, Y., OLESEN, O. & NORDGULEN, Ø. 2005. Is there evidence for magmatic underplating beneath the Oslo rift? *Terra Nova*, **17**, 129-134.

ERCIT, T.S. 2005. *REE-enriched granitic pegmatites*. In Rare-Element Geochemistry and Mineral Deposits (R.L. Linnen & I.M. Samson, eds.). Geologocal Association of Canada, Short Course Notes 17, 175-199.

FOUGHT, H. 1993. Geological descriptions of pegmatites in the Einerkilen-Ånestølkilen area, South Norway (in Dansih). Unpublished MSc thesis, University of Copenhagen.

FROST, B.R., BARNES, C.G., COLLINS, W.J., ARCULUS, R.J., ELLIS, D.J. & FROST, C.D. 2001. A geochemical classification for granitic rocks. *Journal of Petrology*, **42**, 2033-2048.

FUJIMAKI, H. 1986. Partition coefficients of Hf, Zr, and REE between zircon, apatite and liquid. *Contributions to Mineralogy and Petrology*, **94**, 42-45.

GELLEIN, J. 2007. Gravimetrisk residualkart, Mandel, Målestokk, 1:250,000. Norges Geologiske Undersøkelse.

http://georem.mpch-mainz.gwdg.de/ Accessed February 2012.

GINSBURG, A.I., TIMOFEYEV, I.N. & FELDMANN, L.G. 1979. *Principles of geology of the granitic pegmatites*, Moscow, Nedra, pp. 296.

GLOVER, A.S, ROGERS, W.Z. & BARTON, J.E. 2012. Granitic Pegmatites: Storehouses of Industrial Minerals. *Elements*, **8**, 269-273.

GÖTZE, J. 2009. Chemistry, textures and physical properties of quartz – geological interpretation and technical application. *Mineralogical Magazine*, **73**, 645-671.

GÖTZE, J., PLOTZE, M., GRAUPNER, T., HALLBAUER, D.K. & BRAY, C. 2004. Trace element incorporation into quartz: a combined study by ICP-MS, electron spin resonance, cathodoluminescence, capillary ion analysis and gas chromatography. *Geochemica et Cosmochimica Acta*, **68**, 3741-3759.

GÖTZE, J., PLÖTZE, M., TRAUTMANN, T. 2005. Structure and luminescence characteristics of quartz from pegmatites. *American Mineralogist*, **90**, 13-21.

GÜNTER, D., AUDÉTAT, A., FRISCHKNECHT, R. & HEINRICH, C.A. 1998. Quantitative analysis of major, minor and trace elements in fluid inclusions using laser ablation– inductively coupled plasma mass spectrometry. *Journal of Analytical Atomic Spectrometry*, **13**, 263-270.

GREW, E.S., YATES, M.G., BARBIER, J., SHEARER, C.K., SHERATON, J.W., SHIRAISHI, K. & MOTOYOSHI, Y. 2000. Granulite- facies beryllium pegmatites in the Napier Complex in Khmara and Amundsen bays, western Enderby Land, East Antarctica. *Polar Geoscience*, **13**, 1-40.

HARBEN, P.W. 2002. *The industrial mineral handybook – a guide to markets, specifications and prices*. 4th edition, Industrial Mineral Information, Worcester Park, United Kingdom, pp. 412.

HARLOV, D.E. 2000. Pressure-temperature estimation in orthopyroxene-garnet bearing granulite facies rocks, Bamble Sector, Norway. *Mineralogy and Petrology*, **69**, 11-33.

HEAMAN, L.M. & SMALLEY, P.C. 1994. A U–Pb study of the Morkheia complex and associated gneisses, southern Norway—implications for disturbed Rb–Sr systems and for the temporal evolution of Mesoproterozoic magmatism in Laurentia. *Geochimica et Cosmochimica Acta*, **58**, 1899-1911.

HELLSTRÖM, F.A., JOHANSSON, Å. & LARSON, S.Å. 2004: Age emplacement of late Sveconorwegian monzogabbroic dykes, SW Sweden. *Precambrian Research*, **128**, 39-55.

HENDERSON, I.H.C. & IHLEN, P.M. 2004. Emplacement of polygeneration pegmatites in relation to Sveco-Norwegian contractional tectonics: examples from southern Norway. *Precambrian Research*, **133**, 207-222.

HOEFS, J. 1997. *Stable Isotope Geochemistry, 4th ed*. Springer-Verlay, Berlin, Heidelberg, New York, pp. 199.

HOFMANN, A.E., BAKER, M.B. & EILER, J.M. 2013. An experimental study of Ti and Zr partitioning among zircon, rutile, and granitic melt. *Contributions to Mineralogy and Petrology,* **166**, 235–253.

HÖGDAHL, K., ANDERSSON, U.B. & EKLUND, O. 2004. The Transcandinavian Igneous Belt (TIB) in Sweden: a review of its character and evolution. *Geological Survey of Finland, Special Paper*, **37**, 123 pp.

HÖNIG, S., LEICHMANN, J. & NOVÁK, N. 2010. Unidirectional solidification textures and garnet layering in Y-enriched garnet-bearing aplite-pegmatites in the Cadomian Brno Batholiht, Czech Republic. *Journal of Geosciences*, **55**, 113-129.

HUANG, R. & AUDÉTAT, A. 2013. The titanium-in-quartz (TitaniQ) thermobarometer: A critical examination and re-calibration. *Geochimica et Cosmochimica Acta*, **84**, 75-89.

HUT, G. 1987. *Stable isotope reference samples for geochemical and hydrological investigations* (Rep. Consultants Group Meeting, Vienna, 1985). International Atomic Energy Agency, Vienna, 1-42.

http://www.infomine.com/commodities/ Accessed December 2011

IRVING, A.J. & FREY, F.A. 1978. Distribution of trace elements between garnet megacrysts and host volcanic liquids of kimberlitic to rhyolitic composition. *Geochimica et Cosmochimica Acta*, **42**, 771-787.

JAHNS, R.H. & TUTTLE, O.F. 1963. Layered pegmatite-aplite intrusives. *Mineralogical Society of America Special Paper*, **1**, 78-92.

JAHNS, R.H. & BURNHAM, C.W. 1969. Experimental studies of pegmatite genesis: I. A model for the derivation and crystallisation of granitic pegmatites. *Economic Geology*, **64**, 843-864.

JANSEN, J.B.H., BLOK, R.J., BOS, A. & SCHEELINGS, M. 1985: Geothermometry and geobarometry in Rogaland and preliminary results from the Bamble area, S Norway. *In:* Tobi, A.C. & Touret, J.L. (eds.), *The deep Proterozoic crust in the north Atlantic provinces, NATO Adv. Sci. Inst. Ser*., Reidel, Dordrecht, C158, 499-516.

JERCINOVIC, M.J., WILLIAMS, M.L & LANE, E.D. 2008. In-situ trace element analysis of monazite and other fine-grained accessory minerals by EPMA. *Chemical Geology*, **254**, 197-215.

JOHANSSON, E. & WOLD, S. 1984. Minimising Effects of Closure on Analytical Data. *Analytical Chemistry*, **56**, 1685-1688.

JOLLIFF, B.L., PAPIKE, J.J. & SHEARER, C.K. 1992. Petrogenetic relationships between pegmatite and granite based on geochemistry of muscovite in pegmatite wall zones, Black Hills, South Dakota, USA. *Geochimica et Cosmochimica Acta*, **56**, 1915-1939.

JUNG, L. (ed.) 1992: *High-purity natural quartz. Part 1: High-purity natural quartz for industrial use*. Library of Congress-in-Publication Data, New Jersey, pp. 538.

KNUDSEN, T.-L. & ANDERSEN, T. 1999. Petrology and geochemistry of the Tromøy gneiss complex, South Norway, an alleged example of Proterozoic depleted lower continental crust. *Journal of Petrology*, **40**, 909-933.

KNUDSEN, T.-L., ANDERSEN, T., WHITEHOUSE, M.J. & VESTIN, J. 1997: Detrital zircon ages from Southern Norway – implications for the Proterozoic evolution of the southwestern Baltic Shield. *Contributions to Mineralogy and Petrology,* **130**, 47–58.

KULLERUD, L. & DAHLGREN, S.H. 1993. Sm-Nd geochronology of Sveconorwegian granulite facies mineral assemblages in the Bamble shear belt, south Norway. *Precambrian Research*, **64**, 389-402.

LANDES, K.K. 1933. Origin and classification of pegmatites. *American Mineralogist*, **18**, 33-103.

LARSEN, R.B. 2002. The distribution of rare-earth elements in K-feldspar as an indicator of petrogenetic processes in granitic pegmatites: examples form two pegmatite fields in southern Norway. *The Canadian Mineralogist*, **40**, 137-151.

LARSEN, R.B., POLVÈ, M. & JUVE, G. 2000. Granite pegmatite quartz from Evje-Iveland: trace element chemistry and implications for the formation of high-purity quartz. *NGU-Bull*, **436**, 57-65.

LARSEN, R.B., HENDERSON, I., IHLEN, P.M. & JACAMON, J. 2004. Distribution and petrogenetic behaviour of trace elements in granitic pegmatite quartz from South Norway. *Contributions to Mineralogy and Petrology*, **147**, 615-628.

LONDON, D. (2005a). Geochemistry of alkali and alkaline earth elements in ore-forming granites, pegmatites, and rhyolites, *In:* Linnen, R.L. and

Sampson, I.M. (eds.), *Rare-Element Geochemistry and Mineral Deposits,* GAC Short Course Notes 17, p. 175-199.

LONDON, D. (2005b). Granitic pegmatites: an assessment of current concepts and directions for the future. Lithos, **80**, 281-303.

LONDON, D. 2008. *Pegmatites*, The Canadian Mineralogist, Special Publication 10, Quebec, pp. 347.

LONDON, D. 2009. The origin of primary textures in granitic pegmatites. *The Canadian Mineralogist*, **47**, 697-724.

LONDON, D. 2011. Competing models for the internal evolution of granitic pegmatites. Contribution sot the 5th International Symposium on granitic pegmatites. Asociación Geológica Argentina, Serie D, Publicación Especial, **14**, 131-133.

LONDON, D. 2014. A petrologic assessment of internal zonation in granitic pegmatites. *Lithos*, **184-187**, 74-104.

LONDON, D. & KONTAK, D.J. 2012. Granitic Pegmatites: Scientific wonders and economic bonanzas. *Elements*, **8**, 257-261.

LONDON, D. & MORGAN, G.B. VI. 2012. The Pegmatite Puzzle. *Elements*, **8**, 263-268.

LONDON, D., MORGAN, G.B. VI & ACOSTA-VIGIL, A. 2012. Experimental simulations of anatexis and assimilation involving metapelite and granitic melt. *Lithos*, **153**, 292-307.

MAHOOD, G. & HILDRETH, W. 1983. Large partition coefficients for trace elements in high-silica rhyolites, *Geochim. Cosmochim. Acta*, **47**, 11-30.

MALLÓ, A., FONTAN, F., MELGAREJO, J.C. & MATA, J.M. (1995). The Albera zoned pegmatite field, Eastern Pyrenees, France. Mineralogy and Petrology, 55, 103-116.

MARTIN, R.F. & DE VITO, C. 2005. The patterns of enrichment in felsic pegmatites ultimately depend on tectonic setting. *The Canadian Mineralogist*, **43**, 2027-2048.

MARTIN, R.F., DE VITO, C. & PEZZOTTA, F. 2008. Why is amazonitic K-feldspar an earmark of NYF-type granitic pegmatites? Clues from hybrid pegmatites in Madagascar. *American Mineralogist*, **93**, 263-269.

MCDONOUGH, W.F. & SUN, S.-S. 1995. The composition of the Earth. *Chemical Geology*, **120**, 223-253.

MICHARD, A. 1989. Rare earth element systematics in hydrothermal fluids. *Geochimica et Cosmochimica Acta*, **53**, 745-750.

http://www.mineweb.com/mineweb/view/mineweb/en/page72068?oid=120555&sn=Detail Accessed February 2011.

MÖLLER, C., ANDERSSON, J., LUNDQVIST, I. & HELLSTRÖM, F.A. 2007. Linking deformation, migmatite formation and zircon U-Pb geochronology in polymetamorphic gneisses, Sveconorwegian province, Sweden. *Journal of Metamorphic Geology*, **25**, 727-750.

MÜLLER, A. Personal communication, 2011.

MÜLLER, A., KRONZ, A. & BREITER, K. 2002a. Trace elements and growth patterns in quartz: a fingerprint of the evolution of the subvolcanic Podlesí Granite System (Krušné hory Mts., Czech Republic). *Bulletin of the Czech Geological Survey*, **77**, 135-145.

MÜLLER, A., LENNOX, P. & TRZEBSKI, R. 2002b. Cathodoluminescence and micro-structural evidence for crystallisaiton and defremation preocess of grnaites in the Eastern Lachlan Fold Belt (SE Australia). *Contributions to Mineralogy and Petrology*, **143**, 510-524.

MÜLLER A. & IHLEN P.M. 2011. Trace elements of pegmatitic quartz and their regional distribution in two pegmatite fields of southern Norway. *10th International congress for Applied Mineralogy, abstract proceedings*, pp.7.

MÜLLER A., IHLEN P.M., WANVIK J.E. & FLEM B. 2007. High-purity quartz mineralisation in kyanite quartzites, Norway. *Mineralium Deposita*, **4**, 523-535.

MÜLLER, A., IHLEN, P.M. & KRONZ, A. 2008. Quartz chemistry in polygeneration Sveconorwegian pegmatites, Froland, Norway. *European Journal of Mineralogy*, **20**, 447-463.

MÜLLER, A. & KOCH-MÜLLER, M. 2009. Hydrogen speciation and trace element contents of igneous, hydrothermal and metamorphic quartz form Norway. *Mineralogical Magazine*, **73**, 569-583.

MÜLLER, A., WANVIK, J.E. & IHLEN, P.M. 2012. Petrological and chemical characterisation of high-purity quartz deposits with examples from Norway. *In:* Götze, J. & Wanvik, J.E. (eds.), *Quartz: Deposits, Mineralogy and Analytics*, Springer-Verlag, Berlin, Heidelberg, 71-118.

MORGAN, G.B. VI & LONDON, D. 1999. Crystallisation of the Little Three layered pegmatite aplite dike, Ramona District, California. *Contributions to Mineralogy and Petrology*, **136**, 310-330.

NASH, W.P. & CRECRAFT, H.R. 1985. Partition coefficients for trace elements in silicic magmas. *Geochimica et Cosmochimica Acta*, **49**, 2309-2322.

NEMCHIN, A.A., PIDGEON, R.T. & WHITEHOUSE, M.J. 2006a. Re-evaluation of the origin and evolution of >4.2 Ga zircons from the Jack Hills metasedimentary rocks. *Earth and Planetary Science Letters*, **244**, 218-233.

NEMCHIN, A.A., WHITEHOUSE, M.J. PIDGEON, R.T. & MEYER, C. 2006b. Oxygen isotopic signature of 4.4–3.9 Ga zircons as a monitor of differentiation processes on the Moon. *Geochemica et Cosmochimica Acta*, **70**, 1864-1872.

http://www.norgeskart.no/adaptive2/default.aspx?gui=1&lang=2 Norwegian State Authority's Norgeskart facility. Accessed May 2011.

NORTON, J.J. & REDDEN, J.A. (1990). Relations of zoned pegmatites to other pegmatites, granite, and metamorphic rocks in the southern Black Hills, South Dakota. *American Mineralogist*, 75, 631-655.

http://www.nrm.se/english/researchandcollections/researchdivision/laboratoryforisotopegeology/nordsim/userinformation.91111_en.html Natural History Museum, Sweden. Accessed December 2011.

PEARCE, J.A. & NORRY, M.J. 1979. Petrogenetic implications of Ti, Zr, Y and Nb variations in volcanic rocks. *Contributions to Mineral Petrography*, **69**, 33-47.

PEDERSEN, M. 1993. A geological study of the Flåt complex, Aust-Agder, Norway. *M.Sc. Thesis, Copenhagen University*, pp 128. (in Danish).

PEDERSEN, S. 1981. Rb/Sr age determinations on the late Proterozoic granitoids from the Evje area, south Norway. *Bulletin of the Geological Society of Denmark*, **29**,129-143.

PEDERSEN, S. & KONNERUP-MADSEN, J. 1994: Geology of the Setesdal Region. Excursion Guide to the SNF Excursion, August 1994, Copenhagen University, 55 pp.

PEDERSEN, S. & KONNERUP-MADSEN, J. 2000. Geology of the Setesdalen area, South Norway: Implications for the Sveconorwegian evolution of South Norway. *Bulletin of the Geological Society of Denmark*, **46**,181-201.

PEDERSEN, S., ANDERSEN, T., KONNERUP-MADSEN, J. & GRIFFIN, W.L. 2009. Recurrent Mesoproterozoic continental magmatism in South-Central Norway. *Int J Earth Sci (Geol Rundsch)*, **98**,1151-1171.

PERNY, B., EBERHARDT, P., RAMSEYER, K., MULLIS, J., PANKRATH, R. 1992. Microdistribution of aluminium, lithium and sodium in a quartz: possible causes and correlation with short-lived cathodoluminescence. *American Mineralogist*, **77**, 534-544.

ROLLINSON, H. 1993. *Using geochemical data: evaluation, presentation, interpretation*. Longman, Singapore, pp. 352.

RØNHOLT, K.P. 1990. A geochemical and mineralogical description of metagabbros from the Åvesland area, the Iveland-Gautestad complex, south Norway. *M.Sc. Thesis, Copenhagen University*, pp 137. (in Danish).

SCHÄRER, U., WILMART, E. & DUCHESNE, J.C. 1996. The short duration and anorogenic character of anorthosite magmatism: U-Pb dating of the Rogaland complex, Norway. *Earth and Planetary Science Letters,* **139**, 335-350.

SCHERER, E., MÜNKER, C. & MEZGER, K. 2001. Calibration of the lutetium-hafnium clock. *Science*, **293**, 683-687.

http://seekingalpha.com/article/229254-rare-earth-elements-part-1-the-seventeen-metals-crunch?source=article_lb_author Accessed November 2010.

SEYDOUX, ANNE-MAGALI. Personal communication, 2011.

SEYDOUX, A-M., BINGEN, B., DURAN, C., BOSSE, V., PAQUETTE, J.L., GUILLAME, D., DE PARSEVAL, PH. & INGRIN, J. 2013. Fluid-Mediated Re-equilibration and Self-Irradiation in Complex U-Th-Rich Assemblages of Pegmatites: A Case from Norway and Implications for U-Th-Pb Dating of Ore Deposits. *Mineralogical Magazine*, **77**, 2183.

SEYDOUX, A-M., PAQUETTE, J.L., WIEDENBECK, M., MONTEL, J-M & HEINRICH, W. 2002. Experimental resetting of the U–Th–Pb systems in monazite. *Chemical Geology*, **191**, 165-181.

www.ssrg.com.sg/investinfo/files/**SSRG**%20teaser.pdf Accessed November 2013.

SIMMONS, W.B. 2007. Pegmatite Genesis: recent Advances and Areas for Future Research. *Granitic Pegmatites: The State of the Art – International Symposium, Porto, Portugal, abstract proceedings*.

SIMMONS, W.B., FOORD, E.E. & FALSTER, A.U. 1996. Anatectic origin of granitic pegmatites, Western Maine, USA. GAC-MAC Annual meeting, Winnipeg. Abstracts with programmes.

SIMMONS, W.B., FOORD, E.E., FALSTER, A.U. & KING. V.T. 1995. Evidence for an anatectic origin of granitic pegmatites, western Maine, USA. Geological Society of America Annual meeting, Abstract Programmes, **27**, (6), A411.

SÖDERLUND, U., MÖLLER, C., ANDERSSON, J., JOHANSSON, L. & WHITEHOUSE, M.J. 2002. Zircon geochronology in polymetamorphic gneisses in the Sveconorwgian orogen, SW Sweden: ion microprobe evidence for 1.46-

1.42 Ga and 0.98-0.96 Ga reworking. *Precambrian Research*, **113**, 193-225.

SÖDERLUND, U., ISACHSEN, C.E., BYLUND, G., HEAMAN, L.M., PATCHETT, P.J., VERVOORT, J.D. & ANDERSSON, U.B. 2005. U-Pb baddeleyite ages, and Hf, Nd isotope chemistry constraining repeated mafic magmatism in the Fennoscandian Shield from 1.6 to 0.9 Ga. *Contributions to Mineralogy and Petrology*, **150**, 174-194.

SPEAR, F.S. 1993. *Metamorphic Phase Equilibria and Pressure-Temeprature-Time Paths*. Mineralogical Society of America, BookCrafters, Michigan, pp. 799.

SPRUNT, E.S. 1981. Causes of quartz cathodoluminescence colors. In: In Johari, O. (ed.), *Scanning Electron Microscopy*, Chicago. 525-535.

STEIN, H.J. & BINGEN, B. 2002. 1.05-1.01 Ga Sveconorwegian metamorphism and deformation of the supracrustal sequence at Sæsvatn, South Norway: Re-Os dating of Cu-Mo mineral occurrences. *In*: Blundell, D., Neubauer, F. & von Quadt, A. (eds.), *The timing and location of major ore deposits in an evolving orogen*. Geological Society, London, Special Publications 204, 319-335.

STEWART, D.B. 1978. Petrogenesis of lithium-rich pegmatites. *American Mineralogist*, **63**, 970-980.

STOCKMARR, P. 1994. A description of pegmatites at Åvesland and Evje, South Norway. *M.Sc. thesis, University of Copenhagen* (in Danish).

TANNER, D., HENLEY, R.W., MAVROGENES, J.A. & HOLDEN, P. 2013. Combining in situ isotopic, trace element and textural analyses of quartz from four magmatic-hydrothermal ore deposits. *Contributions to Mineralogy and Petrography*, **166**, 1119-1142.

THOMAS, R. & DAVIDSON, P. 2012a. Evidence of a water-rich silica gel state during the formation of a simple pegmatite. *Mineralogical Magazine*, **76**, 2785-2801.

THOMAS, R. & DAVIDSON, P. 2012b. Water in granite and pegmatite-forming melts. *Ore Geology Reviews*, **46**, 32-46.

THOMAS, R., DAVIDSON, P. & BEURLEN, H. 2012. The competing models for the origin and internal evolution of granitic pegmatites in the light of melt and fluid inclusion research. *Mineralogy and Petrology*, **106**, 55-73.

THOMAS, J.B., WATSON, E.B., SPEAR, F.S., SHEMELLA, P.T., NAYAK, S.K. & LANZIROTTI, A. 2010. TitaniQ under pressure: the effect of pressure and temperature on the solubility of Ti in quartz. *Contributions to Mineralogy and Petrology*, **160**, 743-759.

TINDLE, A.G. & WEBB, P.C. 1990. Estimation of lithium contents in trioctahedral micas using microprobe data: application to micas from granitic rocks. *European Journal of Mineralogy*, **2**, 595-610.

TISCHENDORF, G., FÖRSTER, H.-J. & GOTTESMANN, B. 2001. Minor- and trace element composition of trioctahedral micas: a review. *Mineralogical Magazine*, **65**, 249-276.

TOBI, A.C., HERMANS, G.A.E.M., MAIJER, C. & JANSEN, J.B.H. 1985. Metamorphic zoning in the high -grade Proterozoic of Rogaland-Vest Agder, SW Norway. *In*: Tobi, A.C. & Touret, J.L.R. (eds.), *The deep Proterozoic crust in the North Atlantic Provinces*. *NATO Adv. Sci. Inst. Ser*., Reidel, Dordrecht, C158, 477-497.

VALLEY, J.W. & GRAHAM, C.M. 1996. Ion microprobe analysis of oxygen isotope ratios in quartz from Skye granite: healed micro-cracks, fluid flow, and hydrothermal exchange. Contributions to Mineralogy and Petrology, **124**, 225-234.

VAN DEN KERKHOF, A.M. & HEIN, U.F. 2001. Fluid inclusion petrography. *Lithos*, **55**, 27-47.

VANDER AUWERA, J. & LONGHI, J. 1994. Experimental study of a jotunite (hypersthene monzodiorite): constraints on the parent magma composition and crystallization conditions (P, T, fO2) of the Bjerkreim-Sokndal layered intrusion. *Contributions to Mineralogy and Petrology,* **118**, 60-78.

VANDER AUWERA, J., BOGAERTS, M., LIÉGEOIS, J.P., DEMAIFFE, D., WILMART, E., BOLLE, O. & DUCHESNE, J.C. 2003. Derivation of the 1.0–0.9 Ga ferro-potassic A-type granitoids of southern Norway by extreme differentiation from basic magmas. *Precambrian Research*, **124**, 107-148.

VASYUKOVA, O.V., KAMENETSKY, V.S., GOEMANN, K. & DAVIDSON, P. 2013. Diversity of primary CL textures in quartz from porphyry environments: implication for origin of quartz eyes. *Contributions to Mineralogy and Petrology*, **166**, 1253-1268.

VIGNERESSE, J.L., BARBEY, P. & CUNEY, M. 1996. Rheological transitions during partial melting and crystallization with application to felsic magma segregation and transfer. *Journal of Petrology*, **37**, 1579-1600.

WARK, D.A. & WATSON, E.B. 2006. TitaniQ: a titanium-in-quartz geothermometer. *Contributions to Mineral Petrology*, **152**, 743-754.

WEBBER, K.L., FALSTER, A.U., SIMMONS, W.B. & FOORD, E.E. 1997. The role of diffusion-controlled oscillatory nucleation in the formation of line rock in pegmatite-aplite dikes. *Journal of Petrology*, **38**, 1777-1791.

WEBBER, K.L., SIMMONS, W.B., FALSTER, A.U. & FORD, E.E. 1999. Cooling rates and crystallization dynamics of shallow level pegmatite-aplite dikes, San Diego County, California. *American Mineralogist*, **84**, 708-717.

WHALEN, J.B. AND CHAPELL, B.W. 1988. Opaque mineralogy and mafic mineral chemistry of I- and S-type granites of the Lachlan fold belt, southeast Australia*. *American Mineralogist*, **73**, 281-296.

WHALEN, J.B. 1983. Geochemistry of an Island-Arc Plutonic Suite: the Uasilau-Yau Yau Intrusive Complex, New Britain, P.N.G. *Journal of Petrology*, **26**, 603-632.

WHALEN, J.B., CURRIE, K.L. & CHAPPEL, B.W. 1987. A-type granites: geochemical characteristics, discrimination and petrogenesis. *Contributions to Mineralogy and Petrology*, **95**, 405-419.

WHITE, A.J.R. & CHAPPEL, B.W. 1983. Granitoid types and their distribution in the Lachlan Fold Belt, southeastern Australia. *In*: Roddick, J.A. (ed.), *Circum-Pacific Plutonic Terranes. Geol. Soc. Amer. Memoir*, **159**, 21-24.

WHITEHOUSE, M.J., CLAESSON, S., SUNDE, T. & VESTIN, J. 1997. Ion-micropriobe U-Pb zircon geochronology and correlatio of Archean genisses from the Lewsisian Complex of Gruinard Bay, northwest Scotland. *Geochemica et Cosmochimica Acta*, **61**, 4429-4438.

WHITEHOUSE, M.J. & KAMBER, B.S. 2005. Assigning dates to thin gneissic veins in high-grade metamorphic terranes: a cautionary tale from Akilia, southwest Greenland. *Journal of Petrology*, **8**, 291-318.

WHITEHOUSE, M.J. & NEMCHIN, A.A. 2009. High precision, high accuracy measurement of oxygen isotopes in a large lunar zircon by SIMS. *Chemcial Geology*, **261**, 32-42.

WHITEHOUSE, M.J., KAMBER, B.S. & MOORBATH, S. 1999. Age significance of U-Th-Pb zircon data from early Archaen rocks of west Greenland: a reassessment based on combined ion-microprobe and imaging studies. *Chemical Geology*, **160**, 201-224.

WIENDENBECK, M., ALLE, P., CORFU, F., GRIFFIN, W.L., MEIR, M., OBERLI, F., VON QUADT, A., RODDICK, J.C. & SPIEGEL, W. 1995. Three natural zircon standards for U-Th-Pb, Lu-Hf, trace element and REE analysis. *Geostandards newsletter*, **19**, 1-23.

WILKINSON, J.J. 2001. Fluid inclusions in hydrothermal ore deposits. *Lithos*, **55**, 229-272.

WILLIAMS, M.L., JERCINOVIC, M.J., HARLOV, D.E., BUDZYŃ, B. & HETHERINGTON. C.J. 2001. Resetting monazite ages during fluid-related alteration. *Chemical Geology*, **283**, 218-225.

WILLIAMSON, B.J., WILKINSON, J.J., LUCKHAM, P.F. & STANLEY, C.J. 2002. Formation of coagulated colloidal silica in high-temperature mineralizing fluids. *Mineralogical Magazine*, **66**, 547-553.

WILMART, E. & DUCHESNE, J.C. 1987. Geothermobarometry of igneous and metamorphic rocks around the Ana-Sira anorthosite massif: implications for the depth of emplacement of the South Norwegian anorthosites. *Norsk Geologisk Tidsskrift,* **67**, 185-196.

WINTER, J.D. 2001. *An introduction to igneous and metamorphic petrology*, Prentice Hall, New Jersey, pp. 697.

APPENDIX 1

Sample Summary (including material collected in 2008, 2009, 2020 and 2011)

Sample Number	Location	Easting	Northing	Description
070708-02	Steli	434427	6484276	K-feldspar
070708-04	Steli	434427	6484276	Biotite
070708-05	Steli	434427	6484276	Muscovite
090708-19	Solås	437086	6483790	K-feldspar
090708-20	Solås	437086	6483790	K-feldspar
090708-21	Solås	437086	6483790	Biotite
090708-22	Solås	437086	6483790	Muscovite
100708-14	Hovåsen	437957	6487440	K-feldspar
100708-16	Hovåsen	437957	6487440	Biotite
100708-24	Slobrekka	436143	6487497	K-feldspar
100708-26	Slobrekka	436143	6487497	Biotite
100708-27	Slobrekka	436143	6487497	Muscovite
100708-31	Li Gruva / Li 2	433160	6488069	K-feldspar
120708-01	Landsverk 1	433449	6495851	Hydrothermal quartz crystal collected from vug
120708-02	Landsverk 1	433449	6495851	K-feldspar
120708-04	Landsverk 1	433449	6495851	Muscovite
220609-02	Høvringsvatnet Granite	439326	6497399	Fine-grained monzonite, Høvringsvatnet
220609-03	Høvringsvatnet Granite	439186	6497324	Medium-grained syenomonzonite, Høvringsvatnet
220609-04	Høvringsvatnet Granite	440535	6498989	Medium-grained biotite granite, Høvringsvatnet
240609-05	Slobrekka	436143	6487497	Nortite at contact 10 cm, Slobrekka
240609-06	Slobrekka	436143	6487497	Chilled margin pegmatite, Slobrekka
240609-08	Slobrekka	436143	6487497	Bulk pegmatite, Slobrekka

240609-13	Slobrekka	436143	6487497	Norite 25 m from contact, Slobrekka
260609-01	Hovåsen	437957	6487440	Metagabbro 5 m from contact, Hovåsen
260609-04	Hovåsen	437957	6487440	Norite 10 m from contact, Hovåsen
260609-02	Hovåsen	437957	6487440	Bulk pegmatite (marginal bt zone), Hovåsen
280609-01	Solås	437086	6483790	Bulk pegmatite, Solås
280609-02	Solås	437086	6483790	Migmatitic gneiss from contact, Solås
280609-03	Solås	437086	6483790	Migmatitic gneiss 10 m from contact, Solås
280609-06	Li Gruva / Li 2	433160	6488069	Coarse-grained pegmatitic granite, Li Gruva
280609-07	Solås	437086	6483790	Amazonite
280609-08	Solås	437086	6483790	Pink K-feldspar
290609-01	Li Gruva / Li 2	433160	6488069	Norite 30 m away from contact, Li Gruva
290609-03	Li Gruva / Li 2	433160	6488069	Norite from contact, Li Gruva
040709-08	Høvringsvatnet Granite	439220	6501676	Bt-rich medium-grained granite, Høvringsvatnet
100709-03	Steli	434427	6484276	Coarse-grained pegmattic granite near lower contact, Steli
100709-05	Steli	434427	6484276	Medium-granined granitic facies near lower contact, Steli
100709-08	Steli	434427	6484276	Fine-granined granitic facies from upper contact, Steli
100709-09	Steli	434427	6484276	Granitic gneiss 25 m away from contact, Steli
080910-01	Solås	437086	6483790	Quartz (in plagioclase)
080910-02	Solås	437086	6483790	Quartz (from chaotic quartz/plagioclase zone)
080910-03	Solås	437086	6483790	Graphic quartz (above core)
080910-04	Solås	437086	6483790	Quartz megacryst (core)
080910-05	Solås	437086	6483790	Quartz of Cleavelandite zone
080910-06	Solås	437086	6483790	Quartz from Lower magnetite border zone
080910-07	Solås	437086	6483790	Pink K-feldspar
080910-08	Solås	437086	6483790	Amazonite
080910-09	Solås	437086	6483790	Magnetite (radioactive)
080910-10	Solås	437086	6483790	Allanite

080910-11	Solås	437086	6483790	Polycras/aeschynite
080910-12	Solås	437086	6483790	Fergussonite?
080910-13	Solås	437086	6483790	Tourmaline
080910-14	Solås	437086	6483790	Beryl
080910-15	Solås	437086	6483790	Cleavelandite
080910-16	Solås	437086	6483790	Garnet
080910-17	Solås	437086	6483790	Contact between pegmatite and country rock
080910-18	Solås	437086	6483790	Inclusions of country rock in pegmatite
080910-19	Solås	437086	6483790	Undisturbed country rock adjacent to contact
080910-20	Solås	437086	6483790	Pegmatitic biotite
080910-21	Iveland road section	436768	6479750	Bulk pegmatite (magnetite-bearing)
080910-22	Iveland road section	436768	6479750	Pegmatitic quartz from magnetite-bearing pegmatite
080910-23	Iveland road section	436768	6479750	Iveland road section, banded gneiss; bulk country rock
080910-24	Steli	434427	6484276	Quartz of upper granitic border facies
080910-25	Steli	434427	6484276	Quartz of chaotic quartz/plagioclase intergrowth of intermediate zone
080910-26	Steli	434427	6484276	Quartz from above muscovite splays
080910-27	Steli	434427	6484276	Quartz approximately from core
080910-28	Steli	434427	6484276	Quartz of fine-grained granitic lower border zone
080910-29	Steli	434427	6484276	Quartz of coarse-grained granitic lower border zone
080910-30	Steli	434427	6484276	Colombite?
080910-31	Steli	434427	6484276	Beryl
080910-32	Steli	434427	6484276	Isotope dating (garnet, K-feldspar, biotite)
090910-01	Høvringsvatnet Granite	439199	6501687	Medium-grained, slightly foliated biotite Granite
090910-02	Høvringsvatnet Granite	439261	6501887	Fine-grained Monzonite
090910-03	Høvringsvatnet Granite	439091	6501912	Quartz core from a pegmatite vein
090910-04	Høvringsvatnet Granite	439099	6501682	Medium-grained biotite granite Gautestad, Høvringsvatnet
090910-05	Høvringsvatnet Granite	439794	6501199	Quartz core from a pegmatite vein

090910-06	Høvringsvatnet Granite	439794	6501199	Diorite
090910-07	Høvringsvatnet Granite	439794	6501199	Mafic diorite
090910-08	Høvringsvatnet Granite	440553	6498977	Monzogranite
090910-09	Høvringsvatnet Granite	440553	6498977	Fluorite-sulfide vein
090910-14	Landsverk 1	433449	6495851	Hydrothermal quartz
090910-15	Landsverk 1	433449	6495851	Country Rock enclave in brecciated pegmatite
090910-16	Landsverk 1	433449	6495851	Secondary albite alteration (with calcite?)
100910-01	Li Gruva / Li 2	433160	6488069	Quartz and garnet (from line rock)
100910-02	Li Gruva / Li 2	433160	6488069	Quartz (from megacryst immediately above line rock)
100910-03	Li Gruva / Li 2	433160	6488069	Quartz (from lower core)
100910-04	Li Gruva / Li 2	433160	6488069	Quartz (from upper core, amongst biotite)
100910-05	Li Gruva / Li 2	433160	6488069	Quartz (from chaotic zone above core, amongst biotite)
100910-06	Li Gruva / Li 2	433160	6488069	Quartz (from chaotic zone immediately below granitic margin)
100910-07	Li Gruva / Li 2	433160	6488069	Polycrase
100910-08	Li Gruva / Li 2	433160	6488069	Quartz and garnets
100910-09	Li Gruva / Li 2	433160	6488069	Garnet-bearing Line rock (from bottom)
100910-10	Li Gruva / Li 2	433160	6488069	Biotite-bearing line rock (from roof)
100910-11	Li Gruva / Li 2	433160	6488069	Quartz between biotite
100910-12	Li Gruva / Li 2	433160	6488069	Line rock (orientated for directional studies)
100910-13	Li Gruva / Li 2	433209	488037	K-feldspar with graphic quartz (cupola)
100910-14	Li Gruva / Li 2	433209	488037	Country rock (close to contact)
100910-15	Li Gruva / Li 2	433209	488037	Distal country rock
110910-01	Hovåsen	437957	6487440	Quartz core from mine floor
110910-02	Hovåsen	437957	6487440	Quartz from quartz-plagioclase intergrowth below quartz core
110910-03	Hovåsen	437957	6487440	Beryl-bearing quartz core
110910-04	Hovåsen	437957	6487440	Quartz from quartz-plagioclase intergrowth below quartz core (same zone as 110910-01)
110910-05	Hovåsen	437957	6487440	Quartz from magnetite-/biotite-bearing lower border (contact) zone

110910-06	Hovåsen	437957	6487440	Grey K-feldspar from below quartz core
110910-07	Hovåsen	437957	6487440	Pink K-feldspar from megacrysts 5m from contact
110910-08	Hovåsen	437957	6487440	Garnet
110910-09	Hovåsen	437957	6487440	Beryl
110910-10	Hovåsen	437957	6487440	Border zone with magnetite and accessories
110910-11	Hovåsen	437957	6487440	Colombite and MYSTERY from western albite zone
110910-12	Hovåsen	437957	6487440	(albite zone) (black mineral in beryl)
110910-13	Hovåsen	437957	6487440	Monazite
110910-14	Slobrekka	436143	6487497	Allanite
110910-15	Slobrekka	436143	6487497	Gadolinite (large)
110910-16	Slobrekka	436143	6487497	Gadolinite (and maybe allanite)
110910-17	Slobrekka	436143	6487497	Gadolinite (biggest)
110910-18	Slobrekka	436143	6487497	Polycras
110910-19	Landsverk 1	433449	6495851	Fergussonite
110910-20	Landsverk 1	433449	6495851	Biotite/Magnetite
110910-21	Landsverk 1	433449	6495851	Monaznite between biotite
110910-22	Landsverk 1	433449	6495851	Flourite (violet)
110910-23	Solås	437086	6483790	Colombite
110910-24	Solås	437086	6483790	Fluorite-Y (green) (from cleavelandite zone)
110910-25	Steli	434427	6484276	Monazite in muscovite
110910-26	Kåbuland (Tunnelen)	436467	6489699	Thortveitite
120910-01	Slobrekka	436143	6487497	Quartz from lower quartz/plagioclase layer (next to allanite)
120910-02	Slobrekka	436143	6487497	Massive quartz (from core)
120910-03	Slobrekka	436143	6487497	Massive quartz (adjacent/below gadolinites)
120910-04	Slobrekka	436143	6487497	Quartz 20 cm megacryst (1 m below contact)
120910-05	Slobrekka (West)	436143	6487497	Massive quartz core
120910-06	Slobrekka (West)	436143	6487497	Quartz/plagioclase (1 m from contact)

120910-07	Slobrekka	436143	6487497	K-feldspar
120910-08	Slobrekka	436143	6487497	Allanite (with magnetite?)
120910-09	Slobrekka	436143	6487497	Magnetite, ilmenite, (polycrase)
120910-10	Slobrekka	436143	6487497	Garnet
120910-11	Slobrekka	436143	6487497	Beryl
120910-12	Hovåsen	437957	6487440	Quartz from quartz-plagioclase intergrowth (upper contact, including country rock)
120910-13	Hovåsen	437957	6487440	Pegmatite border zone, Hovåsen (whole rock; upper)
130910-01	Kåbuland (Tunnelen)	436467	6489699	Quartz (assumed from core)
130910-02	Kåbuland (Tunnelen)	436467	6489699	Quartz (1.5 m from contact)
130910-03	Kåbuland (Tunnelen)	436467	6489699	Quartz of quartz-plagioclase intergrowth (30 cm from contact)
130910-04	Kåbuland (Tunnelen)	436467	6489699	Granitic border zone, Kåbuland (whole rock)
130910-05	Kåbuland (Tunnelen)	436467	6489699	Metagabbro at contact, Kåbuland (biotitised metagabbro at contact)
130910-06	Kåbuland (Tunnelen)	436467	6489699	Metagabbro 10 m from contact, Kåbuland
130910-07	Kåbuland (Tunnelen)	436467	6489699	K-feldspar (probably from core)
130910-08	Kåbuland (Tunnelen)	436467	6489699	Biotite
130910-09	Kåbuland (Tunnelen)	436467	6489699	Magnetite in biotised metagabbro
130910-10	Kåbuland (Tunnelen)	436467	6489699	Magnetite in pegmatite
130910-11	Kåbuland (Tunnelen)	436467	6489699	Aeschynite
130910-12	Kåbuland (Tunnelen)	436467	6489699	Allanite
130910-13	Kåbuland (Tunnelen)	436467	6489699	Allanite
130910-14	Kåbuland (Tunnelen)	436467	6489699	Polycrase
130910-15	Kåbuland (Tunnelen)	436467	6489699	Ilmenite
130910-16	Kåbuland (Tunnelen)	436467	6489699	Xenotime
140910-01	Steli	434427	6484276	Bityite $CaAl_2Li$ (Al Be $Si_2)_{10}$ $(OH)_2$
160910-01	Landsverk 1	433449	6495851	Pegmatitc quartz
160910-02	Landsverk 1	433449	6495851	K-Feldspar
160910-03	Landsverk 1	433449	6495851	Fergusonite

160910-04	Landsverk 1	433449	6495851	Euxenite
160910-05	Landsverk 1	433449	6495851	Monazite
160910-06	Landsverk 1	433449	6495851	Ilmenised biotite and monazite
160910-07	Landsverk 1	433449	6495851	Garnet
160910-08	Landsverk 1	433449	6495851	Hydrothermal quartz 1
160910-09	Landsverk 1	433449	6495851	Hydrothermal quartz 2 and stilpnomelane and chlorite
160910-10	Landsverk 1	433449	6495851	Hydrothermal quartz 3 and stilpnomelane
160910-11	Landsverk 1	433449	6495851	Hydrothermal quartz 4 and stilpnomelane
160910-12	Landsverk 1	433449	6495851	Epidotised muscovite
160910-13	Landsverk 1	433449	6495851	Fluorite
160910-14	Landsverk 1	433449	6495851	Adularia and chlorite and pyrite
160910-15	Landsverk 1	433449	6495851	Adularia and quartz and 'green soft mineral'
160910-16	Landsverk 1	433449	6495851	Chlorite
160910-17	Landsverk 1	433449	6495851	Brecciated host rock in pegmatite
160910-18	Landsverk 1	433449	6495851	Metagobbro at contact, Landsverk 1
160910-19	Landsverk 1	433449	6495851	Metagabbro 4 m from contact, Landsverk 1
170910-01	Li Gruva / Li 2	433160	6488069	Grey K-feldspar from core
170910-02	Li Gruva / Li 2	433160	6488069	Pink K-feldspar from upper layer
170910-03	Li Gruva / Li 2	433160	6488069	Polycrase
170910-04	Li Gruva / Li 2	433160	6488069	Unknown mineral and polycrase
170910-05	Li Gruva / Li 2	433160	6488069	Monazite
170910-10	Steli	434427	6484276	Granitic facies at lower contact, Steli (whole rock)
170910-11	Steli	434427	6484276	Granitic facies at upper contact, Steli (whole rock)
040611-01	Landsverk area	32832	95497	Aplite sheet
040611-02	Landsverk area	32691	94447	Granitic wall rock
040611-03	Landsverk area	32691	94447	Quartz from core
040611-04	Landsverk area	32907	94515	Quartz from core periphery

040611-05	Landsverk area	32907	94515	Quartz from core
050611-01	Landsverk area	33155	94970	Quartz from core
050611-02	Landsverk area	33330	94767	Quartz from pod
050611-03	Landsverk area	33335	94870	Quartz from core
060611-01	Landsverk area	33286	95019	K-fld from intermediate zone
060611-02	Landsverk area	33286	95019	K-fld from core
060611-03	Steli	434427	6484276	Garnet from intermediate K-fld and graphic quartz, and two random pieces
070611-01	Landsverk area	33158	95154	Quartz core from micro pegmatite
070611-02	Landsverk area	33206	95296	Quartz from central pod
070611-03	Landsverk area	33116	95550	Gneiss-hosted quartz vein
070611-04	Landsverk area	33140	96120	Gneiss-hosted quartz vein
070611-05	Landsverk area	33378	96255	Quartz core from massive boulder
070611-06	Landsverk area	33378	96255	K-fld from massive boulder
070611-07	Landsverk area	33378	96255	Int zone adjacent to excavation and therefore probably core
080611-01	Landsverk area	33599	94956	Quartz from pod
080611-02	Landsverk area	33600	95165	Quartz from core
080611-03	Landsverk area	33948	418	Quartz from pod
080611-04	Landsverk area	33868	94866	Quartz from core
080611-05	Landsverk area	33868	94866	K-fld from core
080611-06	Landsverk area	33888	94898	Quartz from core
080611-07	Landsverk area	33888	94898	K-fld from core
080611-08	Landsverk area	33806	95207	Quartz from core
100611-01	Landsverk area	33613	96208	Quartz (from core?)
100611-02	Landsverk area	33613	96208	K-fld (from core?)
100611-03	Landsverk area	33587	96225	Quartz from vein/pod
100611-04	Landsverk area	33587	96225	K-fld from 'core'
100611-05	Landsverk area	33587	96225	K-fld/quartz/plag groundmass

100611-06	Landsverk area	33565	96328	Quartz from core
100611-07	Landsverk area	33565	96328	K-fld from core
100611-08	Landsverk area	33819	96006	Quartz (from boulder)
100611-09	Landsverk area	33819	96006	White K-fd (from boulder)
100611-10	Landsverk area	33509	95547	Quartz from pod
100611-11	Landsverk area	33457	95518	Quartz from core
100611-12	Landsverk area	33457	95518	K-fld from core
110611-01	Landsverk area	33909	95789	Quartz from core
110611-02	Landsverk area	33909	95789	K-fld from core
110611-03	Landsverk area	33853	95803	Quartz from mass
110611-04	Landsverk area	33853	95803	K-fld
110611-05	Landsverk area	33693	95526	Quartz from boulder in core
110611-06	Landsverk area	33693	95526	K-fld from core edge
110611-07	Landsverk area	33693	95500	Quartz from core
110611-08	Landsverk area	33693	95500	K-fld from core
110611-09	Landsverk area	33700	95277	Quartz
110611-10	Landsverk area	33700	95277	K-fld; white, tending to cleavelandite?
110611-11	Landsverk area	33700	95277	Quartz from adjacent vein
110611-12	Landsverk area	33235	94947	Quartz from SW core
110611-13	Landsverk area	33235	94947	K-fld from SW core
110611-14	Landsverk area	33235	94947	Quartz from central core
110611-15	Landsverk area	33235	94947	K-fld from central core
120611-01	Landsverk area	33984	95866	Quartz vein; variably Fe stained, pyritised and epidotised
120611-02	Landsverk area	34230	95300	Quartz from pod
120611-03	Landsverk area	34423	95336	Quartz core
140611-01	Landsverk area	35074	95326	Quartz pod
140611-02	Landsverk area	34864	95291	Quartz pod

150611-01	Landsverk area	34646	94622	Quartz pod
150611-02	Landsverk area	34402	94661	Quartz 'core'
150611-03	Landsverk area	34264	94391	Quartz from pod
150611-04	Landsverk area	34129	94661	Quartz from pod
150611-05	Landsverk area	34029	94516	Quartz from pod
150611-06	Landsverk area	34029	94516	K-fld adjacent to pod
150611-07	Landsverk area	33998	94394	Quartz from pod
160611-01	Landsverk area	34526	95066	Quartz from pod
160611-02	Landsverk area	34500	950029	Quartz from 'vein'
160611-03	Landsverk area	34458	95001	Quartz from pod
160611-04	Landsverk area	34062	95134	Quartz from pod
160611-05	Landsverk area	33457	95812	Quartz from pod
160611-06	Landsverk area	33539	95896	Quartz rich intermediate zone
180611-01	Landsverk 1	433449	6495851	Quartz with granular garnet from excavation floor
180611-02	Landsverk 1	433449	6495851	Quartz from north wall amid brecciated K-fld megacrysts
180611-03	Landsverk 1	433449	6495851	Quartz from north wall amid brecciated K-fld megacrysts, plus lump from floor
180611-04	Landsverk 1	433449	6495851	Quartz from east wall amid brecciated K-fld megacrysts
180611-05	Landsverk 1	433449	6495851	Quartz on secondary clay
180611-06	Landsverk 1	433449	6495851	Quartz from cavity in east wall, plus garnet
180611-07	Landsverk 1	433449	6495851	Quartz from north wall adjacent to muscovite
180611-08	Landsverk 1	433449	6495851	Quartz crystal from floor, zoned
180611-09	Landsverk 1	433449	6495851	Garnets from floor
180611-10	Landsverk 1	433449	6495851	Garnets from floor
180611-11	Landsverk 1	433449	6495851	Quartz from upper level
180611-12	Landsverk 1	433449	6495851	Quartz from upper level close to country rock

APPENDIX 2

Data tables for geochemical results

Whole rock element compositions (ICP-ES and ICP-MS) of the Høvringsvatnet granites and pegmatite border zones (analyses removed for Ag, Cd and Hg as these fell below LOD; excepting 0.1 ppm Ag in Bulk pegmatite, Solås)

		Detection Limit	Fine-grained monzonite, Høvringsvatnet	Medium-grained syenomonzonite, Høvringsvatnet	Medium-grained biotite granite, Høvringsvatnet	Bt-rich medium-grained granite, Høvringsvatnet	Medium-grained biotite granite Gautestad, Høvringsv.	Chilled margin pegmatite, Slobrekka	Bulk pegmatite, Slobrekka	Bulk pegmatite (marginal bt zone), Hovåsen	Bulk pegmatite, Solås	Coarse-grained pegmatitic granite, Li Gruva	Coarse-grained pegmatitic granite near lower contact, Steli	Medium-grained granitic facies from lower contact, Steli	Fine-grained granitic facies from upper contact, Steli	Iveland road section, bulk pegmatite	Pegmatite border zone, Hovåsen	Granitic border zone, Kåbuland	Granitic border zone lower contact, Steli	Granitic border zone upper contact, Steli
Sample number			220609-02	220609-03	220609-04	040709-08	090910-04	240609-06	240609-08	260609-02	280609-01	280609-06	100709-03	100709-05	100709-08	080910-21	120910-13	130910-04	170910-10	170910-11
SiO_2	[%]	0.01	72.62	55.54	67.58	62.52	63.48	75.48	73.85	74.21	79.8	77.34	70.52	73.99	68.47	69.58	78.12	77.93	71.45	73.63
Al_2O_3	[%]	0.01	14.11	13.57	15.31	16.05	15.03	13.79	13.93	15.24	11.31	13.05	16.01	13.58	16.97	14.63	12.81	12.83	15.97	13.68

Sample number			220609-02	220609-03	220609-04	040709-08	090910-04	240609-06	240609-08	260609-02	280609-01	280609-06	100709-03	100709-05	100709-08	080910-21	120910-13	130910-04	170910-10	170910-11
Fe_2O_3	[%]	0.04	2	7.98	2.93	4.86	4.68	1.55	1.36	0.72	0.8	0.56	2.66	1.4	1.98	6.07	0.65	0.83	1.79	1.55
MgO	[%]	0.01	0.26	4.79	0.67	1.53	1.61	0.1	0.21	0.15	0.03	0.07	0.17	0.24	0.42	0.05	0.28	0.18	0.4	0.28
CaO	[%]	0.01	0.7	5.65	1.34	2.54	2.86	2.16	1.1	1.88	0.56	0.81	1.14	0.67	2.29	3.17	2.09	2.74	2.69	0.98
Na_2O	[%]	0.01	3.46	3.24	3.71	3.88	3.55	4.74	3.3	6.07	4.31	5.08	5.74	2.66	4.64	4.69	4.96	4.34	5.35	3.21
K_2O	[%]	0.01	5.68	4.01	6.43	6.02	5.56	1.21	5.42	0.9	2.32	2.5	2.26	6.77	4.3	0.98	0.36	0.38	1.19	5.3
TiO_2	[%]	0.01	0.24	1.44	0.42	1.02	0.98	0.06	0.12	0.06	0.03	0.03	0.07	0.12	0.21	0.15	0.06	0.06	0.18	0.14
P_2O_5	[%]	0.01	0.05	1.34	0.14	0.36	0.42	0.01	0.02	<0.01	0.02	0.02	0.02	0.03	0.04	<0.01	0.01	0.01	0.03	0.03
MnO	[%]	0.01	0.02	0.11	0.04	0.07	0.06	0.03	0.04	0.05	0.04	0.08	0.91	0.04	0.04	0.05	0.03	0.01	0.04	0.05
Cr_2O_3	[%]	0.002	0.01	0.02	0.006	0.007	0.002	0.009	0.009	0.009	0.011	0.01	0.009	0.008	0.006	0.003	0.002	0.002	<0.002	<0.002
Sc	[ppm]	1	2	15	3	7	7	3	6	9	2	8	14	5	7	2	9	2	6	6
LOI	[%]	-5.1	0.6	1.5	1	0.4	1.2	0.7	0.5	0.6	0.7	0.4	0.4	0.3	0.4	0.5	0.6	0.6	0.8	1
TOTAL	**[%]**	**0.01**	**99.7**	**99.22**	**99.57**	**99.24**	**99.41**	**99.84**	**99.82**	**99.91**	**99.92**	**99.95**	**99.89**	**99.82**	**99.77**	**99.85**	**99.99**	**99.96**	**99.89**	**99.86**
Ba	[ppm]	1	940	3123	1549	3216	2714	471	320	81	4	6	113	621	656	127	37	198	194	500
Be	[ppm]	1	4	4	3	3	4	7	4	12	18	12	19	3	5	6	25	3	12	5
Co	[ppm]	0.2	2.5	27.5	3.3	10.5	10	1.2	1.7	1.9	0.6	0.4	1.4	1.6	3.4	3.5	1.7	2	2.9	1.8
Cs	[ppm]	0.1	0.9	0.7	1.8	1.7	1.7	9.5	4	1.4	159.8	11.6	21.5	6.7	15.2	0.6	9.1	1	17.1	8.4
Ga	[ppm]	0.5	18.7	18.2	20.1	21.8	21	20.8	21.6	27.9	23.1	28.3	36.7	18.3	21.9	29	22.2	14.9	28.2	20.9
Hf	[ppm]	0.1	8.3	12.5	12.4	13	13.1	2.3	4.9	3.8	5.3	1.7	5.7	4.7	6.8	24.6	1.3	5.1	7.4	11
Nb	[ppm]	0.1	17.5	12.3	17.7	18.4	21	14.9	85.5	36.3	52.8	34.1	41.7	28.6	23.2	2.5	19.3	1.5	28.7	33.6
Rb	[ppm]	0.1	173.7	107.5	194.9	166.4	188.7	155.7	306.5	101.2	592	262.8	226.7	377.3	248.7	28.3	140.8	23.5	172.2	366.9
Sn	[ppm]	1	2	2	3	3	3	2	4	3	3	3	7	4	2	3	2	<1	5	5
Sr	[ppm]	0.5	481.8	1165	621.2	1529	1131	299.2	156.9	156.6	9.7	6.2	49.2	103.8	195.6	260.5	213.7	272.9	184	100.6
Ta	[ppm]	0.1	1.4	0.6	1.2	1	1.1	1.8	6.5	3.5	9.1	7.6	24.6	2.8	1.4	0.3	1.4	0.1	1.6	2.3
Th	[ppm]	0.2	38.2	12.3	39.9	15.3	14.2	26.9	50.3	22.2	19.5	8	13.9	51.6	87.9	200.8	8.7	14	86	49.7
U	[ppm]	0.1	3.1	3.1	3.4	2.8	3.8	20.5	54.3	19.7	15.5	5.4	14.8	18.4	8	34.7	12.4	2.2	12.2	37.8
V	[ppm]	8	16	129	28	63	71	<8	<8	<8	<8	<8	<8	<8	24	76	<8	8	12	<8
W	[ppm]	0.5	<0.5	7.5	<0.5	<0.5	<0.5	<0.5	0.8	<0.5	1.2	1.7	1.2	<0.5	<0.5	<0.5	<0.5	<0.5	<0.5	<0.5
Zr	[ppm]	0.1	243.5	439.4	375.9	522.7	538	45.9	95.6	54.6	63.5	13.8	33.2	124.2	202.1	714.9	23.4	158	211.5	274.6
Y	[ppm]	0.1	40.3	28.8	40.6	28.2	31.7	96.7	266.3	44.3	89.7	34	118.2	115.5	36.6	12.1	16.3	2.6	53.3	146.2
La	[ppm]	0.1	118.4	171.6	172.3	131.6	114.2	15.2	18.1	7.4	3.4	12.5	19.9	51.4	98.5	3.3	23.1	8.2	66.2	38.6

Sample number			220609-02	220609-03	220609-04	040709-08	090910-04	240609-06	240609-08	260609-02	280609-01	280609-06	100709-03	100709-05	100709-08	080910-21	120910-13	130910-04	170910-10	170910-11
Ce	[ppm]	0.1	244.8	375.4	349	310.6	269.2	31.8	37.4	16.3	6.3	34.5	60.7	108.8	218.7	4.8	9.7	20.5	152.6	84.7
Pr	[ppm]	0.02	24.03	42.68	35.8	34.44	30.34	4.57	5.98	1.89	0.77	4.11	8.5	12.75	23.01	0.57	1.11	1.98	16.36	9.92
Nd	[ppm]	0.3	79	163.6	119.1	123.6	113.7	19.2	26.1	7.2	3.4	15.9	34.9	49.2	83.6	2.1	4.2	6.8	64.1	38.3
Sm	[ppm]	0.05	11	20.6	14.28	16.81	15.35	5.91	9.41	2.65	2.79	5.11	17.29	11.29	16.17	0.65	1.31	1.34	12.69	9.88
Eu	[ppm]	0.02	1.34	4.55	2.09	3.19	2.92	0.77	0.66	0.33	0.15	0.06	0.25	0.87	1.43	0.67	0.29	0.4	1.1	0.78
Gd	[ppm]	0.05	6.73	10.08	7.61	8.83	8.19	8.15	17.61	3.49	5.65	3.96	13.69	12.23	11.52	1	1.48	0.81	9.91	12.2
Tb	[ppm]	0.01	1.23	1.29	1.32	1.24	1.21	1.8	4.37	0.83	1.54	0.81	3.15	2.35	1.66	0.2	0.32	0.11	1.6	2.64
Dy	[ppm]	0.05	6.48	5.64	6.7	5.84	5.76	11.98	33	5.25	10.55	4.46	16.62	15.14	7.56	1.49	2	0.5	8.87	18.37
Ho	[ppm]	0.02	1.37	0.92	1.42	1.04	1.03	2.98	8.72	1.22	2.54	0.86	2.51	3.68	1.29	0.41	0.46	0.08	1.75	4.52
Er	[ppm]	0.03	3.91	2.25	4.13	2.7	2.81	9.77	29.08	4.29	9.4	2.96	6.98	12.02	3.4	1.43	1.55	0.23	5.31	15.3
Tm	[ppm]	0.01	0.63	0.31	0.62	0.43	0.42	1.6	4.57	0.9	2.05	0.66	1.52	2.04	0.53	0.26	0.31	0.05	0.81	2.49
Yb	[ppm]	0.05	3.99	2	4.08	2.7	2.55	10.59	30.53	7.63	17.32	5.74	12.3	14.09	3.26	1.97	2.67	0.35	5.64	18.02
Lu	[ppm]	0.01	0.55	0.26	0.57	0.38	0.38	1.56	4.55	1.38	2.93	1.05	1.63	2.22	0.5	0.39	0.47	0.07	0.9	2.87
TOT/C	[%]	0.02	0.05	<0.02	0.07	0.02	0.04	<0.02	<0.02	<0.02	<0.02	<0.02	<0.02	<0.02	0.03	0.02	<0.02	<0.02	<0.02	<0.02
TOT/S	[%]	0.02	<0.02	0.03	0.02	0.04	0.04	<0.02	<0.02	<0.02	<0.02	<0.02	<0.02	<0.02	<0.02	<0.02	<0.02	<0.02	<0.02	<0.02
Mo	[ppm]	0.1	3.6	1.2	2.1	2	0.6	2.8	2.5	2.5	2.9	2.7	2.9	2.2	1.8	0.2	0.1	0.2	0.3	0.4
Cu	[ppm]	0.1	5.6	22.8	7.1	16.8	16	2.3	1.9	2.2	1.7	1.4	1.5	1	2.6	1.6	3.5	4	0.6	0.7
Pb	[ppm]	0.1	35.5	26.6	40.7	14.8	14.1	15.4	17.2	20.8	18.1	13.1	13.2	18.7	16.3	22.3	4.6	7.7	10.1	15.7
Zn	[ppm]	1	24	64	37	80	86	14	23	13	21	8	26	33	42	19	20	11	48	37
Ni	[ppm]	0.1	23.2	63.8	8.4	11.2	13.1	4.4	1.9	13.9	3.6	2.1	2.7	2.4	3.7	5.6	11.8	4.1	1.9	1.4
As	[ppm]	0.5	<0.5	<0.5	0.6	0.5	<0.5	<0.5	<0.5	<0.5	3.5	<0.5	0.7	<0.5	<0.5	<0.5	<0.5	<0.5	0.6	0.6
Sb	[ppm]	0.1	<0.1	<0.1	<0.1	<0.1	<0.1	<0.1	<0.1	<0.1	1.3	<0.1	0.1	<0.1	<0.1	<0.1	<0.1	<0.1	<0.1	<0.1
Bi	[ppm]	0.1	<0.1	<0.1	<0.1	<0.1	<0.1	<0.1	<0.1	<0.1	1.3	<0.1	0.2	<0.1	<0.1	<0.1	0.2	<0.1	<0.1	<0.1
Au	[ppb]	0.5	<0.5	<0.5	<0.5	<0.5	<0.5	<0.5	<0.5	<0.5	<0.5	0.6	<0.5	1	<0.5	<0.5	0.9	<0.5	<0.5	<0.5
Tl	[ppm]	0.1	<0.1	0.2	0.1	0.6	0.6	0.2	0.3	0.1	0.3	<0.1	<0.1	0.5	0.9	<0.1	1	0.1	0.9	0.7
Se	[ppm]	0.5	0.6	<0.5	<0.5	<0.5	0.6	<0.5	0.6	<0.5	<0.5	<0.5	<0.5	<0.5	<0.5	<0.5	<0.5	<0.5	0.7	0.8

Whole rock element compositions (ICP-ES and ICP-MS) of the country rocks in the Evje-Iveland region

		Detection Limit	Norite at contact 10 cm, Slobrekka	Norite 25 m from contact, Slobrekka	Migmatitic gneiss from contact, Solås	Migmatitic gneiss 10 m from contact, Solås	Norite 30 m away from contact, Li Gruva	Norite from contact, Li Gruva	Metagabbro at contact, Kåbuland	Metagabbro 10 m from contact; Kåbuland	Metagabbro 5 m from contact, Hovåsen	Norite 10 m from contact, Hovåsen	Metagabbro at contact, Landsverk 1	Metagabbro 4 m from contact, Landsverk 1	Granitic gneiss 25 m away from contact, Steli	Iveland road section, banded gneiss
Sample number			240609-05	240609-13	280609-02	280609-03	290609-01	290609-03	130910-05	130910-06	260609-01	260609-04	160910-18	160910-19	100709-09	080910-23
SiO_2	[%]	0.01	55.25	54.71	62.03	53.42	45.32	51.41	45.44	48.77	52.07	48.48	33.71	45.54	42.63	54.63
Al_2O_3	[%]	0.01	19.5	19.42	16.56	13.54	18.57	19.38	14.22	15.77	19.19	15.28	14.24	12.23	13.52	15.84
Fe_2O_3	[%]	0.04	6.33	7.11	7.38	14.67	11.86	4.63	20.47	10.29	6.79	14.27	18.82	16.05	25.45	8.75
MgO	[%]	0.01	3.19	3.33	2.28	2.59	8.83	7.46	4.27	7.21	6.12	5.9	8.16	6.28	5.97	5.8
CaO	[%]	0.01	5.07	7.93	3.54	6.83	10.73	9.64	2.59	12.43	9.28	8.5	9.13	6.07	7.83	7.21
Na_2O	[%]	0.01	5	4.72	4.22	3.52	2.37	3.29	2.59	2.7	4.11	3.5	0.02	2.39	1.91	3.51
K_2O	[%]	0.01	2.16	0.53	2.22	0.89	0.26	1.12	4.72	0.34	0.58	0.25	1.99	1.79	0.51	1.86
TiO_2	[%]	0.01	1.43	0.78	0.82	2.51	0.84	0.14	3.04	1.07	0.54	2.15	5.21	4.88	1.28	0.7
P_2O_5	[%]	0.01	0.74	0.27	0.2	1.23	0.06	0.01	1.19	0.15	0.05	0.38	2.23	1.61	0.3	0.37
MnO	[%]	0.01	0.12	0.13	0.11	0.21	0.17	0.14	0.51	0.17	0.12	0.18	0.2	0.15	0.4	0.19
Cr_2O_3	[%]	0.002	0.011	0.01	0.009	0.007	0.017	0.06	0.002	0.074	0.014	0.024	0.024	0.021	0.021	0.02
Ni	[ppm]	20	90	39	<20	<20	140	142	29	88	103	106	105	82	55	70
Sc	[ppm]	1	15	20	17	33	31	17	95	47	18	26	27	22	35	22

LOI	[%]	-5.1	0.7	0.8	0.4	0.2	0.7	2.5	0.2	0.8	0.9	0.7	5.8	2.5	-0.1	0.8
Sample number			240609-05	240609-13	280609-02	280609-03	290609-01	290609-03	130910-05	130910-06	260609-01	260609-04	160910-18	160910-19	100709-09	080910-23
TOTAL	**[%]**	**0.01**	**99.54**	**99.7**	**99.77**	**99.62**	**99.73**	**99.76**	**99.29**	**99.8**	**99.71**	**99.67**	**99.5**	**99.52**	**99.73**	**99.66**
Ba	[ppm]	1	657	557	412	555	31	382	124	62	347	217	126	1287	85	681
Be	[ppm]	1	7	2	4	2	<1	2	6	<1	<1	2	2	2	<1	3
Co	[ppm]	0.2	18	17.8	15	21.1	62	30.7	31.3	39.2	30.9	40.4	57.1	44.7	38.8	28.9
Cs	[ppm]	0.1	6.9	0.6	8.2	1.4	0.8	2.7	16.8	0.3	2.6	0.3	0.1	0.8	1.7	3
Ga	[ppm]	0.5	27.2	20.9	23	23.6	17.5	16.9	62.6	18.4	15.7	20.6	29.3	19.5	18.2	18.9
Hf	[ppm]	0.1	26.8	2.4	3.7	17.1	0.6	0.3	14	1.9	1	5.7	9.3	8.6	2.3	2.8
Nb	[ppm]	0.1	27.9	5	15.8	24.6	0.6	6.2	184	2.7	1.4	12.9	26.7	21.5	11.4	5.6
Rb	[ppm]	0.1	220.5	6.3	140.7	11.8	4.2	80.6	723.4	2.9	29.9	7.8	62.7	100.3	12	117.8
Sn	[ppm]	1	9	<1	2	4	<1	3	42	<1	<1	2	6	3	1	4
Sr	[ppm]	0.5	731.8	833	496.6	395.1	274.7	303.5	74.6	214.3	767.5	612.8	835.2	575.8	135.2	746.9
Ta	[ppm]	0.1	3.9	0.3	1.1	1	<0.1	0.4	9.2	0.2	<0.1	0.6	1.4	1	0.5	0.3
Th	[ppm]	0.2	4.2	0.4	1.6	0.2	<0.2	0.4	159.1	0.5	0.3	0.3	6.6	5.4	1	4.3
U	[ppm]	0.1	5.3	0.3	2.1	0.4	<0.1	0.2	67.5	0.2	0.2	0.2	6.7	1.9	0.3	1.8
V	[ppm]	8	81	112	133	154	181	46	195	278	94	195	354	342	152	170
W	[ppm]	0.5	<0.5	<0.5	<0.5	0.6	<0.5	<0.5	0.7	<0.5	<0.5	1.2	1.2	0.6	<0.5	<0.5
Zr	[ppm]	0.1	1159	84.7	125.9	726.5	12.9	8.3	455.3	57.5	33.3	226.6	364.5	335.4	87.2	110.6
Y	[ppm]	0.1	62.4	24.2	26.8	90.5	8.4	18.3	2237	31.1	10.8	35.6	42.7	28.8	97.1	27.2
La	[ppm]	0.1	52.5	24.3	12.6	47.8	2	3.9	32.7	6.3	8.9	26.7	122.6	87.2	12.5	53.6
Ce	[ppm]	0.1	112.2	51	23.7	124.2	6.6	7.8	88.6	16.7	18.4	62	269.5	194.6	35	124.6
Pr	[ppm]	0.02	13.96	6.42	2.95	16.81	1.05	1.34	13.71	2.45	2.36	8.52	30.61	22.97	4.94	15.51
Nd	[ppm]	0.3	55.1	26.8	11.9	75.3	5.6	6.1	69.2	12.5	9.8	37.7	119.8	91.4	24.4	64.5
Sm	[ppm]	0.05	10.44	5.27	2.93	16.8	1.47	1.83	42.39	3.46	1.99	7.78	19.12	14.3	8.06	10.54
Eu	[ppm]	0.02	1.74	2.1	0.84	4.58	0.73	0.4	1.72	1.23	0.86	2.62	3.85	2.94	1.69	2.8
Gd	[ppm]	0.05	8.68	4.7	3.39	17.37	1.65	2.12	113	4.7	1.98	7.46	12.8	9.26	12.47	7.24
Tb	[ppm]	0.01	1.58	0.78	0.67	2.84	0.28	0.42	26.48	0.87	0.34	1.22	1.75	1.28	2.61	1
Dy	[ppm]	0.05	8.92	4.39	4.02	15.79	1.5	2.32	218	5.44	1.8	6.65	8.31	6.17	16.31	5.03
Ho	[ppm]	0.02	1.82	0.85	0.93	3.32	0.32	0.55	61.13	1.18	0.37	1.31	1.42	0.98	3.72	0.88
Er	[ppm]	0.03	5.7	2.47	2.88	9.17	0.89	1.78	222.7	3.38	1.12	3.54	3.81	2.47	10.93	2.52

Tm	[ppm]	0.01	1.02	0.37	0.47	1.32	0.13	0.33	37.22	0.52	0.15	0.51	0.51	0.33	1.69	0.39
Sample number			240609-05	240609-13	280609-02	280609-03	290609-01	290609-03	130910-05	130910-06	260609-01	260609-04	160910-18	160910-19	100709-09	080910-23
Yb	[ppm]	0.05	7.69	2.32	3.08	8.33	0.8	2.24	285.5	3.48	0.99	3.24	3.24	2.06	10.75	2.44
Lu	[ppm]	0.01	1.21	0.34	0.47	1.25	0.12	0.38	48.6	0.52	0.15	0.47	0.5	0.29	1.65	0.37
TOT/C	[%]	0.02	<0.02	<0.02	<0.02	0.02	0.04	<0.02	<0.02	0.06	<0.02	0.07	0.06	<0.02	0.03	<0.02
TOT/S	[%]	0.02	0.06	0.06	0.02	<0.02	0.15	<0.02	<0.02	0.1	0.03	0.13	<0.02	0.29	0.19	0.13
Mo	[ppm]	0.1	1.2	1.2	1.3	1.7	0.7	0.5	0.3	1	1.5	1.2	0.5	0.8	1.7	0.2
Cu	[ppm]	0.1	18	26.6	3.8	30.9	130.2	1.8	4	55	12	52.7	13.7	68.1	42.5	70.9
Pb	[ppm]	0.1	4.6	0.8	3.2	1.3	2	10.4	15.8	0.7	1.6	2.1	340.4	6.3	2.2	2.6
Zn	[ppm]	1	88	32	111	105	13	21	352	21	18	50	279	72	68	65
Ni	[ppm]	0.1	89.2	18.5	14.6	8.2	60	45.4	26.4	44.5	43.5	69.6	104.1	53	22	47.3
As	[ppm]	0.5	1.3	<0.5	<0.5	1.5	<0.5	<0.5	1.4	<0.5	<0.5	0.6	2.5	1.7	0.7	0.6
Cd	[ppm]	0.1	<0.1	<0.1	<0.1	0.1	<0.1	<0.1	<0.1	<0.1	<0.1	<0.1	0.1	<0.1	0.1	0.1
Sb	[ppm]	0.1	<0.1	<0.1	<0.1	<0.1	<0.1	<0.1	<0.1	<0.1	<0.1	<0.1	<0.1	<0.1	<0.1	<0.1
Bi	[ppm]	0.1	<0.1	<0.1	<0.1	0.3	<0.1	<0.1	<0.1	<0.1	<0.1	<0.1	0.1	<0.1	<0.1	<0.1
Ag	[ppm]	0.1	<0.1	<0.1	<0.1	<0.1	<0.1	<0.1	<0.1	<0.1	<0.1	<0.1	<0.1	<0.1	0.2	<0.1
Au	[ppb]	0.5	<0.5	0.8	1.1	<0.5	4.9	<0.5	<0.5	<0.5	1.1	1.4	<0.5	<0.5	<0.5	<0.5
Hg	[ppm]	0.01	<0.01	<0.01	<0.01	<0.01	<0.01	<0.01	<0.01	<0.01	<0.01	<0.01	<0.01	<0.01	<0.01	<0.01
Tl	[ppm]	0.1	2	<0.1	1	<0.1	<0.1	<0.1	5.9	<0.1	0.1	<0.1	<0.1	<0.1	<0.1	0.8
Se	[ppm]	0.5	0.5	<0.5	<0.5	<0.5	<0.5	<0.5	2.7	<0.5	<0.5	<0.5	<0.5	0.7	<0.5	<0.5

XRF data for K-feldspar chemistry (analyses removed for MgO, MnO, Cr_2O_3, CuO, HfO_2, NiO, V_2O_5, ZnO, ZrO_2, Ag, As, Cd, Ce, Co, Cr, La, Nb, Nd, Sb, Sc, Th, V, W, Yb, Zr, Cl, F, S, Bi, Br, Hg, I, Se, Sm and Ta as these fell below LOD)

Pegmatite		**Steli**	**Solås**	**Solås**	**Solås**	**Solås**	**Hovåsen**	**Slobrekka**	**Li Gruva**	**Landsverk1**	**Kåbuland**
Sample		**070708-02**	**090708-19**	**090708-20**	**280609-07**	**280609-08**	**100708-14**	**100708-24**	**100708-31**	**120708-02**	**130910-07**
SiO_2	[%]	65.5	65.4	65.8	64.9	64.2	66.7	64.9	65.9	65.6	65.1
Al_2O_3	[%]	18.4	18.6	18.3	18.2	18.3	18.8	18.2	18.5	18.3	18.5
Fe_2O_3	[%]	0.057	0.065	0.032	0.021	0.066	0.048	0.059	0.062	0.093	0.072
TiO_2	[%]	<0.01	0.011	<0.01	<0.01	<0.01	<0.01	<0.01	<0.01	<0.01	<0.01
CaO	[%]	0.054	0.068	0.02	<0.01	0.052	0.054	0.063	0.083	0.019	0.083
Na_2O	[%]	3.38	2.78	4.79	2.18	2.71	3.97	3.23	3.34	3.4	2.64
K_2O	[%]	12.2	12.7	10	13.2	12.8	11.3	12.3	12.2	12.2	12.5
P_2O_5	[%]	0.018	<0.01	<0.01	<0.01	<0.01	0.03	<0.01	<0.01	0.01	<0.01
Gl.tap	[%]	0.04	0.129	0.031	0.13	0.158	0.025	0.044	0.131	0.086	0.11
TOTAL	**[%]**	**99.7**	**99.9**	**98.9**	**98.7**	**98.3**	**101**	**98.8**	**100**	**99.6**	**99**
BaO*	[%]	<0.025	0.512	<0.025	<0.025	0.328	<0.025	<0.025	<0.025	<0.025	<0.025
PbO*	[%]	0.018	<0.01	0.013	0.013	<0.01	0.017	0.032	0.025	0.022	0.024
SrO*	[%]	<0.04	0.102	<0.04	<0.04	0.086	<0.04	<0.04	<0.04	<0.04	<0.04
Ba	[ppm]	30	3900	15	53	2500	54	22	37	51	167
Cu	[ppm]	<2	<2	<2	2.4	<2	2.1	<2	<2	<2	<2
Ga	[ppm]	27.9	15.1	51.3	70.3	15.3	51.5	27.4	25.2	43.1	25.2
Mo	[ppm]	<1	<1	<1	1.9	<1	2.2	<1	<1	<1	<1
Ni	[ppm]	7.5	2.5	19.8	46.9	2.3	48.1	6.2	4.3	9.9	8.9
Pb	[ppm]	162	85.1	133	129	99.1	136	278	231	233	169
Rb	[ppm]	1010	444	3350	7530	356	7550	939	738	1690	697
Sn	[ppm]	<10	11	<10	<10	<10	<10	<10	<10	<10	<10
Sr	[ppm]	7.6	678	9.4	19.9	599	25.3	26.1	18.9	9.8	72
U	[ppm]	2.9	4	9.4	23.4	3.9	23.3	2.7	2.3	4.9	3
W	[ppm]	<5	<5	<5	0.4	0.4	<5	<5	<5	<5	<5
Y	[ppm]	1.9	1.7	12.8	68.4	1.4	79.8	2.4	2	3.9	1.6
Zn	[ppm]	<1	<1	1.7	2.4	<1	1.7	<1	<1	<1	<1
Cs*	[ppm]	16	16	346	1230	<10	216	<10	17	33	15
Ge*	[ppm]	2.4	<1	11.8	18.6	<1	14	2.1	1.6	6.2	8.9
Hf*	[ppm]	<5	<5	<5	<5	<5	<5	<5	<5	<5	10.6

Sample		070708-02	090708-19	090708-20	280609-07	280609-08	100708-14	100708-24	100708-31	120708-02	130910-07
Te*	[ppm]	<10	<10	13	15	<10	11	<10	10	13	13
Tl*	[ppm]	10	<10	33	84	<10	77	<10	<10	17	<10

LA-ICP-MS data for quartz chemistry from the Evje-Iveland pegmatite field. Values are arithmetic means of three analyses for each sample

Pegmatite Sample	Li	Be	B	Mn	Ge	Rb	Sr	Sb	Na	Al	P	K	Ca	Ti	Fe	Zn	Ga
LOD	*0.85*	*0.23*	*2.49*	*0.18*	*0.16*	*0.05*	*0.03*	*0.04*	*4.41*	*3.52*	*2.71*	*20.77*	*14.47*	*0.75*	*2.27*	*0.57*	*0.00*
Li Gruva 100910-04	23.13	1.41	1.01	0.01	0.04	0.54	0.44	0.03	166.00	69.91	0.67	1.64	215.66	16.12	0.19	12.67	0.00
Li Gruva 100910-05	16.86	0.20	1.29	0.92	0.57	0.32	0.06	0.05	7.42	219.96	0.76	28.80	18.92	27.51	3.41	11.05	0.41
Li Gruva 100910-06	13.67	0.81	3.79	2.81	0.58	0.00	0.02	0.01	1.73	43.85	4.65	1.95	57.64	16.63	0.93	9.07	0.00
Li Gruva 100910-13	7.19	0.34	3.82	0.51	1.72	0.00	0.11	0.04	31.31	48.87	2.52	7.89	12.21	42.34	13.20	7.53	0.00
Hovåsen 110910-01	22.75	0.20	0.77	0.51	7.97	0.18	0.58	0.23	8.46	74.73	2.28	0.70	21.74	1.33	0.16	10.77	0.00
Hovåsen 110910-02	17.13	0.35	1.02	0.14	2.41	0.03	0.05	0.02	0.00	47.45	3.22	1.86	10.49	9.76	0.33	9.02	0.00
Hovåsen 110910-03	9.37	0.30	0.57	0.17	3.98	0.00	0.05	0.01	4.85	36.22	0.12	0.26	0.00	6.43	0.14	11.52	0.00
Hovåsen 110910-04	16.75	0.32	1.44	0.35	3.73	0.09	0.06	0.03	0.92	73.02	6.96	3.44	27.13	7.58	1.14	9.29	0.00
Landsverk 1 120708-01 (Multiple points)	25.55	0.00	0.66	0.07	0.00	0.03	0.01	0.23	0.00	316.93	3.67	1.49	0.00	0.00	0.00	8.59	0.00
	61.10	0.03	0.77	0.30	0.05	0.03	0.01	0.38	0.00	834.66	6.97	4.67	0.00	0.00	0.34	14.44	0.00
	61.99	0.00	0.63	0.25	0.26	0.06	0.03	0.32	14.90	818.81	8.50	4.55	0.00	0.00	0.00	13.45	0.00
	27.06	0.15	1.00	0.24	0.03	0.00	0.12	0.23	0.00	686.34	3.80	6.10	0.44	0.00	0.63	10.81	0.00
	9.77	0.00	0.73	0.24	0.16	0.03	0.05	0.15	0.00	70.56	0.82	0.00	34.70	0.00	0.00	9.66	0.00
	6.86	0.00	0.66	0.23	0.00	0.04	0.06	0.13	0.00	89.44	2.70	4.30	18.63	0.00	0.21	12.32	0.00
	18.46	0.11	0.18	0.44	0.00	0.06	0.01	0.21	0.00	128.03	0.00	3.29	0.00	0.00	0.17	10.52	0.00

	0.00	0.00	0.85	0.29	0.05	0.00	0.00	0.28	0.00	0.00	2.54	0.00	0.00	0.00	0.11	14.22	0.00
	2.61	0.00	0.37	0.30	0.16	0.03	0.00	0.10	4.85	11.56	1.99	0.00	0.00	0.00	0.41	9.79	0.00
	0.60	0.00	1.13	0.07	0.02	0.00	0.06	0.00	0.00	53.45	0.85	1.48	0.00	0.00	0.76	6.24	0.00
	1.05	0.17	0.43	0.22	0.33	0.01	0.05	0.02	0.00	4.78	0.00	0.88	0.00	0.00	0.00	12.19	0.00
	0.63	0.00	0.72	0.31	0.28	0.06	0.10	0.04	0.00	8.02	2.98	0.02	30.48	0.00	0.32	8.08	0.00
LOD	*0.34*	*0.13*	*0.35*	*0.06*	*0.10*	*0.05*	*0.02*	*0.04*	*14.24*	*5.56*	*1.41*	*6.42*	*36.40*	*1.54*	*0.33*	*1.17*	*0.00*
Solås 080910-01	8.25	0.11	0.65	0.22	1.49	0.00	0.08	0.02	0.00	43.84	1.34	0.85	0.00	26.17	0.25	1.16	0.00
Solås 080910-02	10.31	0.03	0.42	0.15	1.26	0.00	0.08	0.02	0.00	36.17	4.27	1.33	22.53	15.69	0.18	0.00	0.03
Solås 080910-03	9.71	0.17	0.84	0.20	3.15	0.00	0.07	0.02	0.00	33.89	2.46	0.10	0.00	15.88	0.22	0.00	0.00
Solås 080910-04	8.64	0.50	1.13	0.65	3.49	1.62	0.03	0.08	5.67	82.08	3.35	7.44	8.93	13.15	0.40	1.57	0.12
Solås 080910-05	6.71	0.08	1.63	0.30	11.72	0.03	0.06	0.09	0.00	12.12	2.92	2.14	0.00	0.96	0.14	0.00	0.00
Solås 080910-06	4.94	0.07	0.98	0.30	1.87	0.05	0.17	0.10	0.00	15.98	4.53	0.86	0.00	17.09	0.16	0.00	0.00
Steli 080910-24	7.56	0.12	0.51	0.20	0.98	0.01	0.03	0.02	0.00	16.25	2.92	0.59	0.50	13.28	0.34	0.00	0.00
Steli 080910-25	9.50	0.08	0.76	0.28	1.80	0.07	0.05	0.12	4.37	50.54	0.64	7.50	0.07	6.45	0.75	0.00	0.00
Steli 080910-26	11.63	0.18	0.48	0.35	2.10	0.00	0.02	0.25	0.00	44.30	4.13	1.67	10.06	3.02	0.45	0.00	0.00
Steli 080910-27	9.04	0.08	0.52	0.19	3.26	0.00	0.01	0.24	0.37	36.44	5.78	1.39	0.00	5.28	0.18	0.00	0.00
Steli 080910-28	10.73	0.05	1.99	0.76	0.88	0.02	0.08	0.01	14.27	20.80	0.00	0.77	15.63	13.18	0.02	1.41	0.00
Steli 080910-29	9.71	0.00	0.77	0.12	1.00	0.01	0.05	0.01	0.00	25.27	0.00	1.40	2.03	11.05	0.21	0.32	0.00
Li Gruva	5.10	0.06	0.59	0.15	3.39	0.00	0.04	0.01	0.00	7.90	1.81	0.69	0.37	15.68	0.13	0.40	0.00

100910-01																	
Li Gruva 100910-02	9.04	0.74	0.51	0.43	2.03	0.29	0.05	0.03	0.00	91.15	4.13	7.45	5.48	21.52	0.65	0.95	0.00
Li Gruva 100910-03	6.12	0.24	0.51	0.18	1.92	0.02	0.06	0.03	0.00	24.16	6.43	0.27	4.21	23.40	0.03	0.00	0.00
Hovåsen 100910-05	20.01	0.14	0.59	0.24	1.32	0.03	0.05	0.01	0.00	65.17	0.62	1.51	0.00	12.30	0.17	0.14	0.00
Slobrekka 120910-01	10.21	0.06	0.61	0.28	2.07	0.03	0.03	0.02	0.00	25.08	0.40	2.14	9.77	17.64	0.20	0.08	0.00
Slobrekka 120910-02	4.51	0.16	0.89	0.35	8.11	0.31	0.03	0.07	0.00	53.96	6.06	9.88	15.21	4.35	0.37	0.00	0.08
Slobrekka 120910-03	9.60	0.21	0.84	0.36	4.76	0.03	0.05	0.05	0.00	52.25	5.08	0.40	3.06	6.37	0.46	0.00	0.00
Slobrekka 120910-04	8.57	0.23	0.75	1.01	2.11	0.49	0.04	0.02	0.00	86.66	6.08	19.16	13.62	25.16	0.34	0.00	0.00
Slobrekka 120910-05	10.79	0.51	0.88	1.41	2.72	1.03	0.02	0.10	0.00	175.27	2.75	30.86	6.76	27.81	1.30	0.00	0.00
Slobrekka 120910-06	6.06	0.02	0.44	0.24	1.30	0.02	0.06	0.01	1.67	10.09	5.91	0.25	7.69	26.09	0.30	0.00	0.00
Hovåsen 120910-12	19.08	0.07	0.41	0.26	1.44	0.00	0.07	0.01	0.00	53.85	5.09	0.73	49.09	25.89	0.02	0.00	0.00
Kåbuland 130910-01	10.12	0.13	0.28	0.29	1.19	0.01	0.01	0.05	0.00	105.09	5.44	4.70	0.00	33.37	1.93	0.00	0.00
Kåbuland 130910-02	10.50	0.32	0.45	1.47	2.17	0.27	0.05	0.03	0.00	145.24	6.11	43.57	67.32	23.26	1.15	0.00	0.00
Kåbuland 130910-03	12.03	0.23	1.06	0.88	1.76	0.16	0.07	0.31	2.62	80.28	6.68	10.54	5.03	29.30	1.47	0.00	0.00
Landsverk 1 160910-01	24.27	0.21	2.11	0.45	0.15	1.47	23.28	0.08	1080.69	169.90	4.66	153.99	595.83	0.00	1.00	0.62	0.00

LA-ICP-MS data for quartz chemistry for the Landsverk pegmatites. Values are arithmetic means of two/three analyses for each sample

Sample	Li	Be	B	Mn	Ge	Rb	Sr	Sb	Na	Al	P	K	Ca	Ti	Fe	Zn	Ga
040611-03	3.89	0.02	1.39	0.07	0.78	0.02	0.17	0.06	0.00	29.50	0.81	0.84	0.00	28.41	0.09	0.00	0.00
040611-04	4.47	0.02	1.28	0.06	1.20	0.01	0.02	0.10	0.00	76.63	0.05	24.53	1.17	26.28	3.55	0.18	0.01
040611-05	2.47	0.00	1.41	0.13	0.72	0.02	0.03	0.16	0.00	52.47	10.61	0.80	0.40	34.50	0.22	0.15	0.02
050611-01	4.73	0.09	2.19	0.14	1.16	0.00	0.02	0.38	4.57	93.78	3.39	0.91	0.00	28.39	0.73	0.22	0.03
050611-02	2.17	0.01	1.24	0.07	0.76	0.01	0.02	0.02	1.76	12.40	2.82	0.56	0.00	17.92	0.16	0.00	0.01
050611-03	4.61	0.20	0.97	0.19	1.68	0.02	0.03	0.05	2.20	34.49	6.95	0.44	0.00	26.10	0.18	0.05	0.00
070611-01	4.37	0.08	1.15	0.14	1.03	0.02	0.02	0.05	0.00	38.58	0.30	0.31	0.00	31.44	0.27	0.04	0.01
070611-02	2.20	0.04	1.05	0.07	1.11	0.00	0.03	0.11	0.00	16.51	2.99	0.59	1.14	22.35	0.07	0.44	0.00
070611-03	2.11	0.01	1.06	0.18	0.92	0.02	0.03	0.08	0.00	22.76	4.56	0.57	0.00	25.51	0.10	0.17	0.00
070611-04	2.40	0.01	1.28	0.06	0.76	0.00	0.02	0.10	0.00	18.01	2.16	0.24	0.41	23.05	0.03	0.16	0.00
070611-05	4.11	0.05	1.20	0.31	1.60	0.08	0.11	0.06	0.00	53.57	5.46	4.02	1.26	23.08	0.30	0.08	0.00
080611-01	10.84	0.16	1.62	0.32	1.15	0.00	0.03	0.10	44.16	67.85	3.41	0.82	0.65	29.31	0.77	0.10	0.01
080611-02	5.16	0.14	0.97	0.10	1.51	0.01	0.07	0.02	0.00	38.68	3.51	0.26	0.00	28.43	0.24	0.16	0.00
080611-03	0.00	0.04	0.93	0.27	1.38	0.04	0.20	0.17	0.00	25.55	4.88	2.51	4.40	12.35	2.43	0.14	0.00
080611-04	2.34	0.12	1.25	0.08	1.88	0.00	0.01	0.04	0.00	32.12	6.93	1.85	0.00	21.04	0.42	0.00	0.00
080611-06	0.09	0.06	1.13	0.09	1.76	0.01	0.12	0.07	0.00	9.68	3.79	0.53	6.23	13.95	0.31	0.09	0.00
080611-08	2.00	0.16	1.30	0.32	1.83	0.01	0.03	0.02	0.00	121.26	4.88	0.51	0.00	42.46	3.21	0.90	0.01
100611-01	5.04	0.19	1.56	0.20	1.87	0.14	0.08	0.42	0.00	69.27	0.31	8.48	2.10	32.43	0.27	0.20	0.00
100611-03	3.58	0.08	1.24	0.16	1.28	0.02	0.05	0.11	2.98	46.43	3.49	2.77	1.02	26.57	0.76	0.17	0.01
100611-06	3.45	0.14	0.89	0.47	1.53	0.03	0.02	0.04	0.00	183.62	6.17	21.35	0.54	35.45	2.77	0.00	0.08
100611-08	2.79	0.05	1.00	0.25	1.58	0.00	0.03	0.11	0.00	18.31	0.52	0.13	0.00	30.75	0.12	0.00	0.00
100611-10	3.89	0.06	0.90	0.14	1.19	0.01	0.03	0.10	0.00	28.33	1.99	0.00	0.00	29.81	0.20	0.00	0.00
100611-11	6.86	0.06	1.02	0.11	0.10	0.02	0.15	0.22	0.00	76.90	6.51	0.54	8.25	0.00	0.05	0.22	0.00
110611-01	2.25	0.15	1.10	0.07	1.22	0.00	0.04	0.10	0.00	27.58	3.88	0.18	0.14	23.47	0.18	0.00	0.00

110611-03	3.58	0.05	0.91	0.14	1.27	0.02	0.02	0.07	0.00	33.00	3.18	1.31	0.00	28.12	0.21	0.07	0.00
110611-05	5.39	0.12	1.18	0.21	0.99	0.01	0.05	0.03	0.00	88.83	7.83	0.73	1.02	32.14	2.29	0.08	0.02
110611-07	5.89	0.16	1.20	0.99	1.66	0.26	0.07	0.06	0.00	132.96	5.22	17.28	13.56	21.96	0.81	0.12	0.01
110611-09	5.37	0.32	1.88	0.41	10.35	0.36	0.04	0.25	0.00	96.44	4.21	5.65	0.59	8.75	0.66	0.52	0.03
110611-11	3.10	0.34	0.69	0.10	2.58	0.00	0.02	0.06	0.00	53.21	5.56	0.00	0.00	21.82	0.92	0.19	0.01
110611-12	5.73	0.32	1.14	0.18	1.72	0.15	0.02	0.05	0.00	73.63	5.42	2.83	0.00	24.13	0.20	0.00	0.00
110611-14	5.21	0.16	1.58	0.67	1.62	0.64	0.04	0.43	0.00	100.32	3.03	16.45	5.11	43.60	0.32	0.35	0.00
120611-01	2.39	0.06	1.24	0.15	0.93	0.01	0.09	0.08	0.00	32.61	2.45	0.62	0.38	11.36	0.19	0.00	0.00
120611-02	3.83	0.00	1.21	0.09	0.98	0.01	0.03	0.11	0.00	20.80	2.54	0.04	0.00	22.42	0.08	0.00	0.00
120611-03	3.85	0.07	0.76	0.10	1.22	0.01	0.09	0.09	0.00	20.51	0.39	0.54	0.00	22.43	0.06	0.09	0.00
140611-01	0.51	0.00	0.75	0.14	1.20	0.02	0.06	0.11	0.00	13.90	5.56	0.16	1.11	17.71	0.30	0.18	0.00
140611-02	1.83	0.08	0.79	0.13	1.58	0.01	0.07	0.12	0.00	23.19	0.13	0.56	1.22	12.10	0.07	0.41	0.00
150611-01	7.37	0.02	1.03	0.18	1.66	0.14	1.81	0.58	383.25	50.27	3.09	25.00	184.49	30.67	1.75	1.51	0.00
150611-02	0.25	0.02	1.64	2.32	1.79	0.07	1.28	0.31	1.16	14.10	1.20	27.68	122.29	10.32	8.89	1.30	0.00
150611-03	8.30	0.30	0.82	0.97	1.82	0.84	0.33	0.05	22.11	153.41	2.89	18.70	10.07	30.02	0.75	0.28	0.00
150611-04	0.04	0.21	0.67	0.15	0.69	0.06	1.16	0.37	16.01	17.36	2.40	6.30	9.68	27.78	10.19	0.49	0.00
150611-05	1.61	0.10	0.88	0.15	2.21	0.07	0.11	0.21	0.00	20.19	0.00	2.42	3.40	19.80	0.61	0.94	0.00
150611-07	4.53	0.08	0.46	0.27	2.25	0.02	0.07	0.12	0.00	38.72	0.00	1.50	5.80	23.14	0.24	1.05	0.00
160611-01	0.35	0.04	0.71	0.15	1.26	0.11	0.17	0.07	13.26	9.52	0.00	3.50	0.11	17.49	0.51	0.00	0.00
160611-02	5.79	0.14	0.87	0.44	0.00	0.38	4.83	1.20	112.49	34.72	6.38	21.68	43.15	0.00	0.55	0.00	0.00
160611-03	1.27	0.32	0.92	0.59	1.05	0.00	0.19	0.13	0.00	163.15	0.00	3.08	1.34	97.35	4.85	0.19	0.00
160611-04	5.15	0.04	1.24	0.28	1.69	0.01	0.04	0.33	0.00	13.71	0.00	1.34	7.54	16.11	0.53	1.34	0.00
160611-05	6.10	0.06	0.48	0.27	1.73	0.00	0.10	0.08	5.00	94.99	0.00	3.08	0.00	32.18	2.24	0.00	0.04
160611-06	2.71	0.05	0.97	0.03	2.91	0.00	0.06	0.60	0.00	14.71	2.52	2.45	16.65	11.55	0.30	0.18	0.00
180611-01	35.80	0.00	0.25	0.00	3.63	0.92	2.35	0.64	211.58	85.01	34.07	13.10	12.60	0.00	1.75	1.18	0.00
180611-02	2.62	0.00	1.44	0.02	0.19	0.14	0.86	0.11	0.00	37.92	8.62	0.00	0.00	0.00	0.22	0.00	0.00
180611-04	2.68	0.00	0.89	0.04	0.05	0.46	5.71	0.18	422.76	3.39	0.00	38.55	222.70	0.00	0.19	0.86	0.00

180611-06	1.06	0.00	0.63	0.11	0.04	0.00	0.11	0.41	11.84	11.63	3.33	2.65	0.00	0.00	0.43	0.32	0.00
180611-07	1.55	0.32	0.63	0.23	0.05	0.08	1.08	0.54	25.80	3.47	1.59	1.44	13.52	0.00	1.84	0.00	0.00
180611-08	93.13	0.14	1.25	0.35	0.86	0.17	0.25	1.07	74.52	823.22	16.56	0.00	32.70	0.00	0.00	0.00	0.00
180611-10	3.44	0.05	0.80	0.29	0.00	0.03	0.16	0.08	37.73	11.26	0.59	4.60	19.09	0.00	0.21	0.00	0.00
180611-11	2.11	0.05	1.22	0.23	0.03	0.11	0.54	0.33	46.98	12.31	1.28	5.37	33.57	0.00	0.28	0.00	0.00
180611-12	7.72	0.18	0.72	0.14	0.19	0.00	0.23	0.07	4.45	43.12	3.98	1.16	2.92	0.00	0.25	0.00	0.00

XRF data for mica chemistry. FeO_{TOT} calculated from Fe_2O_3. Analyses removed for Cr_2O_3, CuO, HfO_2, NiO, SrO and ZrO_2 as these fell below LOD. Atomic proportions i.e. number of ions in formula (**at. pro.**) are provided (excluding P_2O_5, BaO, PbO and V_2O_5 as these typically fall below LOD, producing atomic proportions of 0.00%).

	SiO_2 wt%	Al_2O_3 wt%	FeO_{TOT} wt%	TiO_2 wt%	MgO wt%	CaO wt%	Na_2O wt%	K_2O wt%	MnO wt%	ZnO wt%	P_2O_5 wt%	BaO wt%	PbO wt%	V_2O_5 wt%	H_2O wt%	TOTAL wt%
	at. pro.	at. pro.	at. pro.	at. pro.	at. pro.	at. pro.	at. pro.	at. pro.	at. pro.	at. pro.					at. pro.	
Biotite Steli 070708-04	35.10	17.40	26.54	2.13	3.82	0.01	0.18	8.93	0.75	0.13	<0.01	<0.03	<0.01	<0.02	5.01	94.99
	5.42	3.17	3.43	0.25	0.88	0.00	0.05	1.76	0.10	0.01					5.16	
Biotite Solås 090708-21	37.20	15.60	20.79	3.35	8.09	<0.01	0.14	9.49	1.06	0.12	0.02	0.03	<0.01	0.02	4.10	95.90
	5.67	2.80	2.65	0.38	1.84	0.00	0.04	1.84	0.14	0.01					4.23	
Biotite Hovåsen 100708-16	36.10	15.60	22.95	3.04	6.72	<0.01	0.19	9.38	1.26	0.12	<0.01	<0.03	<0.01	<0.02	4.64	95.36
	5.54	2.82	2.95	0.35	1.54	0.00	0.05	1.84	0.16	0.01					4.75	
Biotite Slobrekka 100708-26	36.50	16.70	21.69	2.75	6.67	0.14	0.14	9.17	1.17	0.10	<0.01	<0.03	<0.01	<0.02	4.98	95.02
	5.53	2.98	2.75	0.31	1.51	0.02	0.04	1.77	0.15	0.01					5.02	
Biotite Kåbuland 130910-08	36.40	15.00	21.78	2.93	9.11	0.13	0.05	8.54	0.34	0.06	<0.01	0.03	0.01	0.03	5.59	94.41
	5.45	2.65	2.73	0.33	2.03	0.02	0.01	1.63	0.04	0.01					5.65	
Muscovite Steli 070708-05	45.30	32.50	4.42	0.16	0.42	<0.01	0.75	10.20	0.08	0.02	<0.01	<0.03	<0.01	<0.02	6.17	93.83
	6.03	5.10	0.49	0.02	0.08	0.00	0.17	1.73	0.01	0.00					5.47	
Muscovite Solås 090708-22	45.30	31.30	4.54	0.28	0.39	<0.01	0.68	10.10	0.31	0.09	<0.01	<0.03	<0.01	<0.02	7.02	92.98
	5.99	4.88	0.50	0.03	0.08	0.00	0.15	1.70	0.03	0.01					6.19	
Muscovite Slobrekka 100708-27	45.20	30.30	4.72	0.81	1.00	<0.01	0.72	10.30	0.13	0.01	<0.01	<0.03	<0.01	<0.02	6.80	93.20
	6.01	4.75	0.52	0.08	0.20	0.00	0.16	1.75	0.01	0.00					6.02	
Muscovite Landsverk 1 120708-04	45.40	29.70	5.19	0.75	0.99	0.03	0.77	10.10	0.25	0.05	<0.01	<0.03	<0.01	<0.02	6.77	93.23
	6.05	4.66	0.58	0.08	0.20	0.00	0.18	1.72	0.03	0.01					6.01	

Atomic proportions are calculated using the method described in Deer, Howie and Zussman (1966); the calculation is included for sample 070708-04 (biotite from Steli). H_2O wt% is estimated by subtracting TOTAL wt% from 100%. Li was not included in the calculation as it could not be estimated from F or Rb (as these fell below LOD) or from SiO_2 (the abundancy of which would grossly overestimate Li). The fact that the Evje-Iveland NYF pegmatites lack Li by definition further justifies this choice.

	(1) wt% of oxides	(2) mol. pro. of oxides (devide (1) by molecular weight)	(3) at. pro. of O from each mol. (multiply (2) by no. of O)	(4) Anions on basis of 24 (multiply (3) by 9.28)	(5) Ions in formula (divide (4) by ratio of O to cations)
SiO_2	35.10	0.58	1.17	10.85	5.42
Al_2O_3	17.40	0.17	0.51	4.75	3.17
FeO_{tot}	26.54	0.37	0.37	3.43	3.43
TiO_2	2.13	0.03	0.05	0.50	0.25
MgO	3.82	0.09	0.09	0.88	0.88
CaO	0.01	0.00	0.00	0.00	0.00
Na_2O	0.18	0.00	0.00	0.02	0.05
K_2O	8.93	0.09	0.09	0.88	1.76
MnO	0.75	0.01	0.01	0.10	0.10
ZnO	0.13	0.00	0.00	0.01	0.01
TOTAL	94.99	0.28	0.28	2.58	5.16
H_2O	5.01				
Total	100		2.59		
		24/2.59 =	9.28		